Assay Development, Identification, Optimization and Pharmacological Characterization of Inhibitors for Ecto-5′-nucleotidase (CD73)

Dissertation

zur Erlangung des Doktorgrades (Dr. rer. nat.)

der

Mathematisch-Naturwissenschaftlichen Fakultät

der

Rheinischen Friedrich-Wilhelms-Universität Bonn

vorgelegt von

Christian Philipp Renn

Aus Remscheid

Bonn 2019

Angefertigt mit Genehmigung der Mathematisch-Naturwissenschaftlichen Fakultät der Rheinischen Friedrich-Wilhelms-Universität Bonn.

Die vorliegende Arbeit wurde von Juni 2015 bis Juli 2019 am Pharmazeutischen Institut der Rheinischen Friedrich-Wilhelms-Universität Bonn unter der Leitung von Frau Prof. Dr. Christa E. Müller angefertigt.

Table of content

List of figures

List of tables

List of abbreviations

[2,8-^{3}H]AMP	tritiated AMP at position 2 and 8
4T1.2	triple-negative breast cancer cells from mouse derived clone 4T1.2
6xHis-Tag	6 times histidine tag
A_{280}	absorption at 280 nm
ABL	Abelson murine leukemia viral oncogene homolog
ADME	absorption, distribution, metabolism, and excretion
ADP	adenosine-5′-diphosphate
AMP	adenosine-5′-monophosphate
AOPCP	α,β-methylene-ADP
AP	alkaline phosphatase
APS	ammonium peroxydisulfate
ATP	adenosine-5′-triphosphate
BALB/c	mice: albino, laboratory-bred strain of the house mouse
Bq	Becquerel
BSA	bovine serum albumin
b-TNAP	bovine tissue-non-specific alkaline phosphatase
CD73	ecto-5′-nucleotidase
cDNA	complementary DNA
CDP	cytidine-5′-diphosphate
c-IAP	tissue-specific calf intestinal alkaline phosphatase
CMP	cytidine-5′-monophosphate
COPCP	α,β-methylene-CDP
ddH$_2$O	double-distilled water
DMEM	Dulbeccos's modified eagle medium
DMSO	dimethyl sulfoxide
DNA	deoxyribonucleic acid
EC_{50}	half maximal effective concentration for activators
ECL	enhanced chemiluminescence
EDTA	ethylenediaminetetraacetic acid
ER	estrogen receptor
EtOH	ethanol

f.c.	final concentration
FAD	flavin adenine dinucleotide
FBS	fetal bovine serum
FDA	The U.S. Food and Drug Administration
g	g-force
GMP	guanosine-5′-monophosphate
GPCR	G protein–coupled receptor
GPI	glycosylphosphatidylinositol
H118A	mutation: histidine is replaced at position 118 to alanine
Hepes	4-(2-hydroxyethyl)piperazine-1-ethanesulfonic acid
HER2/neu	human epidermal growth factor receptor 2
HPLC	high-performance liquid chromatography
HTS	high-throughput screening
IBD	inflammatory bowel disease
IC_{50}	half maximal inhibitory concentration
IMP	inositol-5′-monophosphate
IR	injury ischemia-reperfusion injury
kDa	kilodalton
K_i	inhibition constant
K_M	Michaelis constant, substrate concentration at half V_{max}
LB media	lysogeny broth media
LGIC	ligand-gated ion channel
LOD	limit of detection
Ma.Mel65	melanoma cells from human clone Ma.Mel65
mAbs	monoclonal antibodies
mCi	millicurie
MDA-MB-231	triple-negative breast cancer cells from human derived clone MDA-MB-231
MeOH	methanol
$MgCl_2$	magnesium chloride
Milli-Q water	purified water (grade 1 (ISO 3696))
MTBST	milk powder in TBST-buffer
MW	molecular weight

NaCl	sodium chloride
NADH	nicotinamide adenine dinucleotide
NANC nerve	non-adrenergic, non-cholinergic nerve
NCI-H292	mucoepidermoid pulmonary carcinoma cells
Ni^{2+}-NTA	nickel ions chelated with nitrilotriacetic acid
NTPDase	ecto-nucleoside triphosphate diphosphohydrolase
PBS	phosphate-buffered saline
POM1	polyoxotungstate
PR	progesterone receptor
PTM	post-translational modification
rpm	rounds per minute
RPMI medium	Roswell Park Memorial Institute medium
RT	room temperature
S/B	signal-to-background ratio
sCD73	soluble CD73 (ecto-5′-nucleotidase)
SCID	severe combined immunodeficiency mice
SDS-PAGE	sodium dodecyl sulfate polyacrylamide gel electrophoresis
SEM	standard error of the mean
Sf9	insect cells derived from *Spodoptera frugiperda 9*
T175	culture flask with a surface of 175 cm^2
T25	culture flask with a surface of 25 cm^2
T75	culture flask with a surface of 75 cm^2
TBS	tris-buffered saline
TBST	TBS with Tween® 20
TEMED	*N,N,N′,N′*-tetramethylethane-1,2-diamine
TNBC	triple-negative breast cancer
Tris	tris(hydroxymethyl)aminomethane
UDP	uridine-5′-diphosphate
UMP	uridine-5′-monophosphate
UOPCP	α,β-methylene-UDP
V	velocity
V_{max}	maximal velocity
wt	wild-type

1   Introduction

1.1   Drug discovery

The development of a drug against a specific disease is a long journey unique for every disease. The first findings about a disease and possible therapeutic approaches often come from basic research. Once it has been recognized how a disease develops and progresses on a cellular and molecular level, key structures can be identified that are responsible for the pathological course of the disease. Based on this information, a drug can be developed. This thesis touches many areas in the field of drug development. For a better understanding, the process of drug development including the definition of many technical terms is explained in this chapter.

1.1.1   Drug

A pharmaceutical drug applied to the body causes a change of physiological conditions leading to treat, cure, prevent, or diagnose a disease or to promote well-being.[1] This effect is mediated by an active substance within the drug, which usually is a chemical (small molecule) or biologically produced substance (biological) with known structure and characteristics.[2]

1.1.2   Drug target

A drug target is a structure within an organism to which an active substance is directed. The active substance binds to the target, changes its function, thus, leading to a desired physiological effect which cures the disease or promotes healing. Most drugs address proteins; nucleic acids and hormones, on the other hand, play a minor role as drug targets.[3] For example, the β-lactam antibiotic amoxicillin is given in the case of a bacterial infection with gram-negative bacteria. This compound binds to and inhibits the target D-alanine transpeptidase which is essential for bacterial cell division, and the bacteria cannot multiply any further.[4] However, many diseases are not based on pathogens, but on malfunction of body's own signal transduction pathways. In chronic myeloid leukemia, for example, a mutation leads to hyperactivity of the tyrosine kinase ABL. This enzyme is involved in the regulation of cell division. The hyperactivity of this kinase causes the cells to proliferate in an uncontrolled manner and leukemia develops. The drug imatinib binds to this target and thus prevents the proliferation of the affected cells.[5]

Introduction

1.1.3 Assay

Is a drug target identified, a suitable test system (assay) is established to analyze potential drug candidates in the laboratory *in vitro*.[3] Usually, the half-maximal effective concentration (EC_{50}) for activators/agonists or the half-maximal inhibitory concentration (IC_{50}) for inhibitors/antagonists is used as a criterion to describe the potency of compounds quantitatively. This value describes the concentration of a compound at which it induces a 50% change of response in the assay.[6]

1.1.4 Hit identification

After establishing a suitable assay, it is necessary to identify a chemical compound that binds to the target and affects its activity. Most often, the endogenous ligand of a receptor or a substrate in case of an enzyme is known. This compound interacts with the target and its chemical modification might lead to a compound which can modulate the activity of the target in a desired way. A further approach is to test thousands to millions of compounds, which are stored in compound libraries, in high-throughput screening (HTS) campaigns. For this purpose, the developed assay is adapted to a liquid handling workstation, which runs these tests automatically. Compounds which address the target at a certain concentration (usually 10 µM) with a certain effect in the assay are called hits. A variety of HTS is a fragment-based screening approach wherein molecule fragments are screened at higher concentrations leading to hits which are mostly less potent, but not less interesting. Their smaller size offer more potential for the synthesis of potent compounds.[3] A further approach is called virtual screening. Here, the screening of compounds is performed *in silico*. The requirement for virtual screening is the presence of the 3-dimensional structure of the target protein or at least a homology model derived from a protein with a similar amino acid sequence and/or predicted structural similarities. In the virtual screening process, hundreds of thousands to millions of compounds are virtually docked to the target and it is predicted which of these (virtual) compounds might form the most stable complex.[7] These primary hits must then be validated in an assay *in vitro*.

1.1.5 From hit to lead

In the phase from hit to lead (lead generation) structures will be synthesized with slight chemical modifications compared to the structure of the hit compounds. Modifications that lead to more potent compounds will be retained, unfavorable ones will be discarded. These

optimization cycles will be repeated around 3-5 times.[3] In the ideal case, this process leads to the development of compounds that address the target with EC_{50}/IC_{50} values in the low nM range. In addition, this process clarifies the structure-activity relationships of the compound class. Selected compounds are characterized in more detail by analyzing binding modes and selectivity. In addition, the physicochemical properties of compounds from the series are explored to confirm drug-likeness. Medications are mostly taken orally. The likeliness of a compound to cross membranes and to be absorbed by the body is considered likely if the compound meets the criteria of the Lipinski rule of five, which are as follows:[8]

- The molecular weight of the compound is less than 500 Daltons.
- The logP of the compound, which is a measure of lipophilicity, is 5 or less.
- The number of hydrogen bond donors of the compound is 5 or less.
- The number of hydrogen bond acceptors of the compound is 10 or less.

In addition, absorption, distribution, metabolism, and excretion (ADME) properties are investigated *in vitro* by analyzing membrane permeability using colon carcinoma (Caco-2) cells,[9] by investigating the metabolic stability and intrinsic clearance using human liver microsomes,[10] by analyzing the potential influence to the metabolism using cytochrome P450 inhibition/induction studies[11] and the distribution of propensity of the drug for protein binding.[12] Furthermore, possible toxic effects are excluded by the examination of cytotoxicity, hepatotoxicity and genotoxicity studies.[3] Potent, selective and nontoxic compounds with desirable ADME properties and appropriate pharmacokinetics are then investigated in primary animal models. If the compound does not meet the expected characteristics of these tests, the chemical structure will be further optimized in the stage of lead optimization.

1.1.6 What comes after the stage of drug discovery?

The U.S. Food and Drug Administration (FDA) listed the drug discovery as the first of five steps of drug development. The second step, as mentioned above, is the subsequent preclinical research; here the drugs undergo laboratory and animal testing to answer basic questions about safety. In the following third step, called clinical research, the drugs are tested first on small groups (phase I) of healthy volunteers to ensure drug safety. Followed by trials with larger groups (phase II and III) to make sure their effectiveness. The fourth step is the FDA review. Here, the FDA examines all of the submitted data related to the drug

and makes a decision to approve or reject it. After market launch the FDA further monitors all drugs safety issues and this fifth step is called: FDA post-market safety monitoring.[13] The industry estimates from the beginning of drug discovery till the launch of the drug to the marked is around 12-15 years.[14, 15]

The enzyme ecto-5′-nucleotidase is the drug target studied in this thesis. This enzyme is one of the key elements within the purinergic signaling pathway. This pathway is physiologically and pathophysiologically very important and its key players are described in the following chapters.

1.2 Purinergic signaling pathway

1.2.1 History

First signs that purines play a role as extracellular signaling molecules were found in the regulation of the cardiovascular system by Drury & Szent-Györgyi in 1929 (Figure 1). Purine-enriched tissue extracts or AMP solutions (which is presumably converted to adenosine according to the present state of knowledge) intravenously injected into guinea-pig, rabbit, cat or dog led to the same pharmacological effects, including a negative chronotropic effect up to a cardiac arrest of the heart, dilatation of coronary blood vessels and inhibition of spontaneously active intestinal smooth muscles.[16, 17]

In the 1970s, Geoffrey Burnstock and coworkers postulated ATP to act as a neurotransmitter in non-adrenergic, non-cholinergic (NANC) nerves.[18] Back in those days, these findings were debated controversially, because the concept of NANC nerves was not fully accepted, and the role of ATP was believed to be limited to intracellular energy transfer metabolism only.[17] However, further experimental evidence led to the concept of the "purinergic" nerve[19] and purines and pyrimidines as extracellular signaling molecules became more and more accepted. Since then, the purinergic signaling pathway has been extensively investigated until today.[17]
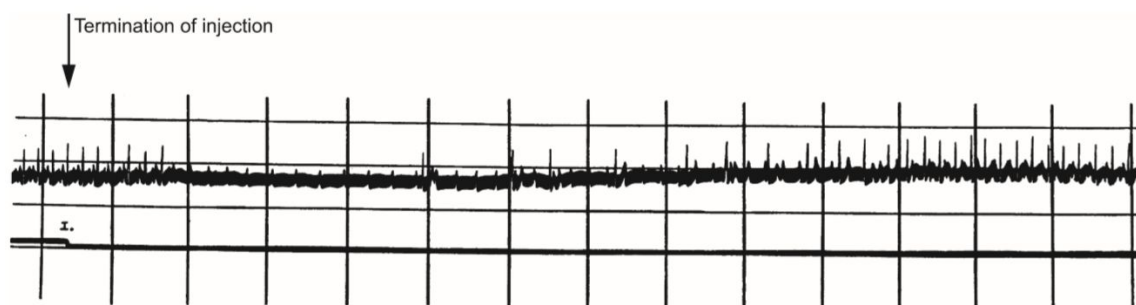
Figure 1. Purine-enriched extract and its effect on the heart. Electrocardiogram shows the influence of intravenous injection of the extract to the heart (injection starts three seconds before termination as indicated by the arrow; time maker = 1 second).[17]

Introduction

1.2.2 Purinergic Receptors

The membrane-bound receptors (purinergic receptors) which are activated by nucleosides and nucleotides were originally classified by Burnstock into P1 and P2 receptors, respectively.[20] Since that time altogether 19 purinergic receptors have been identified in human (Figure 2), which made a further subdivision of the receptors necessary. The P1 family representing G protein-coupled receptors (GPCR) was divided into 4 subtypes (A_1, $_{2A}$, $_{2B}$, $_3$), the P2 family was further subdivided into P2Y receptors (8 subtypes: $P2Y_{1, 2, 4, 6, 11-14}$) representing GPCRs and P2X receptors (7 subtypes: $P2X_{1-7}$) representing ligand-gated ion channels (LGIC).[20–23]

The P2Y subtypes ($P2Y_{3, 5, 7-10}$) are non-mammalian receptors or share sequence homology to P2Y receptors, but are not activated by nucleotides. Besides P1 and P2 receptors, adenine receptors, so called P0 receptors, were identified in rodents, but have not yet been identified in humans.[23] A brief characterization of human purinergic receptors, their endogenous ligands, tissue expression, biological function and medications targeting them, is given in the next chapters.
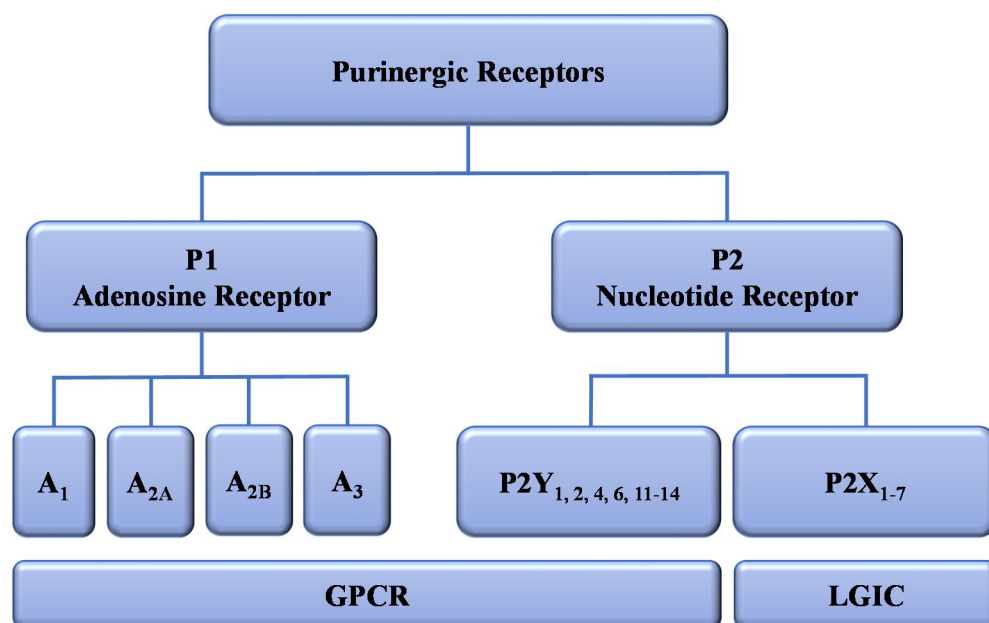
Figure 2. Purinergic receptors identified in humans. Human purinergic receptors are classified as P1 (activated by the nucleoside adenosine) and P2 receptors (activated by nucleotides). P1 consists of four adenosine receptor subtypes, P2 is further divided into P2Y and P2X. P1 and P2Y are G protein-coupled receptors (GPCR) and P2X receptors are ligand-gated ion channels (LGIC), adapted from[24].

1.2.2.1 P1 receptors

Adenosine is the endogenous ligand of the P1 or adenosine receptors. Adenosine regulates various physiological processes. It acts as a (CNS) depressant and anticonvulsant. It is sleep promoting and has an antidiuretic effect. It leads to a negative inotropic and negative chronotropic effect to the heart muscle. It has immunosuppressive and anti-inflammatory properties and induces angiogenesis.[25] The stimulating effect of caffeine is based on the antagonism of adenosine receptors.[26] The A_1 and A_{2A} receptors have high and A_{2B} and A_3 receptors low affinity to adenosine.[27, 28] The xanthine derivative istradefylline is the first-in-class, non-dopaminergic, selective adenosine A_{2A} receptor antagonist and was approved in 2013 for the treatment of Parkinson's disease in combination with L-DOPA in Japan.[29] In addition, A_{2A} is further targeted by the regadenoson, an agonist which was approved by the FDA in 2008[30] as a coronary vasodilator and is used in cardiac imaging.[31] Several A_{2A} receptor antagonists are currently investigated in clinical trials. For example for cancer therapy Ciforadenant (CPI-444) is tested in combination with the anti-PD-L1 antibody atezolizumab for non-small cell lung and refractory renal cell cancer in phase I and NIR178 in combination with an anti-PD-1 antibody PDR001 in phase II for a variety of advanced malignancies.[32–35]

1.2.2.2 P2Y receptors

The main endogenous ligands for $P2Y_{1,11-13}$ receptors are adenine di- or triphosphates, $P2Y_{4,6,14}$ receptors are activated by uracil nucleotides and the $P2Y_2$ receptor can be stimulated by both ATP and UTP. The P2 receptor family is expressed in almost all tissues and it has been found that many P2Y receptors form homo- or hetero-oligomers, which influence their pharmacological properties. The receptors have manifold biological activities and are involved in the regulation of vasodilation, immune response and blood platelet aggregation.[36]The active metabolite of the antiplatelet medication clopidogrel is an irreversible allosteric inhibitor of $P2Y_{12}$, which was approved by the FDA in 1997[37] and reduces the adverse cardiovascular outcomes in patients with cardiovascular diseases.[38] Diquafosol, an agonist of $P2Y_2$ receptor was approved in Japan and other Asian countries as a treatment for dry eye disease.[23]

1.2.2.3   P2X receptors

In contrast to previously described receptors, which are all GPCRs, the P2X receptors are cation (Ca^{2+}, Na^+, K^+) channels gated by extracellular ATP. P2X receptors are expressed with different preference in almost every tissue and most subunits can form functional homomeric or heteromeric receptors. The receptors play key roles in inter alia afferent signaling, regulation of renal blood flow, vascular endothelium, and inflammation and are associated to rheumatoid arthritis, pain, and cough.[39–41] Due to the wide involvement of P2X receptors in physiology and pathophysiology, agonists and antagonists have been developed and were investigated. However, no medication that addresses any of the P2X receptors has been developed so far, but several P2X small molecule antagonists are currently in clinical trials.[42] Besides the receptors, important ectonucleotidases including ecto-5′-nucleotidase are involved in the purinergic signaling pathway, too. They will be discussed in the next chapter.

1.2.3 Ectonucleotidases

1.2.3.1 Overview

Besides receptors, an orchestra of ectonucleotidases is involved in the purinergic signaling pathways (Figure 3). These ectonucleotidases are a family of membrane-bound enzymes, which together hydrolyze extracellular nucleotides to the related nucleosides and inorganic phosphate. The ecto-nucleoside triphosphate/diphosphohydrolases (E-NTPDases) cleave nucleosidetriphosphates to di- and further to monophosphates, the nucleotide pyrophosphatase/phosphodiesterase (E-NPP) family hydrolyzes a broad spectrum of nucleotides to their related monophosphates, and the ecto-5′-nucleotidase (CD73, *e*N, NT5E, E5'-NT) hydrolyzes nucleosidemonophosphates to the related nucleoside.[43] In the following chapters the ectonucleotidases are described in more detail, whereby the main focus is on ecto-5′-nucleotidase.
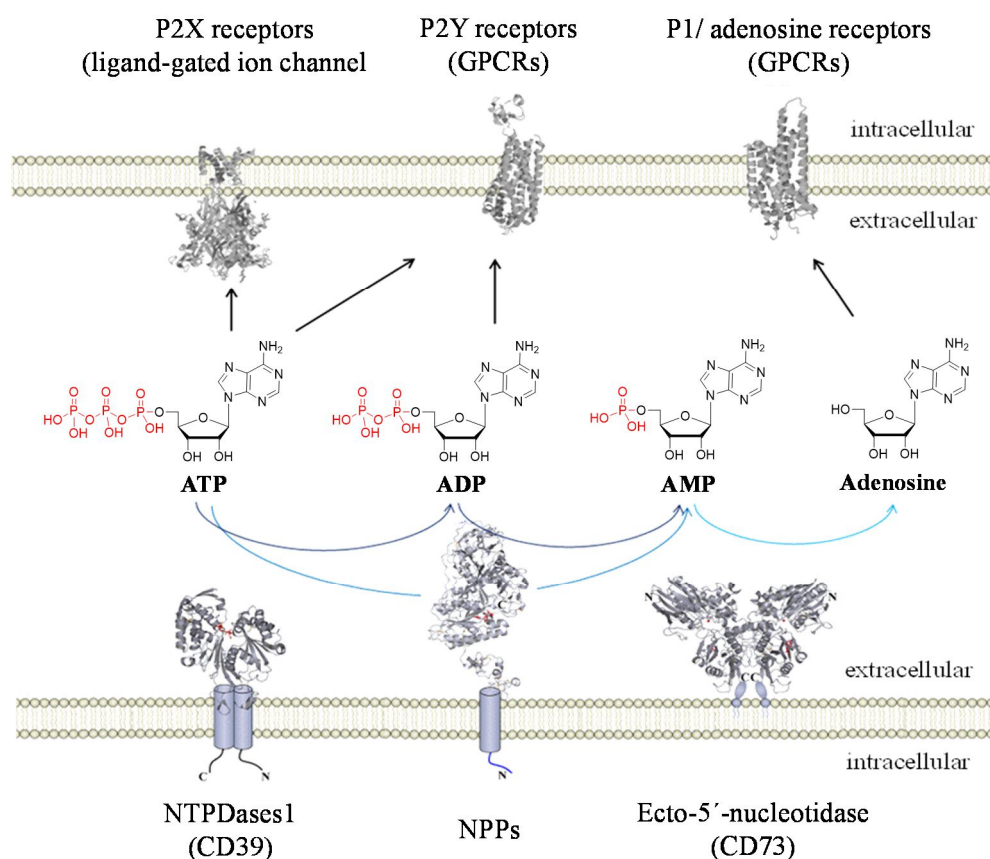
Figure 3. Ectonucleotidases in purinergic signaling. Ectonucleotidases hydrolyze extracellular nucleotides, here exemplarily shown for ATP via ADP and AMP to adenosine. ATP affects members of the P2X ligand-gated ion channels (LGICs) and together with ADP the activity of the G protein-coupled P2Y receptors. Formed adenosine activates adenosine receptors (P1); modified based on [24, 25, 44].

1.2.3.2 Ecto-nucleoside triphosphate/diphosphohydrolases

The family ecto-nucleoside triphosphate diphosphohydrolases hydrolyzes nucleoside tri- and diphosphates (NTPDases) to the related nucleoside monophosphates. Eight homologues were identified in humans (EC 3.6.1.5). NTPDase1, NTPDase2, NTPDase3, and NTPDase8 hydrolyze any kind of nucleoside tri/diphosphates, are N-glycosylated and located as monomers to tetramers at the cell surface with two transmembrane domains (TMDs). In contrast, for NTPDase4 to NTPDase7 the substrate spectrum is more limited and they are mainly localized in membranes of intracellular organelles. Therefore, they play a minor role for extracellular purinergic signaling. All enzymes require millimolar concentrations of Ca^{2+} or Mg^{2+} as cofactors and show highest activity in a pH range between 7 and 8. NTPDases have a wide tissue distribution, but are mostly expressed by specific cells, for example in epithelial cells. NTPDase1 is the most investigated homologue and is often abbreviated as CD39, especially in an immunological context. It is a leucocyte activation marker, and is expressed in many immune cells. Thus, it is critically involved in immune responses. As a drug target for cancer immunotherapy it is as promising as ecto-5′-nucleotidase.[45]

NTPDase1 further hydrolyzes prothrombototic ADP in vascular endothelium, and thus regulates fluidity and thrombosis. Since the NTPDases influence the purinergic signaling pathway at a very early stage by lowering ATP levels, producing a certain quantity of ADP/AMP or together with ecto-5′-nucleotidase producing adenosine, they affect physiological conditions by tuning P1 and P2 receptor activity. Examples are P2Y receptor-dependent vasorelaxation, P2Y receptor-mediated bile ductular proliferation in liver, vascular hemostasis, proliferation and immune responses. Until now no medication is targeting NTPDase1 or is in clinical trial, nevertheless knockout mice of NTPDase1 revealed a key role of this enzyme in thrombosis, in vascular permeability in angiogenesis, tumor growth and metastasis, which makes it interesting as a potential drug target.[43, 45] Furthermore, a therapeutic antibody (IPH52) and a sodium polyoxotungstate (POM1) as small molecules for cancer immunotherapy are promising tools or preclinical candidates.[46]

1.2.3.3 Nucleotide pyrophosphatase/phosphodiesterases

The family of ecto-nucleotide pyrophosphatase/phosphodiesterase (E-NPPs) belongs to the alkaline phosphatase (AP) superfamily and consists of seven members (NPP1-NPP7). These enzymes are located at the cell surface; they are either secreted or integrated into the cell membrane facing with their catalytic domain towards the extracellular space.[47] Among these, NPP1-4 are known to hydrolyze nucleotides, whereby NPP1 showed the highest activity hydrolyzing of ATP to AMP, and NPP2 has only weak nucleotide-metabolizing activity.[43, 48] NPP2 mainly hydrolyzes phospholipids and NPP5 cleaves nicotinamide adenine dinucleotide (NAD).[49] NPP6 and NPP7 (alkaline sphingomyelinase) only hydrolyze phospholipids. AMP or UMP are not hydrolyzed but exert competitive product inhibition of NPPs.[43]

NPP1–NPP3 have a wide tissue distribution and can be co-expressed. Like NTPDase, NPPs are often expressed in epithelia, for example in lung, liver, kidney and on intestinal epithelial surfaces. NPP6 is mainly expressed in brain, kidney and testis.[50] NPP1 and NPP3 are homodimeric membrane proteins and NPP2 is a secreted monomeric protein. The secreted NPP2 is found in body fluids including serum, seminal plasma and cerebrospinal fluid. Besides NPP2, soluble forms prepared by shedding of NPPs were also reported for NPP1, NPP3, NPP6, and NPP7.[43]

NPP1 is involved in the regulation of calcification. In addition, it is a marker for antibody-producing B cells. High expression of NPP1 has been found in astrocytic brain tumors,[51] and NPP1 is further associated with insulin resistance and type 2 diabetes. NPP2 is also involved in calcification and it has been further linked to promotion of cancer cell invasion, cell migration, lymphocyte trafficking, and angiogenesis. NPP3 has been shown to promote differentiation and invasion of glial cells, and NPP4 acts as a procoagulant enzyme on the surface of vascular endothelium.[43, 52] The physiological role of NPP6 is not completely clear.[43, 50]

NPP7 was found to be involved in inflammation and is associated with inflammatory bowel disease.[43] In general, NPPs influence the purinergic signaling pathway by hydrolyzing P2 receptor agonists, and together with ecto-5′-nucleotidase they produce adenosine. Thus, malfunction of these enzymes also affects those diseases that are primarily connected to purinergic receptors.[43, 48, 53] No medication currently targets NPPs, no small molecule, but an antibody–drug conjugates (AGS16F) targeting NPP3 for renal cell carcinoma is currently being evaluated in clinical trials phase II.[54, 55]

Introduction

1.3 Ecto-5′-nucleotidase

1.3.1 Ecto-5′-nucleotidase: structure, properties and characteristics

In the purinergic pathway ecto-5′-nucleotidase (CD73, eN, EC 3.1.3.5) is the final enzyme in the cascade of ectonucleotidases. The enzyme binds and requires Zn^{2+} as cofactor for catalytic activity. CD73 mainly hydrolyzes AMP to adenosine and inorganic phosphate. With lower turnover rates, it hydrolyzes further 5′-monophosphates (CMP, UMP, IMP, GMP), nicotinamide-mononucleotide to nicotinamide-riboside and NAD^+ to adenosine and/or nicotinamide ribosides.[43, 56] Bacterial ecto-5′-nucleotidase shows a broader substrate spectrum and also hydrolyzes ATP and ADP. These nucleotides bind to the vertebrate CD73 in a competitive manner. In contrast to the bacterial enzyme, however, they act as inhibitors of the reaction.[43] The enzyme ecto-5′-nucleotidase is encoded by the gene *NT5E* which is located on human chromosome 6q 14–21. The cDNA sequence encodes for a precursor of 574 amino acids of which 26 belong to an N-terminal signal peptide and further 25 hydrophobic amino acids are located at the C-terminal. Based on the cDNA sequence the molecular weight is 63 kDa, but purified proteins were identified with higher weights (68-72 kDa), probably due to the attachment of carbohydrates. Altogether five N-linked glycosylation sites were identified for CD73.[35] The mature form of CD73 lacks the signal peptide and the 25 hydrophobic amino acids,[57] thus contains 523 amino acids with a molecular weight of 61 kDa.[58] It is glycosylphosphatidylinositol (GPI)-anchored in the membrane facing the extracellular space and it is present as non-covalent homodimer (Figure 4).[35, 43, 59] Ser523 located at the C-terminal is the anchor attachment site for the GPI anchor.[57, 60]
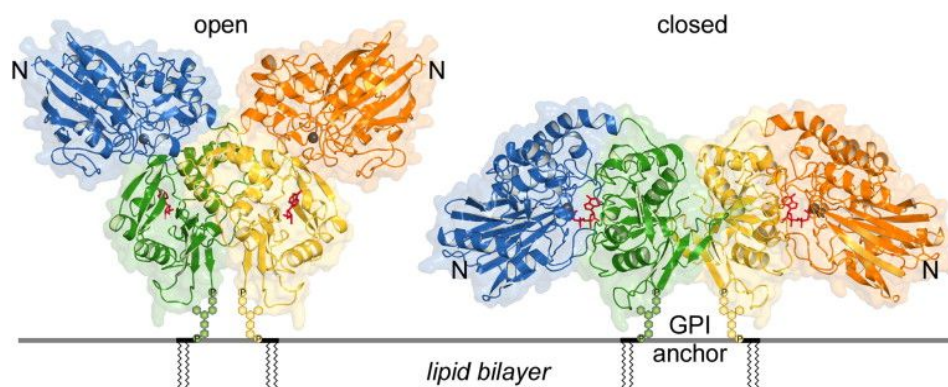
Figure 4. Homodimer of human CD73. The enzyme is connected with GPI-anchors to the plasma membrane. The catalytic domain is extracellularly located and consists of the N- and C-terminal domain, which undergo a conformational change after substrate binding from 'open' to 'closed'. (blue/orange: N-terminal domain; green/yellow: C-terminal domain: red: adenosine/AOPCP; PDB: 4H2G & 4H2I).[59]

Eight cysteine residues are present in the amino acid sequence of CD73 and all eight form intramolecular S-S bonds.[43, 59] The sequence of CD73 is highly conserved in multiple species.[35] Intracellular, so called cytosolic 5′-nucleotidases are structurally and phylogenetically not related to CD73.[43, 61] CD73 can be released by different mechanisms into tissues and body fluids like serum[62] and synovial fluid.[63] It can be released as a GPI-anchored variety via microvesicles or exosomes[64, 65] or it can be shedded by proteolytic degradation releasing a truncated variety of CD73. It was found that the activity of this soluble CD73 in bull seminal plasma was different from the membrane-bound variety.[66] Endogenous phospholipase C can cleave the GPI anchor and release CD73. In contrast to the truncated variety of CD73, the same catalytic activities were found for this variety compared to the membrane-bound one.[43, 67]

Several bacteria crystal structures of CD73 are available, and the human CD73 was crystallized in different conformations, with bound adenosine or the inhibitor AOPCP in the substrate binding pocket in 2012.[59] Each subunit of the CD73 dimer contains a C-terminal domain (residues: 337-549) where the substrate binding site is located, and a larger N-terminal domain (residues: 27-317), which contains the metal ion binding site. These domains are connected with a flexible α-helical hinge region, which enables two different conformations of the monomer. The substrate AMP binds to the C-terminal domain in the 'open' conformation, afterwards, the N-terminal domain rotates by 114° towards the 'closed' conformation (Figure 4). In this conformation two bounded metal ions and catalytically relevant amino acids of the N-terminal domain are in the right position for the hydrolytic reaction. Afterwards, the enzyme opens up again and releases the products.[43, 59] The co-crystallization of CD73 in a closed conformation with the inhibitor AOPCP (nucleotide derivatives as CD73 inhibitors are discussed more precisely in chapter 1.5.1, page 26) revealed that the inhibitor binds in the active site near the zinc ions, which are necessary for the hydrolysis of AMP to adenosine and phosphate (Figure 5A). The adenine base is stacked via π-stacking interactions between two phenylalanines (F417 and F500). R354, R395 and D506 form hydrogen bonds with the ribose, and the diphosphonate moiety interacts via hydrogen bonds with the amino acids N245, R354, R395, N117 and H118. H118 is highly conserved and it was shown that an exchange of H118 to alanine led to a complete loss of enzymatic activity.[68] In addition to these hydrogen bonds, the β-phosphonate group is coordinated to the zinc ions. The crystal structure of the binding site also shows that a large sub-pocket of about 210 Å^3 with bound water molecules is formed next to the C2 carbon

atom of the adenine moiety (Figure 5B), which might be interesting for the development of inhibitors.[59]
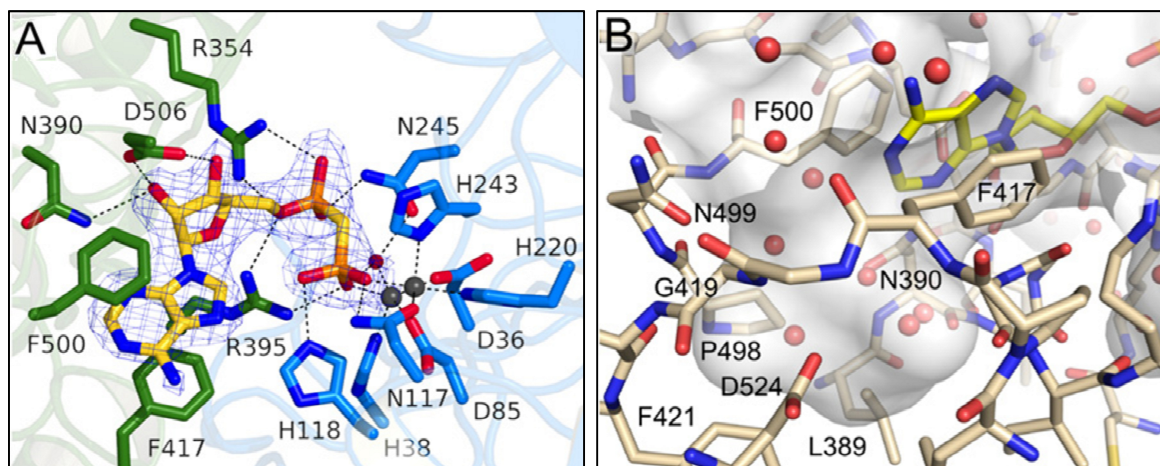
Figure 5. Binding site of CD73 with bound inhibitor AOPCP. (**A**) AOPCP within the binding site of CD73. Nucleobase and the ribose moiety mainly interact with amino acids from the C-terminal domain (colored in green) and with the diphosphonate with amino acids of the N-terminal domain (colored in blue) and the coordinated zinc ions (colored in gray). (**B**) A large sub-pocket with bound water molecules of about 210 Å^3 is formed next to the C2 atom of the adenine base.[59]

Ecto-5′-nucleotidase has a wide tissue distribution. Higher expression levels in healthy humans are found in T- and B-lymphocytes, macrophages, uterus, placenta, thyroid, cardiomyocytes, smooth muscle cells and in bronchial epithelia cells.[43, 69, 70] CD73 is involved in many physiological processes. The majority of the processes are related to the production of adenosine, which leads to signaling via P1 receptors. It was found that CD73 due the production of adenosine protects tissues and organs from ischemia-reperfusion (IR) injury. These injuries occur when after ischemia the blood supply is restored which is the case in many serious diseases like e.g. myocardial infarctions and strokes, after surgeries or organ transplants after transplantation. It was found that in a renal IR injury model that CD73 knockout mice have more injuries and vascular permeability than wild-type mice and that the effect can be restored by the addition of adenosine to CD73 knockout mice.[71, 72]

CD73 has a checkpoint function in immunity and inflammation by producing immunosuppressive adenosine and lowering together with CD39 proinflammatory ATP/ADP. Hereby, it regulates endothelial barrier functions during inflammation, leukocyte trafficking and is involved in the progression of inflammatory bowel disease (IBD).[72] The

effect of adenosine towards the regulation of immune cells and anticancer immune response is highlighted in the following chapter.

1.3.2 Ecto-5′-nucleotidase as potential target for cancer immunotherapy

In the previous chapter we already got to know the actuators of the purinergic signaling pathway and their different physiological and pathophysiological properties. Focusing on the anti-cancer immune response, the balance between the extracellular signal molecule ATP and adenosine are of great importance. ATP as an extracellular signal molecule acts as a proinflammatory danger signal and leads to the activation of immune cells by activating P2X and P2Y purine receptors. In contrast, adenosine acts as immunosuppressive signal molecule by activating adenosine receptors. The ectonucleotidases, especially CD39 and CD73 together balance the concentration of these signaling molecules. In many cancers the expression of the ectonucleotidases is upregulated leading to high concentrations of adenosine in the tumor microenvironment.[73] Especially CD39 and CD73 are upregulated in solid tumors under hypoxic conditions. Here, the induction of hypoxia inducible factor (HIF) modulates among others the expression of CD73 in the tumor area.[74] Adenosine leads to multiple effects on immune cells which are illustrated in Figure 6. Thus, overproduction of adenosine by CD73 suppresses antitumor immune responses and is associated with proliferation, angiogenesis, and metastasis.[35, 75, 76]
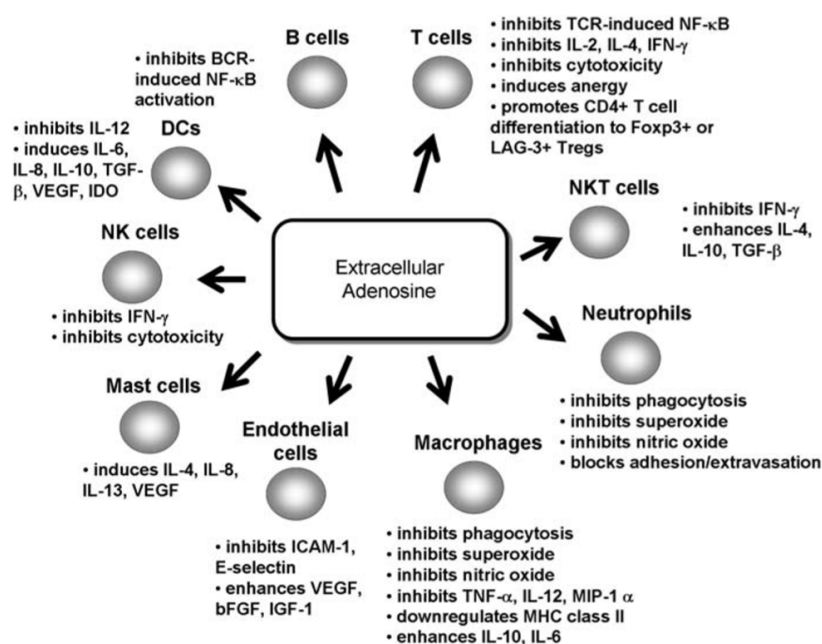
Figure 6. Extracellular adenosine and its immunosuppressive properties. Taken from[73].

Introduction

In many studies the expression of CD73 in cancer patients has been used as a prognostic marker for the progression of the disease.[77] In breast cancer, the overexpression of CD73 correlates with disease progression and poor prognosis. Furthermore, it is associated with the pro-metastatic potential of breast cancer and melanoma.[75] Triple-negative breast cancer (TNBC), one of the most aggressive tumors, refers to breast cancer that lack the expression of the estrogen receptor (ER), progesterone receptor (PR) and human epidermal growth factor receptor 2 (HER2/neu).[78] Estrogen suppresses the expression of CD73 and in a study of 122 patients with TNBC it was shown that the patients with high levels of CD73 expression and low levels of tumor-infiltrating leukocytes had the worst clinical outcome.[79] Furthermore, mice with CD73 knockout have an increased antitumor immunity and are resistant to experimental metastasis.[80] In addition, it seems that not only the catalytic properties of CD73 in generating immunosuppressive adenosine are connected with cancer progression. Results from experiments on severe combined immunodeficiency (SCID) mice revealed that CD73 expression has also a pro-metastatic effect which is mainly related to CD73 as adhesion molecule.[81, 82] To conclude, it seems that CD73 is a key checkpoint in tumor growth, angiogenesis and metastasis, indicating the potential of CD73 as a drug target for cancer immunotherapy. Until now, no medication is addressing CD73 as a target for cancer immunotherapy, but antibodies or small molecules have been developed that inhibit CD73 in animal tumor model. The blockage of CD73 using the small molecule inhibitor AOPCP was related to tumor regression, T-cell response and increased survival in a mouse xenograft model of ovarian cancer.[35, 83, 84] A derivative of AOPCP is about to enter clinical trial phase I[85] (for more details of nucleotide derivatives as CD73 inhibitors see chapter: 1.5.1, page 26). Moreover, antibodies against CD73 activity or CD73 as adhesion molecule were developed and it was shown that the anti-CD73 mAbs TY/23 and AD2 led to reduced tumor growth and metastasis in mice. [81, 86] Interestingly, the mode of action of the AD2 antibody is independent from inhibiting the catalytic activity of the enzyme. In contrast, the antibody induces the internalization of CD73.[86] The antibody MEDI9447 (Oleclumab) targets CD73 and is now in clinical trial phase II for cure of triple-negative breast cancer and metastatic pancreatic ductal adenocarcinoma.[35, 87, 88] Outcomes of these studies will illuminate whether CD73 will be a validated target for cancer immunotherapy.

1.4 Enzyme kinetics

In this chapter basic concepts about enzyme kinetics, mode of inhibition and the potency of inhibitors are described. Unless otherwise stated, the origin of this information are the English and German editions of the textbook "Biochemistry".[89, 90]

1.4.1 Michaelis-Menten kinetics and Lineweaver-Burk plot

Enzymes are biocatalysts which drive the adjustment of a chemical equilibrium by decreasing the activation energy of the reaction. Enzyme (E) and substrate react to the enzyme-substrate complex [ES] with the rate k_1 and the reverse reaction whereby the enzyme-substrate complex decays to the substrate and enzyme with k_{-1}. Product formation and release of product (P) and the enzyme are further described by the rate constant k_2 and the reverse reaction k_{-2}. At the beginning of a reaction when the product concentration is low, the reverse reaction does not take place (k_{-2} [P] $\approx$ 0) and the reaction equation can be simplified:

$$E + S \underset{k_{-1}}{\overset{k_1}{\rightleftharpoons}} ES \xrightarrow{k_2} E + P \tag{1}$$
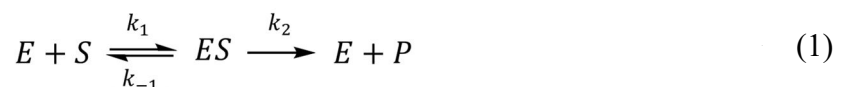
Under the assumption that the substrate concentration is manifold than the concentration of the enzyme what is always the case with enzyme reactions, then the velocity (v) of product formation only depends on the concentration of the formed ES-complex and the rate constant k_2:

$$v = \frac{d\,[P]}{dt} = k_2[ES] \tag{2}$$

The formation of the ES-complex depends on the concentration of enzyme, substrate and the rate constant k_1. At the same time, the concentration is lowered by the reverse reaction and formation of the product. Thus, the concentration of the ES-complex is described as follows:

$$\frac{d\,[ES]}{dt} = k_1[E][S] - k_{-1}[ES] - k_2[ES] \tag{3}$$

The equation cannot be integrated, but it is possible to simplify the equation with different assumptions. Here, we concentrate on the simplest and most common option which is the assumption of the steady-state proposed in 1925 by George Briggs and John Haldane. Mixing the enzyme with the substrate, which is in great excess over the enzyme, leads

imminently (within milliseconds) to the formation of the ES-complex. After this transition phase the concentration of the ES-complex is constant during the enzymatic reaction till the depletion of the substrate at the end of the reaction. Thus, $d[ES]/dt = 0$, which simplifies and allows to rearrange the equation (3) as follows:

$$\frac{[E][S]}{[ES]} = \frac{k_{-1} + k_2}{k_1} \tag{4}$$

The term on the right hand side describes kinetic properties of the enzyme which are independent of both the enzyme and the substrate concentration. This term is described with the Michaelis-constant K_M:

$$K_M = \frac{k_{-1} + k_2}{k_1} \tag{5}$$

Introducing the K_M value into equation (3) and rearrangement:

$$[ES] = \frac{[E][S]}{K_M} \tag{6}$$

In order to generate values which can be determined in experiments further assumption are necessary. The ES-complex and the free enzyme (E) are not measurable, but the sum of them is the total amount of enzyme within the reaction and this value is determined by the protein concentration ($[E]_T = [E] + [ES]$). Rearranging the equation to ($[E] = [E]_T - [ES]$) and substitution of [E] in equation (6):

$$[ES] = \frac{([E]_T - [ES])\,[S]}{K_M} \tag{7}$$

This allows to combine ES elements and after rearmament the following equation is obtained:

$$[ES] = [E]_T \frac{[S]}{[S] + K_M} \tag{8}$$

Introducing this equation into the equation (2) for the catalysis velocity it results:

$$v_o = k_2[E]_T \frac{[S]}{[S] + K_M} \tag{9}$$

The maximal velocity is reached when all catalytic binding sites of the enzyme are saturated ($[ES] = [E]_T$):

18

$$V_{max} = k_2[E]_T \tag{10}$$

Inserting it into equation (9), the Michaelis-Menten equation is obtained. Now, the velocity can be calculated by known parameters like enzyme and substrate concentration and by parameters like V_{max} and K_M which can be both determined by experimental procedures.

$$v_0 = V_{max}\frac{[S]}{[S]+K_M} \tag{11}$$

If the substrate concentration is much lower than the K_M value than the enzyme reaction is first-order reaction ($V_0 = (V_{max}/K_M)[S]$) and the velocity is proportional to the substrate concentration. At high concentration, when [S] is much higher than K_M the velocity is described as a zero-order reaction ($V_0 = V_{max}$) described by a saturation of the velocity (Figure 7).
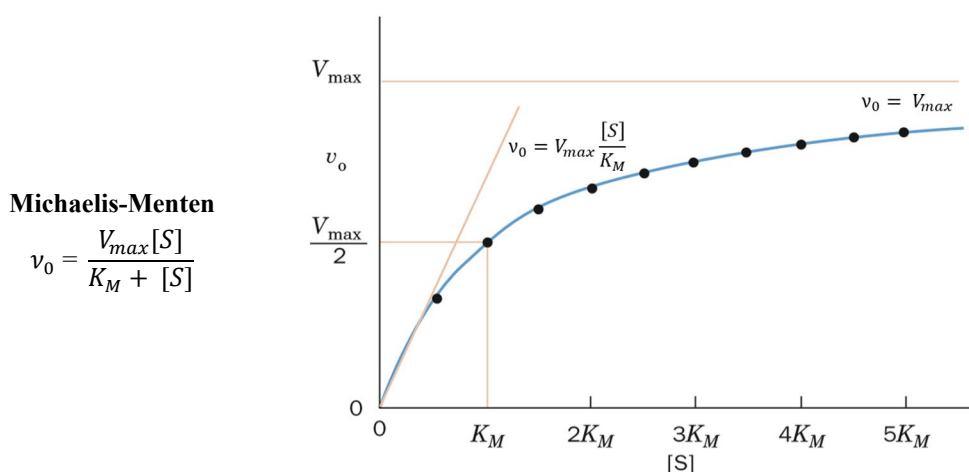
Figure 7. Michaelis-Menten kinetics. Plotting the Michaelis-Menten kinetics leads to a saturation function, whereby the velocity at low substrate concentrations is linear and described by the term $v_0 = (V_{max}/K_M)[S]$. At high concentration the velocity is characterized by an increasing saturation and approaches $v_0 = V_{max}$; modified based on [90].

The K_M value is the substrate concentration at half of V_{max}. Thus, it further describes the binding affinity of enzyme and substrate. A low K_M value describes a high affinity of the substrate to the enzyme binding site. As already mentioned, this value is theoretically constant. However, buffer conditions, pH value and temperature also influence the binding of the substrate to the enzyme. Thus, literature values slightly differ under chosen assay and reaction conditions. In contrast, the V_{max} value depends directly on the enzyme concentration

and further to a much greater extent than the K_M value on the reaction conditions. To determine the kinetic parameters (V_{max} and K_M) experiments with different substrate concentrations (Michaelis-Menten kinetics, Figure 7) are conducted and plotted. Graphical determinations of the values are prone to errors, because of the asymptotic approximation of V_{max}. To circumvent this problem, the kinetic curve is linearized by using the reciprocal values of both, the substrate concentration and the measured values. These values are then plotted in a double-reciprocal plot also named after its inventors Lineweaver-Burk plot (Figure 8). In this plot the intercept with the y-axis corresponds to the reciprocal value of V_{max}, and the intercept with the x-axis corresponds to the reciprocal value of K_M.
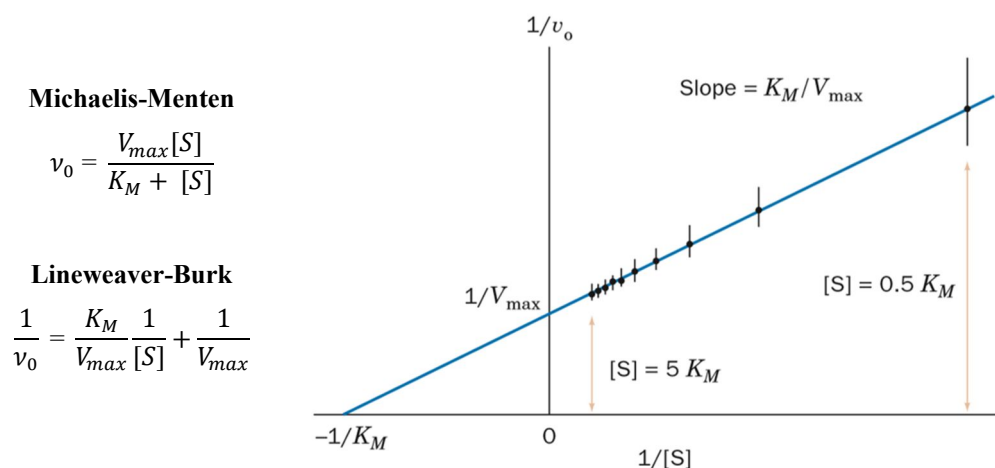
Figure 8. Lineweaver-Burk plot. Linearization of Michaelis-Menten kinetic enables the graphical determination of K_M (x-axis intercept: $-1/K_M$) and V_{max} value (y-axis intercept: $1/V_{max}$), adapted from[90].

A drawback of the Lineweaver-Burk plot is that measurement values for low substrate concentration, which usually have high data variability, influence the linear fit the most (Figure 8). Nowadays, software can perform nonlinear fits, and the K_M and V_{max} values can directly be determined from the Michaelis-Menten kinetics. Nevertheless, the Lineweaver-Burl-plot is a very useful tool for the illustration of the mode of inhibition, which is described in the following paragraph. However, it is recommended to create the Lineweaver–Burk plot with calculated values of the non-linear fit of the Michaelis–Menten kinetic (slope: K_m/V_{max} and x-axis intercept: $-1/K_m$).[91]

1.4.2 Enzyme inhibition

Enzyme inhibitors reduce the product formation of an enzymatically catalyzed reaction. Based on the mode of inhibition, they are divided into the three classes: competitive, uncompetitive and mixed inhibition (often described as non-competitive). In the following chapters, these three types are discussed. Figure 9 gives an overview of these three inhibitors and at which point they interfere with the enzyme.

$$E + S \xrightleftharpoons[k_{-1}]{k_1} ES \xrightarrow{k_2} E + P$$

$$K_I = \frac{[E][I]}{[EI]} \qquad K_I \qquad K'_I \qquad K'_I = \frac{[ES][I]}{[ESI]}$$

$$EI \qquad ESI$$

competitive   uncompetitive
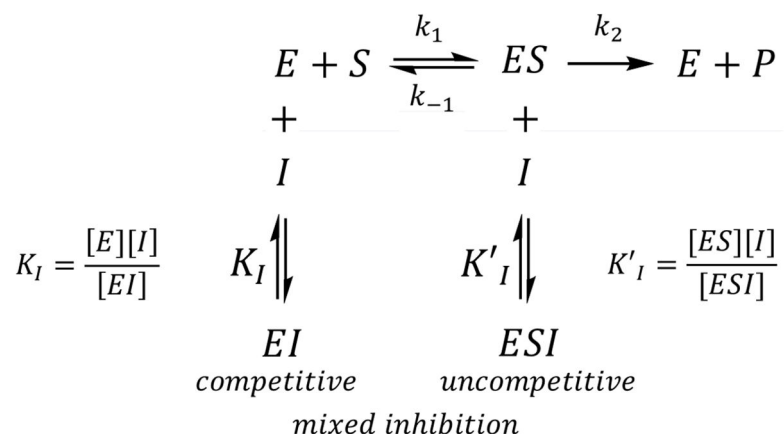
mixed inhibition

Figure 9. Modes of enzyme inhibition. Inhibitors are classified by the mode of inhibition into: competitive, uncompetitive and mixed inhibition (non-competitive), modified based on[89, 90].

1.4.2.1 Competitive inhibition

If an inhibitor binds to the active site, it competes with the substrate for the binding site of the enzyme. Thus, it is a competitive inhibitor. Here, the product formation is reduced, because higher concentrations of the substrate are necessary to produce the same concentrations of the ES-complex compared to a not inhibited reaction. This leads in the Michaelis-Menten kinetics at a fixed inhibitor concentration to an increased K_M value. If the substrate concentration is much higher than the inhibitor concentration (($[S] >>> [I]$), the binding equilibrium of inhibitor and substrate will be shifted to the substrate and V_{max} values will be recorded as for a non-inhibited reaction. The K_I (also K_i) value describes the binding equilibrium between the inhibitor and the enzyme. After including the K_I into the Michaelis-Menten equation, after simplification and the defining of α as:

$$\alpha = \left(1 + \frac{[I]}{K_I}\right) \tag{12}$$

the Michaelis-Menten and Lineweaver-Burke equations are altered as described in Figure 10. It is obvious as discussed above that α only has an influence on the K_M value and

not on the V_{max} value which can be observed very well in the Lineweaver-Burk plot (Figure 10).

<div style="text-align:center">

Type of inhibition
competitive

Michaelis-Menten
$$v_0 = \frac{V_{max}[S]}{\alpha K_M + [S]}$$

Lineweaver-Burk
$$\frac{1}{v_0} = \frac{\alpha K_M}{V_{max}}\frac{1}{[S]} + \frac{1}{V_{max}}$$

Effect of Inhibitors
increase of K_M

</div>
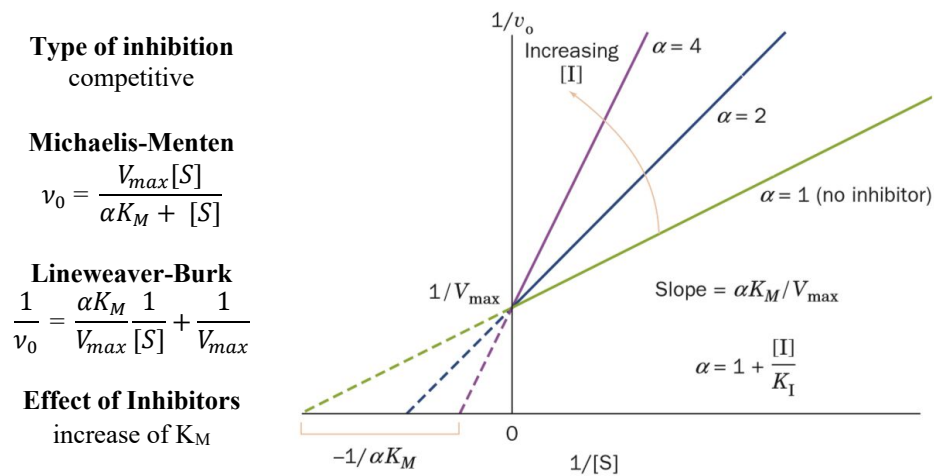
Figure 10. Kinetic characteristics of a competitive inhibitor. Lineweaver-Burk plot for different concentrations of a competitive inhibitor consists of lines with different slopes ($\alpha K_M/V_{max}$), the same intercept of the y-axis, and different intercepts of the –axis at $-1/\alpha K_M$.

1.4.2.2   Uncompetitive inhibition

If an inhibitor binds to the ES-complex and not to the free enzyme, it is called uncompetitive inhibitor (Figure 9). The binding of the inhibitor will influence the active site or the enzyme in a way that the catalysis is decreased. In contrast to competitive inhibition, V_{max} is lowered also at high substrate concentrations. In addition, this kind of inhibition is not observed when the substrate concentration is very low ($[K_M]>>>[S]$). Thus, the K_M value is also lowered. Including the equilibrium of the inhibitor and the ES-complex described by K'$_I$ into the Michaelis-Menten equation and defining a α' analogous to the competitive inhibitors:

$$\alpha' = \left(1 + \frac{[I]}{K'_I}\right) \tag{13}$$

the Michaelis-Menten and Lineweaver-Burke equations are altered as described in Figure 11.

Type of inhibition
uncompetitive

Michaelis-Menten
$$\nu_0 = \frac{V_{max}[S]}{K_M + \alpha'[S]}$$

Lineweaver-Burk
$$\frac{1}{\nu_0} = \frac{K_M}{V_{max}}\frac{1}{[S]} + \frac{\alpha'}{V_{max}}$$

Effect of Inhibitors
increase of K_M and
decrease of V_{max}
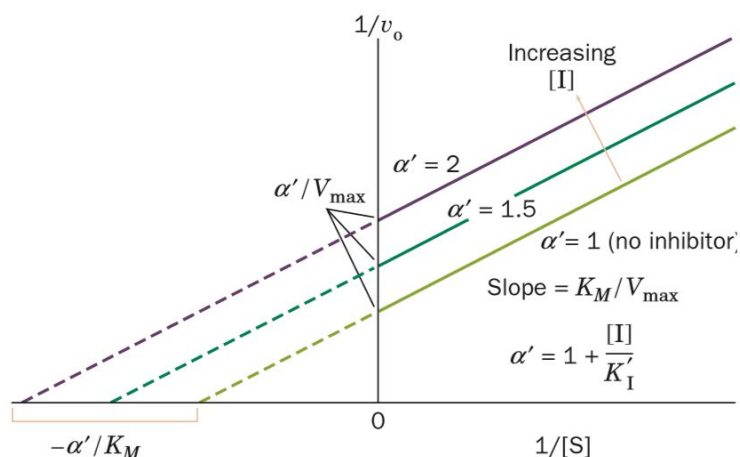
Figure 11. Kinetic characteristics of an uncompetitive inhibitor. Lineweaver-Burk plot for different concentrations of an uncompetitive inhibitor consists of a family of parallel lines with the same slope (K_M/V_{max}) and intercepts of the y- and x-axis at α'/V_{max} and $-\alpha'/V_{max}/K_M$, respectively, modified based on[90].

1.4.2.3 Mixed inhibition (non-competitive)

Most inhibitors bind to the free enzyme and to the ES-complex and lower the catalytic properties of the enzyme. Thus, both K_I and K'_I need to be considered and both terms α and α' can be found in the Michaelis-Menten equation (Figure 12). Since, this type of inhibition has the characteristics of both competitive and uncompetitive inhibition, it is referred to as mixed inhibition.

Type of inhibition
Mixed inhibition/non-
competitive

Michaelis-Menten
$$\nu_0 = \frac{V_{max}[S]}{\alpha K_M + \alpha'[S]}$$

Lineweaver-Burk
$$\frac{1}{\nu_0} = \frac{\alpha K_M}{V_{max}}\frac{1}{[S]} + \frac{\alpha'}{V_{max}}$$

Effect of Inhibitors
increase of V_{max}; K_M can
be in- or decreased
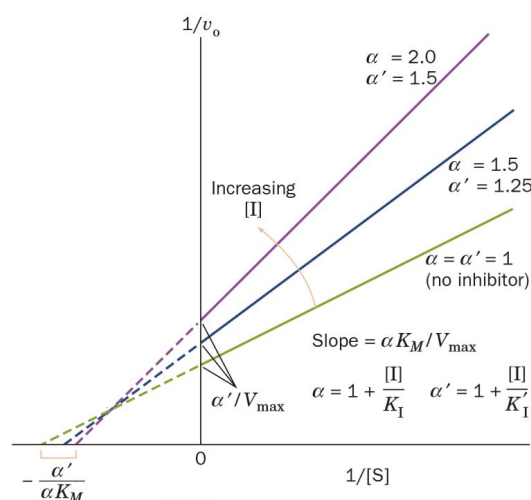
Figure 12. Kinetic characteristics of a mixed inhibition. Lineweaver-Burk plot for different concentrations of an inhibitor which shows mixed inhibition properties. The slope is described by $\alpha K_M/V_{max}$ like for competitive inhibition, the intercept with the y-axis results in the V_{max} value described with the term $-\alpha'/V_{max}$, like in uncompetitive inhibition mode and the intercept of all lines lays in quadrant II of the coordinated system. If this intercept additionally lays on the x-axis than $\alpha = \alpha'$, which represents a classical non-competitive mode of inhibition, modified based on.[90]

23

In the Lineweaver-Burk plot, the V_{max} value is described at the y-axis intercept with α'/V_{max} like for an uncompetitive inhibition and the slope with $\alpha K_M/V_{max}$ like for a competitive inhibition. Depending on the values of α and α' and thus of K_I and K'_I the K_M value increases (competitive) or decreases (uncompetitive) with increasing inhibitor concentrations. If the affinity of the enzyme and of the ES-complex to the inhibitor are the same ($K_I = K'_I$) then the K_M value is independent of the presence or concentration of the inhibitor. All lines will intercept on the x-axis at the same point. This special case of a mixed inhibition is a classical non-competitive inhibition.

1.4.3 Potency of inhibitors

For the development of enzyme inhibitors, it is important to determine the potency of inhibitors in order to elucidate the structure-activity relationship. The potency of inhibitors is often described by using the value of the half-maximal inhibitory concentration (IC_{50}) as already mentioned. The IC_{50} value is the concentration of an inhibitor at which the activity of the enzymatic reaction is reduced by 50%. This value can be determined experimentally with a concentration-response curve. Here, the enzymatic activity is measured at constant substrate, but different inhibitor concentrations. The measured values are normalized, plotted against the logarithm of the inhibitor concentrations, a sigmoidal curve is fitted and the IC_{50} is read out or computer calculated.

Considering the kinetics discussed above, it can be seen that the IC_{50} value of competitive inhibitors depends on the concentration of the substrate. For the comparison of inhibitors, whose IC_{50} value was determined at different substrate concentrations, the IC_{50} is therefore an inaccurate comparison parameter. In contrast, the K_i value is independent of the substrate concentration and thus, is more suitable. The K_i value can be calculated from the kinetics described above. The experimental effort for the analysis of an inhibitor, on the contrary, is considerably greater than the experimental determination of the IC_{50} value. If, however, the K_M value of the enzyme in the same assay and under the same assay conditions is known, the Cheng-Prusoff equation can be used to convert the IC_{50} into the K_i value.[92]

$$K_i = \frac{IC_{50}}{1 + \frac{[S]}{K_M}} \tag{14}$$

In the following chapter different CD73 inhibitors are discussed. If possible, the K_i value instead of the IC_{50} is given. However, there are also inhibitors, which probably competitively bind to the target, but in the corresponding literature IC_{50} values are given. A useful consideration is that based on the Cheng-Prusoff equation, the K_i value can never be greater than the IC_{50} value.

1.5 State of the art CD73 inhibitors

1.5.1 Nucleotides as CD73 inhibitors

Endogenous inhibitors for CD73 are ATP and ADP (Figure 13A and B). Both inhibit rat CD73 in the low µM range with K_i values of 8.9 and 3.4 µM, respectively.[93] *In vivo*, this so-called feed forward inhibition leads to the effect, that first ATP and ADP are hydrolyzed by CD39 and NPPs to AMP, which is then further metabolized by CD73 to adenosine. The drawback of these types of inhibitors is their instability, because they can get metabolized by CD39 and NPPs.[43] The exchange of the diphosphate group of ADP to a non-hydrolyzable diphosphonate group led to the inhibitor α,β-methylene-ADP (AOPCP, AMPCP, APCP) with increased stability in human blood plasma (Bhattarai *et al.*, unpublished) and increased potency with K_i values of about 197 nM in recombinantly produced soluble rat CD73, 88.4 nM in recombinantly produced soluble human CD73 and with 487 nM less potent in human serum (Figure 13C).[94]

ATP
K_i rat sCD73: 8900 nM[93]

ADP
K_i rat sCD73: 3380 nM[93]

AOPCP
K_i rat sCD73: 197 nM[94]
K_i human sCD73: 88.4 nM[94]
K_i human serum: 487 nM[94]
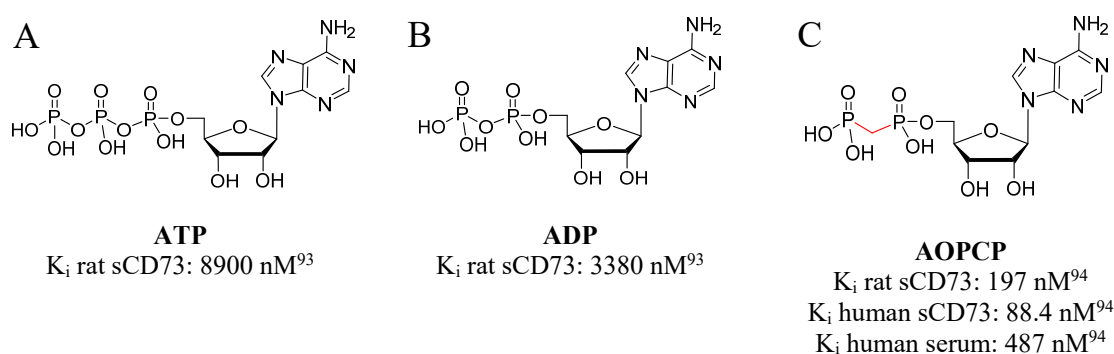
Figure 13. Nucleotide inhibitors of ecto-5′-nucleotidase (I). ATP **(A)** and ADP **(B)** are endogenous and unstable inhibitors of CD73. **(C)** The replacement of the oxygen of the pyrophosphate of ADP to a carbon atom (labeled in red) led to α,β-methylene-ADP (AOPCP) a more potent and stable CD73 inhibitor.

AOPCP was first synthesized by Myers *et al.* in 1965[95] and was firstly mentioned as ecto-5′-nucleotidase inhibitor in 1970 by Burger and Lowenstein.[96] From then on, it was used as a tool compound for studying CD73 *in vitro* and *in vivo*. In contrast to its plasma stability, the stability of AOPCP in human liver microsomes was as low as for ADP. (Bhattarai *et al.*, unpublished). In addition, *in vivo* data on the metabolism of AOPCP, which was investigated in BALB/c mice, showed that the blood concentration of AOPCP dropped rapidly from 38.6 to 6.4 μM within 60 minutes.[97] A further drawback of AOPCP is that one of its hydrolysis product may be adenosine which activates P1 receptors.

A

PSB-12379
K_i rat sCD73: 9.03 nM[94]
K_i human sCD73: 2.21 nM[94]
K_i human serum: 18.8 nM[94]

B

PSB-12489
K_i rat CD73: 0.746 nM
(Bhattarai *et al.*, unpublished)
K_i human sCD73: 0.318 nM
(Bhattarai *et al.*, unpublished)

C

AB680
IC_{50} human sCD73: 0.043 nM[98]
IC_{50} human CD73-CHO: 0.070 nM[98]
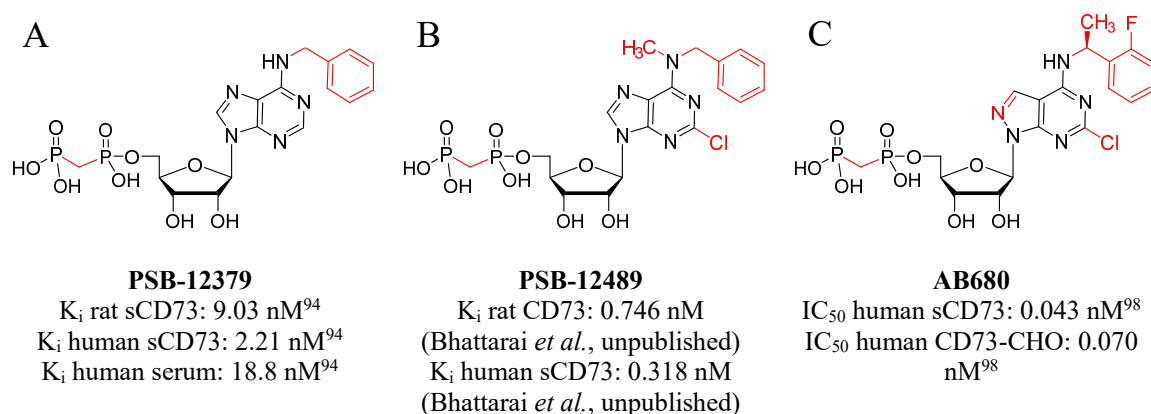
Figure 14. Nucleotide inhibitors of ecto-5′-nucleotidase (II). (A) Benzyl substitution of AOPCP at the N^6-position (PSB-12379) increased the potency and the stability in human plasma and liver microsomes. **(B)** Further methyl substitution at N^6 and 2-chloro substitution increased potency further. **(C)** AB680 an inhibitor from the company Arcus Biosciences Inc..

50 years after the first synthesis of AOPCP, its structure was further optimized to increase potency, stability and selectivity. For this purpose, modifications of the adenine moiety were investigated in 2015 in our group by Bhattarai *et al.*.[94] It turned out that substitution of N^6 of adenine is favorable and many inhibitors were synthesized in this study, which were measured with potencies in the low nM range at rat and human CD73. N^6-benzyl substitution yielded one of the most potent compounds (PSB-12379, Figure 14A). In addition to its high potency of 2.21 nM versus human soluble CD73, it was characterized by high stability in human plasma and in human liver microsomes.[94] Co-crystallization of PSB-12379 with human CD73 revealed a comparable binding behavior as described for AOPCP (see chapter 1.3.1, page 12). Just the amino acid N186 was shifted to provide space for the N^6-benzyl substituent, which further interacts with the carbon atoms of the amino acids D121, S185 and N186 (Figure 15A).

Introduction

Data from crystallography studies suggested that the benzyl group has a high flexibility within the binding site. Further N^6-methylation was beneficial (Figure 14B). In addition, the C2-position was chlorinated targeting a sub-pocket which was observed in the crystal structure of BSB-12379. The combination of these further beneficial modification led to the inhibitor PSB-12489 which displayed subnormal potencies for rat and human CD73 (Figure 14B). Co-crystallization of PSB-12489 with human CD73 showed that the chlorine forms a hydrogen bond with the N390 side chain and a water molecule coordinated to CO^{N499} is also in hydrogen bonding distance (Figure 15B). Based on these finding the inhibitor AB680 (Figure 14C) was developed by the company Arcus Biosciences Inc. which will be investigated in clinical trial phase I[85] (Bhattarai *et al.*, unpublished).
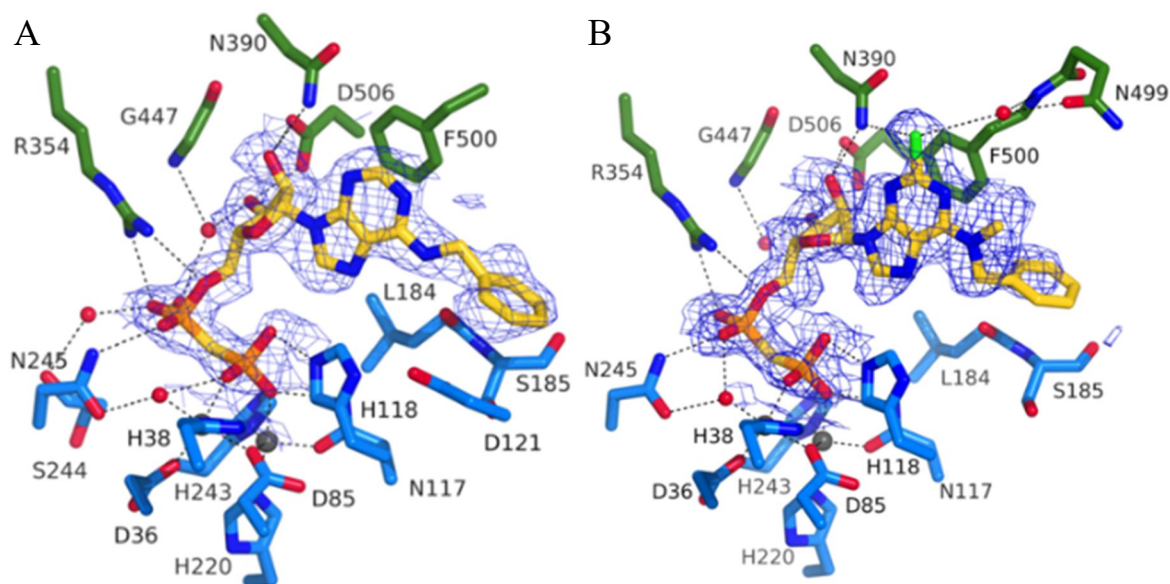
Figure 15. Co-crystal structures of AOPCP analogs with human CD73. PSB-12379 **(A)** and PSB-12489 **(B)** within the substrate binding site of human CD73 (yellow: AOPCP derivatives; blue: amino acid formed by the N-terminal domain; green: amino acids of the C-terminal domain; Bhattarai *et al.*, unpublished).

Besides the discussed structures, further structures derived from AOPCP and nucleotide mimetics were synthesized and evaluated as CD73 inhibitors. Clofarabine, a purine nucleoside antimetabolite for the treatment of acute myeloid leukemia (AML)[99] was compiled with the diphosphonate group of AOPCP ("Clofarabine"PCP, Figure 16A). This compound inhibited recombinant soluble CD73 with an IC50 of 180 nM and the membrane-bound variety using MDA-MB-231 breast cancer cells and NCI-H292 mucoepidermoid pulmonary carcinoma cells with IC50 values of 3200 and 240 nM, respectively.[100] Nucleotide mimetics like 5,6-dihydrouracil with 5′-terminal dicarboxylic acids, uridine and adenosine

derivatives with 5′-terminal phosphoric acids or phosphoric acids ester were investigated in capillary electrophoresis assay using recombinant soluble rat CD73.[101] Overall, compounds showed a moderate inhibition of CD73 in the low μM range. Interestingly, the potency depends on the pH value. The 5,6-dihydrouracil derivative with a 5′-terminal dicarboxylic acids showed the highest potencies (Figure 16B) with a K_i value of 11.5 μM at a pH of 7.4, but was less potent with a K_i value of 72.5 μM at pH of 5.6. Terminal phosphoric acids or phosphoric acid esters were less potent or inactive, but the combination of adenine derivatives with the favored 5′-terminal dicarboxylic acids, which probably would be more potent, have not been investigated.[101, 102]

A

B

("Clofarabine"PCP)
K_i human sCD73: 180 nM[100]
IC_{50} human CD73-MDA-MB-231: 3200 nM[100]
IC_{50} human CD73-NCI-231: 240 nM[100]

AMB566.1
K_i rat sCD73 (pH 7.4): 11.5 μM[101]
K_i rat sCD73 (pH 5.6): 72.5 μM[101]
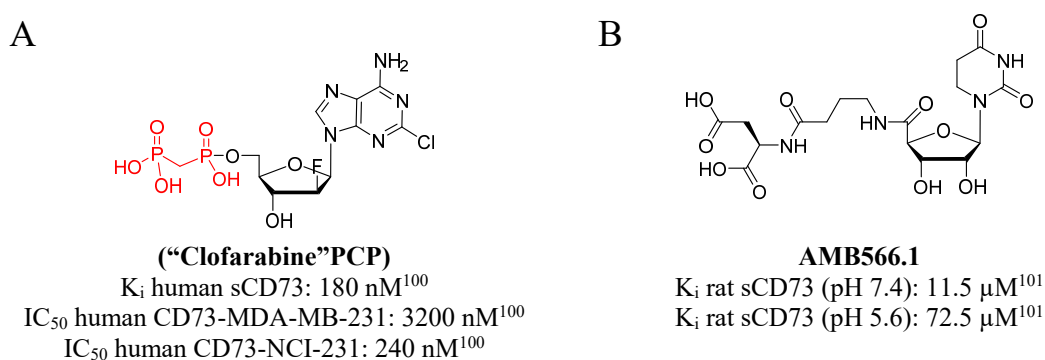
Figure 16. Nucleotide analogs as inhibitors of ecto-5′-nucleotidase. (A) A combination of the anticancer drug Clofarabine (black) and the diphosphonate of AOPCP (red) as inhibitor of CD73. **(B)** The 5,6-dihydrouracil connected to the 5′-terminal dicarboxylic acids by D-aspartic acid as a nucleotide mimetic CD73 inhibitor.

In 2015, the company Vitae Pharmaceuticals Inc. patented a variety of nucleotides and nucleotide mimetic structures as CD73 inhibitors. Within this patent they showed the synthesis of about 150 exemplary compounds and their biological evaluation in two different assays. The majority of these structures has differently substituted adenines as a base, the ribose is usually untouched and at the 5′-position different substituents like carboxylic acids or esters, monophosphonates and amides or combinations were inserted as bioisosteric replacement of the pyrophosphate or diphosphonate depending on whether ADP or AOPCP was used as a lead structure (exemplary structures are shown in Figure 17). 39 of these compounds inhibited CD73 with an IC_{50} value of 100 nM or below in both assays.[103] Interestingly, the compounds were measured against CMP as substrate instead of AMP. The K_M value of CMP is several times higher than the K_M value of AMP.[104] Therefore, higher substrate concentrations can be employed, which one the on hand increase the sensitivity of

the used malachite green assay, on the other hand inhibitors are measured with a lower IC_{50} than it would have been with AMP. Thus, their potency is overrated and it makes it difficult to compare them to inhibitors analyzed with AMP as substrate. However, in the patent the IC_{50} value for AOPCP is reported to be 12-25 nM.[103] Hence, it can be estimated that the compounds are about 8-16 times less potent than IC_{50} measured with AMP as a substrate. However, since only inhibition ranges are given, it is not possible to calculate what this would actually mean for the IC_{50} values.

A

B

C

Example 61

Example 88
IC_{50} human sCD73: ≤ 100 nM
IC_{50} human U138 glioma cells: ≤ 100 nM

Example 98
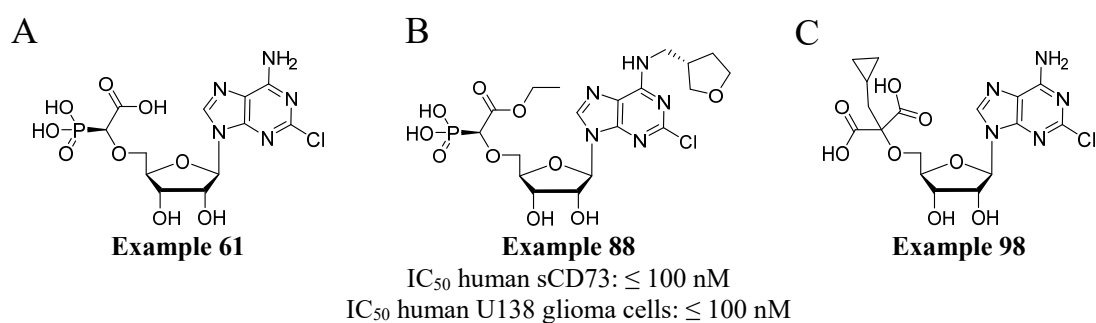
Figure 17. Nucleotide derivatives from Vitae Pharmaceuticals Inc.. (A, B, C) Exemplary structures of nucleotide derivative patented by Vitae Pharmaceuticals Inc. as CD73 inhibitors.

Besides Vitae Pharmaceuticals Inc., the company Calithera Biosciences Inc. also patented a variety of nucleotides and nucleotide mimetic structures as CD73 inhibitors. In the patent they showed about 300 different derivatives. The majority of these structures were 2-chloro-2′-deoxy-2′-fluoroadenosine (Clofarabine, see above Figure 16) derivatives with a 5′-substituent consisting of a dicarboxylic acid and different more bulky, mainly lipophilic residues (Figure 18). The potencies of these compounds were usually in the nM range.[105]

A

B

C

Example 150
IC_{50} human sCD73: 9 nM[105]

Example 179
IC_{50} human sCD73: 9 nM[105]

Example 181
IC_{50} human sCD73: 16 nM[105]
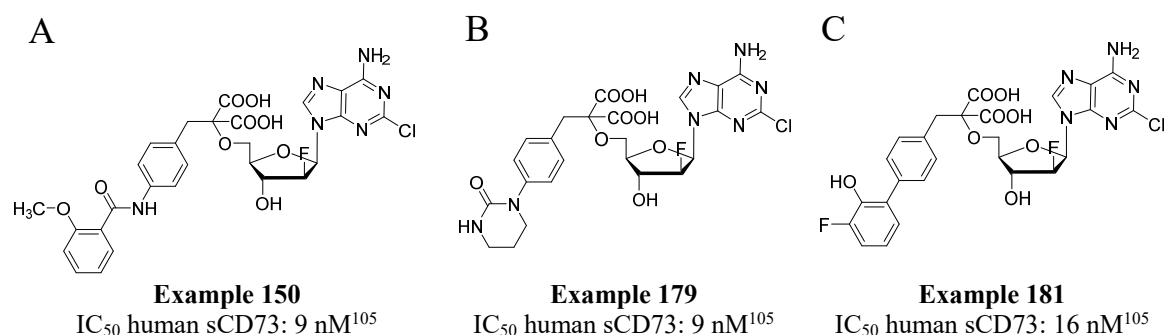
Figure 18. Nucleotide derivatives from Calithera Biosciences Inc.. (A, B, C) Exemplary structures of nucleotide derivative patented by Calithera Biosciences Inc. as CD73 inhibitors.

1.5.2   Non-nucleotides as CD73 inhibitors

The plant alkaloids candimine and lycorine were reported to inhibit ecto-5′-nucleotidase of the parasite *trichomonas vaginalis*, which causes trichomonas infections, a non-viral sexually transmitted disease. However, the inhibitory effects were only visible after 24-hour treatment of the parasite with the alkaloids before analyzing enzymatic activity, and the alkaloids were not selective because they also inhibited NTPDase. Unfortunately, inhibition of the purified enzymes was not investigated.[24, 106] Nevertheless, the study exemplarily illustrates the potential of CD73 expressed in bacteria/parasites as a target for the treatment of infection diseases.[106–108]

Further naturally occurring CD73 inhibitors were discovered in the group of flavonoids. Quercetin and Myricetin were identified as inhibitors with potencies in the low µM range (1.4 and 1.1 µM).[109] In contrast, in another study quercetin showed an IC$_{50}$ value of 45.3 µM.[110] Baicalin was also reported as a weak inhibitor. Nevertheless, it was possible to use baicalin as an inhibitor for co-crystallization with CD73 to get more information about the binding behavior of this polyphenol.[24, 59, 111]

The natural xanthine derivatives caffeine und theophylline were described as weak competitive inhibitors of CD73. Besides their weak potency, which is in the low mM range, these compounds are non-selective and show activity towards many different target structures including adenosine receptors.[24, 112, 113] In a screening campaign of 321 compounds at 10 µM concentration, 14 inhibitors were identified which share structural moieties with the xanthine scaffold and hence will be here described as xanthine derivatives. The two most potent compounds (Figure 19), an *N*,*N*-dimethyllumazine (PZB08511001A) and a bicyclic 2-aminopyrimidine derivative (PZB08511180A), displayed IC$_{50}$ values of 5.77 and 4.90 µM, respectively at rat CD73.[24]

A
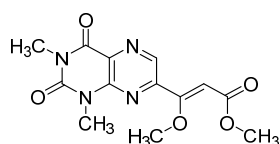
PZB08511001A
IC$_{50}$ rat sCD73: 5.77 µM[24]

B
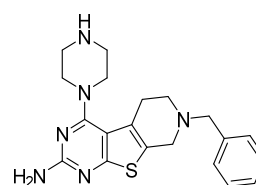
PZB08511180A
IC$_{50}$ rat sCD73: 4.90 µM[24]

Figure 19. Xanthine-like derivatives as CD73 inhibitors. (A) *N*,*N*-dimethyllumazine (PZB08511001A) and **(B)** a bicyclic 2-aminopyrimidine derivative as CD73 inhibitors.

Introduction

The anthraquinone (AQ) dye Reactive Blue (RB-2) was identified as a CD73 inhibitor with a K_i value of 3.07 µM. It further acts as a non-selective P2 receptor agonist and as an NTPDase inhibitor. Acid Blue (AB-25, Figure 20A), which is a much smaller AQ was found to be only slightly less potent than RB-2 (15.2 µM) and was used as a lead structure for further optimization. Small substituents at the 4-position of the AQ core structure were investigated and led to PSB-0963 (Figure 20B) with a potency of 150 nM and to PSB-0952 (Figure 20C), a more selective compound against P2Y receptors, which inhibited CD73 slightly less potently with a K_i of 260 nM.[111, 114]

Acid Blue (AB-25)
K_i rat sCD73: 15.2 µM[114]

PSB-0963
K_i rat sCD73: 150 nM[114]

PSB-0952
IC_{50} rat sCD73: 260 nM[114]
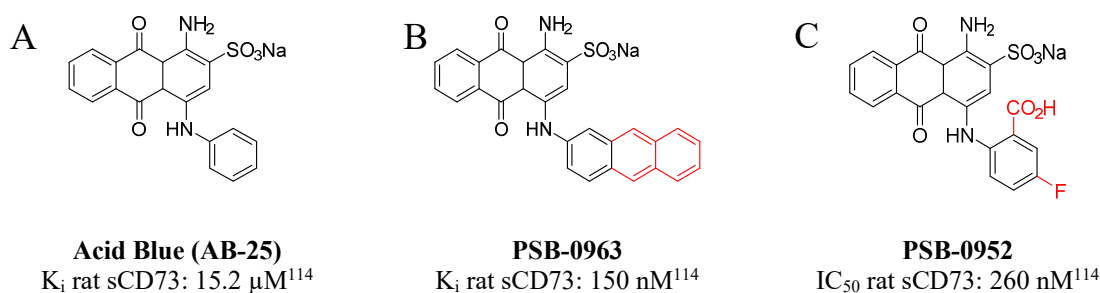
Figure 20. Anthraquinone derivatives as ecto-5′-nucleotidase inhibitors. (A) Acid Blue is an anthraquinone dye which inhibits ecto-5′-nucleotidase. The expansion of the lipophilic phenyl moiety in the N^4-position of the AQ core to anthracene (red) **(B)** increased the potency of the derivative. **(C)** 2-Carboxy-4-fluorophenyl substitution (red) of the phenyl moiety (PSB-0952) led to a slightly less potent compound, but with a higher selectivity against P2Y receptors.

Sulfonic acids were reported as CD73 inhibitors in two studies using recombinant rat and human CD73. Overall, the inhibitors were active in the medium to low µM range.[115, 116] The only more potent compound was 2,4-dinitrobenzenesulfonate which was the most potent inhibitor at human CD73 with a K_i value of 0.61 µM (Figure 21A)[115]. However, nitro groups may lead to toxic effects in some compounds.[117, 118] The most potent compound of the second study was 6-amino-4-hydroxynaphthalene-2-sufonic acid (Figure 21B) with an IC_{50} value of 1.32 µM at human CD73. Both compounds were less active at rat CD73 (Figure 21). They are with 248 and 239 Da relatively small which enable further modifications to increase their potency.[24, 116]

A

2,4-Dinitrobenzenesulfonic acid
K_i rat sCD73: 32 μM[115]
K_i human sCD73: 0.61 μM[115]

B

6-Amino-4-hydroxynaphthalene-2-sufonic acid
IC_{50} rat sCD73: 1.32 μM[116]
IC_{50} human sCD73: 10.4 μM[116]
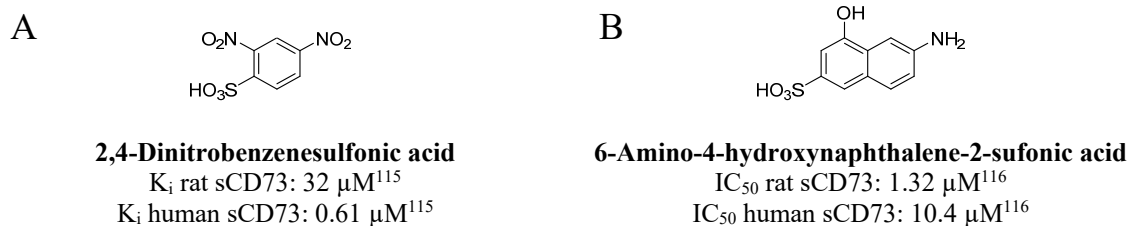
Figure 21. Sulfonic acid derivatives as ecto-5′-nucleotidase inhibitors. (A) 2,4-Dinitrobenzenesulfonate inhibited human CD73 in the high nM range and **(B)** 6-amino-4-hydroxynaphthalene-2-sufonic acid in the low μM range.

Isonicotinohydrazones and -thiazoles were identified as CD73 inhibitors of rat and human CD73. The inhibitors were active in the low μM or high nM range and the most potent isonicotinohydrazone at human CD73 was (*E*)-*N*′-(1-(3-(4-fluorophenyl)-5-phenyl-4,5-dihydro-1*H*-pyrazol-1-yl)ethylidene)isonicotinohydrazide illustrated in Figure 22A. This compound was reported to inhibit human CD73 with an IC_{50} value of 0.19 μM. Besides CD73, all tested isonicotinohydrazones were also inhibitors of bovine tissue-non-specific alkaline phosphatase (b-TNAP) and tissue-specific calf intestinal alkaline phosphatase (c-IAP).[119] The most potent thiazole derivative was (*E*)-1-(4-methyl-2-(2-(pyridin-3-ylmethylene)hydrazinyl)thiazol-5-yl)ethanone with an IC_{50} of 0.32 μM at human CD73 (Figure 22B). In both studies, molecular modeling suggested a competitive binding mode of the inhibitors, but this was not experimentally confirmed. The hydrazone moiety present in both compounds is labile and may be hydrolyzed.[120] However, the stability of the compounds has not been studied.[119, 121]

A

(*E*)-*N*′-(1-(3-(4-Fluorophenyl)-5-phenyl-4,5-dihydro-1*H*-pyrazol-1-yl)ethylidene)isonicotinohydrazide
IC_{50} rat sCD73: 0.36 μM[119]
K_i human sCD73: 0.19 μM[119]

B

(*E*)-1-(4-Methyl-2-(2-(pyridin-3-ylmethylene)hydrazinyl)thiazol-5-yl)ethanone
IC_{50} rat sCD73: 7.81 μM[121]
IC_{50} human sCD73: 0.32 μM[121]
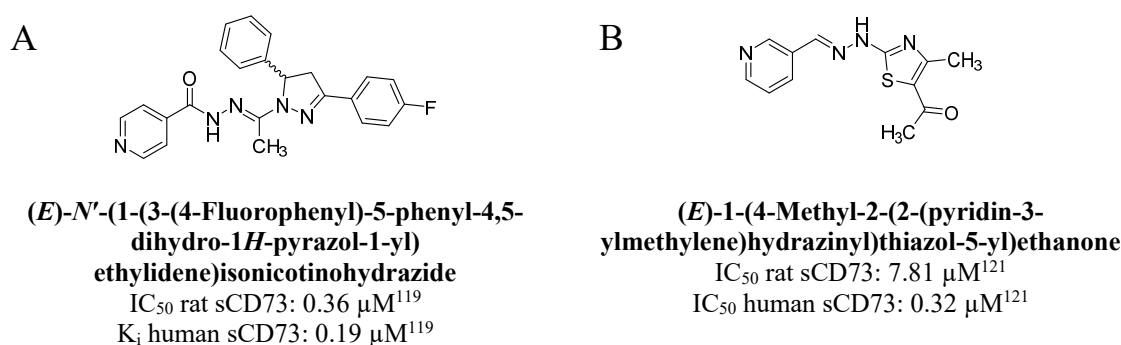
Figure 22. Isonicotinohydrazones and thiazoles as ecto-5′-nucleotidase inhibitors. (A) (*E*)-*N*′-(1-(3-(4-Fluorophenyl)-5-phenyl-4,5-dihydro-1*H*-pyrazol-1-yl)ethylidene)isonicotinohydrazide and **(B)** (*E*)-1-(4-methyl-2-(2-(pyridin-3-ylmethylene)hydrazinyl)thiazole.

Introduction

Monastrol (Figure 23A) is a small molecule inhibitor of kinesin-5. The inhibition of this motor protein leads to monopolar spindles during mitosis and thus to cell cycle arrest and reduced cell proliferation rates.[122, 123] A derivative of Monastrol, LaSOM 63 (Figure 23B), was identified as a CD73 inhibitor. It reduced glioma cell viability and cell growth. However, its IC_{50} value was not determined at the purified enzyme, and the estimated IC_{50} value based on whole cell experiments was with around 200 µM relatively high. Thus, further studies are necessary to assess whether this compound could be a suitable lead structure.[24, 111, 124]
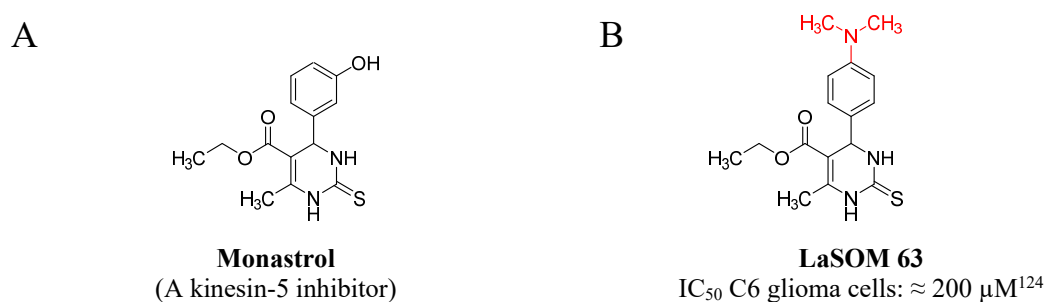
Figure 23. LaSOM 63, a monastrol derivative as CD73 inhibitor. (A) The kinesin-5 inhibitor monastrol and **(B)** the derivative which was found to be an inhibitor of ecto-5′-nucleotidase.

In 2017 GlaxoSmithKline patented 187 substituted benzothiadiazine derivatives as CD73 inhibitors. The structure of the most potent compounds (IC_{50} at CD73 (undefined species): 15.8 nM) is illustrated in Figure 24A.[125]
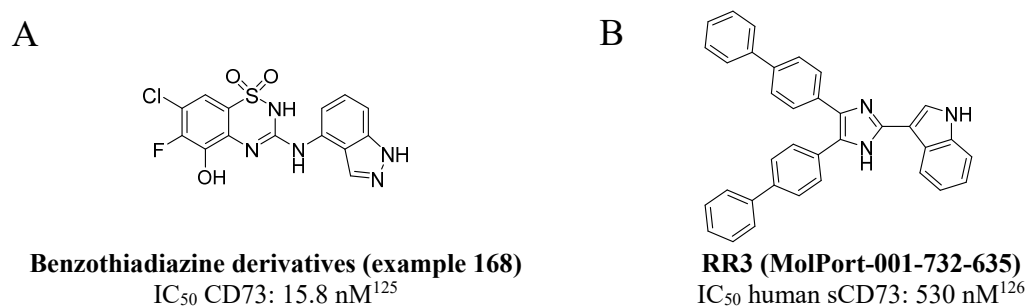
Figure 24. Benzothiadiazine and (aza)indole derivatives as CD73 inhibitors. **(A)** Exemplary benzothiadiazine derivatives from a GlaxoSmithKline patent and **(B)** RR3 (MolPort-001-732-635) a non-competitive inhibitor which targets the dimerization interface of CD73.

Most studies aimed at identifying competitive inhibitors for CD73. In contrast, a virtual screening campaign aimed to identify non-competitive inhibitors which interact in the region of the dimerization interface between two CD73 monomers. Several hit compounds were identified and validated *in vitro* showing moderate potencies in the low micromolar range (most potent inhibitor, see Figure 24B). Overall, the identified inhibitors were relatively large and characterized by high lipophilicity, thus, further optimization to improve potency and drug-like properties would be required.[126]

In a structure-based virtual screening approach sulfonamides were identified as CD73 inhibitors in our group. In this study 51 identified hit compounds were selected and the potencies were determined in *in vitro* experiments. A total of 13 of these molecules were validated using a sensitive radioassay (assays for CD73 will be described in the next chapter) at rat CD73.

The most potent inhibitor from this series was 6-chloro-2-oxo-N-(4-sulfamoylphenyl)-2*H*-chromene-3-carboxylic acid amide with an IC_{50} value of 1.90 µM (Figure 25D).[24, 127]

The identified hits mainly consisted of two different phenyl-sulfonamide structures, one with a lipophilically substituted hydrazone (Figure 25A, in black, MAF74; IC_{50}: 5.79 µM) and one with a coumarin moiety (Figure 25C, in black, MAF43; IC_{50}: 2.21 µM). These structures were used as lead structures, and further compounds were synthesized by Dr. Marianne Freundlieb to increase their potency. In the structural class of hydrazones, the compound (*E*)-4-(2-((6-methoxynaphthalen-2-yl)methylene)hydrazinyl)-3-propyl benzene-sulfonamide (MAF77) with a IC_{50} value of 1.66 µM was the most potent derivative (Figure 25B). In contrast, in the coumarin series the potency of the identified hit compound could not be increased. The binding mode of the inhibitor was described to be competitive.[24, 127] In contrast, another study published in 2018 reported that the IC_{50} value of this inhibitor was independent of the substrate concentration, suggesting a non-competitive mechanism of inhibition.[128]
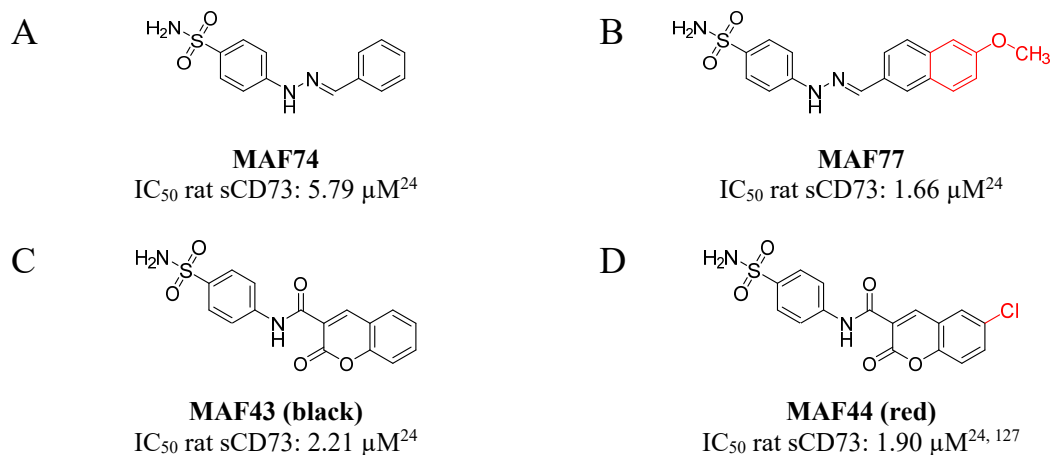
Figure 25. Sulfonamide derivatives as ecto-5′-nucleotidase inhibitors. (A) Hydrazone lead structure and **(B)** the most potent derivative. **(C)** Coumarin lead structure and **(D)** the most potent derivative out of this series.[24, 127]

Besides organic chemistry compounds, inorganic polyoxometalates (POMs) were also identified in our group to inhibit CD73. POMs are complexes of transition metal ions like tungsten, molybdenum, niobium, antimony and vanadium. The ions are typically bridged by oxo ligands (O^{2-}) resulting in a negative charge of POMs. Some of them are stable under physiological conditions and were explored as inhibitors of enzymes of the purinergic signaling pathway.[129, 130] The most potent POM for CD73 inhibition consisting of a rhenium cluster with the formula $K_4[(Re_6S_8)(HCOO)_6]\cdot 3H_2O$, is non-competitive and inhibits CD73 with an IC_{50} of 4.57 µM.[101] However, it is not selective since it inhibits NTPDase1-3 and NPP1 as well. In general, all POMs which inhibited CD73 also inhibited other ectonucleotidases.[24, 101, 130]

1.6   Assays for ecto-5′-nucleotidase

Suitable assay systems are required for the determination of enzymatic kinetics, to identify new inhibitors in screening campaigns and to analyze the potency of CD73 inhibitors. Parameters which are often used in the characterization of an assay are the detection limit (limit of detection, LOD), the signal-to-background ratio and the Z′-factor.[131]

The limit of detection (LOD) describes the lowest amount of analyte in a sample which can be detected, but not necessarily quantitated as an exact value (ICH guideline, Q2/R1).[132] The way to determine the LOD depends on the type of analytical method. In the present study it was calculated according to the following formula (ICH guideline, Q2/R1):[132]

$$Limit\ of\ detection = \frac{3.3 \cdot \sigma}{S} \tag{15}$$

σ: standard deviation of the blank

S: slope of the calibration curve

The signal-to-background ratio (S/B) describes the ratio between the mean of the response signal to the mean of the blank. Thereby it describes the so-called signal window between no response (noise) and response and is calculated according to the following formula:

$$S/B = \frac{\mu_+}{\mu_-} \tag{16}$$

μ_+: mean of signal

μ_-: mean of background

An assay with a high signal-to-background ratio usually stands for a more robust assay compared to one with a low value, but the determination of S/B do not take the variability of the mean of response and the mean of blank (noise) into account. Thus, an assay with a small signal-to-background ratio, but small variability in the response and blank values can be more robust than an assay with a large assay window (high S/B) with high variability within the blank and/or the response (signal) values. To overcome this drawback, the Z′-factor was established by Zhang and coworkers and has since been used for the determination of the performance of assays. It is calculated according to the following formula:[133]

$$Z' - factor = 1 - \frac{(3\sigma_{c+} + 3\sigma_{c-})}{|\mu_{c+} - \mu_{c-}|} \tag{17}$$

σ_{c+}: *standard deviation of the positive controls*

σ_{c-}: *standard deviation of negative controls (blank)*

μ_{c+}: *mean of the positive controls*

μ_{c-}: *mean of the negative controls (blank)*

Z′-factor values of 1 would describe an ideal assay and values between 0.5 and 1 are characteristic of an excellent assay also suitable for automated screening campaigns.

To identify and to analyze ecto-5′-nucleotidase-modulating substances, different assay systems have been reported. These include colorimetric, chromatographic/spectroscopic, luminescent and radiometric procedures.[93, 128, 134–153] The detection of produced inorganic phosphate by different colorimetrically detectable dyes has been explored and optimized for decades. Under acidic conditions, ammonium heptamolybdate and phosphate form a phosphomolybdate complex, which is the basis for the colorimetric phosphate assays. The analysis of different cationic dyes, which convert the colorless complex into a colorful one, has revealed that the use of the organic dye malachite green is most sensitive. Under acidic conditions (pH < 2), malachite green is present in its protonated, yellow species. In the presence of the negatively charged phosphomolybdate complex, malachite green attaches via electrostatic interaction to the complex. Thereby, malachite green is present in its non-ionic form, which is characterized by a blue-green color, which is photometrically detectable.[152] The assay is easy to handle, inexpensive, but less sensitive than other reported assays for CD73.

Further assays are based on coupled enzyme reactions[143, 145, 146, 150, 154] including the luciferase reaction.[146] Luciferase converts luciferin under ATP consumption to oxyluciferin, AMP and emits photons as bioluminescence. In the described assay, unconverted AMP of the ecto-5′-nucleotidase reaction inhibits the luciferase reaction. Thus, a high ecto-5′-nucleotidase activity is reflected by a high ATP hydrolysis and high luminescence signal. This assay has some drawbacks. It requires a substrate concentration of 300 µM AMP which is about 10 times higher than the K_M value of ecto-5′-nucleotidase (1-59 µM)[43, 155, 156] which makes the identification of competitive inhibitors difficult. Furthermore, ATP which is used for the readout reaction itself is a competitive inhibitor of ecto-5′-nucleotidase ($K_i = 8.9$ µM[93]). Moreover, luciferase inhibition by test compounds leads to false-positive hits.

Recently, a sensitive RapidFire–tandem mass spectrometry (RF-MS/MS)-based multiplex assay was developed which is suitable for HTS. Enzymatic reactions were performed, each with one of four different isotopes of AMP, namely $[^{13}C]_5$-AMP, $[^{2}H]_2$-AMP, $[^{15}N]_5$-AMP, $[^{13}C]_{10}[^{15}C]_5$-AMP. Afterwards, the four reactions were pooled and the formed adenosine was quantified simultaneously with a rapidfire MS technology.[128] It is not mentioned in the publication, but it can be assumed that this assay is very sensitive. However, the radioisotopes as well as the complex rapidfire MS device makes this assay costly.

One of the most sensitive assays for ecto-5′-nucleotidase is a radiometric assay (LOD: 0.028 ± 0.002 μM adenosine), which was developed by Dr. Freundlieb in our group and allows the use of low substrate concentrations, thus enabling the identification of weak competitive inhibitors (Figure 26). In this assay, radiolabeled $[2,8-^{3}H]$AMP is converted to $[2,8-^{3}H]$adenosine. Unconverted substrate and phosphate is precipitated by the addition of lanthanum(III) chloride. The soluble adenosine is separated from the precipitate by filtration and is further quantified by scintillation counting, reflecting enzymatic activity of CD73.[151] Advantages and disadvantages of the different assays are summarized in Table 1.
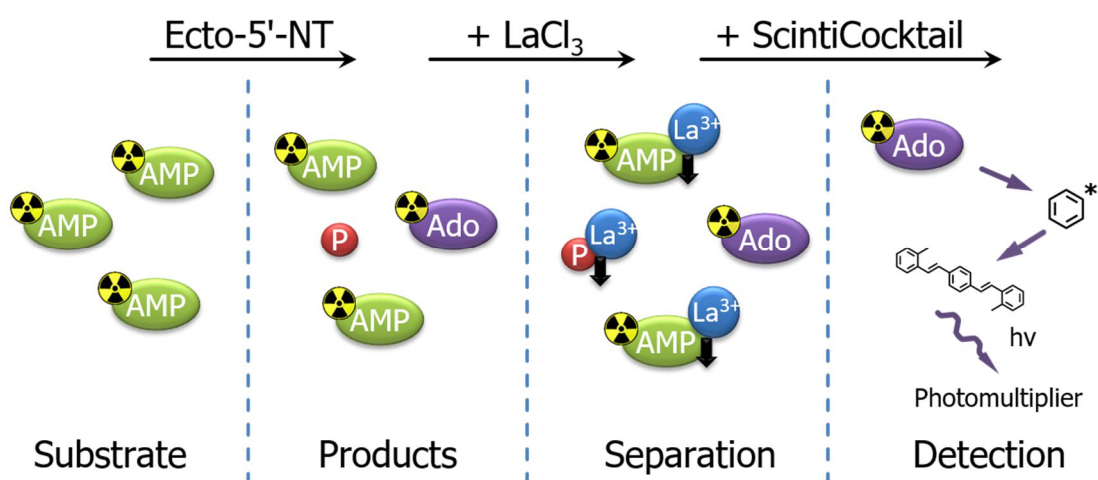
Figure 26. Principle of a sensitive radiometric ecto-5′-nucleotidase assay.[151]

Introduction

Table 1. Advantages and disadvantages of different reported CD73 assays (-: disadvantage, -/+: neither, +: advantage; modification and extension of[24, 25]).

Assay	Sensitivity	HTS-compatible	Natural substrate	Detection of product	Low costs	Low cost of laboratory equipment
Capillary electrophoresis[93, 101]	-	-	+	+*	+	-/+
HPLC[157]	-	-	+	+*	+	-/+
Enzyme-coupled reactions (e.g. luciferase)[146]	-	+	+	-	+	+
Radiometric assay[151]	+	-/+**	+	+	-	-***
RapidFire–tandem mass spectrometry[128]	+	+	+	+	-	-***
Colorimetric assays (e.g. malachite green)[152]	-	+	+	-	+	+

* It is possible to detect the substrate as well as the product; ** Possible with great effort and costs; *** Besides the technical equipment, the laboratory needs to be certified for the work with radioisotopes.

1.7 Objectives and work strategy

The purinergic pathway is involved in many physiological and pathophysiological processes. The enzyme ecto-5′-nucleotidase (CD73) is one of the key players in purinergic signaling. To investigate its roles and functions *in vitro* and *in vivo*, it is required to develop potent and selective inhibitors for this enzyme. These so-called tool compounds can then be used in animal models of disease to investigate their effects and to validate CD73 as a drug target.

To identify, optimize and characterize inhibitors, expression and purification of the enzyme is required. Rat CD73 has previously been expressed and provided to our group by Prof. Herbert Zimmermann, University of Frankfurt. Even though rat and human CD73 share a high sequence identity of 87%, it cannot be excluded that species differences exist, especially for allosteric antagonists. Therefore, we aim to

- recombinantly express and purify human soluble CD73.

For this purpose, different vector constructs will be explored, and human soluble CD73 will be recombinantly expressed in *Spodoptera frugiperda* (Sf9) insect cells and purified by affinity chromatography. Soluble CD73 is not bound to the membrane, and amino acid tags have to be added for purification. Therefore, we additionally aim to

- obtain membrane-bound human CD73 for establishing a less artificial test system.

For this purpose, we will produce membrane preparations from the triple-negative breast cancer (TNBC) cell line, MDA-MB-231, and use this as a natural source for CD73. To identify, optimize and to characterize inhibitors different assays are required. We aim to

- establish and optimize the previously developed sensitive radioassay (see chapter 1.6) employing different sources of CD73, and additionally
- develop an assay suitable for automated screening of compound libraries.

For the analysis of our proprietary in-house compound library consisting of several thousand compounds, it is necessary to have an assay, which is transferable to an automatic screening

Introduction

station. This screening assay should be straightforward with only few pipetting steps, be fast, robust, inexpensive, non-radioactive and running in a microtiter plate format. We will explore the possibility to use malachite green for the determination of phosphate as a product of CD73. After screening, we plan to validate the identified hits by applying the sensitive radioassay as an orthogonal method.

Besides hit validation, we will further use the radioassay to investigate the structure-activity relationships of AOPCP and sulfonamide derivatives with the following objectives:

- We aim to replace the base adenine by different (substituted) purine and pyrimidine moieties to increase potency and selectivity.
- The ribose and the diphosphonate of AOPCP have not been well investigated so far; therefore, we aim to modify the ribose or to replace it by acyclic structures.
- The diphosphonate group is charged under physiological conditions, which is expected to result in low oral bioavailability. We plan to replace this moiety by bioisosteres to increase drug-likeness.
- We aim to develop a radioligand for CD73 based on previous results of nucleotidic inhibitors.
- We want to increase the potency of the sulfonamide derivatives.
- Selected compounds of these projects will be further characterized by analyzing their mode of inhibition and their potency at human soluble and human membrane-bound CD73.

Besides small-molecules, we plan to analyze the potency of antibodies for CD73, produced by a cooperation partner for potential therapeutic use.

This project is aimed to result in improved CD73 assays, novel tool compounds, and potential diagnostics and therapeutics for CD73. The result is expected to lead to significant advances and deepened knowledge on CD73, which represents a novel drug target for cancer immunotherapy.

2 Methods

2.1 Various sources and types of ecto-5′-nucleotidase

2.1.1 Recombinant ecto-5′-nucleotidase from the species rat

Recombinantly produced CD73 derived from the species rat were provided by the research group of Prof. Dr. Herbert Zimmermann (University of Frankfurt, Germany). The enzyme was expressed as soluble glutathione S-transferase/ecto-5′-nucleotidase fusion protein in insect cells (Sf9) using the baculovirus expression system. The protein was purified by affinity chromatography with cross-linked glutathione agarose.[158] These stocks (20 mM Hepes pH 7.4) were defrosted, diluted 1:1 in 25 mM Tris buffer pH 7.4 plus 4 mM iodacetamide, and 50% glycerol were added. Aliquots were subsequently frozen and stored at -80°C.

2.1.2 Expression and purification of soluble human CD73

2.1.2.1 Overview

The cDNA of human CD73 was provided by Prof. Dr. Norbert Sträter (University of Leipzig, Germany) and is based on the Genbank accession no. NM_002526 and the natural variation T376A identified in leukocytes (P21589/VAR_022091, UniProtKB/Swiss-Prot). In order to generate a soluble enzyme the signaling sequence for anchoring the protein to the membrane via a GPI-anchor had been omitted (N-terminal residues: 1-27, C-terminal residues: 550-574 including GPI-anchor attachment site).[59] In addition, a polyhistidine-tag (6xHis-Tag) was fused to the C-terminus. Prof. Dr. med. Michael Hölzel (Institute of Clinical Chemistry and Clinical Pharmacology, University of Bonn) used this sequences and integrated it into two different vectors. Both vector types (pACG2T and pACGP67B) are suitable for the expression and secretion of the produced fusion protein into the supernatant of baculovirus-infected Sf9 insect cells. Moreover, the vector pACG2T provides an N-terminal located glutathione S-transferase (GST). The secretion signal peptide (gp67) is cleaved during transport across the cell membrane,[159] and the sequence of the expressed fusion proteins are as follows (full amino acid sequences are provided in the appendix, page 143):

pACGP67B-sCD73: ADLGS-(W^{27}ELT-CD73-IKFS^{549})-GGSHHHHHH

pACG2T-sCD73:   ADLGS-(GST)-LVPRGS-(W^{27}ELT-CD73-IKFS^{549})-GGSHHHHHH

43

Methods

2.1.2.2 Cell culture of insect cells

Sf9 cells were grown in Insect-XPRESS™ medium (#: BE12-730Q, Lonza, Switzerland) with 10 mg/l gentamicin and split at a ratio of 1:3 every fourth day. Therefore, old culture medium was discarded and renewed with 5, 10 or 15 ml medium for 25 cm^2, 75 cm^2 or 175 cm^2 culture flasks, respectively. Afterwards, adherent cells were detached by tapping onto the culture flask and cells were transferred to a fresh 25 cm^2, 75 cm^2 or 175 cm^2 culture flask previously filled with the related volume of medium (see above).

2.1.2.3 Transfection

For each vector construct (pACG2T-sCD73, pACGP67B-sCD73), Sf9 cells were seeded in 25 cm^2 culture flasks (60-70% confluence). 100 µl of cell medium and 1 µl of the vector DNA (1000 ng/µl) were mixed with 2.5 µl of baculovirus genomic ProEasy™ vector DNA (AB vector, San Diego, CA, USA) and combined with premixed 100 µl of cell medium and 8 µl of Cellfectin™ II Reagent (Thermo Fisher Scientific, Waltham, MA, USA). The transfection mixture was incubated for 30 min at room temperature and then dropwise added to the cells in a 25 cm^2 culture flask. The cells were incubated for 30 min at room temperature and afterwards overnight at 27°C. The medium was renewed and cells were incubated for further four days at 27°C.

2.1.2.4 Amplification of baculovirus

Cells from the transfection procedure were detached from the bottom of the culture flaks and centrifuged for 5 min at 2000g. 1.5 ml of the supernatant (viral stock P1) was transferred to a 75 cm^2 culture flask with seeded uninfected Sf9 cells (60-70% confluence) and incubated for four days at 27°C. Then 1.5 ml of the supernatant were taken and added to uninfected Sf9 cells in a 75 cm^2 culture flask. This was repeated five more times, using more cells and larger flasks after the third round of infections (175 cm^2 to which 3.0 ml of supernatant were added). The final stock P7 was further used as a virus solution. The procedure from transfection to the virus solution was also done with non-transfected cells to monitor possible cross-contaminations between the different vector constructs.

2.1.2.5 Protein expression

The baculoviruses related to the vector pACGP67B-sCD73 were used for further protein expression. For this purpose, 150 ml of cell medium containing $2x10^6$ uninfected Sf9 cells/ml were transferred to a 500 ml Erlenmeyer flask, and 3 ml of the working virus solution were mixed together and incubated for 4 days at 27°C (150 rpm).

2.1.2.6 Protein purification

Cell suspensions were transferred to 50 ml falcon tubes and centrifuged for 15 min at 5000g (4°C). Afterwards, the supernatants were frozen to -80°C or further processed by protein ultrafiltration with Amicon® Ultra-15 (10 kDa cut-off, Merck Millipore, Burlington, MA, USA). Therefore, 12 ml of supernatant were transferred to the Amicon® tube and centrifuged for 15-30 min at 5000g (4°C). The flow-through was discarded and the process was repeated two more times. The concentrated protein was removed from the filter membrane and the filter was washed by up and down pipetting with 2 ml of Tris buffer (25 mM Tris, pH 7.4). The protein was frozen to -80°C or further processed by purification with HisPur™ Ni^{2+}-NTA spin columns (#: 88226, Thermo Fisher Scientific, Waltham, MA, USA). The column purification was proceeded as recommended in the instruction manual with adjusting the incubation time for protein binding to 1 h at 4°C with an end-over-end mixer (Kisker Biotech, Steinfurt, Germany) and an additional incubation step of 2 min with the elution buffer before eluting the protein. For removal of imidazole and phosphate, a dialysis tube (Membra-Cel™, 14 kDa cut-off, 250 mm x 44 mm x 0.02 mm, Carl Roth, Germany) was preincubated for 1 h in Tris buffer (25 mM Tris, pH 7.4). Afterwards, one site of the tube was locked with a dialysis clamp, elution fractions were pooled, transferred to the tube and the upper end of the tube was locked. The dialysis tube was incubated at 4°C in Tris buffer (25 mM Tris, pH 7.4), whose volume was adjusted to 40 times the volume of the elution fraction. The buffer was renewed after 30, 60 and 120 min.

The proteins were concentrated with Amicon® Ultra-15 (10 kDa cut-off) as described above. After the protein was concentrated, a five-fold volume of Tris buffer (25 mM Tris, pH 7.4) was added to the Amicon® tube and centrifuged as described above. This washing step was repeated two more times. Afterwards, the proteins were aliquoted and frozen to -80°C. For all steps of the purification procedure, samples for measuring the protein concentration and the enzymatic activity were collected.

Methods

2.1.2.7   Analysis of protein concentration

The protein concentration of collected samples was analyzed during the purification process by measuring the absorption at 280 nm (A_{280} = 1 equals 1 mg/ml protein, Colibri Microvolume Spectrometer, Titertek Berthold, Pforzheim, Germany) and/or with Lowry-assay.[160] For this purpose, protein samples were diluted 1:20 in Tris buffer (25 mM Tris, pH 7.4), 1 ml of reagent C (62 mM Na_2CO_3, 0.62 mM Cu_2SO_4, 1 mM sodium L-tartrate, 0.1 N NaOH) were added, samples were vortexed and incubated 20 min at room temperature. Afterwards, 100 µl of reagent D (Folin-Ciocalteu's phenol) were added, samples were vortexed and incubated for further 30 min at room temperature. Solutions were transferred to halfmicro-cuvettes (Ratiolab®, Ratiolab, Dreieich, Germany) and the absorption at 500 nm was distinguished (DU® 530, Beckman Coulter, Brea, CA, USA). Protein concentrations were calculated with system stored calibration curve.

2.1.2.8   Sodium dodecyl sulfate polyacrylamide gel electrophoresis (SDS-PAGE)

Protein samples were mixed with 4x SDS-loading buffer (250 mM Tris, 8% sodium dodecyl sulfate (SDS), 20% ß-Mercaptoethanol, 0.04% bromophenol blue, 15% glycerol, pH 6.8), incubated 5 min at 95°C and centrifuged for 5 min at 23000g. Afterwards, the proteins were separated according to their molecular weight in discontinuous polyacrylamide gel after the procedure of Laemli[161] (Mini-PROTEAN® 3 Cell Bio-Rad Laboratories, Hercules, CA, USA). In 6% stacking gel the samples were focused for 15-20 min at 120 V (PowerPac Universal™, Bio-Rad Laboratories, Hercules, CA, USA) and afterwards separated in 10% running gel for 60 min at 200 V (recipe for the gels and buffers for the SDS-PAGE, see page 62). To estimate the molecular weight of the separated proteins a His-tagged protein standard (10 - 160 kDa, BenchMark™, Thermo Fischer Scientific, Waltham, MA, USA) marker was used.

2.1.2.9   Western blot

Protein samples separated with SDS-PAGE were transferred to a nitrocellulose blotting membrane (Amershan™ Protan™ 0.45 µm, GE HealthCare, Chicago, IL, USA) with the wet protein transfer procedure (Mini-Trans Blot cell®, Laboratories, Hercules, CA, USA). For each polyacrylamide gel two filter papers (Gel-blotting-Papier, Carl Roth, Karlsruhe, Germany) and two filter sponges were soaked in transfer buffer and a nitrocellulose membrane was activated in Milli-Q water. Afterwards, the filter paper, sponges, gel and

membrane were stacked and proteins were transferred to the membrane for 90 min at 90 V (PowerPac Universal™, Bio-Rad Laboratories, Hercules, CA, USA at a cooled blocking chamber, see Figure 27.)
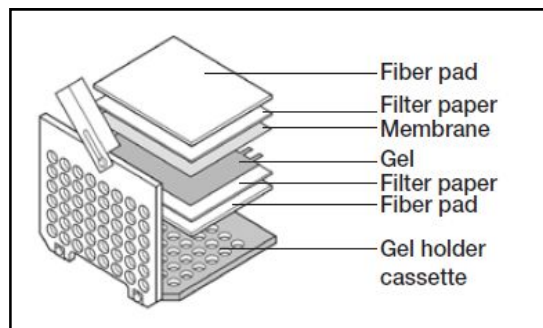
Figure 27. Transfer of proteins to a nitrocellulose membrane by wet-blotting.[162]

After the transfer, the membrane was incubated with M-TBST (5% powdered milk, 20 mM Tris, 137 mM NaCl, 0.1% Tween® 20, pH 7.6) for 1 h with constant shaking at room temperature. Then, the blocking solution was removed and the membrane was shaking-incubated overnight at 4°C with a 1:3000 dilution of a His-Tag antibody (#: Ma1-21315-HRP, Thermo Fischer Scientific, Waltham, MA, USA). Afterwards, the membrane was washed three times for 15 min with TBST (20 mM Tris, 137 mM NaCl, 0.1% Tween® 20, pH 7.6). The membrane was treated 5 min with 1 ml enhanced chemiluminescence (ECL) substrate (Bio-Rad, Hercules, CA, USA) and the luminescence produced by the horseradish peroxidase, which is conjugated to the antibody was detected with x-ray films (CL-x Posure™ Film 20 x 25 cm, Thermo Fischer Scientific, Waltham, MA, USA; developer: Cawomat 200 IR, CAWO Photochemisches Werk GmbH, Schrobenhausen, Germany; recipe for the buffers for the western blot see page 62).

Methods

2.1.3 Preparation of cell membrane fractions as a source for CD73

2.1.3.1 Cell culture of mammalian cells

2.1.3.1.1 Culture conditions

Mammalian cells were cultured in cell culture flasks (25 cm^2, 75 cm^2 or 175 cm^2 culture flask) in their specific culture medium (Table 2) at 37°C with 5% CO_2. Cells were split every 72 h (at 80-90% cell confluence) to their specific split ratio (Table 2). To detach the adherent cells, culture medium was removed, cells were washed with phosphate-buffered saline (PBS, 25 cm^2: 2.5 ml, 75 cm^2: 5 ml, 175 cm^2: 10 ml) and incubated with trypsin/EDTA (0,05%/0.6 mM; 25 cm^2: 0.5 ml, 75 cm^2: 1.5 ml, 175 cm^2: 3 ml) for 5 min at ambient temperature or in the incubator at 37°C. Detached cells were diluted with culture medium (25 cm^2: 2 ml, 75 cm^2: 5 ml, 150 cm^2: 10 ml) and transferred to new culture flasks containing culture medium (25 cm^2: 5 ml, 75 cm^2: 10 ml, 175 cm^2: 15 ml).

Table 2. Culture conditions for different types of mammalian cells.

Cell line	species	Culture medium	Split ratio
Triple-negative breast cancer (MDA-MB-231)	human	Dulbecco's Modified Eagle Medium (DMEM, #: 41966, Thermo Fisher Scientific, Waltham, MA, USA), plus 100 U/ml penicillin/ 100 µg/ml streptomycin (#: P06-07100, PAN Biotech, Aidenbach, Germany, 10% fetal bovine serum (FBS, #: P30-1502, PAN Biotech, Germany)	1:20 every 72 h
Triple-negative breast cancer (4T1.2)	mouse	Roswell Park Memorial Institute (RPMI) medium GlutaMAX™ Supplement, (#: 61870036, Thermo Fisher Scientific, Waltham, MA, USA) plus 100 U/ml penicillin/100 µg/ml streptomycin, 10% FBS	1:20 every 72 h

2.1.3.1.2 Defrosting of cryo-conserved cells

Cryo-conserved cells were defrosted, diluted 1:10 in culture medium and centrifuged for 5 min at 3000*g*. The supernatant was discarded, cells were resuspended in 10 ml culture medium and transferred to a 75 cm^2 culture flask.

2.1.3.1.3 Cryo-conservation of cell lines

Cells were expanded in 175 cm^2 culture flasks to 80-90% cell confluence. Culture medium was removed, cells were washed with PBS and detached with trypsin/EDTA solution. Afterwards, 10 ml of culture medium were added, the cell number was distinguished with a Neubauer counting chamber (Paul Marienfeld GmbH & Co.KG, Lauda Königshofen,

Germany) and the cell suspension was centrifuged for 5 min at 3000g. The supernatant was discarded and the cells were resuspended in desirable volume of culture medium containing 20% FBS and 10% DMSO resulting in a cell concentration of $1x10^7$ cells/ml. Each cryo-conservation vial was filled with 500 µl of the cell solution. Vials were frozen at -80°C using a freezing container (-1°C/min, Mr. Frosty™ Freezing Container, Thermo Fischer Scientific, Waltham, MA, USA). After 24 h samples were stored at -80°C or at -150°C.

2.1.3.1.4 Membrane preparations

Cells were expanded in 175 cm² culture flasks to 80-90% cell confluence. After detachment by trypsin/EDTA, equal amounts of the solution were transferred to 10 cell culture dishes (150 cm²) and incubated for 4 days at 37°C with 5% CO_2. Culture medium was removed, each dish was washed with 10 ml PBS and cells were frozen to -20°C. Afterwards, the dishes were treated with 1 ml of ice-cold scraping buffer (50 mM Tris, 2 mM EDTA, pH 7.4), scraped off, collected in a conical tube and centrifuged for 10 min at 1000g (4°C). The supernatant was discarded, the pellet resuspended in membrane buffer (0.5 ml/dish; 25 mM Tris, 1 mM EDTA, 320 mM sucrose, 1:1000 protease inhibitor cocktail (#: P8340, Sigma-Aldrich, MO, USA), pH 7.4) and homogenized three times for 30 s (20500 rpm, Ultraturrax, IKA-Labortechnik, Germany). After a centrifugation step (10 min, 1000g, 4°C), the supernatant was collected and centrifuged for 30 min at 48000g at (4°C). The resulting supernatant was discarded and the pellet was resuspended in washing puffer (0.5 ml/dish; 50 mM Tris, pH 7.4) and centrifuged again (same conditions). This step was repeated three times. Finally, the pellet was resuspended in washing buffer (0.1 ml/dish), the protein concentration was determined as described above, samples were aliquoted and frozen at -80°C.

Methods

2.2 Characterization of CD73 and inhibitors with a radiometric enzyme assay

2.2.1 Variations of the radioassay

In this study two general variations of the assay[151] were used:

1) The composition of the assay reaction buffer was: 25 mM Tris, 140 mM sodium chloride, 25 mM sodium dihydrogen phosphate, pH 7.4. After the reaction, the samples were placed on ice and 500 µl of cold precipitation buffer (100 mM lanthanum chloride, 100 mM sodium acetate, pH 4.0) were added to stop the reaction and to facilitate the precipitation.

2) The composition of the assay reaction buffer was: 25 mM Tris, 140 mM sodium chloride, 2 mM magnesium chloride, 1 mM calcium chloride, pH 7.4. After the reaction, the samples were placed on ice and two buffers were added to stop and to facilitate the precipitation. First, 100 µl of cold 25 mM sodium dihydrogen phosphate pH 4.0 and second, 500 µl of the cold precipitation buffer were given to the reactions.

2.2.2 Michaelis-Menten kinetics of CD73

For the determination of the K_M and V_{max} values of CD73, the AMP hydrolysis of different substrate concentrations in the range from 0.97 to 500 µM AMP were analyzed with a sensitive radio assay using the first variation of the assay. A 10-fold solution of AMP (5000 µM) were prepared in assay reaction buffer with addition of [2,8-³H]AMP (specific activity: 2 mCi/mmol, American Radio-labeled Chemicals, MO, USA, distributed by Hartmann Analytic, Braunschweig, Germany). A two-fold serial dilution was performed in assay reaction buffer. After addition of 10 µl of the diluted samples to 80 µl of assay reaction buffer, the mixture was preincubated for 5 min at 37°C in a shaking water bath. The reactions were initiated by the addition of 10 µl prewarmed (37°C) CD73 solutions leading to a final amount of 16.3, 3.65 and 74 ng for rat soluble, human soluble and human membrane-bound CD73, respectively. After the reaction, which was performed for 25 min at 37°C in a shaking water bath, the enzymatic reaction was stopped and precipitation of free phosphate and unconverted [2,8-³H]AMP was performed like described above for the first variation of the assay. After the precipitation was completed (after at least 30 min on ice) the mixture was separated by filtration through GF/B glass fiber filters (Whatman™ GE Healthcare, Chicago, IL, USA) using a cell harvester (M-48, Brandel, Gaitherburg, MD, USA). After washing each reaction vial three times with 400 µl of cold (4°C) Milli-Q water, 5 ml of the scintillation cocktail ULTIMA Gold XR (PerkinElmer) was added and radioactivity was

measured by scintillation counting (counting efficacy: 49-52%, TRICARB 2900 and 2810 TR, PerkinElmer, Waltham, MA, USA). Moreover, two calibration curves without addition of CD73 were recorded. One curve was determined including the filtration step, which presents background, the other curve was determined without filtration corresponding to 100%. Reactions were performed in duplicates, background activities were subtracted of the resulted data, the concentration of produced adenosine were quantified with use of the calibration curve and the velocity (v (µmol/min/mg protein)) was calculated. The mean result of three independent experiments was plotted with GraphPad Prism 6 program (GraphPad Software, La Jolla, USA) and the Michaelis-Menten kinetic were fitted.

2.2.3 Determination of specific enzymatic activity

The AMP hydrolysis of different samples obtained during the expression and purification of human CD73 (cell supernatants or samples of the protein purification procedure) was analyzed with the radio assay using the first variation of the assay. Multiple 10-fold dilutions of each sample were performed in assay reaction buffer. After addition of 10 µl of protein sample to 80 µl of assay reaction buffer, the reaction mixture was preincubated for 5 min at 37°C in a shaking water bath. The enzymatic reaction was initiated by the addition of 10 µl of [2,8-^{3}H]AMP (specific activity: 20 mCi/mmol), American Radio-labeled Chemicals, MO, USA, distributed by Hartman Analytic, Braunschweig, Germany) resulting in a final substrate concentration of 5 µM AMP. The reaction and precipitation was performed as described above.

In each experiment two control samples as duplicates were incubated without adding a CD73-containing solution. Two were included in the filtration step representing background activity and two were measured without filtration representing 100%. Background activities were subtracted of the resulted data, the concentration of produced adenosine was quantified with use of the 100% samples. Values in the range of 10% AMP hydrolysis were selected for the calculation of the specific activity (U/mg protein). Data were plotted with "GraphPad Prism 6".

2.2.4 Enzyme titrations with various sources of CD73

The hydrolysis of the radiolabeled AMP to adenosine by different concentrations of membrane preparations or recombinant human CD73 was analyzed using the first assay variation. Membrane preparations or recombinant produced human CD73 was diluted in

reaction buffer and the final AMP concentration was set to 5 µM. The experiment was performed as described above in 2.2.3, page 51.

2.2.5 Inhibition assay

Stock solutions (10 mM) for hydrophilic small molecules (usually nucleotides) were prepared in Milli-Q water. Further dilutions were performed in assay reaction buffer. When pipetting the assay, 10 µl of these solutions were given to the test vial (final volume 100 µl). For more lipophilic compounds (usually sulfonamides), the stock solutions (10 mM) and further dilutions were prepared in DMSO. This is also valid for samples of the compound library which are usually provided as 10 mM DMSO stocks. When pipetting the assay, 1 µl of these solutions was given to the test vial (final volume 100 µl).

Antibodies against CD73 were diluted under sterile conditions in assay reaction buffer and 10 µl were used in the assay (final volume 100 µl).

To analyze the potency of the different CD73 modulating substances, full concentration-inhibition curves in a desirable concentration range were prepared in assay reaction buffer. 10 µl for water soluble compounds and antibodies and 1 µl for samples in DMSO were added to 70 µl or 79 µl of assay reaction buffer, respectively. After the addition of 10 µl of CD73 solution leading to a final amount of 16.3, 3.65 and 74 ng for rat soluble, human soluble and human membrane-bound CD73, respectively, the reaction was initiated by the addition of 10 µl of $[2,8-^3H]$AMP (specific activity: 20 mCi/mmol), American Radio-labeled Chemicals, MO, USA, distributed by Hartman Analytic, Braunschweig, Germany) resulting in a final substrate concentration of 5 µM. Two controls were included and measured as duplicates. One reaction was performed without the inhibitor resulting in 100% enzyme activity (positive control) and one was incubated without the inhibitor and the enzyme and served as background control. The reactions were performed as described above (2.2.3, page 51). All nucleotides and sulfonamides were measured with the first variation of the assay. Compounds from the screening campaign were analyzed with the second variation of the assay. In addition, these compounds were preincubated for 20 min at 37°C with CD73 before the induction of the reaction. Antibodies were preincubated for 30 min at 37°C with CD73.

Resulted data were subtracted from the background and were normalized with the positive control. The results were plotted and a sigmoidal curve was fitted with "GraphPad Prism 6". The mean $IC_{50} \pm$ SEM from three independent experiments was calculated. For competitive

inhibitors the K_i value was calculated with the Cheng-Prusoff equation (see introduction 1.4, page 17).

2.2.6 Enzyme titration using cell lines MDA-MB-231 and 4T1.2

MDA-MB-231 and 4T1.2 cells were grown in their specific culture medium cells in 175 cm^2 culture flasks to 80-90% cell confluence. After detachment by trypsin/EDTA, 195 to 5x10^4 cells per well for MDA-MB-231 and 49 to 5x10^4 cells per well for 4T1.2 were transferred to the wells of a 96-well-plate (Nunclon^{TM} Delta Surface, Thermo Fischer Scientific, Waltham, MA, USA) and incubated for 48 h at 37°C with 5% CO$_2$. After the incubation time, culture medium was removed and cells were washed three times with 100 µl of assay reaction buffer (25 mM Tris, 140 mM sodium chloride, 2 mM magnesium chloride, 1 mM calcium chloride, pH 7.4). After addition of 110 µl of assay reaction buffer to the wells, the reaction mixture was preincubated for 30 min at 37°C in a shaking plate incubator and the enzymatic reaction was initiated by the addition of 10 µl of [2,8-^{3}H]AMP (specific activity: 20 mCi/mmol), American Radio-labeled Chemicals, MO, USA, distributed by Hartman Analytic, Braunschweig, Germany) resulting in a final substrate concentration of 5 µM AMP. After the reaction, which was performed for 20 min at 37°C in a shaking plate incubator, 100 µl volume of each well were transferred to 4 ml plastic test tube to enablable precipitation and filtration procedures. These steps of the experiment were performed as described above in 2.2.3, page 51.

2.2.7 Ecto-5′-nucleotidase radioassay using MDA-MB-231 and 4T1.2 cells

To analyze the inhibition of CD73-targeting antibodies, 1000 cells for MDA-MB-231 or 500 cells for 4T1.2 were transferred to each well of a 96-well-plate and incubated for 48 h at 37°C with 5% CO$_2$. Removal of culture medium and washing steps were performed as described above. Antibodies were tested by measuring full concentration-inhibition curves in a concentration range of 30 µg/ml to 0.003 µg/ml or at a single concentration of 100 µg/ml. Antibody preparations were diluted under sterile conditions in assay reaction buffer. After addition of 10 µl of the antibody solution to 100 µl (final volume of 110 µl) of assay reaction buffer, the reaction mixture was preincubated for 30 min at 37°C in a shaking plate incubator and further proceeded as described above in 2.2.6, page 53. Controls and data analysis were performed as described in 2.2.5, page 52.

In a modified experimental setup, for the analysis of the antibody TY/23 at a single concentration of 100 µg/ml, the preincubation time was increased to 5 h; one time in reaction buffer and the other time in cell culture medium before the washing step and before initiating enzymatic reactions.

2.3 Optimization of malachite green assay for high-throughput-screening

2.3.1 Optimization of malachite green assay

2.3.1.1 Overview

Reactions were performed in assay buffer consisting of 25 mM Tris, 2 mM $MgCl_2$, 1 mM $CaCl_2$, 140 mM NaCl, pH 7.4. The reaction volume was set to 50 µl. For each reaction, 40 µl reaction buffer including AMP (final concentration 30 µM) were transferred to a well of a 96-well half-area microplate (clear, Greiner Bio-One, Kremsmünster, Austria) and preincubated for 5 min at 37°C (300 rpm). Afterwards, the reaction was initiated by adding 10 µl of 5-fold enzyme solution (assay buffer added with 0.01% BSA) to each test well (final amount 25 ng). The mixture was incubated for 10 min at 37°C (300 rpm). To stop the reaction and enable phosphate detection, 20 µl of detection reagent I (final concentration 120 µM malachite green oxalate, 0.06% polyvinyl alcohol) and 30 µl of the detection reagent II (final concentration: 6 mM ammonium heptamolybdate, 0.45 M H_2SO_4) were added. The plate was incubated at ambient temperature for 20 min at 500 rpm. The absorption of the colorimetric complex was analyzed at 600 nm (PHERAstar FS, BMG Labtech, Ortenberg, Germany).

2.3.1.2 Phosphate calibration curve

To determine the sensitivity of the test system, the absorbance at 600 nm was blotted against the phosphate concentration in a concentration range from 1 to 50 µM. The assay was performed as described above, but without the addition of the enzyme. The results of three independent experiments were pooled and fitted to a linear regression curve using "GraphPad Prism 7" program (GraphPad Software, La Jolla, CA, USA). The limit of detection (LOD) of the test system was determined according to equation listed in the introduction 1.6, page 37.

2.3.1.3 Optimization of detection wavelength

To determine the optimal detection wavelength an absorbance spectra was recorded. For this purpose, 50 µl of assay buffer with, and without 10 µM of phosphate were transferred to the wells of a 96-well plate and treated as described above. The absorption spectra of each sample was recorded in a range from 400 to 800 nm. To obtain difference spectra, absorbance values of the sample with phosphate were subtracted with the related values obtained without phosphate and plotted with "GraphPad Prism 7".

2.3.1.4 Optimization of BSA concentration

To determine the optimal concentration of BSA for stabilization of enzymatic activity and not influencing the absorbance readout, two experiments were performed: First, a logarithmic dilution series of BSA in the concentration range from 0.00002 to 0.2% BSA was generated in assay buffer, once with 10 µM phosphate and once without. The difference spectra was generated as described in the previous section. Second, a logarithmic dilution series of BSA in the range of 0.0001 to 0.01% was added to a five-fold enzyme stock solution and stored at 4°C. At different time points ($t_0 = 0$ min, $t_1 = 240$ min, $t_2 = 1350$ min), 10 µl of the enzyme solutions were used to facilitate the enzymatic reaction as described above in 2.3.1.1, page 54. Results were normalized to the corresponding absorbance value of t_0, plotted and an exponential decay was fitted with "GraphPad Prism 7".

2.3.1.5 Enzyme titration

For the determination of the optimal enzyme concentration, an enzyme titration was performed. Eleven different enzyme concentrations between 0.06 and 2.0 µg/ml were incubated with a substrate concentration of 30 µM AMP for 10 min at 37°C. The readout of the reaction was performed as described above. Three separate assays were performed, each in triplicates. Absorbance values were converted to phosphate concentrations with the equation resulted from the phosphate calibration curve.

2.3.1.6 Determination of apparent K_M value

For the determination of the apparent Michaelis–Menten constant (K_M), twelve different substrate concentrations of AMP between 0.5 and 1000 µM were used. The enzymatic reaction was carried out using a final amount of 25 ng ecto-5′-nucleotidase. Reactions were performed as described above. Three separate assays were performed, each in duplicates.

K_M and V_{max} values were calculated by fitting of the Michaelis–Menten equation with "GraphPad Prism 7".

2.3.2 Assay validation

For the validation of the newly developed malachite green assay, the absorbance of a series of positive and negative controls was analyzed. In the negative control, 50 µl of assay buffer including AMP (final concentration 30 µM) were used. For the positive controls, 10 µl of enzymatic solution (final amount: 25 ng) were mixed with 40 µl of assay buffer including AMP (final concentration 30 µM). The assay was performed as described above. Three independent experiments were performed. For each of the controls 24 values were generated. To quantify the assay, the Z′-factor[133] and the signal-to-noise ratio (SNR) were calculated according to the equations listed in the introduction 1.6, page 37.

2.3.3 Inhibition assay

For further validation of the assay, the standard inhibitor AOPCP was analyzed under explored assay conditions. Therefore, 10 µl of aqueous inhibitor solution was added to 30 µl of assay buffer included AMP (final concentration 30 µM). The mixture was preincubated for 5 min at 37°C and reactions were initiated by the addition of 10 µl of the enzyme (final amount: 25 ng). The readout reaction was performed as described above. To obtain full concentration-response curves, twelve inhibitor concentrations were used in the range from 0.0003 to 100 µM. Three separate inhibition assays were performed, each in triplicates. To obtain the IC_{50} value the concentration–response curves were fitted using the sigmoidal concentration–response curve of "GraphPad Prism 7" software. To calculate the corresponding K_i value of the competitive inhibitor AOPCP the Cheng-Prusoff equation[92] (see introduction 1.6, page 37) was used.

2.3.4 Automatization for screening

The assay was adapted to a liquid handling workstation (Biomek, NXMC 96-well head/pod and NXspan 8, Beckman Coulter, Brea, CA, USA), which is controlled by SAMI Runtime software (Beckman Coulter, Brea, CA, USA). Pipette tips (Biomek, P50-tips, Beckman Coulter, Brea, CA, USA), microplates (96-well half-area microplates, Greiner Bio-One, Kremsmünster, Austria) and compound plates (96-Well V-bottom Microplates, Greiner Bio-One, Kremsmünster, Austria) with fivefold concentration of test compounds in column 2 to

11 and controls in 1 and 12 (final concentration 10 µM (2% DMSO)) were stored in the labware hotel (Cytomat hotel, Thermo Fisher Scientific, Waltham MA, USA). Assay buffer included AMP (final concentration 30 µM), malachite green and ammonium molybdate solutions were stored in upside down orientated lids of pipette tip boxes at the deck of the NXMC. Ecto-5′-nucleotidase with 0.01% BSA was supplied in a 96-well plate (Well V-bottom Microplates, Greiner Bio-One, Kremsmünster, Austria) in column 2 to 11. In addition, 4 wells of column 1 and 12 also contained ecto-5′-nucleotidase as positive control and 4 wells without the enzyme as negative control. Controls were arrayed alternately on both sites to reduce edge and plate-effects.[163] The plates were stored on the deck of NXMC module and cooled to 4°C (CPAC Ultraflat HT 2-TEC, INHECO Industrial Heating & Cooling GmbH, Planegg, Germany). Cover lids, which prevent evaporation, were placed on the deck of NXspan 8.

Reactions were performed in a total volume of 50 µl. First, 30 µl reaction buffer with AMP were transferred to each well of the reaction plate. 10 µl of test substances/controls were added from the compound plate. After this step, the absorbance was spectroscopically measured (Pherastar FS, BMG Labtech, Ortenberg, Germany) at 600 nm to analyze, the self-absorbance of the compounds at this wavelength. Afterwards, the plate was lidded and preincubated (Incubator Shaker, INHECO Industrial Heating & Cooling GmbH, Planegg, Germany) to 37°C for 5 minutes. Enzymatic reactions were started by the addition of 10 µl of ecto-5′-nucleotidase followed by further incubation at 37°C for 10 min at 300 rpm. For phosphate detection, 30 µl of ammonium molybdate and 20 µl of malachite green solution were added. After an incubation step of 20 min at ambient temperature (500 rpm) the formed phosphomolybdate-malachite green complex was detected at 600 nm (PHERAstar FS, BMG Labtech, Ortenberg, Germany). For the validation of the assay performed by the liquid handling station, the Z′-factor and the signal-to-noise-ratio was distinguished three times with 48 positive and 48 negative controls. For the analysis of screening results, the percentage inhibition was calculated using the equation listed in introduction 1.6, page 37.

2.3.5 Determination of binding mode of small molecules

The enzymatic activity was measured with different substrate concentrations in the range of 1.95 to 1000 µM AMP. For each inhibitor three different curves were proceeded; 1) without inhibitor, 2) inhibitor concentration half of the IC_{50} value and 3) inhibitor concentration double of the IC_{50} value. Inhibitors and substrate were diluted in assay reaction buffer. As

duplicates, 20 µl assay reaction buffer, 10 µl of the inhibitor and 10 µl of CD73 (final amount: 25 ng) were transferred to half-area microplates (clear, Greiner Bio One). After a preincubation of 5 min at 37°C (300 rpm), the reaction was initiated by the different dilutions of AMP and further incubated at 37°C for 20 min (300 rpm). Readout reaction and spectroscopic analysis was performed as described above (2.3.1.1, page 54). Blank values of different AMP concentrations were subtracted from measured absorption values and conversion rates (µmol phosphate/min/mg protein) were calculated with use of the phosphate calibration curve (Figure 53). The mean conversion rate of three independent experiments wasplotted against the substrate concentration and the Michaelis-Menten saturation curve was fitted with "GraphPad Prism 7". Based on distinguished K_M- and V_{max} value from the non-linear fit, a Lineweaver–Burk plot was created for better illustration of binding modes (The software "GraphPad Prism 7" explains, why a double reciprocal plotting of measured values and linear regression for the creation of this plot is error-prone. Therefore, Prism recommends to create the lines for the Lineweaver–Burk plot with calculated values of the non-linear fit of the Michaelis–Menten kinetic (slope: K_M/V_{max} and x-axis intercept: $-1/K_M$).[91]

3 Technical Equipment and Materials

3.1 Technical Equipment

Centrifuges

Allegra X-30 and Avanti J-20XP (Beckman Coulter, Brea, CA, USA); ROTOFIX 32 and Mikro 200R (Hettich, Kirchlengern, Germany)

Counting chamber

Neubauer counting chamber (Paul Marienfeld GmbH & Co.KG, Lauda Königshofen, Germany)

Electrophoresis and Western blot

Cawomat 200 IR (CAWO Photochemisches Werk, Schrobenhausen, Germany); ChemiDoc MP Imaging System, PowerPac 300, PowerPac Universal^{TM}, Mini-PROTEAN$^®$ 3 Cell, Mini-Trans Blot cell$^®$ (Bio-Rad Laboratories, Hercules, CA, USA); Transilluminator UVStar (Analytik Jena AG, Jena, Germany)

Freezing container

Mr. Frosty™ Freezing Container, Thermo Fischer Scientific, Waltham, MA, USA

Incubators

CO_2 Incubator (Binder, Tuttlingen, Germany); CO_2 Incubator ICO150med (Memmert, Schwabach, Germany); New Brunswick Innova 4200 Incubator Shaker (Eppendorf, Hamburg, Germany)

Laminar airflow cabinets

Bioair Safeflow 1.2 (BIOAIR, Siziano, Italy); Microflow Biological Safety Cabinet (BioQuell, Hampshire, United Kingdom); Safe 2020 (Thermo Fisher Scientific, Waltham MA, USA)

Material

Liquid handling workstation

Biomek, NXMC 96-well head/pod, NXspan 8 (Beckman Coulter, Brea, CA, USA); CPAC Ultraflat HT 2-TEC Incubator Shaker (INHECO Industrial Heating & Cooling GmbH, Planegg, Germany); Cytomat Hotel (Thermo Fischer Scientific, Waltham, MA, USA) PF3400 SCARA robot (Precise Automation, Fremont, CA, USA)

Microscopes

Axiovert 25 (Carl Zeiss, Jena, Germany); Wilovert 30 (Helmut Hund, Wetzler, Germany)

Pipettes

Accu-jet® pro (Brand, Wertheim, Germany); Eppendorf Research® plus (2.5, 10, 100, 200 and 1000 µl); Multichannel Xplore (100 µl 12 channels); Multipette® (M4, E3/E3x and plus; Eppendorf, Hamburg, Germany)

pH meter

FiveEasy™ pH/mV-meter FE20 (Mettler Toledo, Columbus, OH, USA)

Plate sealer

Fluidx X-SEAL Thermal Microplate Sealer (HTA Singulex, Brescia, Italy)

Scales

CPA 2250 (Satorius AG, Göttingen, Germany); PCB 2000-1 and 440-47N (Kern & Sohn, Balingen, Germany); SBC 42 (Scaltec Instruments, Heiligenstadt, Germany); XA 205 Dual Range (Mettler Toledo, Columbus, OH, USA)

Scintillation counter

TRICARB 2900 and 2810 TR (PerkinElmer, Waltham, MA, USA)

Shaker and heating devices

ARE Heating Magnetic Stirrers (VELP Scientifica, Usmate, Italy); End-over-end mixer (Kisker Biotech, Steinfurt, Germany); Grant Instruments™ Microplate-Thermo-Shaker PHMP-4 (Thermo Fisher Scientific, Waltham MA, USA); KühlThermoMixer MKR23 (HLC Biotech, Bovenden, Germany); MS1 Minishaker, Ultraturrax and Vortexer Genius 3

(IKA-Labortechnik, Staufen, Germany); Thermomixer Comfort (Eppendorf, Hamburg, Germany); Vortex-Schüttler vv3 and Advanced Digital Shaker (VWR, Radnor, PA, USA)

Software

ChemDraw Professional 15.0 (PerkinElmer, Waltham, MA, USA); Citavi 6 (Swiss Academic Software, Wädenswil, Switzerland); Clone Manager 9 (Scientific & Educational Software, Denver, CO, USA); GraphPad Prism 6 and 7 program (GraphPad Software, La Jolla, USA); Microsoft Office 2013 - Professional Plus (Microsoft Corporation, Redmond, WA, USA); SAMI Runtime software (Beckman Coulter, Brea, CA, USA)

UV/VIS-Spectrometer

Colibri Microvolume Spectrometer (Titertek Berthold, Pforzheim, Germany); DU$^®$ 530 (Beckman Coulter, Brea, CA, USA); PHERAstar FS (BMG Labtech, Ortenberg, Germany)

Water baths

1083 (Gesellschaft für Labortechnik, Burgwedel, Germany); Sonorex Digitec DT100H (Bandelin, Berlin, Germany)

3.2   Consumables

Assay plates

96-well-plate (Nunclon^{TM} Delta Surface, Thermo Fischer Scientific, Waltham, MA, USA); half-area microplates clear and 96-well V-bottom Microplates (Greiner Bio-One, Kremsmünster, Austria)

Cell culture

Cell Scraper (BD Bioscience, Bedford, Ma, USA), CryoPure 1.8 ml, TC Dish 150 cm^2, culture flasks TC Flask T25, T75, T175, Standard (Sarstedt, Nümbrecht, Germany)

Filters for radioactive assay

GF/B glass fiber filters (WhatmanTM GE Healthcare, Chicago, IL, USA)

Material

Pipettes and pipette tips

Biosphere® Filter Tip 20, 200 and 1000 µl, pipette tips 20, 200 and 1000 µl, serological pipettes 5, 10, 20 and 50 ml (Sarstedt, Nümbrecht, Germany); Combitips advanced® 1, 2.5, 5 ml (Eppendorf, Hamburg, Germany); Ritips® professional 0.5, 1 and 5 ml (Ritter Medical, Schwabmünchen, Germany); P50 Biomek Sterile 50 µl-Tips (Beckman Coulter, Brea, CA, USA); Sterile aerosol pipette tips 10 µl (Bioenzym Scientific, Hessisch Oldendorf, Germany)

Protein purification consumables

Amicon® Ultra-15 (10 kDa cut-off, Merck Millipore, Burlington, MA, USA); dialysis tube Membra-Cel™, 14 kDa cut-off, 250 mm x 44 mm x 0.02 mm, Carl Roth, Germany); HisPurTM Ni2+ NTA spin columns, #: 88226 (Thermo Fischer Scientific, Waltham, MA, USA)

Reaction tubes and cuvettes

0.5, 1.5, and 2 ml reaction tubes Biosphere® SafeSeal 1.5 and 0.5 reaction tubes, Multiply®-Pro 0.2 and 0.5 ml reaction tubes (Sarstedt, Nümbrecht, Germany); 5 ml reaction tubes; Ratiolab® halfmicro-cuvettes (Ratiolab Dreieich, Germany); Falcon® 15 and 50 ml High Clarity PP Centrifuge Tube (Corning, Corning, NY, USA); Scintillation vial, Midi-Vial, 8 ml (PerkinElmer, Waltham, MA, USA);

Western blot consumables

CL-x Posure™ Film 20 x 25 cm (Thermo Fischer Scientific, Waltham, MA, USA); Gel-blotting-paper (Carl Roth, Karlsruhe, Germany); Nitrocellulose blotting membrane Amershan™ Protan™ 0.45 µm (GE Healthcare, Chicago, IL, USA)

3.3   Buffers and recipes

SDS-PAGE and western blot

Cathode buffer: 25 mM Tris-base, 192 mM glycine, 0.1 % SDS, pH 8.3; stacking-gel buffer: 0.25 M Tris-base, 0.4 % SDS, pH 6.8; running-gel buffer: 0.75 M Tris-base, 0.4 % SDS, pH 8.8; TBST buffer: 20 mM Tris, 137 mM NaCl, 0.1% Tween® 20, pH 7.6; MTBST buffer: 5% powdered milk in TBST-buffer; transfer buffer: 2.5 mM Tris-base, 19.2 mM glycine, 20% methanol

SDS-PAGE gels (recipe for two gels (101 x 73 x 1 mm))

6% stacking gel: 2.4 ml Milli-Q water, 1 ml stacking gel buffer, 0.6 ml 30%, acrylamide solution (Rotiphorese® gel 30, Roth), 50 µl of 10% ammonium, persulfate solution, 6 µl *N,N,N′,N′*-Tetramethylethane-1,2-diamine (TEMED 30, Roth)

10% running gel: 5 ml Milli-Q water, 3 ml running gel buffer, 4 ml 30%, acrylamide solution 160 µl 10% ammonium, persulfate solution, 12 µl TEMED 30

3.4 Culture media

Mammalian cell culture

Dulbecco's Modified Eagle Medium, DMEM, #: 41966 and Roswell Park Memorial Institute (RPMI) medium 1640, #: 21875034 (Thermo Fisher Scientific, Waltham, MA, USA)**;** Penicillin-Streptomycin, #: P06-07100, fetal bovine serum and (FBS), #: P30-1502 and Trypsin/EDTA #: P10-022100 (PAN Biotech, Aidenbach, Germany)

Insect cell culture

Insect-XPRESS™ media, #: BE12-730Q (Lonza, Basel, Switzerland)

3.5 Test compounds

Table 3. Test compounds, compound libraries and tested antibodies.

Test compound or name of compound library	Information
Bispecific antibodies	Produced in the research group of Professor Ditzel (University of Southern Denmark, Denmark) by Odd Lilleng Gammelgaard
ChemBridge library	From Professor Herdewijn (University of Leuven, Netherlands)
ChemDiv library	From Professor Herdewijn (University of Leuven, Netherlands)
Chromenone library	Chromenones synthesized in the research group of Professor Müller by Dr. Anne Meyer
Fragment library	In-house library; synthesized in the research group of Professor Müller
Herdewijn library	Internal library of Prof. Dr Herdewijn (University of Leuven, Netherlands)
Interbioscreen library	From Professor Herdewijn (University of Leuven, Netherlands)
Internal approved drug library	Commercially available active substances[164]
KD library	Compound Synthesized in the research group of Professor Kieć-Kononowicz (Jagiellonian University, Kraków, Poland)
Nucleotide derivatives	Synthesized in the research group of Professor Müller by Sanjay Bhattarai (SB-compounds), Dr. Stephanie Federico (SF-compounds), Georg Rolshoven (GR-compounds) and Constanze Schmies (CS-compounds). Synthesized in the research group of Professor Jacobsen (National Institutes of Health, Bethesda, USA) by Dr. Anna Junker (MRS-compounds). Synthesized in the research group of Dr. Anna Junker (University of Münster, Germany) by Clemens Dobelmann (JMS-compounds). Synthesized in the research group of Professor Bilha Fisher (University of Bar-lla, Israel by Molhm Nassir) (MN-compounds). Synthesized by Petra Doláková (PD-compounds) in the Institute for Organic Chemistry and Biochemistry Prague, Czech Republic
Proschak library	From Professor Proschak (Goethe University, Frankfurt am Main, German)
Stark library	From Professor Stark (Heinrich-Heine-University, Düsseldorf, Germany)
Sulfonamide derivatives	Synthesized in the research group of Professor Müller by Dr. Thanigaimalai Pillaiyar, Dr. Marianne Freundlieb and others
Tocris library	Structural diverse and address more than 300 pharmacological targets (distributed by TOCRIS (Bristol, United Kingdom)[165, 166]
Xanthine library	Xanthine derivatives synthesized in the research group of Professor Müller or cooperation partners

3.6 Chemicals

AB vector (San Diego, CA, USA)

Baculovirus genomic ProEasy™ vector DNA

Acros Organics (Geel, Belgium)

Polyvinyl alcohol (98% hydrolyzed, average MW 16.000)

American Radio-labeled Chemicals (St. Louis, MO, USA)

[2,8-^{3}H]AMP (specific activity: 20 Ci/mmol, concentration: 1 mCi/mmol, solvent: ethanol:water (1:1)) distributed by Hartmann Analytic, Braunschweig, Germany)

AppliChem (Darmstadt, Germany)

Bromophenol blue sodium salt; Tween$^®$ 20

BIOLOG Life Science Institute (Bremen, Germany)

Adenosine 5′-O-(α,β-methylene)diphosphate (AMPCP, AOPCP)

Biomol (Hamburg, Germany)

Gentamycin sulfate

Carl ROTH (Karlsruhe, Germany)

4-(2-hydroxyethyl) piperazine-1-ethanesulfonic acid (Hepes); D(+)-Sucrose; dimethyl sulfoxide (DMSO); Lanthanum(III) chloride heptahydrate; powdered milk; Rotiphorese$^®$ NF-Acrylamid/Bis-Solution 30 % (29:1); sodium chloride; sodium dihydrogen phosphate monohydrate; tetramethylethylendiamin (TEMED); tris(hydroxymethyl)aminomethane (Tris)

Grüsing GmbH (Filsum, Germany)

Sodium acetate

Merck KGaA (Darmstadt, Germany)

adenosine-5′-monophosphate; sulfuric acid; Folin-Ciocalteu's phenol reagent; ethanol

PerkinElmer (PerkinElmer, Waltham, MA, USA)

ULTIMA Gold XR

Sigma-Aldrich (St. Louis, MO, USA)

ß-Mercaptoethanol; ammonium persulfate (APS); albumin from bovine serum (BSA); calcium chloride dihydrate, magnesium chloride, ammonium molybdate tetrahydrate (Bio Ultra); glycerol; malachite green oxalate; protease inhibitor cocktail (#: P8340); sodium hydroxide

Material

Tokyo Chemical Industry (Tokyo, Japan)

Iodoacetamide

Thermo Fisher Scientific

Cellfectin™ II Reagent; His-Tag antibody (#: Ma1 21315-HRP); Protein standard (#: LC560610 - 160 kDa, BenchMark™)

University of Bonn (Bonn, Germany)

Copper(II) chloride; sodium carbonate

VWR Life Science (Radnor, PA, USA)

Methanol; sodium dodecylsulfate (SDS)

4 Results and Discussion
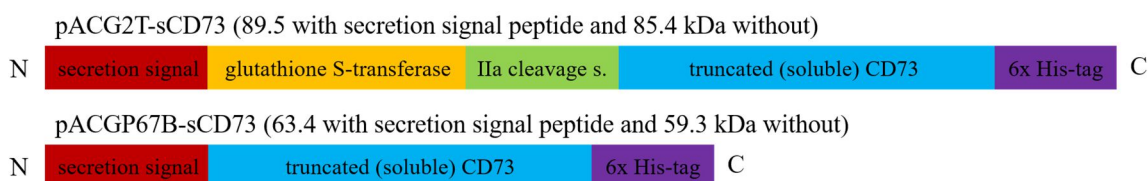
4.1 Various sources of CD73

The determination of ecto-5′-nucleotidase activity is the basis for identification, characterization and further development of compounds which modulate its activity, no matter, those be inhibitors or activators. The source of CD73 is therefore as important as the used assay system. Rat CD73, was produced by the research group of Professor Zimmermann, and has frequently been used in different assay systems for the successful development of CD73 inhibitors.[24, 94, 167] Human and rat CD73 are similar (87% sequence identity, BLAST algorithm),[168, 169] and the active site only differs in a single amino acid residue. The phenylalanine at position 500 in the human enzyme is replaced by a tyrosine in rat.[94, 170] Inhibitors, developed with the use of rat CD73 had shown comparable or higher potency for the human CD73.[24, 94, 167] In the present study, rat CD73 was mainly used for characterization of inhibitors by measuring their potencies and mode of inhibition. Furthermore, it was used for the identification of new scaffolds by automated screening of compound libraries. Although the properties of human and rat CD73 are similar, most potent compounds were also analyzed at the human CD73. For this purpose, human soluble CD73 protein was recombinantly produced, purified and characterized. Both, the rat and human variety of the recombinant enzyme had tags for expression and purification strategies and are truncated soluble versions instead of the GPI-anchored, membrane-bound bound CD73 as it is present in the cell. To analyze the developed inhibitors in a less artificial environment, membrane preparations of the CD73-overexpressing triple-negative breast cancer cell line MDA-MB-231 were produced. The results of the production of recombinant soluble human CD73 as well as the preparation of the membrane-bound variety of CD73 are discussed in the following chapters.

Results and Discussion

4.1.1 Expression and purification of soluble human ecto-5′-nucleotidase

4.1.1.1 Overview

Prof. Dr. med. Michael Hölzel (Institute of Clinical Chemistry and Clinical Pharmacology, University of Bonn) provided two different vector constructs with cloned CD73. Both vector types (pACG2T and pACGP67B) are suitable for the expression and secretion of the produced fusion protein into the supernatant of baculovirus-infected Sf9 insect cells. The expressed fusion proteins share the secretion signal peptide gp67 at the N-terminus, which is cleaved during transport across the cell membrane and a C-terminal 6x polyhistidine-tag for purification by affinity chromatography (Ni^{2+}-NTA, Figure 28, full protein sequences are provided in the appendix, page 143).

pACG2T-sCD73 (89.5 with secretion signal peptide and 85.4 kDa without)

| N | secretion signal | glutathione S-transferase | IIa cleavage s. | truncated (soluble) CD73 | 6x His-tag | C |

pACGP67B-sCD73 (63.4 with secretion signal peptide and 59.3 kDa without)

| N | secretion signal | truncated (soluble) CD73 | 6x His-tag | C |

Figure 28. Schematic representation of the fusion proteins (N- and C-: N- and C-terminus; IIa: thrombin cleavage site).

In addition, the fusion proteins encoded by pACG2T provide glutathione S-transferase, which is fused between the secretion signal and the truncated N-terminus of CD73 with a thrombin cleavage site. This enables purification with glutathione sepharose affinity chromatography and cleavage of it after purification. The calculated molecular weight for the matured fusion protein (without secretion signal peptide) of pACG2T-sCD73 and for pACGP67B-sC73 is 85.4 and 59.3 kDa, respectively. First, both vector constructs were transfected into Sf9 cells and both viruses were amplified. The construct which showed higher expression rates was more suitable for purification with the available equipment was selected for expression and purification in larger scales.

4.1.1.2 Transfection and virus amplification

The first signs of a successful virus infection of the Sf9 cells appeared during the second cycle of virus amplification (P2-P3) marked by a reduced proliferation rate of infected cells compared to the control cells. Morphological signs of infected cells, big and irregularly formed cells with increased density as described in the literature[171, 172] were observed from P5 on.

The AMP hydrolysis of the cell supernatants of the virus stocks P7 was analyzed (Figure 29). Results revealed that the supernatant of the CD73 infected cells hydrolyzed AMP and that the control cells didn't show this ability. AMP hydrolysis was inhibited by the selective CD73 inhibitor **AOPCP** indicating that CD73 was responsible for the AMP hydrolysis of the cell supernatant. Thus, the transfection, virus amplification, production of recombinant CD73 proteins and secretion into the cell supernatant were successful.
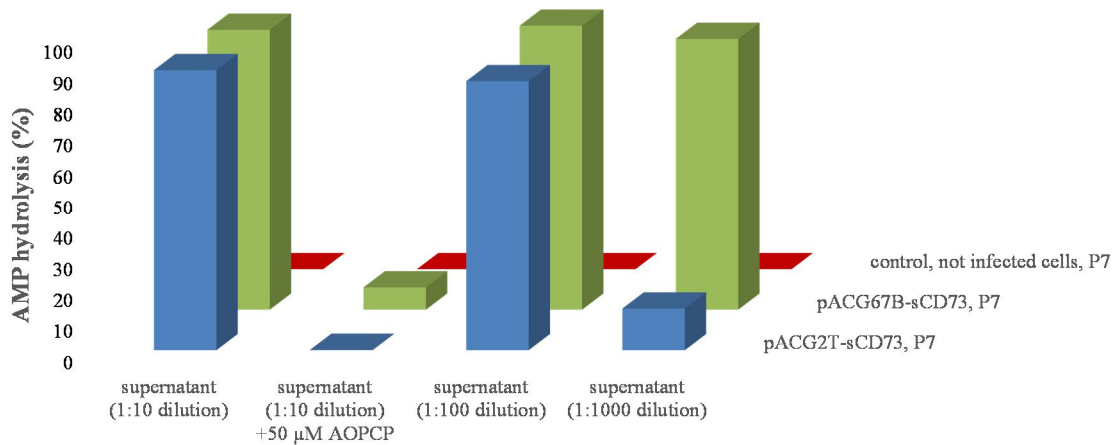
Figure 29. Analysis of AMP hydrolysis of cell supernatants. The supernatant of CD73 vector constructs infected insect cells hydrolyzed AMP. The selective CD73 inhibitor **AOPCP** inhibited this effect; supernatants of the control cells did not show any activity.

The hydrolysis of AMP was analyzed with 1:10, 1:100 and 1:1000 dilutions of the cell supernatant with the radiometric assay system. The measurements of 1:10 and 1:100 dilutions of the supernatants from both constructs showed similar values for AMP hydrolysis, because enzymatic activity of both samples was very high, and the enzymatic reactions were saturated. In contrast, a further dilution step to 1:1000 showed that the cell supernatant from cells infected with construct pACGP67B-sCD73 had a higher activity compared the construct pACG2T-sCD73. This is not surprising since the protein encoded by the vector pACG2T-sCD73 has a size of 85.4 kDa and of vector pACGP67B-sCD73 59.3 kDa. It can be assumed that the cells produced significantly more of a small than of a larger protein. For upscaling the expression of CD73, the vector type (pACGP67B) was selected, because of the higher expression of CD73.

4.1.1.3 Optimization of protein purification

The protein purification was optimized by monitoring the enzyme activity in each step. Figure 30 illustrates the development of the purification strategy over time.
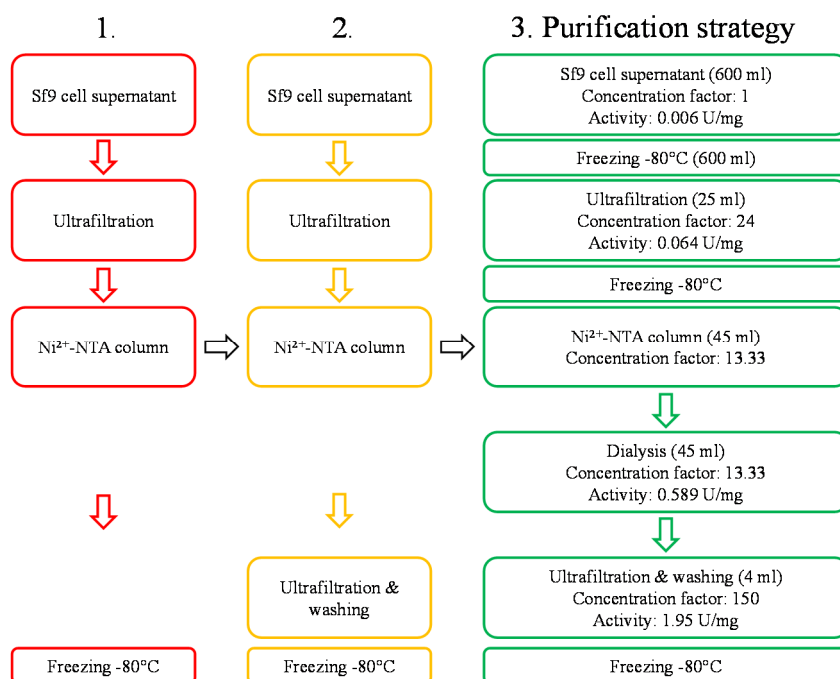

Figure 30. Strategies for the production and purification of human ecto-5′-nucleotidase. The first cycle of purification was performed by ultrafiltration of harvested Sf9 cell supernatant and by affinity chromatography with a Ni^{2+}-NTA column. To concentrate the final protein and to reduce the amount of imidazole and phosphate, an additional step of ultrafiltration and washing was introduced in the second cycle of purification. Since the membrane of the Amicon® was not stable towards the high imidazole concentration, the final procedure of purification was performed with an additional dialysis step followed by ultrafiltration of the protein.

In the first cycle of purification, the whole procedure from harvesting the supernatant until freezing of the pure eluted protein was performed without freezing the samples in between, because freezing and un-freezing in non-optimal buffer conditions might lead to reduction or loss of enzymatic activity.[173] However, it was also analyzed if a freezing step after harvesting the cell supernatant or after ultrafiltration is possible without loss of enzymatic activity. For this purpose, samples were frozen at -80°C, subsequently defrosted and enzymatic activity was recorded and compared to the unfrozen samples. Results showed that it is possible to freeze the protein at both steps with only a slight loss of enzymatic activity (Figure 31). Since later performed purification strategies were more time consuming, it was necessary to interrupt the procedure at both of these steps and freeze the protein to -80°C (Figure 30).
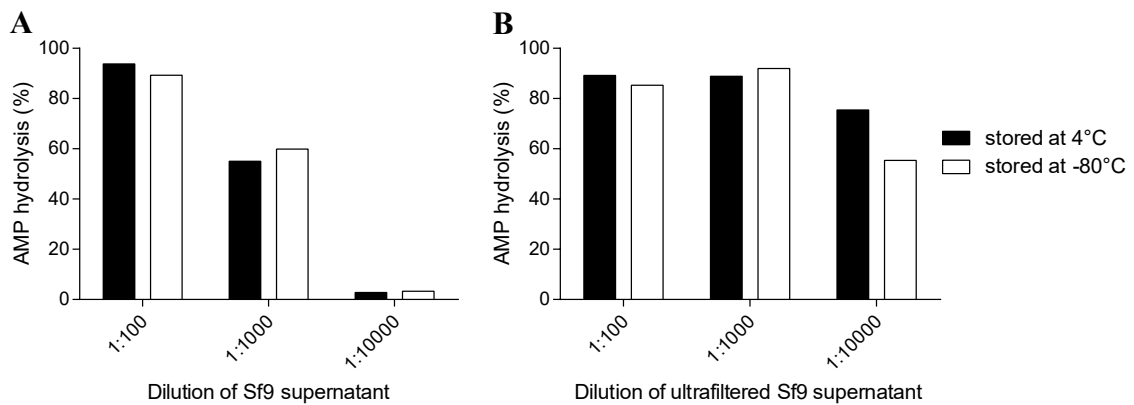
Figure 31. Freezing steps during protein purification. (A) It is possible to freeze the supernatant (A) and ultrafiltered supernatant **(B)** without or, with only negligible loss of enzymatic activity.

The first cycle also proved that the general purification procedure with use of a Ni^{2+}-NTA column worked. The eluted protein was used to investigate the storing conditions for purified human CD73. For this purpose, glycerol was investigated at different temperatures (Figure 32). This analysis revealed that the enzymatic activity is stabilized by directly freezing it to -80°C or storage with 50% glycerol at -20 or 4°C. Therefore, all further purified proteins were frozen to -80°C. For future application of the enzyme, it would be possible to use these aliquots directly or mix them 1:1 with storing buffer (f.c. 25 mM Tris, 4 mM iodacetamide and 50% glycerol) for short term use. This buffer also successfully stabilized the enzymatic activity of rat CD73.
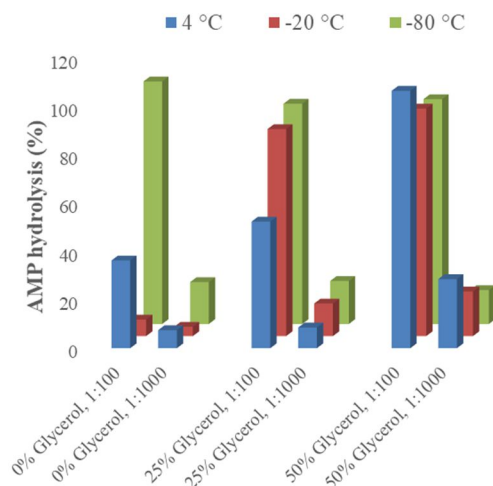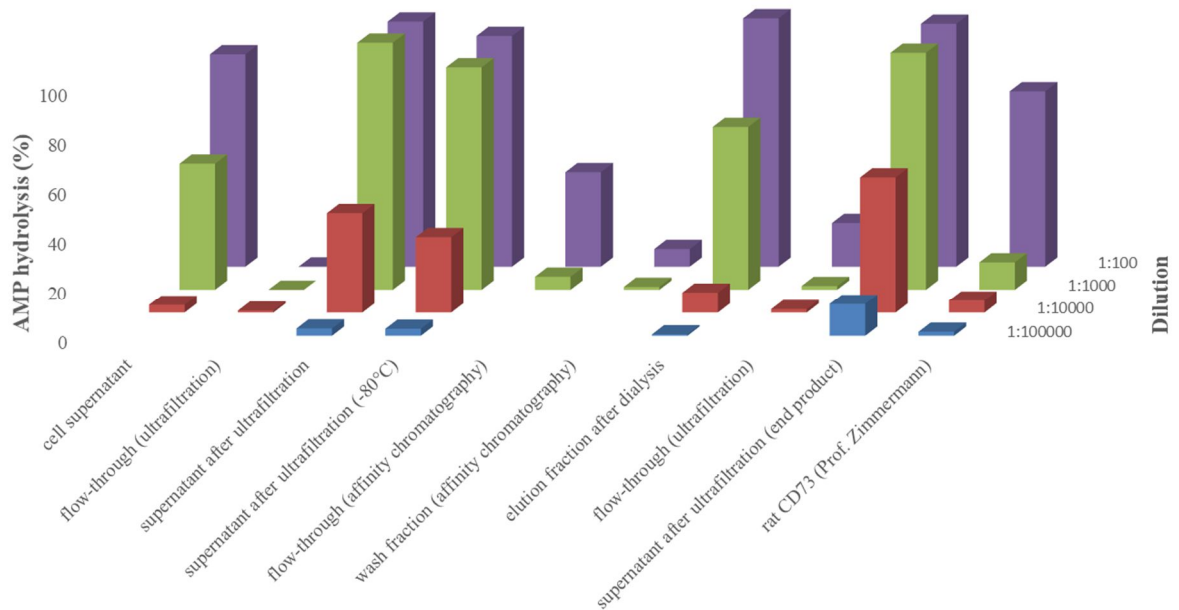

Figure 32. Analysis of AMP hydrolysis in elution fractions. The freezing of eluted human CD73 to -80°C or the addition of 50% glycerol stabilized enzymatic activity independent of the investigated storing temperatures.

Results and Discussion

In the second optimization step, proteins eluted from the column were pooled and again ultrafiltered to increase the protein concentration. In addition, the concentrated protein was washed three times with Tris buffer to remove imidazole and phosphate. In this case, the removal of phosphate plays a special role, because the enzyme solution should also be used in the malachite green assay, and phosphate contaminations would raise the background signal. However, it was found that the ultrafiltration membrane was not stable against the high imidazole concentration of 250 mM. This problem was found by detecting high absorption values of the solution at 280 nm. The user manual of the Amicon® recommends imidazole concentrations less than 100 mM.[174] Thus, for the third and final purification strategy, an additional dialysis step was introduced to reduce the imidazole concentration before ultrafiltration of the pooled elution fractions (Figure 30).

The monitored enzyme activities of the final protein purification are illustrated as percent of AMP hydrolysis in Figure 33. The supernatant of infected cells showed significant hydrolysis of AMP to adenosine in the radioassay. After all, the supernatant converted more than 50% of the substrate at a dilution of 1:100. Interesting in this context is the focus on specific activity. The specific activity relates the measured activity to the protein concentration as illustrated in Figure 34. In addition to the secreted human CD73, the supernatant of the cells contains further proteins and especially amino acids of the culture medium. Therefore, it is not surprising that a high protein concentration of 14.2 mg/ml was measured and that the resulting specific activity was therefore with 0.006 U/mg protein rather low. The 600 ml of cell supernatant were concentrated to 25 ml with ultrafiltration. As expected, the flow-through of the filtration process with a 10 kDa cutoff showed no activity. The ability to hydrolyze AMP was increased in the supernatant (Figure 33) and also the specific activity (Figure 34), since many small proteins and free amino acids were no longer present in the supernatant during filtration. The subsequent freezing of the samples to -80°C and thawing showed, as already described above, only a slight loss of enzymatic activity of about 10%.

**Figure 33. Analysis of AMP hydrolysis during protein purification.**

Comparing this activity of the preparation with the activities of the pooled elution fractions after the affinity chromatography, it is found that the activity was dropped by the half, and that also the specific activity was just slightly increased. This is probably due to the fact that the elution volume was twice as large as the sample volume before chromatography, and that the elution buffer's pH value and high imidazole and salt concentration might affect a proper enzymatic reaction. In this context, the increase in substrate hydrolysis and specific activity after the dialysis is interesting and suggests that an exchange against Tris buffer with a pH 7.4 leads to more optimal reaction conditions, or that the activity of misfolded and thus inactive enzyme was restored. Anyway, the further ultrafiltration reduced the volume to 4 ml. As expected, the AMP hydrolysis increased (Figure 33), but unexpectedly also the specific activity. The formation of protein aggregates was observed during ultrafiltration. After the filtration, they were separated from the solution by centrifugation. It can be speculated that the removal of these inactive enzymes reduced the protein concentration and thus increased the specific enzymatic activity. Around 4 ml of soluble human CD73 with a concentration of 0.7 mg/ml with a specific activity of 1.95 U/mg were produced.

Results and Discussion
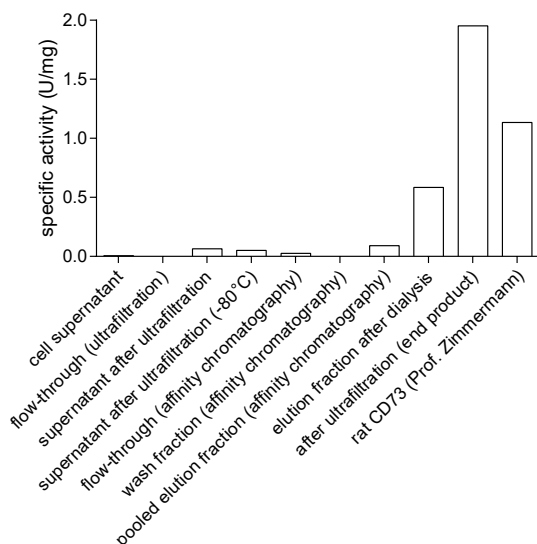
Figure 34. Analysis of specific enzymatic activity during protein purification. The analysis of the enzymatic activity in relation to the protein concentration revealed that the elution fraction and the further ultrafiltered elution fraction showed high specific activity.

The identity of the presumed human CD73 protein was clarified by a Western blot analysis (Figure 35). At a molecular weight of about 60 kDa, the polyhistidine tag-specific antibody detected the expressed fusion protein (calculated molecular weight: 59.3 kDa). It was well detected for 1 µg and weak for 0.1 µg of the purified protein, even weaker in 20 µg of the cell supernatant.
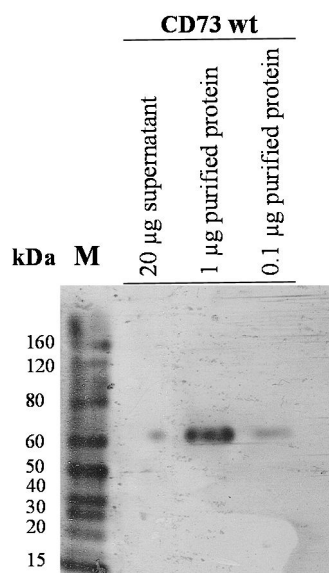
Figure 35. Western blot analysis of human CD73. Detection of His-tagged CD73 by His-tag antibody at around 60 kDa (calculated molecular weight 59.3 kDa; illumination time: 1 min, M: BenchMark™ His-tagged Protein Standard).

4.1.2 Membrane preparations

Many human tumor cell lines overexpress CD73, and membrane preparation of these cells can be used for analyzing CD73 modulating substances. Human CD73-containing membrane preparations are, in contrast to recombinantly expressed enzymes, less artificial. The enzyme is not truncated or has additional amino acid sequences such as the secretion signal or a poly-histidine tag like the human recombinantly expressed one. Furthermore, it is attached to the membrane, is present as a dimer and has the natural post-translational modifications (PTMs), which all might affect proper inhibitor binding and inhibitory potency. The cell line MDA-MB-231 serves as an *in vitro* system for triple-negative breast cancer and had previously been used for the development of therapeutic antibodies against CD73 (see introduction 1.3.2, page 15).[86, 87, 175–177] Thus, this cell line was selected for the determination of potential inhibitors. MDA-MB-231 membranes were prepared yielding 2 ml of membrane suspension with a protein concentration of 1.23 mg/ml.

4.1.3 Characterization of various sources of CD73 using the radioassay

The enzymatic activity of different types of CD73, namely recombinantly produced rat and human CD73, and the membrane fractions of the cell line MDA-MB-231, were analyzed in the radioassay. Therefore, the Michaelis-Menten kinetics were recorded for the different preparations of CD73 (Figure 36). The Michaelis-Menten constant (K_M value) was measured to be 53.0 µM for the rat enzyme, while for the human recombinantly produced enzyme 17.0 µM, and for the membrane-bound form of the enzyme 14.8 µM were measured. These data are well in line with the literature data for CD73.[43, 155, 156] The same rat enzyme had been tested in a previous study in the same assay system providing a K_M value of 59 µM.[151] In measurements where AMP analogs were tested as inhibitors against both enzymes, it was found that inhibitors are in general two to three times more potent at the human CD73 than on the rat enzyme.[94] The results of the K_M determination reflected these findings, because also AMP binds with a three times higher affinity to human CD73.

Regarding the V_{max} value it needs to be mentioned, that the values for the recombinantly produced and purified ecto-5′-nucleotidase of rat and human CD73 are higher (rat: 2.14 ± 0.06; human: 2.51 ± 0.21 µmol/min/mg) compared to the CD73 activity of the membrane preparation (0.111 ± 0.004 µmol/min/mg). The maximal velocity is calculated considering the total protein concentration. Since the membrane fraction contains besides CD73 many different membrane proteins, the maximal velocity is much lower compared to

the recombinantly produced and purified enzymes. With the assumption that the recombinant enzymes are pure and functional and that all proteins in the membrane fraction share the same size, it can be estimated that every twentieth membrane protein in the used triple-negative breast cancer cell line is CD73. This, demonstrates the very concentration of CD73 in this cancer cell line.
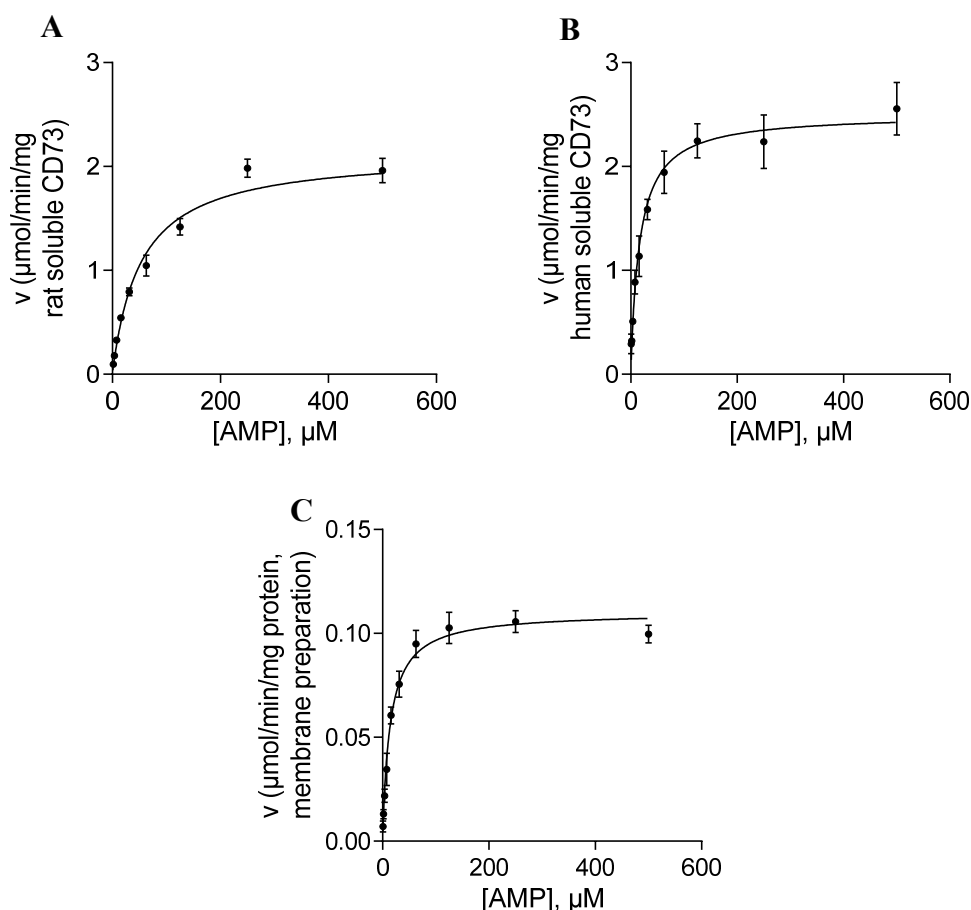
Figure 36. Michaelis-Menten kinetics of CD73. (A) Determination of kinetic parameters of soluble rat CD73 (K_M: 53.0 ± 4.1 µM and V_{max}: 2.14 ± 0.06 µmol/min/mg). **(B)** Determination of kinetic parameters of human soluble CD73 (K_M: 17.0 ± 2.1 and V_{max}: 2.51 ± 0.21 µmol/min/mg). **(C)** Determination of kinetic parameters of human membrane-bound CD73 utilizing a membrane preparation of MDA-MB-231 (K_M: 14.8 ± 2.1 µM and V_{max}: 0.111 ± 0.004 µmol/min/mg). Data points are means ± SEM from at least three separate experiments performed in duplicates.

Comparison with the literature is rather difficult, because in most cases, the expression levels are measured on the mRNA level, or total protein concentration is provided, but in this case just the membrane fraction was analyzed. However, this sensitive method could be used to compare the CD73 activity of different tissues or cancer cell lines to generate, besides mRNA or proteomic comparisons, additional functional data that are more relevant.

The radioassay had been developed for the recombinant rat CD73.[151] The optimal enzyme concentration for the assay was found to be 16.3 ng in 100 µl reaction volume. For the other two sources of CD73, an enzyme titration was performed to optimize the concentration of CD73 for the radioassay (Figure 37A). It has been found that an amount of 3.65 ng of human CD73 and 74 ng of the membrane fraction resulted in 10% AMP hydrolysis, and these amounts were used for further experiments.
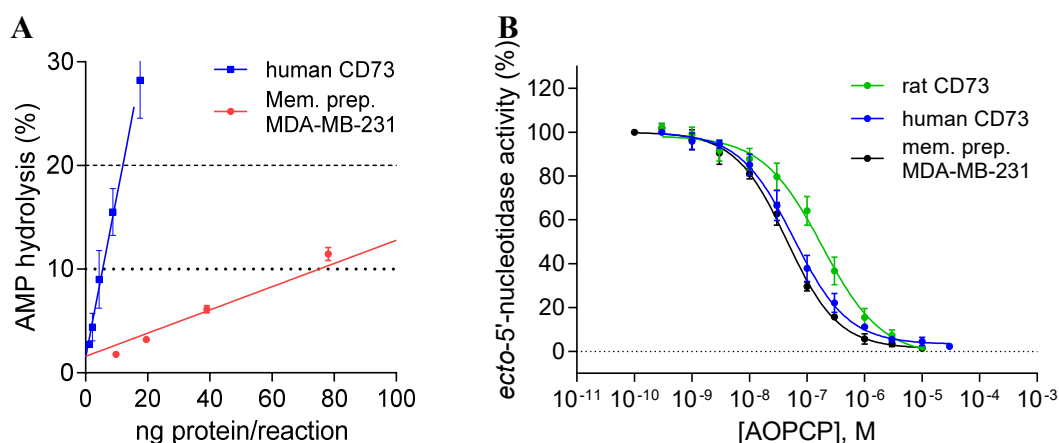
Figure 37. Assay optimization and validation. (A) Enzyme titration to optimize the amount of recombinantly produced human CD73 and membrane-bound CD73 in a membrane preparation of MDA-MB-231 cells. **(B)** Concentration-response curve of the reference inhibitor **AOPCP** using the different sources of CD73 (Data points are means ± SEM from at least three separate experiments performed in duplicates).

The potency of the reference inhibitor **AOPCP** was determined on the different sources of CD73 (Figure 37B and Table 4). At the rat enzyme, a K_i value of 167 ± 54 nM was measured. The analysis of both human varieties revealed higher potencies with K_i values of 49.9 ± 14.5 and 39.0 ± 7.0 nM for the recombinant human CD73 and the membrane preparation, respectively. In a previous study under the same conditions, a comparable value for the rat enzyme was obtained. In contrast, a twofold lower potency had been measured for human CD73 in human serum.[94]

Table 4. Parameters for the radioassay with different sources of CD73 (means ± SEM from at least three separate experiments performed in duplicates).

Variation of CD73	Concentration (µg protein/ml)	$K_M \pm$ SEM (µM)	$V_{max} \pm$ SEM (µmol/min/mg)	AOPCP $K_i \pm$ SEM (nM)
Recombinant rat	0.163	53.0 ± 4.1	2.14 ± 0.06	167 ± 53
Recombinant human	0.0365	17.0 ± 2.1	2.51 ± 0.21	49.9 ± 14.5
Membrane-bound	0.740	14.8 ± 2.1	0.111 ± 0.004	39.0 ± 7.0

4.2 Structure-activity relationships of nucleotides as CD73 inhibitors

4.2.1 Overview

The nucleotidic ecto-5′-nucleotidase inhibitor **AOPCP** was used as a lead structure. Multiple modifications and substitutions were performed in different positions. The diphosphonate group is charged under physiological conditions, and substitutions, modifications or bioisosteric replacements of this moiety were driven by the aim to increase the drug-like properties without losing potency. The ribose connects the diphosphonate group with the adenine base. It was tried to replace the ribose by a flexible alkyl linker. Multiple modifications of adenine or exchange of the base by substituted purine or pyrimidine rings were explored and will be presented in the following chapter. In general, rat CD73 and the sensitive radioassay were used to conduct these structure-activity relationships. The most potent compounds were additionally analyzed using the recombinantly produced human CD73 and membrane preparations of the triple-negative breast cancer cell line MDA-MB-231.

A part of the results of nucleotides as CD73 inhibitors were already published in the journals *Purinergic Signalling* (**2019**)[178] and *Journal of Medicinal Chemistry* (**2019**).[179]

4.2.2 Modification of adenine

A number of modifications of the adenine moiety had been explored in earlier studies which led to the most potent CD73 inhibitor so far (see introduction, page 26). What has not been investigated was the removal of the nitrogen atoms of purine leading to **1-, 3-** and **7-deaza-AOPCP** (Table 5). Based on data from crystallography and molecular modeling, N1 interacts with a structural water molecule, while N3 interacts via hydrogen bonding with Asn390 (Figure 38).

The test results reflected these interactions of the nitrogen atoms with the amino acids of the target, and a loss of inhibitory potency was observed for **1-** and **3-deaza-AOPCP**. In contrast, **7-deaza-AOPCP** was found to be two times more potent than **AOPCP** (**2g**, 88.6 nM) and the N7-nitrogen atom shows no interaction with amino acid residues in the binding site.
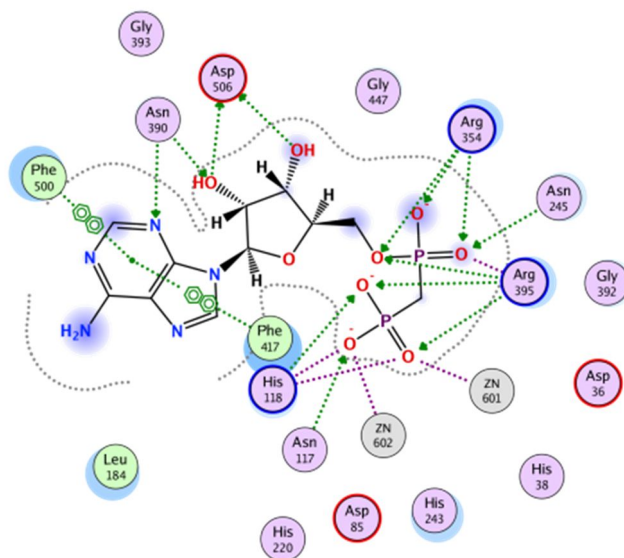
Figure 38. 2D-interaction diagram of AOPCP with human ecto-5′-nucleotidase. Molecular modeling studies were performed by Dr. Vigneshwaran Namasivayam.

Table 5. Potencies of AOPCP derivatives modified at the adenine moiety at rat CD73. If not otherwise indicated, X, Y and Z are nitrogen atoms (N, means ± SEM from at least three separate experiments performed in duplicates).

.
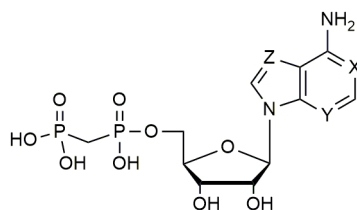
Compound		Substitution	Rat CD73 $K_i \pm$ SEM (nM)*
1	AOPCP		167 ± 53
2	2e	X = CH$_3$	> 1000 (36%)
3	2f	Y = CH$_3$	> 1000 (36%)
4	2g	Z = CH$_3$	88.6 ± 4.03

* or % inhibition at indicated concentration

4.2.3 Cytosine derivatives

The substitution of adenine by cytosine (**COPCP**, 898 nM) led to a 5-fold drop in potency compared to the lead compound **AOPCP** (Table 6 and Figure 39). Substitutions at the 5-position of **COPCP** (**7c-e**) were accepted with minor reduction in potency: 5-methyl (**7e**, 2030 nM) < 5-iodo (**7c**, 502 nM) < 5-fluoro (**7d**, 349 nM). Major increases in potency were generated by the addition of larger lipophilic substitution in the 4-position. The substitution of **COPCP** with a benzoyl moiety led to a 64-fold more potent compound with

Results and Discussion

a K_i value in the low nM range (**7f**, 13.9 nM). For further analysis of this binding pocket an alkoxyimino group was introduced in the 4-position of cytosine, and different lipophilic substituents were studied. Most potent was a naphth-2-ylmethyl- (**9e**, 18.8 nM) followed by a 4-trifluoromethylbenzyl- (**9d**, 30.3 nM), a benzyl- (**9b**, 112 nM) and a methyl-substituent (**9a**, 257 nM). Combination of 4-benzyloxyimino with modifications of the C5- or N3-position were explored (**9f-i**). The introduction of 5-methyl was not beneficial (**9a**, 257 nM) while 5-fluoro was accepted with a slight increase in potency (**9g**, 85.1 nM). Interestingly, the methylation of N1 led to a 30-fold more potent compound (**9h**, 3.67 nM). By expanding the alkyl chain towards an ethyl group the activity was sharply decreased (**9i**, 262 nM).

Table 6. Inhibitory potency of COPCP derivatives at rat CD73. If not otherwise indicated, X and Y are hydrogen atoms (means ± SEM from at least three separate experiments performed in duplicates).


1-6   **7-15**
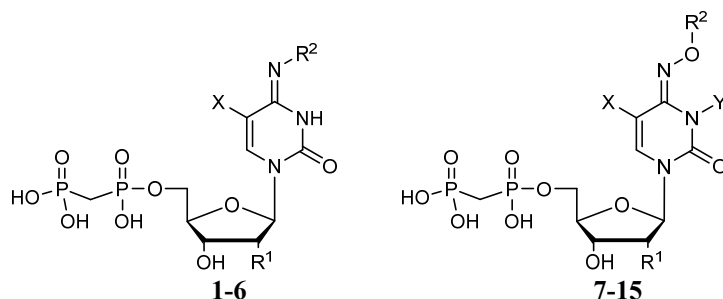
	Compound	Substitution	R^1	R^2	Rat CD73 $K_i \pm$ SEM (nM)*
1	**COPCP, 7a**		OH	H	898 ± 63
2	**7b**		H	H	> 1000 (18%)
3	**7c**	X = I	OH	H	502 ± 83
4	**7d**	X = F	OH	H	349 ± 41
5	**7e**	X = CH$_3$	OH	H	2030 ± 670
6	**7f**		OH	benzoyl	13.9 ± 1.6
7	**9a**		OH	CH$_3$	257 ± 39
8	**9b**		OH	benzyl	112 ± 15
9	**9c**		H	benzyl	780 ± 15
10	**9d**		OH	4-trifluoromethylbenzyl	30.3 ± 4.2
11	**9e**		OH	naphth-2-ylmethyl	18.8 ± 3.2
12	**9f**	X = CH$_3$	OH	benzyl	321 ± 9
13	**9g**	X = F	OH	benzyl	85.1 ± 7.5
14	**9h**	Y = CH$_3$	OH	benzyl	3.67 ± 0.26
15	**9i**	Y = C$_2$H$_5$	OH	benzyl	262 ± 46

* or % inhibition at indicated concentration
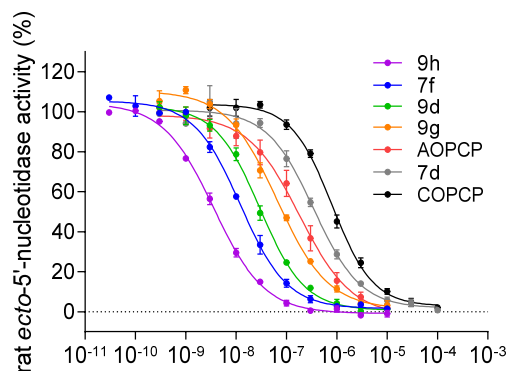
Figure 39. Exemplary concentration-response curves of COPCP analog tested at rat CD73 (data points are means ± SEM from at least three separate experiments performed in duplicates).

Compound **9h** was further investigated in molecular modeling studies (Figure 40). Results of docking studies showed that the diphosphonate group and the ribose form the same interactions to the target as **AOPCP** which leads to the same orientation of **9h** within the binding site. The cytosine moiety mimics the adenine moiety and is stacked by π-π interaction between Phe417 and Phe500 (Figure 40). Asn390 which addresses N3 in adenine, interacts with the keto group in the 2-position of cytosine. This also applies to compound **7f**, which was investigated in docking studies, but whose results are not illustrated due to its similarity to compound **9h**. The larger 4-benzyloxyimino moiety and also the other lipophilic moieties in the 4-position address a large pocket with bound water molecules which is exposed to the surface (Figure 40).
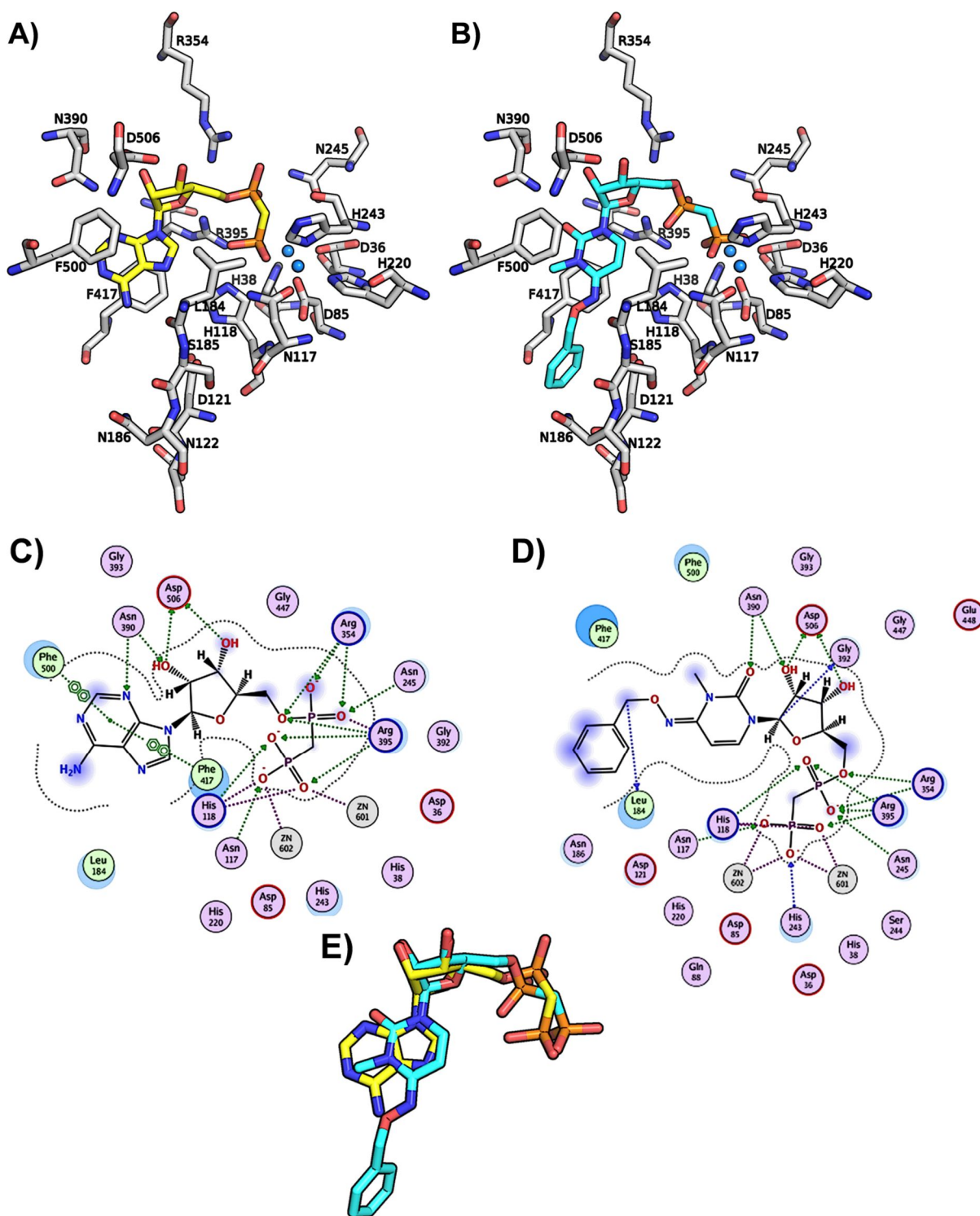
Figure 40. Molecular modeling studies of AOPCP and 9h. (A) The binding pose of AOPCP (yellow) from the X-ray structure (2.0 Å, 4H2I.pdb) and **(B)** the docked pose of **9h** (cyan) within the binding site of the human ecto-5′-nucleotidase. 2D interaction diagram of **(C)** AOPCP and **(D) 9h**. **(E)** Overlay of **AOPCP** (crystal structure) and docked **9h** showing both inhibitors in comparable binding pose (legend: amino acid residues colored gray, **AOPCP** (yellow) and **9h** (cyan) are shown as stick models, zinc ions are colored in marine blue, oxygen atoms in red, nitrogen atoms in blue and phosphorous atoms in orange. Molecular modeling studies were performed by Dr. Vigneshwaran Namasivayam.

4.2.4 Uracil derivatives

Structure-activity relationships of the uracil derivatives were investigated on rat CD73 (Table 7 and Figure 41). The replacement of adenine by unsubstituted uracil led to a 10-fold drop in of potency (**UOPCP**, 1830 nM). Uracil is structurally less related to adenine than cytosine. Therefore, it is not surprising that it is also 2-fold less active compared to **COPCP**. As in the cytosine derivatives, a methylation of N3 was tolerated (**4b**, 1860 nM), but longer and more bulky substituents led to steric clash associated with a total loss of activity (**4c-e**). The substitution of the 5-position was beneficial. Methylation led to a 5-fold (**4f**, 338 nM) and ethynylation to a 6-fold (**4i**, 276 nM) more potent compound. The introduction of 1-chlorovinyl (**4j**, 424 nM) led to a more active compound compared to **UOPCP**, but less active compared to the previously describes substituents. Interestingly, the substitution of 5-position with a small and highly electronegative fluorine resulted in the most potent inhibitor within this series with a K_i of 14.8 nM. Further halogenation of this position led to the series: F > Br = Cl > I. Docking studies revealed that it is possible that the highly electronegative fluorine form a hydrogen bond ether to His118 which is located at a distance of approximately 4 Å away or interact with water molecules (distance of ~3 Å) inside the binding pocket.

Replacement of C6 by a nitrogen (**4v**) and O2 by a sulfur atom (**4y**) as well as the elongation of the diphosphonate group (**4w, 4x**) by an additional carbon atom were not accepted. Within this series of uracil derivatives some modifications of the ribose were also analyzed. The 2-position of the sugar was investigated ether with substituents which are orientated in up or in down position. The results illustrated that most of these changes were accompanied by a strong decrease in potency (**4h, 4q-4s, 4u**). However, 2′-deoxy-2′-fluoro, which was also described in other studies[100, 105] (see introduction, page 29 and 30) to be potent was equipotent to **UOPCP** (**4t**, 1750 nM).

Results and Discussion

Table 7. Inhibitory potency of UOPCP derivatives at rat CD73. If not otherwise indicated, V is a carbon (C), W is an oxygen (O), and X and Y are hydrogen atoms (means ± SEM from at least three separate experiments performed in duplicates).

Compound		Substitution	R^1	R^2	Rat CD73 $K_i \pm$ SEM (nM)*
1	UOPCP, 4a		OH	H	1830 ± 530
2	4b	Y = CH$_3$	OH	H	1860 ± 400
3	4c	Y = C$_2$H$_5$	OH	H	> 1000 (4%)
4	4d	Y = C$_3$H$_7$	OH	H	> 1000 (7%)
5	4e	Y = benzyl	OH	H	> 1000 (3%)
6	4f	X = CH$_3$	OH	H	338 ± 56
7	4g	X = CH$_3$	H	H	639 ± 65
8	4h	X = CH$_3$	OCH$_3$	H	> 1000 (3%)
9	4i	X = ethynyl	OH	H	276 ± 37
10	4j	X = 1-chlorovinyl	OH	H	424 ± 27
11	4k	X = 1-chlorovinyl, Y= CH$_3$	OH	H	1050 ± 290
12	4l	X = F	OH	H	14.8 ± 1.9
13	4m	X = Cl	OH	H	86.7 ± 7.6
14	4n	X = Br	OH	H	88.7 ± 12.5
15	4o	X = I	OH	H	162 ± 4
16	4p		H	H	> 1000 (37%)
17	4q		NH$_2$	H	> 1000 (2%)
18	4r		N$_3$	H	> 1000 (9%)
23	4s		F	H	> 1000 (11%)
19	4t		H	F	1750 ± 380
20	4u		H	OH	> 1000 (8%)
21	4v	V = N	OH	H	> 1000 (21%)
22	4w	n = 2	OH	H	> 1000 (4%)
23	4x	n= 2, X = CH$_3$	OH	H	> 1000 (9%)
24	4y	W = S	OH	H	> 1000 (7%)
25	5a				> 1000 (19%)
26	6a				> 1000 (10%)

* or % inhibition at indicated concentration

84
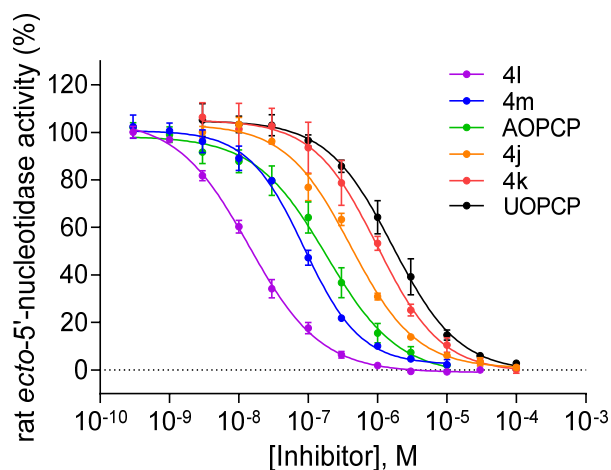
Figure 41. Exemplary concentration-response curves of UOPCP analogs tested at rat CD73 (data points are means ± SEM from at least three separate experiments performed in duplicates).

4.2.5 Modification of the ribose

The structure-activity relationships of ribose substituted at the 2′- and 3′-position were investigated (Table 8). Besides **2′-deoxy-COPCP** (**7b**, 18% inhibition at 1 μM), which was discussed above, the **2′-deoxy-AOPCP** derivative was also found to be less potent (**2a**, 30% inhibition at 1 μM) than **AOPCP**, and (*R*)-**2′-amino-AOPCP** was inactive (**2b**, 2% inhibition at 1 μM). **3′-Deoxy-AOPCP** was found to be more potent than the 2′-deoxy derivative, but still 10-fold less potent (**2d**, 1970 nM) than the lead compound **AOPCP**. Some special cases were also investigated: first, the shift of the diphosphonate group from the 5′ to the 3′-position of the ribose and with an amino group in the 2′-position (**2c**), and secondly, a (*S*)-methanocarba-based nucleotide: both compounds were found to be inactive (**2c**, 8% and **3a**, 12% inhibition at 1 μM).

It can be summarized that modifications of the ribose, especially of the 2′- and 3′-position are in general not beneficial. Molecular modeling showed that hydrogen bonds are formed between the hydroxy groups of the ribose and the amino acids Asn390 and Asp506 (Figure 40, page 82). Thus, the oxygen atoms in these positions are crucial for the correct coordination of the ribose in the binding pocket of ecto-5′-nucleotidase.

Table 8. Inhibitory potency of AOPCP derivatives modified at the ribose moiety (means ± SEM from at least three separate experiments performed in duplicates).
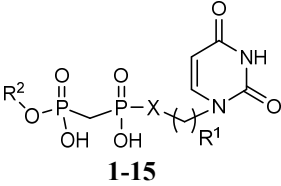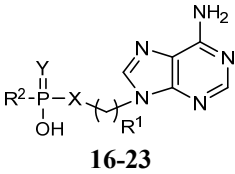

Compound	Substitution	R^1	R^2	Rat CD73 $K_i \pm$ SEM (nM)*
1	AOPCP		OH	OH	167 ± 43
2	2a		OH	H	> 1000 (30%)
3	2b		OH	NH$_2$	> 1000 (2%)
4	2d		H	OH	1970 ± 220
5	2c	5′-OH	OP$_2$O$_5$CH$_5$	NH$_2$	> 1000 (8%)
6	3a				

* or % inhibition at indicated concentration

4.2.6 Exchange of the ribose for an alkyl linker

The starting point for the exchange of ribose for an alkyl linker was based on substances which were primarily synthesized as P2Y receptor antagonists and stored in the in-house compound library. In these compounds, uracil is connected to the diphosphonate group by a linker consisting of alkyl and ether groups of different lengths. The connecting atom between the linker and the diphosphonate group is either an oxygen or a carbon atom. In some derivatives, the diphosphonate group is additionally elongated by a further phosphate residue (Table 9). Because of structural similarity to formerly developed CD73 inhibitors[94] and the cytosine and uracil derivatives described above, these acyclic pyrimidine derivatives were investigated for potential CD73 inhibition. Test results showed that these derivatives inhibited ecto-5′-nucleotidase depending on the length of the linker (Table 9, 1-15 and Figure 42A).

Table 9. Potency of uracil and adenine derivatives with different linker lengths. If not otherwise indicated, X and Y are oxygen atoms (means ± SEM from at least three separate experiments performed in duplicates).

1-15   16-23

Compound		Substitution	R^1	R^2	Rat CD73 $K_i \pm$ SEM (μM)*
1	PD-541	X = CH$_2$	(CH$_2$)$_3$	H	23.4 ± 3.4
2	PD-563	X = CH$_2$	(CH$_2$)$_4$	H	12.6 ± 2.7
3	PD-580	X = CH$_2$	(CH$_2$)$_5$	H	17.4 ± 6.6
4	PD-562	X = CH$_2$	CH$_2$O(CH$_2$)$_2$	H	29.9 ± 7.8[a]
5	PD-530	X = CH$_2$	O(CH$_2$)$_2$	H	43.1 ± 10.6[a]
6	PD-616		(CH$_2$)$_4$	H	38.4 ± 14.1[a]
7	PD-605		(CH$_2$)$_5$	H	8.13 ± 4.34
8	PD-617		(CH$_2$)$_6$	H	35.2 ± 7.9
9	PD-614		(CH$_2$)$_2$OCH$_2$	H	49.8 ± 8.3[a]
10	PD-613		(CH$_2$)$_2$O(CH$_2$)$_2$	H	91.6 ± 19.1[a]
11	PD-627		(CH$_2$)$_4$	OPO$_3$	> 100 (43%)
12	PD-628		(CH$_2$)$_5$	OPO$_3$	30.6 ± 4.5[a]
13	PD-629		(CH$_2$)$_6$	OPO$_3$	> 100 (44%)
14	PD-623		(CH$_2$)$_2$OCH$_2$	OPO$_3$	> 100 (47%)
15	PD-619		(CH$_2$)$_2$O(CH$_2$)$_2$	OPO$_3$	> 100 (43%)
16	SF-31	X = CH$_2$	(CH$_2$)$_4$	CH$_2$PO$_3$	> 10 (37%)
17	SF-18	X = CH$_2$	(CH$_2$)$_5$	OH	> 10 (9%)
18	SF-37	X = CH$_2$	(CH$_2$)$_5$	CH$_2$PO$_3$	5.72 ± 0.58
23	SF-20	X = CH$_2$	(CH$_2$)$_6$	OH	> 10 (22%)
19	SF-21		(CH$_2$)$_5$	OH	> 10 (10%)
20	SF-10		(CH$_2$)$_5$	CH$_2$PO$_3$	3.96 ± 0.54
21	SF-25		(CH$_2$)$_6$	OH	> 10 (28%)
22	SF-35		(CH$_2$)$_6$	CH$_2$PO$_3$	8.21 ± 2.57
23	MN-38		(CH$_2$)$_2$O(CH$_2$)$_2$	CH$_2$PO$_3$	13.9 ± 1.5

* or % inhibition at indicated concentration, [a] estimated by pseudo K_i-curves using inhibition at 100 and 10 μM inhibitor concentration

The acyclic derivative with a C5-alkyl linker and oxygen as connecting atom mimics the ribose moiety best showing a K_i value in the low micromolar range (**PD-605**, 8.13 μM). Compared to the inhibitor **UOPCP** (1.83 μM, Table 7, page 84) it needs to be noted that the loss of potency by exchange of the sugar for a C5-alkyl linker was unexpectedly low. The most potent derivatives with a carbon-linked diphosphonate group was the derivative with a C4-alkyl linker (**PD-563**, 12.6 μM). It was slightly less potent, but the removal of the oxygen in this position suggests a higher metabolic stability and is therefore also an interesting starting point for further optimization. Shorter or longer alkyl linkers or ether groups within the linker were found to be less beneficial (Table 9).

Results and Discussion

A

B

#	X	n	K_i (µM)
PD-605	O	5	8.13
PD-563	C	4	12.6
PD-580	C	5	17.4
PD-541	C	3	23.4
PD-617	O	6	35.2

#	X	n	K_i (µM)
SF-10	O	5	3.96
SF-37	C	5	5.72
SF-35	O	6	8.21
SF-31	C	4	> 10
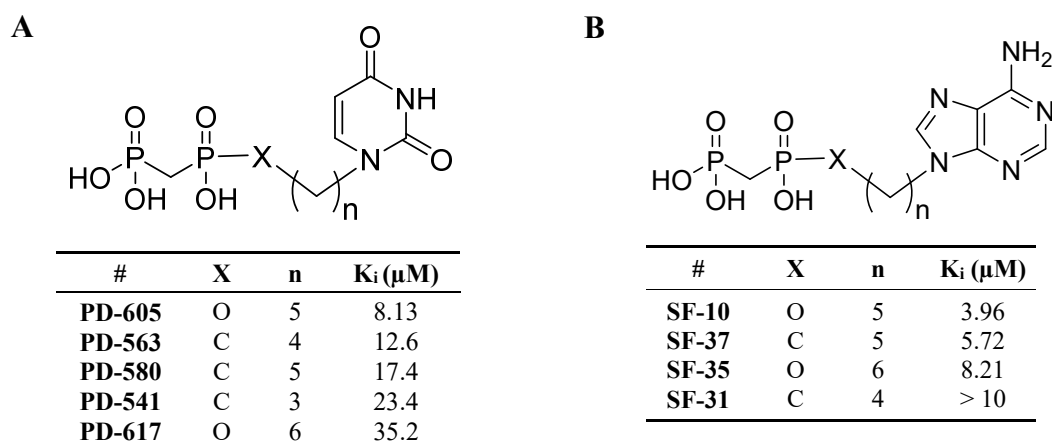
Figure 42. Structure-activity relationships of acyclic AOPCP analogs with different alkyl linker lengths. Structure-activity relationship of uracil **(A)** and adenine **(B)** di-(α/β-methylene) phosphates/phosphonates. Regardless of the base, the phosphate with a C5-alkyl linker length revealed the highest inhibition of rat CD73.

To reach a better comparability to the reference inhibitor **AOPCP**, the uracil moiety was also exchanged for adenine in selected compounds (Table 9, 16-23 and Figure 42B). The exchange from uracil in **UOPCP** to adenine in **AOPCP** had resulted in a 10-fold increase in potency. With a K_i value of 3.96 µM, the oxygen linked derivative with a C5-alkyl linker (**SF-10**) was found to be twice as potent as the corresponding uracil derivative (**PD-605**, 8.13 µM; Table 9 and Figure 42A). In contrast to the uracil series, the most potent acyclic AOPCP analog with a carbon linked diphosphonate group was the compound with a C5-linker (**SF-37,** 5.72 µM). A further compound with a 5-memberd linker was analyzed (**MN-38,** Table 9), which is the adenine analog of compound **PD-613**. It is characterized by a flexible alkyl ether moiety in which the ether atom is located in the middle of the alkyl chain and is flanked by two CH_2 groups each. This form of the linker comes closest to the ribose moiety. The compound (**MN-38)** was displayed with a K_i of 13.9 µM and was thus less potent than those with C5 and C6 linker of acyclic nucleotide analogs within this series. Anyway, in both series of acyclic nucleotide analogs, a C5 linker was best. As a next step, the adenine moiety was substituted with 2-chloro and N^6-benzyl-N^6-methyl residues. These substitutions had been investigated in previous studies in AOPCP derivatives and were found to be around 170-fold more potent (see introduction, page 27, Bhattarai *et al.*, unpublished).[24, 94] The expectation, that these modifications would also push the acyclic analogs with the optimized alkyl linker into the nM range was not met. The potency of C5 (**SF-54**) and C6 (**SF57**) linker-containing target molecules showed K_i values of 1.82 and

2.83 µM, respectively (Figure 43 and Table 10). A variety of bioisosteric moieties (Table 10) abolished CD73-inhibitory potency.
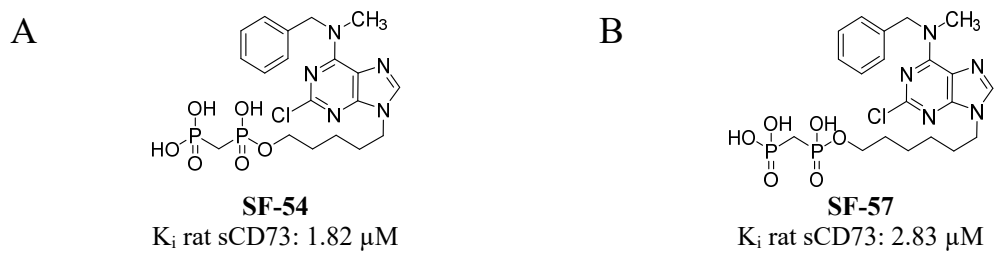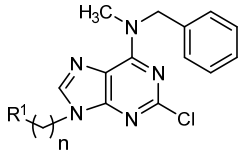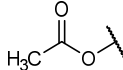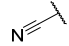
A

SF-54
Ki rat sCD73: 1.82 µM

B

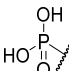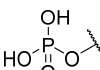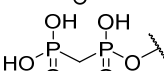**SF-57**
Ki rat sCD73: 2.83 µM
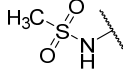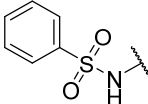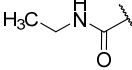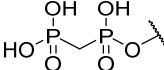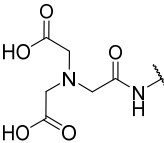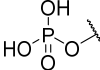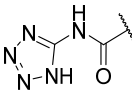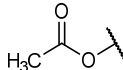
Figure 43. Acyclic analogs of AOPCP substituted at the adenine moiety.
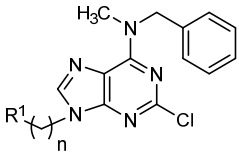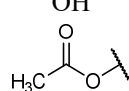
Results and Discussion

Table 10. Bioisosteric replacement of diphosphonate in AOPCP derivatives means ± SEM from at least three separate experiments performed in duplicates).

Compound		n	R¹	Rat CD73 $K_i \pm$ SEM (µM)*
1	SF-39	5		> 10 (16%)
2	SF-44	5		> 10 (-8%)
3	SF-47	5		> 10 (18%)
4	SF-48	5		> 10 (10%)
5	SF-49	5		> 10 (-8%)
6	SF-54	5		**1.82 ± 0.20**
7	SF-61	5		> 10 (-18%)
8	SF-78	5		> 10 (13%)
9	SF-69	5		> 10 (-19%)
10	SF-56	6	OH	> 10 (3%)
11	SF-53	6		> 10 (-6%)
12	SF-68	6		> 10 (24%)
13	SF-79	6		> 10 (23%)
14	SF-57	6		**2.83 ± 0.45**
16	SF-76	7	OH	> 10 (1%)

* or % inhibition at indicated concentration

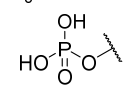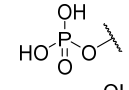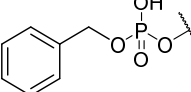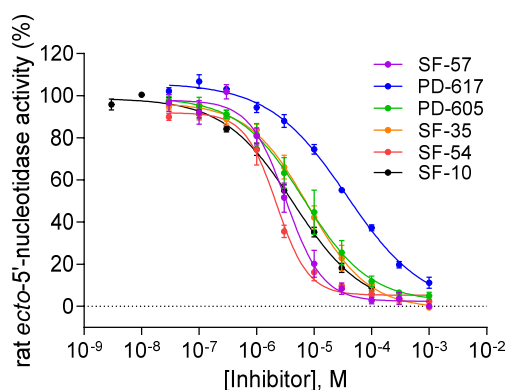**Table 10 (continued). Bioisosteric replacement of diphosphonate in AOPCP derivatives** means ± SEM from at least three separate experiments performed in duplicates).

	Compound	n	R^1	Rat CD73 K_i ± SEM (μM)*
1	SF-76	7	OH	> 10 (1%)
2	SF-74	7		> 10 (5%)
3	SF-80	7		> 10 (25%)
4	SF-71	8		> 10 (39%)
5	SF-75	7		> 10 (31%)

* or % inhibition at indicated concentration

The question is why the substitution of adenine with 2-chloro, methyl and benzyl in the N^6-position did not lead to a stronger inhibition, especially for the oxygen linked diphosphonate with the C5 linker: In these molecules, the substituted adenine and the diphosphonate group maintain binding to the target. The linker is the connection between both and its length needs to be optimal so that each binding site can be addressed as well as possible. It could be speculated that in the situation where the substituted adenine moiety fits perfectly into its binding site, the diphosphonate group is not well oriented and does not address the phosphate binding site sufficiently or *vice versa*.
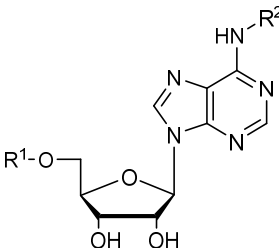

Figure 44. Concentration-response curves of acyclic AOPCP analogs tested at rat CD73 (data points are means ± SEM from at least three separate experiments performed in duplicates, for K_i values see Table 9).
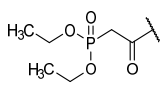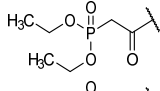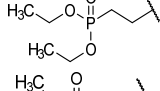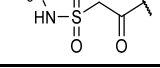
91

4.2.7 AOPCP analogs with monophosphonate groups

In the previous section, the main focus was the replacement of the ribose by a flexible alkyl linker. Additionally, the bioisosteric replacement of the diphosphonate group of acyclic AOPCP and UOPCP analogs were discussed. In this chapter the main focus will be on the bioisosteric replacement of the diphosphonate of the lead structure **AOPCP**. Some structures show additional modifications of the ribose and the adenine rings. As already outlined in the previous chapter, the bioisosteric replacement of the diphosphonate is an important objective to increase the drug-like properties of **AOPCP**. It would be important to avoid negative charges to increase oral bioavailability. The replacement of the diphosphonate by ethylated monophosphonates or a sulfonamide resulted in a series of inactive compounds (Table 11).

Table 11. AOPCP derivatives with bioisosteric replacement of the diphosphonate moiety (means ± SEM from at least three separate experiments performed in duplicates).
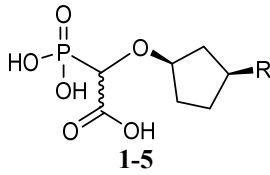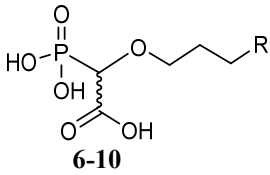
	Compound	R^1	R^2	Rat CD73 $K_i \pm$ SEM (µM)
1	GR-86		H	> 10 (5%)
2	GR-67		benzyl	> 10 (2%)
3	GR-66		benzyl	> 10 (11%)
4	GR-96		benzyl	> 10 (19%)

* or % inhibition at indicated concentration

It can be seen that the size of the binding pocket of CD73 (Figure 38, page 79), where the phosphonate group interacts with the target, is limited. Therefore, it is possible that the ethyl group may cause the inhibitor not to fit sterically into the binding site or at least that the distance to the interacting amino acids or zinc ions is increased in such a way that no proper binding occurs. In addition, it should be noted that there is no negative charge at the position as planned. However, the negative charge may be necessary for a strong binding by

interaction with the cationic amino acids Arg354, Arg395, His118 and/or via complexation with the zinc ions. The same applied to a series of nucleotide analogs with variations of the nucleobase, replacement of the ribose, and bioisosteric exchange of the diphosphonate (Table 12).

Table 12. Potencies of 2-phosphonoacetic acid derivatives at rat CD73. (means ± SEM from at least three separate experiments performed in duplicates).

Compound		R	Rat CD73 $K_i \pm$ SEM (µM)*
1	Cork-28	adenine	> 10 (37%)
2	Cork-60	guanine	> 10 (11%)
3	Cork-25	cytosine	> 10 (35%)
4	Cork-19	thymine	> 10 (5%)
5	Cork-22	uracil	> 10 (41%)
6	JJ-348	adenine	> 10 (32%)
7	JJ-351	guanine	> 10 (23%)
8	JJ-355	cytosine	> 10 (6%)
9	JJ-27	thymine	> 10 (10%)
10	JJ-261	uracil	> 10 (29%)

* or % inhibition at indicated concentration

All compounds inhibited rat ecto-5′-nucleotidase by less than 50% at 10 µM compound concentration. It can be noted that these compounds are in general more potent than the compounds in which the oxygen atoms were ethylated (Table 11). Both types of compounds mimic the diphosphonate group, but the difference is that the 3-phosphonoacetic moiety is negatively charged under physiological conditions which underlines the importance of negative charges at the position of the diphosphonate group. Further modifications of the diphosphonate itself, by a replacement of one or both phosphorus atom(s) by sulfur resulted in compounds with low potency compared to the lead structures **AOPCP (MN-27, MN-34)** showing 44 and 34% inhibition at 10 µM compound concentration, respectively (Table 13).

Results and Discussion

Table 13. Potencies of AOPCP derivatives with replaced phosphorus atoms by sulfur. If not otherwise indicated, X and Y are phosphorus atoms (means ± SEM from at least three separate experiments performed in duplicates).
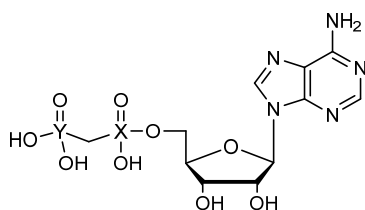
Compound		Substitution	Rat CD73 $K_i \pm$ SEM (µM)*
1	MN-27	Y = S	> 10 (44%)
2	MN-34	X = S, Y = S	> 10 (23%)

* or % inhibition at indicated concentration

4.2.8 Analysis of the most potent nucleotidic CD73 inhibitors at human enzyme

As discussed above, rat CD73 is similar to the human isoform. Nevertheless, the most potent purine and pyrimidine derivatives (**4l**, **7f**, **9d**, **9e**, **9g** and **9h**) and the most potent acyclic derivatives (**SF-35**, **SF-37**, **SF-54** and **SF-57**) were analyzed using recombinant soluble human CD73 (Figure 45A and Table 14). In addition, to study the inhibitors in a more complex, natural environment, membrane-anchored CD73 using membrane preparations derived from the triple-negative breast cancer (TNBC) cell line MDA-MB-231 were employed (Figure 45B and Table 14). The test results from the purine and pyrimidine derivatives confirmed the observation that AOPCP analogs are generally slightly more potent at human CD73 compared to the rat enzyme. Compounds **4l**, **7f**, **9d** and **9e** are 2- to 3-fold more potent, and **9g** is 5-fold more potent. However, the most potent compound at rat CD73 (**9h**, 3.67 nM) was slightly less potent at human CD73 (K_i, soluble CD73, 10.6 nM; membrane preparation, 7.96 nM). All analyzed inhibitors were similarly potent at soluble CD73 as compared to the membrane-bound enzyme.
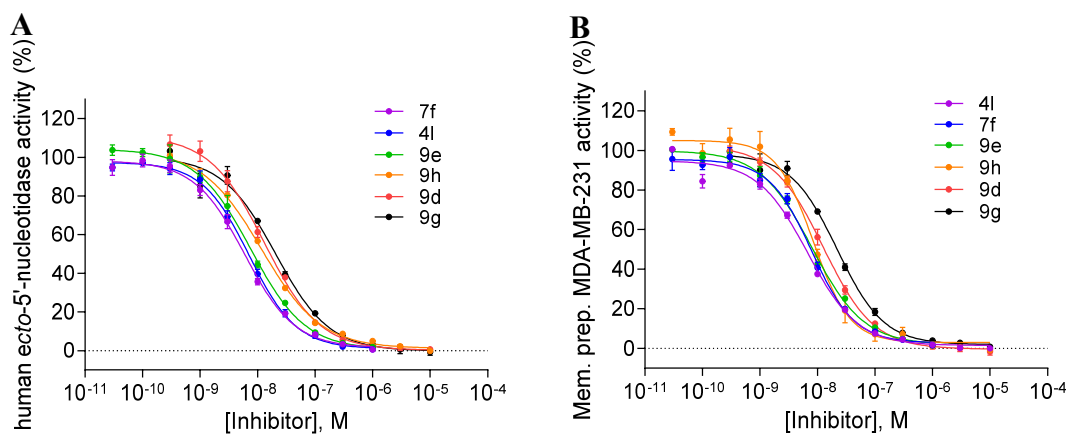
Figure 45. Concentration-response curves of pyrimidine derivatives at human CD73. (A) Analysis with soluble human CD73 and **(B)** with membrane preparation of MDA-MB-231 cells as source for CD73 (data points are means ± SEM from at least three separate experiments performed in duplicates).

Table 14. Potencies of pyrimidine derivatives tested on different sources of CD73 (means ± SEM from at least three separate experiments performed in duplicates).

Compound		Rat CD73 K_i ± SEM (nM)	Human CD73 K_i ± SEM (nM)	MDA-MB-231 Membrane preparation K_i ± SEM (nM)
4l		14.8 ± 1.9	5.33 ± 0.73	4.51 ± 0.13
7f		13.9 ± 1.6	4.58 ± 0.55	5.68 ± 0.75
9d		30.3 ± 4.2	14.0 ± 1.6	10.1 ± 1.4
9e		18.8 ± 3.2	6.88 ± 1.05	6.29 ± 0.45
9g		85.1 ± 7.5	15.9 ± 1.1	16.6 ± 0.7
9h		3.67 ± 0.26	10.6 ± 0.4	7.96 ± 0.57

95
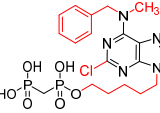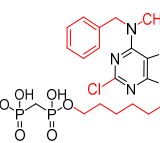
Results and Discussion

Interestingly, data from the analysis of the acyclic AOPCP derivatives showed relatively large species differences between rat and human CD73 (Figure 46 and Table 15). **SF-35**, **SF-37** and **SF-54** were found to be around 5-fold less potent on human than on rat CD73. In contrast, **SF-57** was 5-times more potent and showed K_i values in the medium nM range on soluble human (563 nM) and on human membrane-bound CD73 (481 nM). Like for the purine and pyrimidine derivatives discussed above, the analyzed inhibitors were similarly potent at soluble human CD73 as compared to the human membrane-bound enzyme. This indicates, that the difference in potency is not due to the source, but due to species differences of rat and human CD73. The assumption that the compounds which showed a lower potency were decomposed were ruled out by LC-MS. These results suggest that in the human variant of CD73 a C6-linker in the acyclic AOPCP derivatives is preferred and in rat CD73 a shorter C5-linker is favored. **AOPCP** is a competitive inhibitor and thus also the derivatives should be. Nevertheless, for **SF-57,** the most potent compound in this series, the mode of inhibition was determined and the competitive character of this acyclic class of CD73 inhibitors was confirmed (Figure 47).
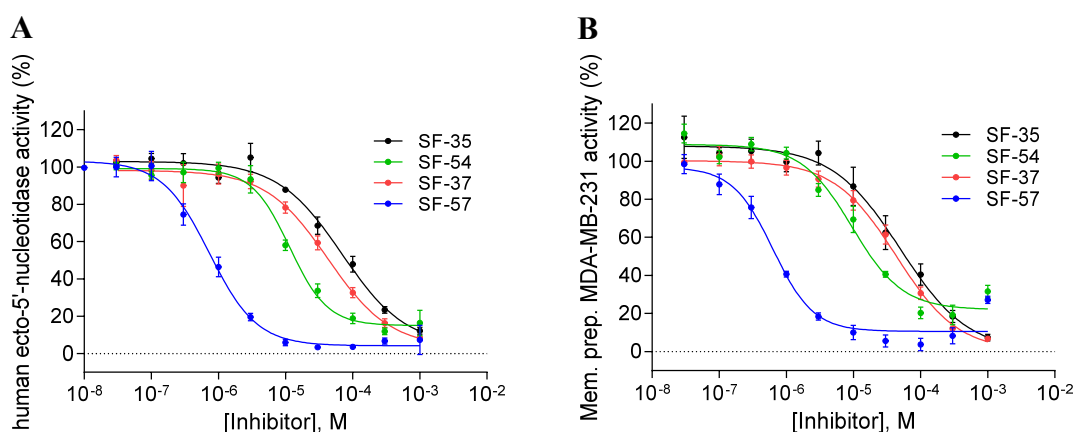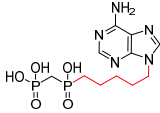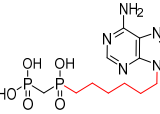

Figure 46. Concentration-response curves of acyclic AOPCP derivatives at human CD73. (A) Analysis with soluble human CD73 and **(B)** with membrane preparation of MDA-MB-231 cells as source for CD73 (data points are means ± SEM from at least three separate experiments performed in duplicates).

Table 15. Potencies of acyclic AOPCP derivatives tested on CD73 of different sources (means ± SEM from at least three separate experiments performed in duplicates).

Compound		Rat CD73 K_i ± SEM (µM)	Human CD73 K_i ± SEM (µM)	MDA-MB-231 Membrane preparation K_i ± SEM (µM)
SF-35		8.21 ± 2.58	55.7 ± 12.2	37.5 ± 9.3
SF-37		5.73 ± 0.59	33.5 ± 1.3	32.8 ± 4.5
SF-54		1.82 ± 0.20	8.51 ± 0.50	7.81 ± 1.02
SF-57		2.83 ± 0.45	0.563 ± 0.087	0.481 ± 0.062
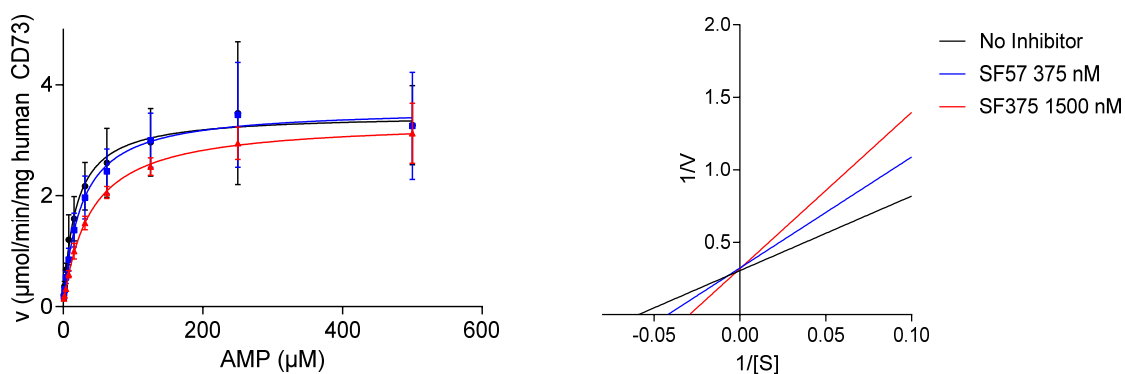
Figure 47. Competitive inhibition mode of the acyclic AOPCP derivative SF-75. (A) Michaelis-Menten kinetics: V_{max} is reached at high substrate concentration independent of the used inhibitor concentration. K_M value is increased for higher inhibitor concentrations. **(B)** Lineweaver-Burk plot shows intercept of all three lines at the y-axis which is typical for a competitive inhibitor (means ± SEM from three separate experiments performed in duplicates).

Results and Discussion

4.3 Structure-activity relationships of sulfonamides as CD73 inhibitors

4.3.1 Overview

In the previous chapter, nucleotides as ecto-5′-nucleotidase inhibitors were discussed. Besides the negative charge of the diphosphonate group, they have the disadvantage that they are structurally related to endogenous substrates. This increases the likelihood of off-target effects, and a fast biodegradation. Clearance of the compound can also be assumed. To overcome these issues of nucleotidic inhibitors, sulfonamide derivatives had been identified (see introduction, page 26) by virtual screening and were evaluated with rat CD73.[24, 127] Based on those results further compounds had been synthesized and tested in the radioassay (Dr. Marianne Freundlieb). The best 15 candidates revealed K_i values in the range of 1.75 to 69.0 µM. Among these candidates two sulfonamide structures, a naphthalene with a hydrazone linker (Figure 48A) and a coumarin derivative with an amide linker were identified as lead structures (Figure 48B). Further optimization led to the most potent compounds of this series, which are illustrated in Figure 48 (modifications are in red). Furthermore, it was found that a nitro group in the 3-position of the benzenesulfonamide moiety is beneficial.[24]
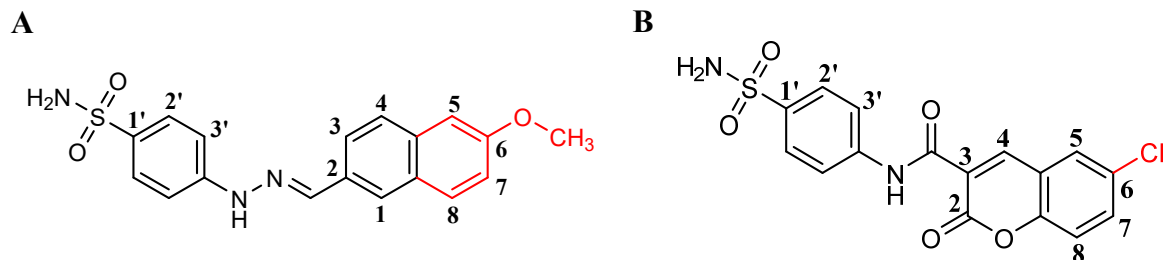
Figure 48. Lead compounds identified by virtual screening, optimized and validated *in vitro*. (A) Hydrazone lead structure with the most potent derivative (red) (K_i: 1.53 µM) and **(B)** coumarin lead structure with the most potent derivative (red) out of this series (K_i: 1.75 µM).[24, 127]

In the present study further sulfonamides were synthesized by Dr. Thanigaimalai Pillaiyar and tested on rat CD73 in the radioassay. In the first section of the following chapter, test results of the hydrazone (lead A), and in the second section results of the coumarin moiety (lead B) will be discussed.

4.3.2 Hydrazone derivatives

The potencies of 18 hydrazone compounds were analyzed on rat CD73 (Table 16 and 17). Measuring full-inhibition curves of the hydrazone derivatives was problematic. Many repeats and the exclusion of outliers by Grubbs test of outliers[180] were necessary to obtain relevant data. Reasons might be the poor solubility of these compounds and the assumption that the hydrazones are unstable. Since it had been found that a nitro group in 3-position of the benzenesulfonamide moiety is beneficial, almost all structures were substituted with a nitro group in this position. For the most potent compound at this time (6-methoxynapthalene, Figure 48A) this modification meant a 6-fold increase in potency (**Yazh-755**, 239 nM). The 6-hydroxy derivative was 2-fold less potent (**Yazh-775**, 488 nM) and the unsubstituted naphthalene was found to be inactive (**Yazh-855**, 14% inhibition at 1 µM concentration) underlining the importance of the substitution in 6-position for strong potency. The introduction of a further methyl group in the hydrazone moiety of the 6-methoxynapthalene derivative was accepted but did not increase the potency (**Yazh-764**, 447 nM).

Table 16. Inhibitory potency of hydrazone derivatives at rat CD73 (I) (means ± SEM from at least three separate experiments performed in duplicates).

	Compound	R^1	R^2	R^3	Rat CD73 K_i ± SEM (nM)*
1	**Yazh-775**	NO_2	H	hydroxy	**488 ± 199**
2	**Yazh-755**	NO_2	H	methoxy	**239 ± 46**
3	**Yazh-855**	NO_2	CH_3	H	> 1000 (14%)
4	**Yazh-764**	NO_2	CH_3	methoxy	**447 ± 73**
5	**Yazh-K19**	Br	H	methoxy	> 1000 (14%)
6	**Yazh-K34**	NO_2	H	H	> 1000 (36%)
7	**Yazh-771**	NO_2	H	2-methoxy	**3527 ± 1377**
8	**Yazh-842**	NO_2	H	4-methoxy	**194 ± 46**
9	**Yazh-766**	NO_2	H	4-dimethylamino	> 1000 (27%)

* or % inhibition at indicated concentration

A different orientation of the substituted naphthalene moiety was also explored (Table 16, 6-9). The unsubstituted naphthalene revealed a higher inhibition (**Yazh-K34**,

Results and Discussion

36% inhibition at 1 µM concentration) compared to the previously discussed orientation of this moiety, but was clearly less active than the substituted naphthalene derivatives described above.

A methoxylation of the 2-position (**Yazh-771**, 3.53 µM) gave a 2-fold more potent compound than the hydroxy derivative (**PR-52,** 6.02 µM[24]). The substitution of the 4-position with a hydroxy group was more beneficial (**Yazh-842**, 194 nM) and led to the most potent inhibitor within this series.

Table 17. Inhibitory potency of hydrazone derivatives at rat CD73 (II) (means ± SEM from at least three separate experiments performed in duplicates).

1-6   7-9

	Compound	R^1	R^2	R^3	Rat CD73 $K_i \pm$ SEM (nM)*
1	Yazh-853	NO$_2$	CH$_3$		> 1000 (16%)
2	Yazh-774	NO$_2$	H		**231 ± 12**
3	Yazh-K20	Br	H		> 1000 (36%)
4	Yazh-780	NO$_2$	H		**345 ± 54**
5	Yazh-773	NO$_2$	H		> 1000 (37%)
6	Yazh-K33	NO$_2$	H		> 1000 (31%)
7	Yazh-823	NO$_2$	H	4-methoxy	> 1000 (31%)
8	Yazh-765	NO$_2$	H	4-dimethylamino	> 1000 (28%)
9	Yazh-852	NO$_2$	CH$_3$	2-methoxy	> 1000 (5%)

* or % inhibition at indicated concentration

The further expansion of the planar aromatic system by the introduction of dibenzofuran was accepted in two different orientations (Table 17). **Yazh-774** and **Yazh-780** were measured with a K_i of 231 and 345 nM, respectively. The exchange of naphthalene against 1,3-

benzodioxyl, 4-(benzoyloxy)-2-hydroxybenzyl or biphenyl, however, was not successful (**Yazh-853,** 16%, **Yazh-773**, 37% and **Yazh-K33**, 31% inhibition at 1 μM concentration). In the virtual screening campaign[24, 127] a compound had been identified which had instead of the naphthalene moiety a 4-hydroxyphenyl substitution (**PR-51**, 7.40 μM[24, 127]). The expectation that a methylation of the hydroxy group will increase the potency was not met (**Yazh-823,** 31% inhibition at 1 μM concentration). Also 2-methoxy and 4-diethylamino substitution of the benzene were not beneficial (**Yazh-852,** 5% and **Yazh-765**, 28% inhibition at 1 μM concentration). For the coumarin derivatives discussed in chapter 4.3.3, it was found that a bromine in the 3-position of the benzenesulfonamide was beneficial. Therefore, the two most potent compounds (**Yazh-755**, **Yazh-774**) were substituted with bromine in the 3-position. However, both compounds were less active (**Yazh-K19**, 14% and **Yazh-K20**, 36% inhibition at 1 μM concentration) than the nitro-substituted analogs.

4.3.3   Coumarin derivatives

For hydrazone derivatives it had been found that a nitro group in the 3-position of the benzenesulfonamide moiety is beneficial. For this reason, the benzenesulfonamide moiety of coumarin derivatives was additionally substituted in the 3-position with methyl, halogens or a nitro group (Table 18). The methylation of the benzenesulfonamide in the 3-position of the lead compound (6-chloro, Figure 48B) led to a 2-fold increase in potency (**Yazh-925**, 797 nM) while a methylation in the 2-position of the same compound led to a less active derivative (**Yazh-K359**, 41% at 1 μM concentration). This indicates that the substitution of the 3-position of the benzenesulfonamide is favorable. Interestingly, methylation in the 3-position and no substitution on the coumarin moiety led to inactive compounds (**Yazh-924**, 8% inhibition at 1 μM) which underlines the importance of an electron-withdrawing substitution in the 6-position of the coumarin moiety. The most beneficial substitution at the 3-postion were halogen atoms with the following order of potency Br > I > F > Cl. Bromine in the 3-position and different coumarin modifications resulted in the most active compounds of this series. Again, the most potent inhibitor was the 6-chloro derivative (**Yazh-937**, 198 nM), which was 9-fold more potent than the lead compound (MAF44, see introduction, page 36). Also 6-bromo- (**Yazh-K291**) and 6-methoxy- (**Yazh-K301**) substituted coumarines were found to be active with K_i values of 446 and 644 nM, respectively.

Results and Discussion
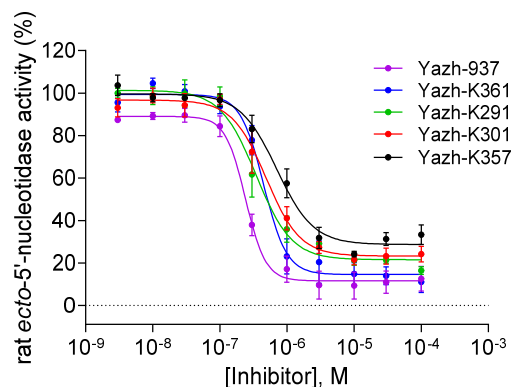
Figure 49. Exemplary concentration-response curves of coumarin derivatives tested at rat CD73 (Data points are means ± SEM from at least three separate experiments performed in duplicates).

Table 18. Inhibitory potencies of coumarin derivatives at rat CD73 (means ± SEM from at least three separate experiments performed in duplicates).
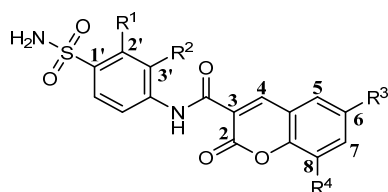
	Compound	R^1	R^2	R^3	R^4	Rat CD73 $K_i \pm$ SEM (nM)*
1	**Yazh-924**	H	CH_3	H	H	> 1000 (8%)
2	**Yazh-925**	H	CH_3	Cl	H	**797 ± 170**
3	**Yazh-K359**	CH_3	H	Cl	H	> 1000 (41%)
4	**Yazh-K343**	CH_3	H	Br	H	> 1000 (12%)
5	**Yazh-K358**	H	F	Cl	H	**414 ± 51**
6	**Yazh-K361**	H	F	Br	H	**391 ± 96**
7	**Yazh-K342**	H	Cl	Cl	H	> 1000 (41%)
8	**Yazh-K290**	H	Br	H	H	> 1000 (22%)
9	**Yazh-937**	H	Br	Cl	H	**198 ± 37**
10	**Yazh-K301**	H	Br	MeO	H	**446 ± 154**
11	**Yazh-K291**	H	Br	Br	H	**644 ± 181**
12	**Yazh-K298**	H	Br	NO_2	H	> 1000 (19%)
13	**Yazh-K366**	H	Br	H	MeO	> 1000 (0%)
14	**Yazh-K475**	H	Br	OH	H	> 1000 (12%)
15	**Yazh-K367**	H	Br	Cl	Cl	> 1000 (42%)
16	**Yazh-K357**	H	Br	Br	Br	**656 ± 185**
17	**Yazh-K310**	H	I	Cl	H	**262 ± 13**
18	**Yazh-K311**	H	I	Br	H	> 1000 (-2%)
19	**Yazh-K343**	H	CF_3	Cl	H	> 1000 (12%)
20	**Yazh-K367**	H	CF_3	Br	H	> 1000 (10%)
21	**Yazh-K295**	H	NO_2	H	H	> 1000 (27%)
22	**Yazh-K293**	H	NO_2	Cl	H	> 1000 (6%)
23	**Yazh-K292**	H	NO_2	Br	H	> 1000 (22%)
24	**Yazh-K314**	H	NO_2	MeO	H	**439 ± 80**
25	**Yazh-K297**	H	NO_2	NO_2	H	> 1000 (19%)

* or % inhibition at indicated concentration

A nitro or hydroxy group in the 6-position or a methoxy group in the 8-position of the coumarin was found to be less active (**Yazh-K298**, 19%; **Yazh-K475**, 12%; **Yazh-K366**, 0% at 1 µM concentration). In the virtual screening campaign a 4,6-dichloro-substituted coumarin had been identified. It had shown a moderate inhibition of CD73 in the medium µM range (**PR-79**, 69.0 µM).[24, 127] Nevertheless, substitution in the 4- and 6-position with chlorine and bromine was investigated. Interestingly, the dibromino derivative resulted in an inhibition of CD73 in the nM range (**Yazh-K357**, 656 nM). The dichloro derivative was less potent (**Yazh-K367**, 42% at 1 µM concentration). The 3-position was further explored with the introduction of a larger lipophilic trifluoromethyl group, but this modification was not accepted (**Yazh-K343**, 12% and **Yazh-K367** 10% at 1 µM concentration). The substitution of the 3-position with a nitro group, which had resulted in the series of hydrazones in the most active compounds, was not beneficial. Only 6-methoxy showed an inhibition higher than 50% in the primary screening and was tested with a K_i value of 439 nM. Very interesting was the result of 6-chloro substitution. This usually best substitution showed in combination with a 3-nitro group no inhibition of CD73 (**Yazh-K293**, 6% at 1 µM concentration).

The exchange of coumarin by 2H-chromene or chromone was explored (Table 19). 2H-chromenon led to compounds with lower activity (**Yazh-K354,** 38% and **Yazh-K355**, 28% inhibition at 1 µM concentration) compared to the structures from which they were derived (**Yazh-937**, 198 nM and **Yazh-K310,** 262 nM). In contrast, the exchange of the coumarin moiety by chromone was successful. Compound **Yazh-K374** which is brominated at the 6-position of the chromone showed a K_i value of 281 nM and was confirmed to be significantly (p<0.05) more potent than the comparable coumarin derivative (**Yazh-K291,** 644 nM).

Results and Discussion

Table 19. Potencies of sulfonamide derivatives with replacement of the coumarin at rat CD73 (means ± SEM from at least three separate experiments performed in duplicates).

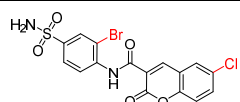|	Compound	R^1	Rat CD73 K$_i$ ± SEM (nM)*
1	Yazh-K354	Br	> 1000 (38%)
2	Yazh-K355	I	> 1000 (28%)
3	Yazh-K364	H	> 1000 (31%)
4	Yazh-K374	Br	**281 ± 29**
5	Yazh-K184		**409 ± 21**

* or % inhibition at indicated concentration

The orientation of the sulfonamide, which is believed to interact with the arginines and zinc ions in the phosphate binding site of CD73 was investigated by shifting the sulfonamide to the 2-position of the benzenesulfonamide, by introduction of a further carbon atom between amide and benzene or between the sulfonamide and the benzene. Also, the replacement of the sulfonamide with boronic acid was analyzed. All three modifications resulted in less active compounds (appendix, Table 32-34, page 145-146).

To sum up, from the hydrazone series compound **Yazh-842** (194 nM) was found to be the most active compound. It is 8-fold more potent than the lead structure (Figure 48A). As discussed above, testing of this compound class was problematic. At high inhibitor concentrations they were insoluble, which led to incomplete curves. Besides the assumed instability of the hydrazone group, the nitro group in the 3-position is problematic for further drug development, too. Nitro-aromatic compounds or their active metabolites were often found to be toxic.[117, 118] In contrast, most potent coumarin derivatives share a bromine substitution in the 3-position. The most active derivative of the coumarin series was **Yazh-937** (198 nM). It is 9-fold more potent than the lead structure (Figure 48B).

This compound was further analyzed as representative for the sulfonamide derivatives with a coumarin moiety at human soluble and membrane-bound CD73. The potency at human and rat recombinantly produced soluble enzyme was equal (Table 20 and Figure 50), but the potency at the membrane-bound variety of CD73 sharply decreased.

Table 20. Potency of Yazh-937 analyzed with different sources of CD73 means ± SEM from at least three separate experiments performed in duplicates).

Compound		Rat CD73 $K_i \pm$ SEM (nM)	Human CD73 $K_i \pm$ SEM (nM)	MDA-MB-231 Membrane preparation $K_i \pm$ SEM (nM)*
Yazh-937		198 ± 37	293 ± 50	> 100000

* or % inhibition at indicated concentration
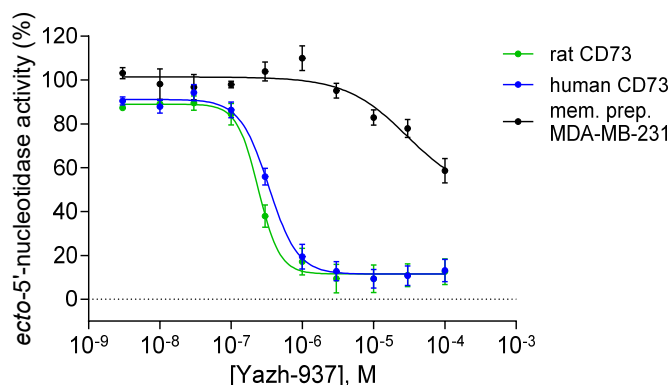
Figure 50. Concentration-response curves of Yazh-937 at different sources of CD73 (means ± SEM from at least three separate experiments performed in duplicates).

Even at a concentration of 100 μM of the compound the inhibition of CD73 on the membrane preparation was not higher than 50%. Thus, it seems that the structural difference between the human soluble and the human membrane-bound variety is responsible for different potencies. The membrane-bound variant is present as a dimer. Due to the dimer formation, it could be that the binding site, to which **Yazh-937** binds, is no longer accessible. Furthermore, the membrane, which sterically "shields" part of the enzyme, must also be considered. If the binding site or the access to the binding site is located within the membrane, it cannot be reached by the inhibitor. The recombinant human soluble enzyme was expressed in insect cells. The three-dimensional structure of a protein, in this case an enzyme, also depends on the post-translational modifications. However, the type and pattern of post-translational modifications in insect cells differs from post-translational modifications in humans.[181] These different post-translational modifications in the human membrane preparation may additionally lead to a different structure of the human CD73 which leads to the inhibitor **Yazh-937** not being able to address the enzyme and thus, not inhibiting the enzymatic reaction. Of course one would rather have an inhibitor that is also potent at the membrane. Nevertheless, data suggest that these types of inhibitors are selective

for the soluble CD73 and do not address the membrane-bound form. Thus, this compound class might be further investigated to developed tool compounds for the analysis of the truncated soluble variety of CD73 in the human plasma.

4.4 Optimization of malachite green assay, automatization and screening

4.4.1 Overview

In previous chapters radiolabeled AMP was used to measure the activity of ecto-5′-nucleotidase and to characterize inhibitors. The radioassay is a very sensitive assay. However, for the automated analysis of thousands of substances the assay is not suitable, because the procedure of the assay involves precipitation/filtration steps, and the transfer to a liquid handling workstation is associated with high costs due to the amounts of radioactive waste. For that reason, the opportunity to measure the enzymatic activity of rat ecto-5′-nucleotidase by analyzing the formed inorganic phosphate by malachite green was explored. In the following chapters, the optimization of the malachite green assay, the validation of the test system, the transfer to the liquid handling workstation and results of the screening of around 6000 compounds are discussed.

4.4.2 Optimization of the malachite green assay

Ecto-5′-nucleotidase hydrolyzes AMP to adenosine and phosphate. Phosphate can be measured by a complex formation reaction with ammonium molybdate and the dye malachite green. Based on the findings of Cogan et al.,[152] who investigated and optimized the complex forming reaction, the malachite green assay was adapted to ecto-5′-nucleotidase.

Cogan and coworkers reported an absorption maximum of the formed complex at 620 nm. In our studies, under the chosen buffer conditions and with the used spectrometer, we identified a maximum at 616 nm. Interestingly, a difference spectra of samples with and without phosphate showed at 600 nm the highest difference, and was therefore selected for further measurements (Figure 51).
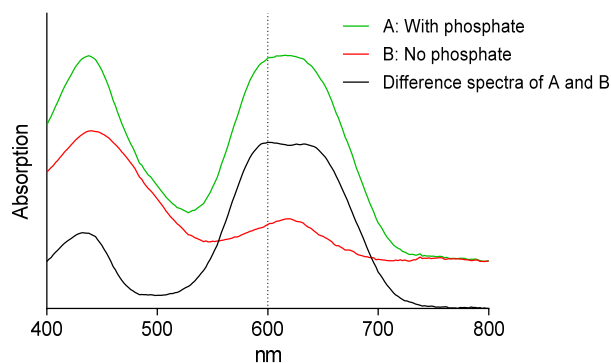
Figure 51. Absorption spectra of the malachite green phosphomolybdate complex. The green line illustrates absorption spectra with phosphate in the sample, the red line without phosphate, and the black line the difference spectrum of both spectra with a difference maximum at 600 nm.

For the transfer of the assay to a liquid handling workstation, it is important that the enzyme activity is maintained during the period of screening. In the utilized system, the enzymatic solution was stored at 4°C. The enzymatic activity of the ecto-5′-nucleotidase was not stable, thus different additives were explored to maintain the activity at least for 12 hours to enable screening overnight. It has been found that 0.01% BSA in the five-fold enzyme working solution stabilized the enzymatic activity with only a slight decrease of activity (10% decrease over 22 h). At this concentration the photometric readout was also not disturbed. (Figure 52). The reaction buffer itself was already optimized by Dr. Marianne Freundlieb.[24] The highest enzymatic activity occurs with a buffer containing 25 mM TRIS, 2 mM $MgCl_2$, 1 mM $CaCl_2$, 140 mM NaCl, pH 7.4. The carrier DMSO was accepted up to a concentration of 5% without any change in enzymatic activity.
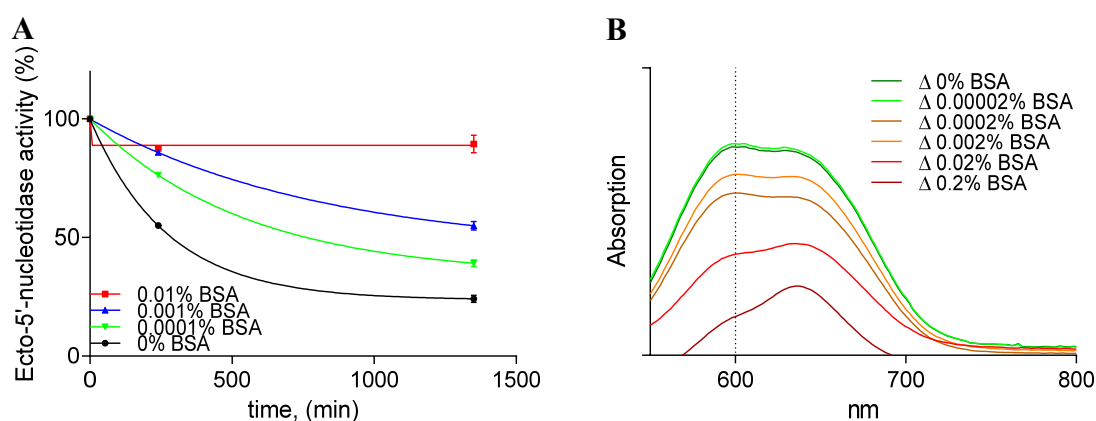

Figure 52. Ecto-5′-nucleotidase activity stabilized with 0.01% BSA. (A) Enzymatic activity is stabilized with 0.01% BSA (five-fold enzyme solution) for about 22 h. **(B)** Difference spectra with different BSA concentrations showed a high signal at this concentration in the assay (0.002% BSA).

Results and Discussion

### 4.4.2.1 Calibration of test system with phosphate calibration curve

The sensitivity was analyzed with a phosphate calibration curve. For this purpose, the absorbance values were plotted against the different phosphate concentrations (Figure 53). The linear regression equation was y = 0.03114x + 0.0262 with a correlation coefficient of 0.997. The limit of detection (LOD) was calculated as a parameter for the sensitivity of the assay and was 0.183 ± 0.086 µM phosphate. The literature describes the sensitivity of the colorimetrically malachite assay to be around 1 µM phosphate.[134, 152] Thus, the assay performed under the optimized conditions is about 4-times more sensitive.
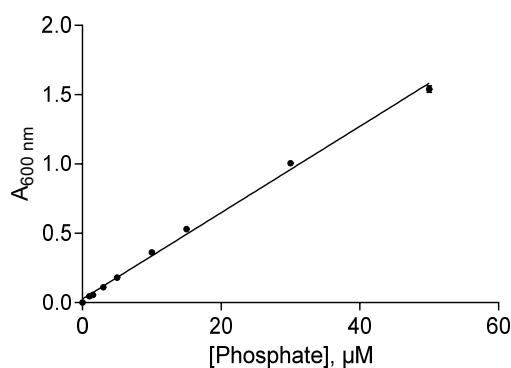
Figure 53. Phosphate calibration curve (means ± SEM from three independent experiments, performed in triplicates. Linear regression: $R^2 = 0.997$, LOD = 0.183 ± 0.086 µM).

4.4.2.2 Optimization of substrate and enzyme concentration

For the identification of potential competitive and non-competitive inhibitors, it is essential to set the substrate concentration in a range between 0.1 x K_M and 10 x K_M. The substrate concentration was set at 30 µM AMP, which is slightly lower than the measured apparent K_M value of 36.5 ± 1.6 µM (4.4.2.3, page, 109) of the newly developed assay. In order to improve the robustness and sensitivity of an assay, it is important to choose an enzyme concentration that generates a large signal window on the one hand, and to carry out the reaction in the linear range of AMP hydrolysis on the other hand. An enzyme titration was performed, to analyze the optimal enzyme concentration (Figure 54). The equation of the linear regression was y = 10.34x + 0.406 with a correlation coefficient of 0.972. The optimal enzyme concentration is at least 20-fold higher than the LOD. The LOD was calculated as described above and was 1.26 ± 0.26 ng per reaction (reaction volume: 50 µl). Thus, an enzyme amount of 25 ng per reaction was used for further enzymatic reactions.
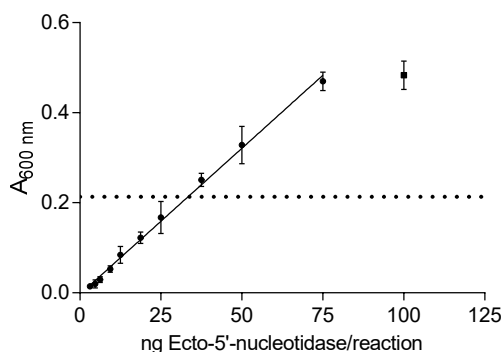
Figure 54. Determination of the optimal enzymatic amount per reaction. Reactions were conducted with 30 µM of AMP and an incubation time of 10 min. An amount of 25 ng ecto-5′-nucleotidase per reaction produced the highest signal intensity without crossing the 20% substrate hydrolysis limit.

The incubation time of the enzymatic reaction was also optimized. Like for the optimization of the enzyme amount used in each reaction, the incubation time should also be optimized so that the signal-to-noise ratio is as high as possible without crossing the 20% threshold of product formation. Therefore, different incubation times were investigated. An incubation time of 10 min was identified which meets the requirements described above. To sum up, the optimized conditions of the newly developed malachite green assay for ecto-5′-nucleotidase were: 30 µM AMP, 25 ng enzyme and 10 min incubation time.

4.4.2.3 Michaelis-Menten kinetics

The parameters of the Michaelis-Menten enzyme kinetics of ecto-5′-nucleotidase vary dependent on the used assay. After the assay parameters had been optimized, the enzymatic parameter K_M and V_{max} were recorded with the newly established assay (Figure 55). The K_M value was calculated using the Michaelis-Menten equation and resulted in a value of 36.5 ± 1.6 µM, which is comparable to the values described in literature.[93, 93, 151, 155, 158]
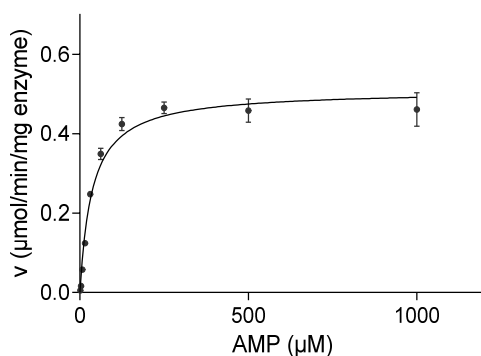
Figure 55. Michaelis–Menten kinetics of rat ecto-5′-nucleotidase. Kinetic parameters: $V_{max} = 0.510 \pm 0.02$ µmol/min/mg ecto-5′-nucleotidase, $K_M = 36.5 \pm 1.6$ µM (means ± SEM from three independent experiments, performed in duplicates).

4.4.2.4 Validation of the optimized assay

The Z′-factor is used as a statistical parameter to analyze if the assay quality is good enough for high-throughput-screening (see introduction, page 38).[133] Thus, before the assay was adapted to the liquid handling workstation, the Z′-factor was investigated in three independent experiments. It was calculated with the equation (17) listed in the introduction, page 38 with a value of 0.82 ± 0.02.

Z′-factors above 0.5 indicate that an assay is suitable for high-throughput-screening. Thus, it was adapted to the liquid handling workstation. Following this, Z′-factor was analyzed again running the assay with the liquid handling workstation. A value of 0.66 ± 0.07 was calculated, which confirmed previous findings conducted with manual pipetting.
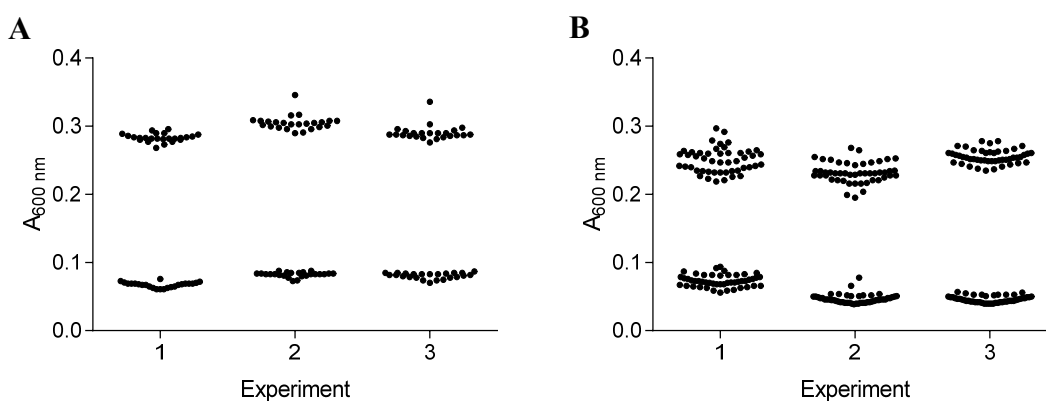
Figure 56. Validation of the optimized assay. Analysis of Z′-factor as a parameter for assay quality pipetted **(A)** manually, and **(B)** in an automated procedure. Both setups revealed Z′-factors above 0.5 indicating a robust assay suitable for high-throughput-screening.

4.4.2.5 Enzyme inhibition assays

For further validation of the developed assay, the potency of the reference inhibitor **AOPCP** was analyzed by recording a full concentration-response curve (Figure 57). The IC_{50} values were analyzed by fitting sigmoidal concentration-response curves and, the corresponding K_i values were calculated with the Cheng-Prusoff equation (14) as listed in the introduction, page 24. The K_i value of **AOPCP** was found to be 42.3 ± 5.67 nM, which was slightly more potent than measured with the radioassay, but still in the same range and consistent with literature values.[93, 158]
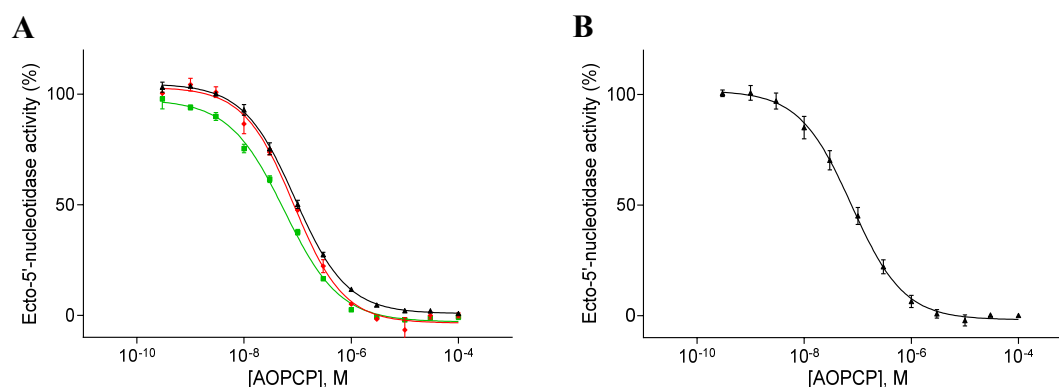
Figure 57. Concentration-response curves of the reference inhibitor AOPCP. (A) Individual measurements. **(B)** Mean curve (IC_{50}: 77.1 ± 10.4 nM; corresponding K_i value: 42.3 ± 5.67 nM (means $\pm$ SEM from three independent experiments, performed in triplicates).

### 4.4.3 Screening of compound libraries

The assay was transferred to a liquid handling system and 5641 compounds from the in-house compound library were analyzed at a test concentration of 10 µM. In addition, 140 fragments (size 250 to 300 g/mol) were tested at 500 µM concentration. The compound library comprises 15 smaller sub-libraries, in which the compounds are either structur- or target-related. The Tocris library is the largest sub-library and consists of 1200 different bioactive compounds (#2890 and #3514 Tocris Biosciences, Bristol, UK). Compounds in this library are well-characterized biologically active compounds which address multiple targets.[165, 166] The second largest library is the xanthine library which currently contains 812 xanthine derivatives. The xanthines were synthesized by our group or cooperation partners in earlier projects. The third largest library is the ChemBridge library which is part of the compound library of Prof. Dr Herdewijn (University of Leuven, Netherlands) and contains 720 compounds. Further libraries are the ChemDiv library also from Professor Herdewijn (560 compound) and the approved drug library (520 compound), which contains different

commercially approved drugs.[164] Further tested sub-libraries are illustrated in chapter 3.5, on page 64.

In the screening campaign, 21 compounds inhibited/activated the enzymatic activity by more than 50%, resulting in a hit rate of 0.36%. Since the hit rate was relatively low, the threshold for defining a hit was decreased to 25% inhibition. With this definition of a hit, the hit rate of the screen was 1.33%. Because the screening was carried out only once, which is usual for HTS campaigns, false-positive and false-negative hits occur. The false-negative hits are not noticeable, because they cannot be identified within the mass of the other negative compounds. However, it is necessary to validate the hits in order to exclude the false-positive ones. It is advantageous to use a different assay for hit validation, since false-positive hits might also be due to the used assay. Thus, for hit validation the previously described radioassay was used, and 20.1% of the identified hits could be validated. Thus, around 80% of the hits identified in the screening campaign were false-positives. Reasons for false-positive hits which are related to the malachite green assay system may, be due to compounds interfering with the complex-forming reaction and/or changing the absorbance properties of the complex. Interestingly, none of the putative activators could be validated. The potency of the validated hits was determined by measuring full concentration-response curves using the sensitive radioassay.
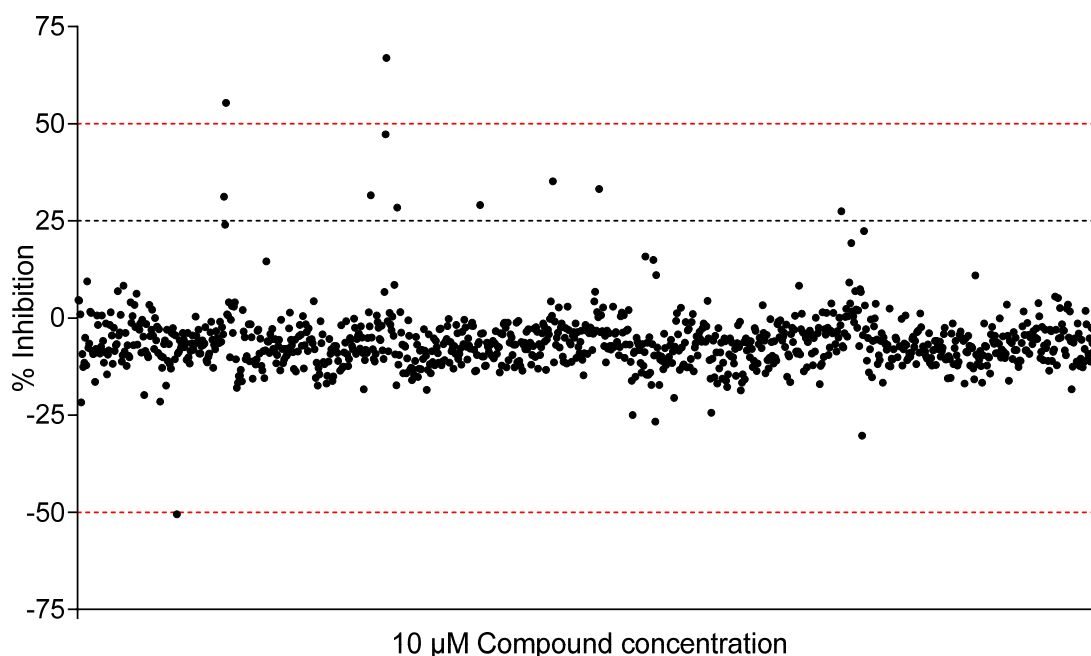

Figure 58. Exemplary screening results of the xanthine sub-library. Each dot represents the inhibition/activation of one compound.

4.4.4   Identified xanthine derivatives as inhibitors of CD73

Most hits were structurally related to xanthines. These xanthine derivatives were originally synthesized as selective adenosine A_{2A} receptor antagonists.[182–191] Since the inhibition of CD73 and the antagonism of adenosine A_{2A} receptors may result in additive or synergetic effects, these structures were of particular interest. The compound library contained further xanthine derivatives which were not stored on screening plates. Because xanthine hits share structural elements, a search towards these elements was performed. The identified compounds were initially screened at 10 µM concentration and if they inhibited CD73 more than 50%, full concentration-response curves were recorded. These results as well as the screening data of structurally similar but inactive compounds, were included into the analysis of the structure-activity relationships of xanthine derivatives for rat CD73. Altogether, the data of 77 compounds were used for the compilation of the structure-activity relationships of the xanthines. For the sake of clarity, not all data are listed in the table of the following chapter. In some cases, examples are given and otherwise reference is made to the appendix.

4.4.5   Structure-activity relationships of xanthine derivatives

The identified xanthine hits generally share alkylation of the N1- and N3-position (xanthine numbering is used, see Figure 59) and a nitrogen atom is attached to the C8-position of the xanthine core structure. This nitrogen is linked to the nitrogen N7 of the xanthine backbone via an aliphatic chain. This chain contains three or four carbon atoms, which ultimately leads to heterocycles consisting of six or seven atoms, respectively. In addition, the nitrogen is substituted with different residues (Figure 59).
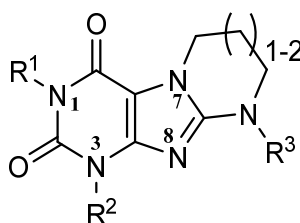
Figure 59. Basic scaffold of identified xanthine derivatives as inhibitors for rat CD73.

Most of the identified tricyclic xanthine hits have methylation groups in the N1- and N3-position and, substituents were superior to ethyl-, propyl- or butyl groups as alkyl side-chains in these positions (Table 21). A good example for these finding is compound **PZB01808014** (23.1 µM) which is methylated in the N1- and N3-position.
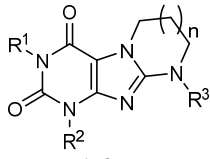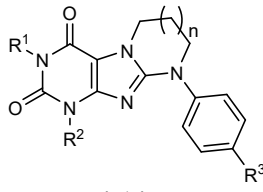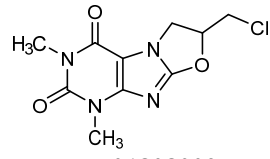
Results and Discussion

Test results of its ethyl-, propyl- or butyl-substituted analogs resulted in inactive compounds. Nevertheless, one compound with a six-membered ring was identified where a propyl-substitution (**PZB01808104**, 7.74 µM) is favored over a methyl group (**PZB01808173**, 10.0 µM). The residue for these both compounds at N^8 is methoxypropyl, which might influence the position of the inhibitor within the binding site of the enzyme, leading to another position where the propyl at the N1- and N3-position is favored over methyl. Another structural feature that all potent compounds share is the substitution of the N^8-position with aliphatic or aromatic side chains. In addition to the substitution with methoxypropyl, which was discussed earlier, and a substitution with cyclohexanol (**PZB01808055**: IC$_{50}$: 13.9 µM), no further structures were potent for either the six- or the seven-membered ring bearing alkyl chains at the N^8-position. Further active compounds were characterized by a substituted phenyl moiety in this position. Benzyl moieties were found to be inactive (for a complete set of xanthine derivatives see Table 35-39, page 148-151).

Compounds with substituents on the phenyl ring were investigated. It turned out that *para*-substituted derivatives are responsible for the potency of the hits in the series of seven-membered heterocycles, where methoxy is the most active one (**PZB01808057**, 3.30 µM). Methylation in this position led to an IC$_{50}$ of 8.47 µM (**PZB01808051**) and other substituents in the *para*-position gave the following sequence of potencies: methoxy > methyl > phenoxy > ethoxy > hydroxy > acetoxy > fluoro. The methoxy substitution was also investigated for the six-membered ring. This substitution was accepted, but the compound was less potent (**PZB01808047**, 25.1 µM, appendix, Table 35, page 148). One further xanthine was identified as a hit which has in contrast to the other hits a five-membered heterocycle with an oxygen instead of a nitrogen attached to the C8-position, resulting in an oxazolidine. This moiety is further substituted with a chloromethyl residue within the aliphatic region (**PZB01808002**) and showed an IC$_{50}$ of 10.4 µM. Further five-membered cycles were found to be not active (appendix, Table 39, page 151).

Table 21. Potencies of xanthine derivatives as inhibitors of rat CD73 (means ± SEM from at least three separate experiments performed in duplicates).

					Rat CD73
	Compound	**n**	**$R^{1,2}$**	**R^3**	**$IC_{50} \pm$ SEM (µM)***
1	PZB01808173	1	methyl	3-methoxypropyl	**10.0 ± 1.14**
2	PZB01808104	1	propyl	3-methoxypropyl	**5.74 ± 4.05**
3	PZB01808055	2	methyl	4-hydroxycyclohexane	**13.9 ± 1.6**
4	PZB01808014	1	methyl	hydroxy	**23.1 ± 8.3**
5	PZB01812022	1	ethyl	hydroxy	> 10 (2%)[a]
6	PZB01812009	1	butyl	hydroxy	> 10 (6%)[b]
7	PZB01812008	1	propyl	hydroxy	> 10 (1%)[b]
8	PZB01808051	2	methyl	methyl	**8.47 ± 1.32**
9	PZB01808054	2	methyl	hydroxy	> 10 (25%)[b]
10	PZB01808057	2	methyl	methoxy	**3.30 ± 0.34**
11	PZB01808053	2	methyl	ethoxy	> 10 (33%)[b]
12	PZB01808056	2	methyl	acetyl	> 10 (27%)[b]
13	PZB01808058	2	methyl	fluoro	> 10 (16%)[a]
14	PZB01808052	2	methyl	phenoxy	~ 10[c]
15	PZB01808002				**10.4 ± 1.55**

* or % inhibition at indicated concentration; [a] tested with malachite green assay (screening); [b] tested with radioassay; [c] problematic to measure, due to solubility issues
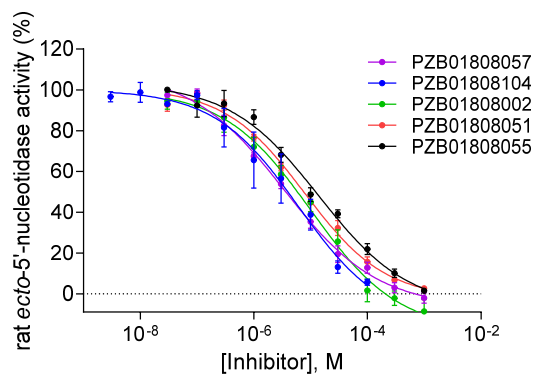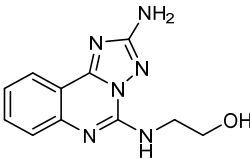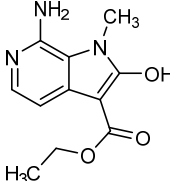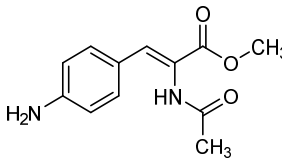

Figure 60. Exemplary concentration-response curves of xanthine derivatives tested at rat CD73 (Data points are means ± SEM from at least three separate experiments performed in duplicates, for IC_{50} values see Table 21).

Results and Discussion

4.4.6 Identified fragments as CD73 inhibitors

A fragment library consisting of 140 compounds which have a molecular weight in the range of 250 to 300 Da was screened. Because of their smaller size and therefore expected lower potencies (introduction, page 1), the initial screening concentration was set to 500 µM. Like for the xanthine library, the hits of the fragment library were validated with the radioassay. In addition to the initial screening concentration of 500 µM, the compounds were analyzed at 100 and 10 µM concentrations, too. Three compounds inhibited rat CD73 by more than 50% at 100 µM concentration. These compounds were further investigated by analysis of full concentration-response curves (Table 22 and Figure 61). The resulting IC_{50} values were measured to be in the medium µM range. Compared to the previous xanthine derivatives, these compounds were less potent, but are still interesting for further investigations, because the smaller size gives space for multiple chemical modifications, which have the potential to increase the potency of these compounds.

Table 22. Potencies of identified fragments at rat CD73 (means ± SEM from at least three separate experiments performed in duplicates).

PZB00609012	PZB00709002	PZB09414102
IC_{50} ± SEM: 32.6 ± 2.6 µM	IC_{50} ± SEM: 37.4 ± 7.4 µM	IC_{50} ± SEM: 96.0 ± 8.0 µM

For fragments which were validated as hits (500 µM), but were less active than 50% inhibition at 100 µM, pseudo-IC_{50} values were determined with the test results obtained by measuring the inhibition at 500, 100 and 10 µM compound concentration (appendix, Table 40, page 152).
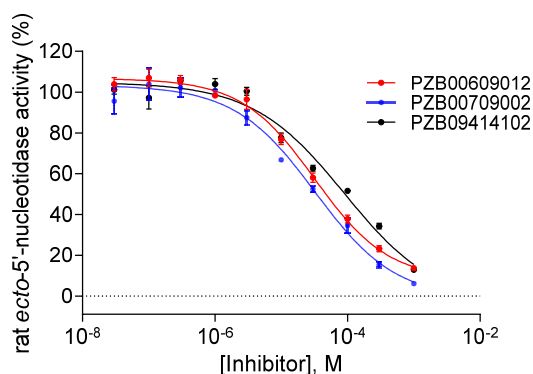
Figure 61. Concentration-response curves of fragment hits tested at rat CD73 (Data points are means ± SEM from at least three separate experiments performed in duplicates).

4.4.7   Further identified inhibitors for CD73

Four further structures were identified by the automated screening and confirmed with the radioassay (Table 23 and Figure 62). Two cationic dyes, Fast Blue B (**PZB20415009**) and Crystal violet (**PZB20415013**), were identified in the internal drug library and measured with IC_{50} values of 2.07 and 16.6 µM, respectively. Besides the dye properties of crystal violet, it also has antibacterial, -trypanosomal, -fungal -angiogenic, and -tumor characteristics.[192, 193] However, both compounds were reported to have multiple cancerogenic effects and thus, are less suitable for further drug development.[194–197]

Table 23. Further identified hits at rat CD73 (I) (means ± SEM from at least three separate experiments performed in duplicates).
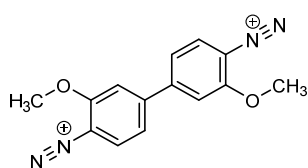
PZB20415009 (Fast Blue B)
IC_{50} ± SEM: 2.07 ± 1.72
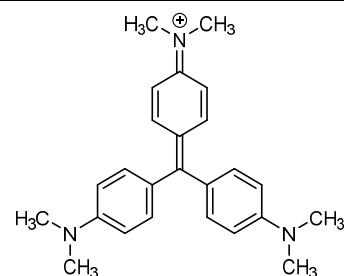
PZB20415013 (Crystal violet)
IC_{50} ± SEM: 16.6 ± 4.8

A further identified hit from the internal drug library was **Levothyroxine**. It inhibited rat CD73 with an IC_{50} of 2.13 ± 0.62 µM (Figure 62). **Levothyroxine** is synthetically produced and corresponds to the body's thyroid hormone thyroxine (T4). Levothyroxine replaces the thyroid hormone thyroxine in hypothyroidism. It leads to an increase of the metabolic rate and further affects the protein, carbohydrate, lipid, nucleic acid and vitamin

117

metabolism.[198, 199] A further hit was a chromenone (**PZB11413020A**), which was originally synthesized by Dr. Anne Meyer and revealed antagonism against the δ-branch orphan G protein-coupled receptors GPR17, 35 and 55 of 10.2, 0.317 and 0.122 μM, respectively.[200] This compound inhibited rat CD73 with an IC_{50} of 0.806 ± 0.424 and was the most active compound from this screening campaign. However, the chromenone acted as partial inhibitor and an efficacy of about 50% was not exceeded at higher inhibitor concentrations. The calculated logP of 5.08[201] suggests that the low efficacy of the compound was, similar to sulfonamides, due to low water solubility. A further drawback for chemical modifications of this structure is the size. The compound is with 544 Da already quite large.
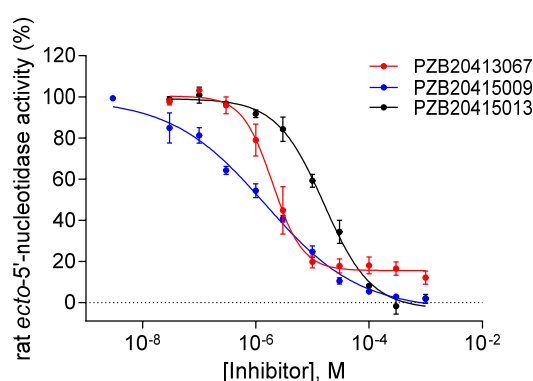
Figure 62. Concentration-response curves of further hits tested at rat CD73 (Data points are means ± SEM from at least three separate experiments performed in duplicates).

Table 24. Further identified hits at rat CD73 (II) (means ± SEM from at least three separate experiments performed in duplicates).
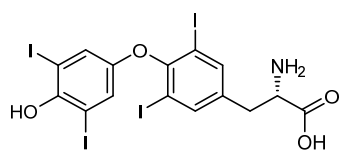

PZB20413067 (Levothyroxine)	PZB11413020A[a]
IC_{50} ± SEM: 2.13 ± 0.62	IC_{50} ± SEM: 0.806 ± 0.424
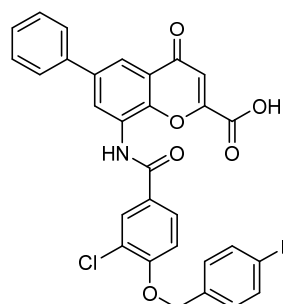
[a] partial inhibitor (inhibition at 100 μM 51 ± 7%)

4.4.8 Determination of mode of inhibition

Two inhibitors of the validated hits were selected and their mode of inhibition was studied. The first inhibitor was the most potent xanthine derivative (**PZB01808057**, 3.30 µM) and the second one was one of the identified fragments (**PZB00709002**, 37.4 µM). Besides these both inhibitors, the well described competitive inhibitor **AOPCP** was also analyzed for validation of the method. To determine the mode of inhibition, Michaelis-Menten kinetics were recorded for rat CD73 with no inhibitor, and with the respective inhibitor at a concentration of 0.5 and 2 x IC_{50} using the optimized malachite green assay. The K_M value of the all non-inhibited enzyme reactions revealed a mean value of 39.7 ± 2.78 µM which is comparable to the K_M value determined previously with the malachite green assay (page 109, $K_M = 32.0 \pm 0.7$ µM). Independent of the inhibitor concentration of **AOPCP** the same V_{max} was reached at high substrate concentration. This characteristic is typical for a competitive inhibitor, because at high substrate concentrations the inhibitor is displaced from the target and the enzymatic reaction is not inhibited, which consequently leads to the same V_{max} value than for the not inhibited reaction (Figure 63).
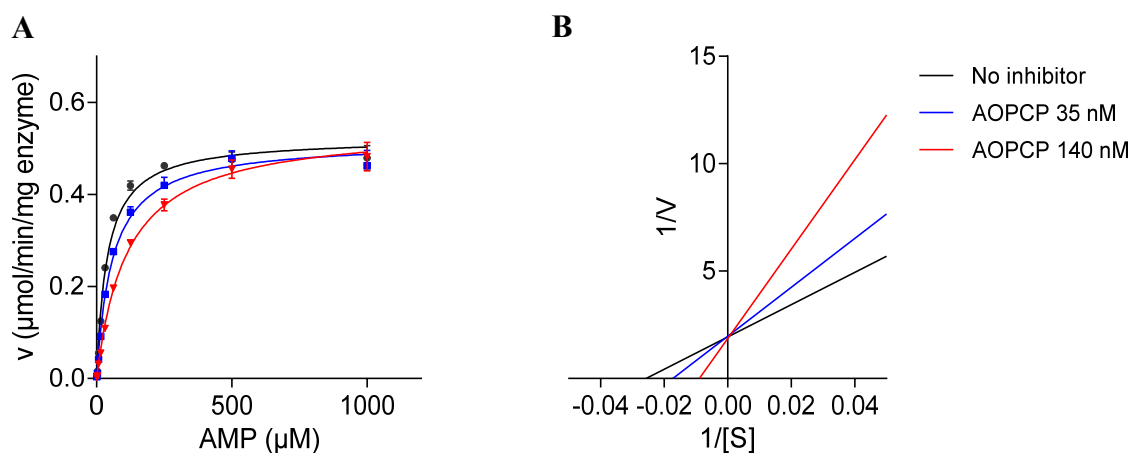
Figure 63. Competitive inhibition mode of AOPCP. (A) Michaelis-Menten kinetics: V_{max} is reached at high substrate concentration independent of the used inhibitor concentration. K_M value is increased for higher inhibitor concentrations. **(B)** Lineweaver-Burk plot shows intercept of all three lines at the y-axis what is typical for a competitive inhibitor (means ± SEM from three separate experiments performed in duplicates).

In the double reciprocal plot (Lineweaver-Burk plot) this behavior is illustrated by the intercept of all three lines nearby the y-axis. The second characteristic of a competitive inhibitor, that the K_M value for the enzymatic reaction is increased depending on the inhibitor concentration, was also observed for **AOPCP**. After it was shown that the competitive mode

of inhibition of **AOPCP** could be confirmed with the used method, the most potent xanthine derivative from the screening campaign **PZB01808057** was analyzed. The inhibitor decreased the V_{max} and increased the K_M value of the enzymatic reaction. In the Lineweaver-Burk plot, the intercept of the three lines lay in quadrant II with $\alpha > 1$. This characteristic indicates mixed inhibition (see Enzyme inhibition, page 21). The inhibitor binds to the enzyme and to the enzyme-substrate complex with different affinities. Thus, the inhibition is not totally independent of the substrate concentration. The observed increase of the K_M value further suggests that the inhibitor favors binding to the free enzyme and thus, the inhibitor has more of a competitive than an uncompetitive character. However, it is not possible to identify the binding site of the inhibitor at rat CD73. The selected compound is a representative for the whole group of identified xanthine derivatives. It can therefore be assumed that also the other xanthines bind to this binding site and also would show a mixed inhibition mode. Interestingly, also the analyzed fragment showed the mixed inhibition mode with comparable kinetics (appendix, Figure 79, page 154). It can be speculated that it also addresses the same binding site as the xanthine derivatives.
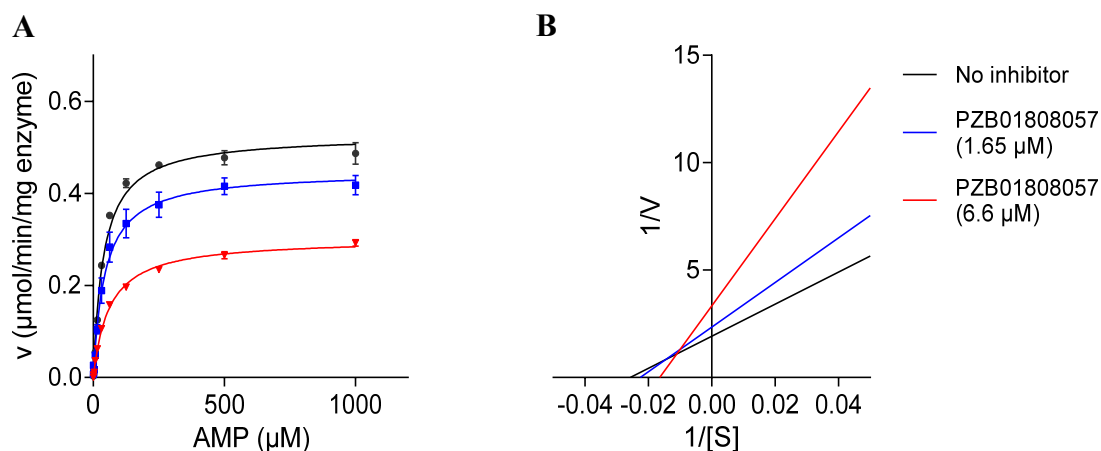
Figure 64. Mixed inhibition mode of PZB01808057. (A) Michaelis-Menten kinetics: V_{max} is decreased at higher inhibitor concentration. The K_M value is increased for higher inhibitor concentrations. **(B)** Lineweaver-Burk plot shows intercept of the lines in quadrant II with $\alpha > 1$ that is typical for a mixed inhibition with a more competitive than uncompetitive character of the inhibition (means $\pm$ SEM from three separate experiments performed in duplicates).

### 4.4.9   Determination of potencies of identified hits at human CD73

Rat CD73 and human CD73 are very similar, especially the substrate binding sites differ only in one amino acid (see introduction). In the previous study of nucleotides as ecto-5′-

nucleotidase inhibitors it was shown that most competitive inhibitors which address rat CD73 also inhibit the human variety of the enzyme (Table 14, page 95). This is not surprising, since the function of the enzyme, binding the substrate and the catalysis from AMP to adenosine, is under greater evolutionary pressure rather than amino acids outside of the binding site. The xanthine derivatives and the analyzed fragments revealed an inhibition mode which suggests that the inhibitors do not bind or do not only bind to the active site of the enzyme. Thus, it was analyzed if the identified inhibitors also inhibit the human soluble and the membrane-bound variety of CD73 (Table 25). In contrast to the nucleotides, it turned out that the compounds identified for the soluble rat CD73 modulated the human soluble enzyme in different ways. Instead of inhibiting the enzyme, most of the xanthine derivatives were found to activate the AMP hydrolysis. For one compound (**PZB01808173**) this effect was higher than 50% at 10 µM concentration, and full concentration-response curves were recorded. Interestingly, the concentration-response curve of the compound showed this activating effect up to a concentration of 30 µM. At higher concentrations activation was decreased again (Table 25 and Figure 65).

Table 25. Potencies of xanthine derivatives analyzed on different sources of CD73 (means ± SEM from at least three separate experiments performed in duplicates).

	Compound	Rat CD73 $IC_{50} \pm$ SEM (µM)*	Human soluble CD73 EC_{50}/or $IC_{50} \pm$ SEM (µM)*	Human membrane-bound CD73 $IC_{50} \pm$ SEM (µM)*
1	PZB01808173	10.0 ± 1.14	0.869 ± 0.173 (activator, 62%)**	> 10 (-15%)
2	PZB01808014	23.1 ± 8.3	6.57 ± 1.0 (inhibitor)	> 10 (-8%)
3	PZB01808055	13.9 ± 1.6	> 10 (-41%)	> 10 (-9%)
4	PZB01808051	8.47 ± 1.32	> 10 (-40%)	> 10 (-15%)
5	PZB01808057	3.30 ± 0.34	> 10 (-42%)	> 10 (-10%)
6	PZB01808002	10.4 ± 1.55	> 10 (24%)	> 10 (-1%)

* or % inhibition at indicated concentration; ** maximum activation
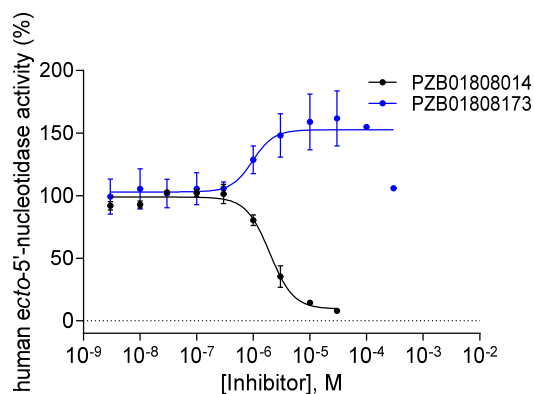
Figure 65. Concentration-response curves of xanthine hits tested at human soluble CD73 (Data points are means ± SEM from at least three separate experiments performed in duplicates).

121

Results and Discussion

This suggests that the binding site at which the xanthines address the rat enzyme does structurally not correspond to the human variety. There are many possible reasons. Rat and human enzyme are very similar but not identical. Even small differences in the primary sequence of the amino acids can lead to structural differences in the enzyme. In addition, due to the binding mode, it must be assumed that the binding site could be located in an area that is exposed to a higher variability as mentioned above. In addition, N- and C-terminus were truncated and an additional His-tag for purification was introduced. This modification can also lead to a different structural conformation of CD73 and thus influences the binding site to which the xanthine derivatives bind in the rat CD73 preparation. Nevertheless, it appears that the xanthines can address the altered binding site, but mainly leads to weak activation at low concentrations and no activation at higher concentrations. However, one of the tested xanthine derivatives showed an inhibition of the human variety of CD73 in the low µM range (**PZB01808014,** 6.57 µM, Figure 65). In addition, the xanthine derivatives were analyzed on the membrane-bound variety of CD73 (Table 25). The results showed that the tested inhibitors were inactive or slightly activating the human membrane-bound variety. The answer to the question why **PZB01808014** is not active on the membrane-bound variety of CD73 is similar to the question why some compounds inhibit rat CD73 but not human CD73. The reason will be a structural difference between both variants. In addition to the reasons listed above, also reasons which were already discussed for the sulfonamide **Yazh-937**, like CD73 is present as a dimer, different PTMs between human and insects, and the influence of the membrane must be taken into account.

The three fragments were analyzed at a concentration of 100 µM on both human variants of CD73 (Table 26). The results were similar to those previously described for xanthines. Two of the three fragments showed an activating behavior (**PZB00709002**, -42% and **PZB09414102** -14% inhibition at 100 µM) and one acted as an inhibitor but with a decreased potency (**PZB00609012,** 125 µM). Measurements on the membrane-bound CD73 showed that the two compounds characterized as activators by the soluble enzyme showed a low activating effect and the inhibitor was tested as an inhibitor, but with a weak potency (**PZB00609012,** 36% at 100 µM). The binding mode of the xanthine derivative **PZB01808057** and the fragment **PZB00709002** was determined in the previous chapter. Both showed a mixed inhibition and may share the same binding mode. These two compounds activated the human soluble enzyme and both showed no activity in membrane preparations. This supports the hypothesis that both might address the same binding site.

Table 26. Potencies of identified fragments analyzed with different sources of CD73 (means ± SEM from at least three separate experiments performed in duplicates).

|	Compound	Rat CD73 $IC_{50} \pm SEM$ (µM)*	Human CD73 $IC_{50} \pm SEM$ (µM)*	Human membrane-bound CD73 $IC_{50} \pm SEM$ (µM)*
1	PZB00609012	32.6 ± 2.6	125 ± 39	> 100 (36%)
2	PZB00709002	37.4 ± 7.4	> 100 (-42%)	> 100 (-15%)
3	PZB09414102	96.0 ± 8.0	> 100 (-14%)	> 100 (-23%)

* or % inhibition at indicated concentration

Further identified hits were also analyzed with both variants of human CD73 (Table 27 and Figure 66). In contrast to the previous structures, none of the compounds showed an activating effect towards human CD73. Levothyroxine (**PZB20413067,** IC_{50}: 0.305 µM**)** and the chromenone (**PZB11413020**, IC_{50}: 4.15 µM) inhibited the human soluble enzyme in the medium nM and the lower µM range, respectively. However, all four tested inhibitors were found to be inactive when tested on the membrane-bound variant of human CD73.

Table 27. Potencies of further identified hits analyzed with different sources of CD73 (means ± SEM from at least three separate experiments performed in duplicates).

	Compound	Rat CD73 $IC_{50} \pm SEM$ (µM)*	Human CD73 $IC_{50} \pm SEM$ (µM)*	Human membrane-bound CD73 $IC_{50} \pm SEM$ (µM)*
1	PZB20413067	2.13 ± 0.62	0.305 ± 0.114	> 10 (5%)
2	PZB20415009	2.07 ± 1.72	> 10 (17%)	> 10 (4%)
3	PZB20415013	16.6 ± 4.8	> 10 (35%)	> 10 (3%)
4	PZB11413020	0.806 ± 0.424	4.15 ± 0.90	> 10 (4%)

* or % inhibition at indicated concentration
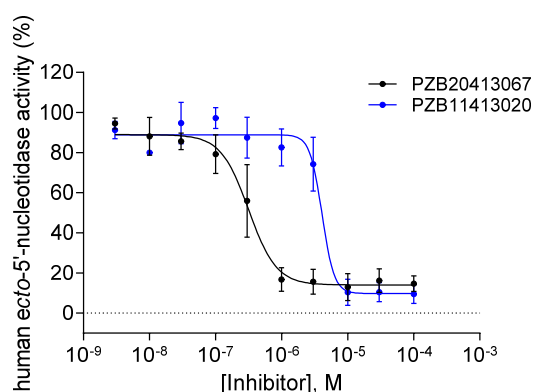
Figure 66. Concentration-response curves of levothyroxine and the chromenone tested at human soluble CD73 (Data points are means ± SEM from at least three separate experiments performed in duplicates).

## 4.5   Development of a radioligand for CD73 binding

In the previously presented studies, the potency of the inhibitors was investigated with a functional enzyme assay. This assay has the advantage to ensure that a bound substance also affects the function of the enzyme by reducing AMP hydrolysis. Nevertheless, for further characterization of an inhibitor or an activator it may be useful to investigate the binding properties of the compound to the target. For this issue, a radioligand binding assay is suitable. The radioligand bound to the target is displaced by a compound to be examined. This displacement can be measured and the binding affinity (K_d) of the substance to be investigated can be deduced. For this purpose, the potential radioligand must be a substance 1) that binds very strongly to the target, 2) where it is known that binding will affect the function of the enzyme, therefore binding in the active site of the enzyme (competitive) is preferred and 3) that it is chemically possible to introduce isotopes into the molecule.[202] As a basis for the radioligand served AOPCP derivatives with 2-chloro and additional N^6-benzyl or 2-chlorobenzyl substituents, which have already been described as potent inhibitors.[24, 94, 167] Seven further compounds were synthesized (Bhattarai and Schmies) carrying additional alkyl groups at the N^6-position and/or at the C1-position of the benzyl moiety. In addition, a compound substituted with a thio-butyl group at C8 was produced.

Table 28. The inhibitory potency of potential radioligands at rat CD73 (means ± SEM from at least three separate experiments performed in duplicates).

	Compound	R₁	R₂	Rat CD73 K_i ± SEM (nM)
1	**SB-826d**	CH_3	H	**2.93** ± 2.25
2	**SB-825d**	CH_2CH_3	H	**76.0** ± 15.3
3	**SB-828a**	$(CH_2)_2CH_3$	H	**21.5** ± 7.6
4	**SB-831d**	CH_2CHCH	H	**19.3** ± 1.4
5	**CS-230**	$(CH_2)_2CH_3$	H	**0.567** ± 0.086
6	**CS-231**[a]	CH_3	CH_3	**0.388** ± 0.095
7	**CS-232**[a]	$(CH_2)_2CH_3$	CH_3	**0.582** ± 0.161
8	**SB-822b**			**2880** ± 625

[a] Racemate

The additional alkyl groups enable the integration of several tritium atoms per molecule, because the last production step of the radioligand is the tritiation of a precursor that carries a triple bond at these positions. The introduction of several tritium atoms leads to a higher specific activity per molecule and thus, to a higher signal. The potency of these compounds was tested at rat CD73 with the radioassay, and results revealed potencies of the N^6-benzyl substituted compounds in the high picomolar range (**CS-230**, 0.567, **CS-231**, 0.388, **CS-232**, 0.582 nM). 2-Chlorobenzyl at this position led to activities in the low to medium nM range (**SB-826d**, 2.93; **SB-825d,** 76.0; **SB-828a**, 21.5; **SB-831d**, 19.3 nM). The thio-butyl compound showed weak potency in the low μM range (**SB-826d**: 2880 nM).
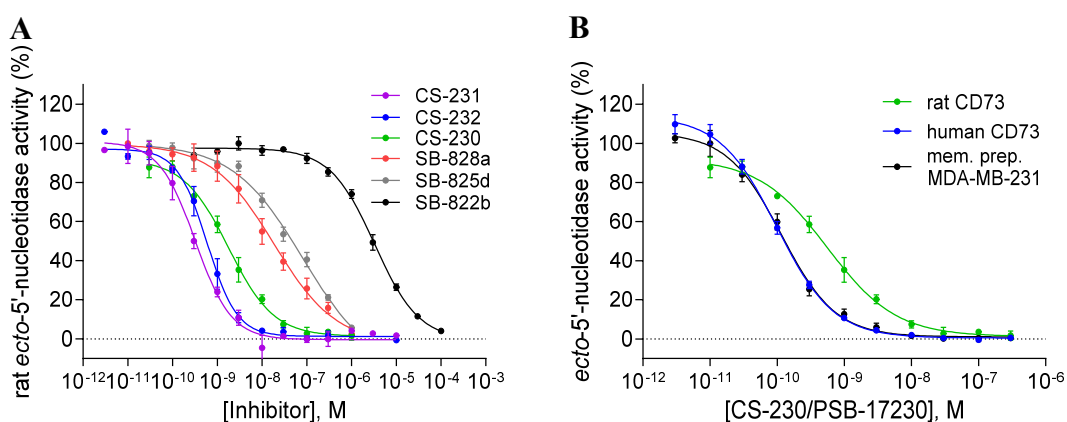

Figure 67. Concentration-response curves of potential radioligands for CD73. (A) Concentration-response curve of potential radioligands measured on rat CD73. **(B)** Concentration-response curves of the potential radioligand CS-230 using different sources of CD73 (means ± SEM from at least three separate experiments performed in duplicates).

CS-231 and **CS-232** are racemic, consisting of a mixture of enantiomers, which could cause problems for a radioassay. Thus, **CS-230** was selected for further investigation in order to avoid potential problems at an early stage. The potency of **CS-230** was also determined on the soluble human enzyme and on the membrane preparation of human TNBC cells revealing K_i values of 73.2 and 89.1 pM, respectively. In the next step the precursor of **CS-230 (**PSB-18327) was submitted to the company RC Tritec AG (Teufen, Switzerland), which produced the desired radioligand (Figure 68). In the future, this radioligand will be used for the development of a radioligand binding assay using the membrane-bound variety of CD73.

Results and Discussion

Table 29. CS-230 (PSB-17230) analyzed on different sources of CD73 (means ± SEM from at least three separate experiments performed in duplicates).

|	Compound	Rat CD73 $K_i \pm$ SEM (nM)	human CD73 $K_i \pm$ SEM (nM)	MDA-MB-231 Membrane preparation $K_i \pm$ SEM (nM)
1	CS-230 PSB-17230	0.567 ± 0.086	0.0732 ± 0.0022	0.0891 ± 0.011
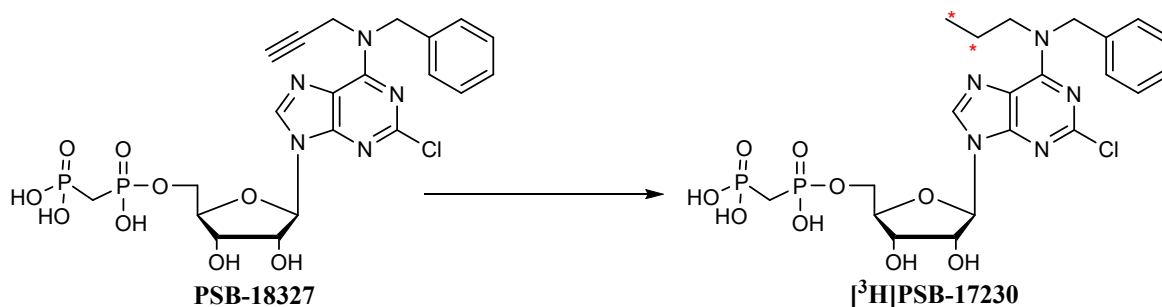
Figure 68. Radiolabeling of PSB-18327 leading to the radioligand [³H]PSB-17230. Precursor PSB-18327 was hydrogenated with tritium gas by the company RC Tritec AG (Switzerland). The resulting radioligand was produced in a purity of 99% (HPLC) and a specific activity of 108 Ci/mmol.

4.6 CD73-inhibitory potency of bispecific antibodies

4.6.1 Overview

In addition to small molecules, therapeutic antibodies have also been established in the recent years as possible drugs for various indications. Especially in the field of cancer immunotherapy antibodies became important therapeutics. Since CD73 is located extracellularly, it became a target of interest for working groups in academia and industry which focus on the production of antibodies. The CD73-addressing antibody **MEDI9447**, which is in clinical trial phase II, underlines the relevance of this approach. Professor Ditzel (University of Southern Denmark, Denmark) and coworkers designed and produced a bispecific humanized antibody with two different functional antigen-binding fragments (Fab) for CD73 (abbreviated as **AD2x1E9**, see Figure 69). One is derived from the antibody **AD2** and the other functional arm from **1E9**. It was reported that both antibodies bind to CD73, **AD2** induces internalization[86] and **1E9** reduces enzymatic activity[203] of the target. Next to this construct they designed control antibodies, which contain one of the functional arms **AD2** or **1E9**, and one contains a Fab fragment of the antibody **b12** which addresses a HIV antigen.[204] Furthermore, they also tested a mixture of the parental antibodies **AD2** and **1E9**, and the **b12** antibody as a negative control. As positive control and benchmark, the cooperation partner produced an antibody with the same biochemical properties as the Medimmune antibody **MEDI9447**.[87, 88]
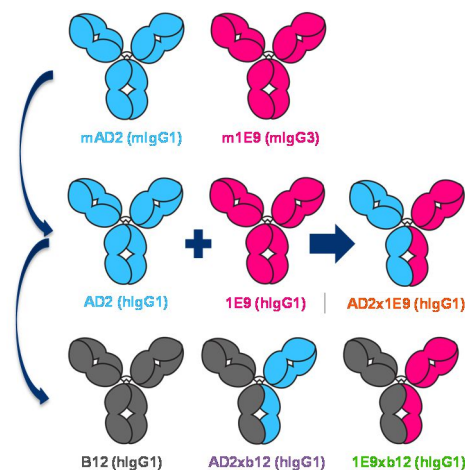

Figure 69. Antibody design. The antibody design is based on two mouse antibodies, **AD2** and **1E9**. These were humanized, a bispecific antibody, which addresses both, the **AD2** and **1E9** epitopes of CD73 (**AD2x1E9**), and controls, were produced, adapted from[205].

In previous work (unpublished) Professor Ditzel and coworkers were able to show the internalization effect of the bispecific antibody, but were unable to measure the inhibition of CD73. In this collaboration project the bispecific antibody **AD2x1E9** and the control antibodies were analyzed towards the inhibition of CD73 using the radioassay. As a source for CD73, the human membrane-bound variety of CD73 was employed using membrane preparations of the triple-negative breast cancer cell line MDA-MB-231. The Fab **AD2** induces internalization of CD73 which lowers the concentration of CD73 at the cell surface, and therefore also the AMP hydrolysis. This effect is only present in living cells. To take this effect into account, the radio assay was optimized to measure the inhibition of CD73 by the antibodies also on living cells of the same cell line.

4.6.2 Optimization of the radioassay for MDA-MB-231 cells

In the first step, the radioassay was optimized to analyze the AMP hydrolysis by living MDA-MB-231 cells. A cell titration revealed that around 1500 seeded cells, after an incubation time of 48 h, led to a substrate turnover of around 20% (Figure 70A). To analyze the initial velocity of the enzyme 1000 cells per well were seeded into a 96-well plate for further experiments.
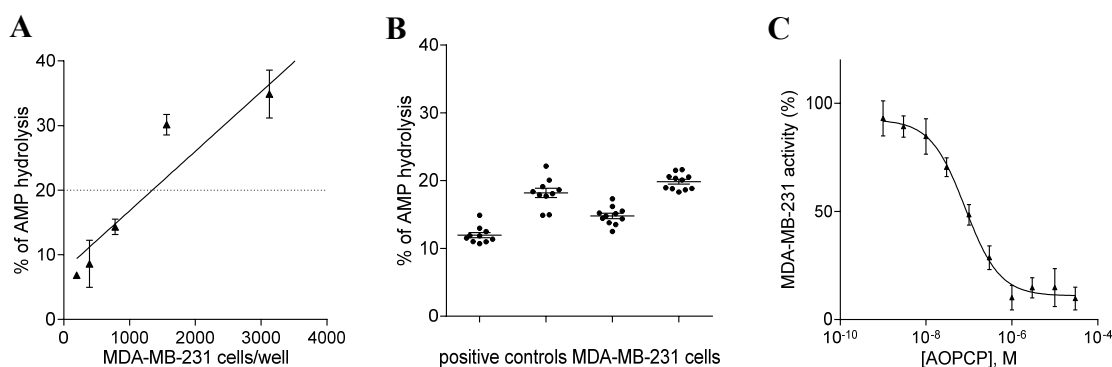
Figure 70. Assay optimization for MDA-MB-231 cells. (A) Cell titration: linear range of mean curve (results of three independent experiments, error bars represent SEM). **(B)** Repeated analysis of ten not inhibited reactions. **(C)** Concentration-response curve of the reference inhibitor **AOPCP** (IC$_{50}$: 98.9 ± 31.5 nM (mean ± SEM from at least three separate experiments performed in duplicates).

Experiments with living cells are often less reproducible, especially when handling low cell numbers like in this assay. To investigate the reproducibility of the assay, the AMP hydrolysis of ten wells, containing the cells, was analyzed in four independent experiments. The results illustrate that the AMP hydrolysis is four times nearby or below the 20% AMP

hydrolysis, and that the data points of each experiment gave comparable values (Figure 70B). For further validation, the reference inhibitor **AOPCP** was analyzed and a IC_{50} value of 98.9 ± 31.5 nM was determined (Figure 70C), which is well in line with literature data.[24, 43, 94]

4.6.3 Analysis of CD73-targeting antibodies

The CD73-targeting bispecific antibody **AD2x1E9**, related controls and the antibody from Medimmune **MEDI9447** were analyzed with membrane preparations of the cell line MDA-MB-231 and with living cells of the same cell line. In contrast to small molecules, in the field of antibodies the IC_{50} is usually provided in mass per volume and not in molarity. To have a better comparison, the IC_{50} of the antibodies and **AOPCP** is illustrated in Table 30 and Table 31 in µg/ml and nM, respectively.

In measurements with membrane preparations as source for CD73, the bispecific antibody **AD2x1E9**, the parental antibody **1E9** and the mixture of both parental antibodies **AD2+1E9** showed comparable potencies (IC_{50}: ca. 1 µg/ml; 5 nM) and high concentrations of these antibodies (30 µg/ml) led nearly to full inhibition of enzymatic activity (Figure 71A).
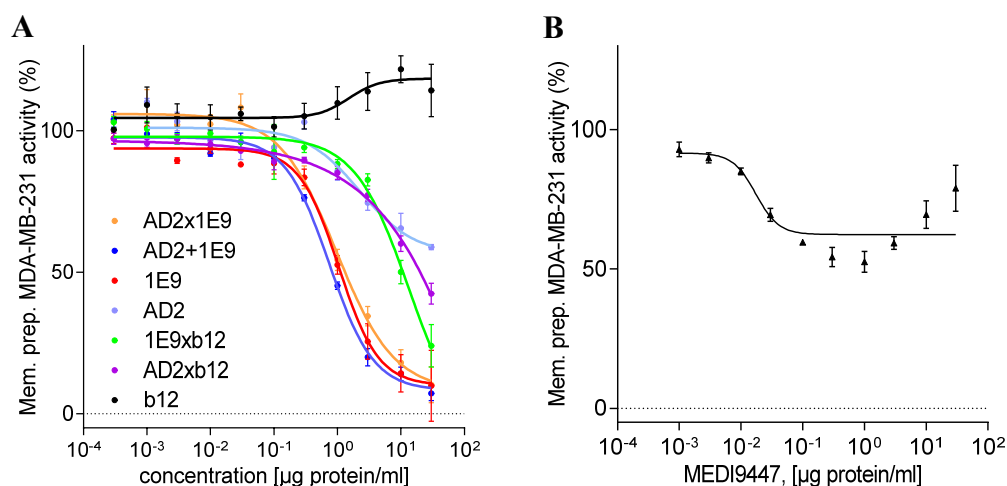
Figure 71. Analysis of CD73-targeting antibodies. (A) Measurement of newly developed antibodies and **(B)** the antibody **MEDI9447** with membrane preparations of MDA-MB-231 cells (means ± SEM from at least three separate experiments performed in duplicates).

129

Results and Discussion

In contrast, the parental antibody **AD2**, die chimeric antibodies **AD2xb12** and **1E9xb12** were less active and did not lead to full inhibition at higher concentrations. Because the Fab arm of **1E9** addresses the enzymatic activity of CD73, the control **1E9xb12** is more active than the parental antibody **AD2** and **AD2xb12**. Nevertheless, it can be recorded that also **AD2** though this one is responsible for internalization also lower the enzymatic activity of CD73 at concentrations above 10 µg/ml.

The measurement of the **MEDI9447** with membrane preparations revealed a higher potency (IC_{50}: 0.017 µg/ml; 0.113 nM) compared to the newly developed bispecific antibody **AD2x1E9**. However, **MEDI9447** acted as partial inhibitor and showed an efficacy of 50% at a concentration of 1 µg/ml which is comparable to the bispecific antibody. Above this concentration, the inhibition of CD73 was decreased (Figure 71B). This, so-called "hook effect" is also described by the developers of the **MEDI9447** antibody and is based on the aggregation of the antibody at higher concentrations.[87] To prevent the formation of drug or protein aggregates non-ionic detergents are often used at concentrations above the critical micelle concentration (CMC) in a range from 0.01 to 0.1%.[206, 207] In this study the detergents Tween 20® and Triton X-100 were employed at different concentrations. No aggregates were formed in these experiments, but the efficacy at higher concentrations of the antibody remained at ca. 50% inhibition of enzymatic activity (appendix, Figure 80, page 154). The measured potencies on living cells were similar to the values obtained on membrane preparations (appendix, Figure 81, page 152). They only differ in the residual AMP hydrolysis at higher antibody concentrations. The residual activity of **AD2x1E9**, **AD2+1E9** and **1E9** were about 25% compared to 10% in the measurements with membrane preparation. For the small molecule **AOPCP** a residual activity of 5% was measured on living cells and 1% with membrane fraction, which suggests that the antibodies are not able to bind to every CD73 molecule and are less efficient in inhibiting CD73 in living cells.

The antibody **MEDI9447** again showed a higher potency, but like in the experiments performed with the membrane preparations an efficacy of 50% was not exceeded. In contrast to the experiment with membrane fractions, the "hook effect" was not observed in the experiments conducted with the cells (appendix, Figure 81, page 155).

Table 30. Measured potencies in μg/ml (means ± SEM from at least three separate experiments performed in duplicates).

Antibody or compound	MDA-MB-231 membrane preparations		MDA-MB-231 cells	
	IC$_{50}$ ± SEM (μg/ml)	Residual enzyme activity (%)	IC$_{50}$ ± SEM (μg/ml)	Residual enzyme activity (%)
AOPCP	0.022 ± 0.004	1 ± 1	0.042 ± 0.013	10 ± 5
MEDI9447	0.017 ± 0.003	53 ± 4**	0.013 ± 0.006	54 ± 5
AD2x1E9	1.02 ± 0.15	10 ± 9	0.648 ± 0.174	20 ± 1
AD2+1E9	0.754 ± 0.064	8 ± 4	0.445 ± 0.032	23 ± 1
1E9	1.01 ± 0.039	13 ± 20	0.877 ± 0.028	47 ± 5
AD2	> 30	59 ± 2	> 30	75 ± 9
1E9xb12	9.04 ± 1.06	24 ± 11	> 30	63 ± 6
AD2xb12	> 30	44 ± 7	> 30	68 ± 11
b12	> 30	114 ± 13	> 30	87 ± 8

**value at 1μg/ml, values >1 μg/ml, "hook effect"

Table 31. Measured potencies nM (means ± SEM from at least three separate experiments performed in duplicates).

| Antibody or compound	MDA-MB-231 membrane preparations		MDA-MB-231 cells	
	IC$_{50}$ ± SEM (nM)*	Residual enzyme activity (%)	IC$_{50}$ ± SEM (nM)*	Residual enzyme activity (%)
AOPCP	52.2 ± 9.4	1 ± 1	98.9 ± 31.5	10 ± 5
MEDI9447	0.113 ± 0.021	53 ± 4**	0.089 ± 0.043	54 ± 5
AD2x1E9	6.82 ± 1.01	10 ± 9	4.32 ± 1.16	20 ± 1
AD2+1E9	5.02 ± 0.43	8 ± 4	2.96 ± 0.22	23 ± 1
1E9	6.73 ± 0.26	13 ± 20	5.84 ± 0.19	47 ± 5
AD2	> 275	59 ± 2	> 275	75 ± 9
1E9xb12	60.2 ± 7.06	24 ± 11	> 275	63 ± 6
AD2xb12	> 275	44 ± 7	> 275	68 ± 11
b12	> 275	114 ± 13	> 275	87 ± 8

*calculated based on a molecular weight of 150 kDa for an antibody; **value at 1μg/ml, values >1 μg/ml, "hook effect"

The tested antibodies from Denmark did not lead to a full inhibition (living cells) of CD73 at high antibody concentration. The question is, if this effect is driven by the antibodies or if it is an artifact of the developed assay system. To address this question, the mouse cell line 4T1.2 and the anti-CD73 antibody **TY/23** were analyzed in the radioassay. Mark J. Smyth developed the anti-CD73 mAb **TY/23**, which showed a significant delay of native 4T1.2 cell tumor growth in immune-competent mice.[81, 208] In this publication, the authors also measured the inhibition of CD73 on living 4T1.2 mouse breast cancer cells (Figure 73). In the first step, the radioassay was optimized to analyze the AMP hydrolysis by the cell line 4T1.2. This was done analogously to the optimization of the MDA-MB-231 cells. It was found that 500 cells per well are optimal to measure the initial velocity of the ecto-5′-

nucleotidase (appendix, Figure 82, page 155). In the second step, the inhibition of CD73 by **TY/23** was measured at a single concentration of 100 µg/ml on the mouse cell line 4T1.2 (Figure 72).
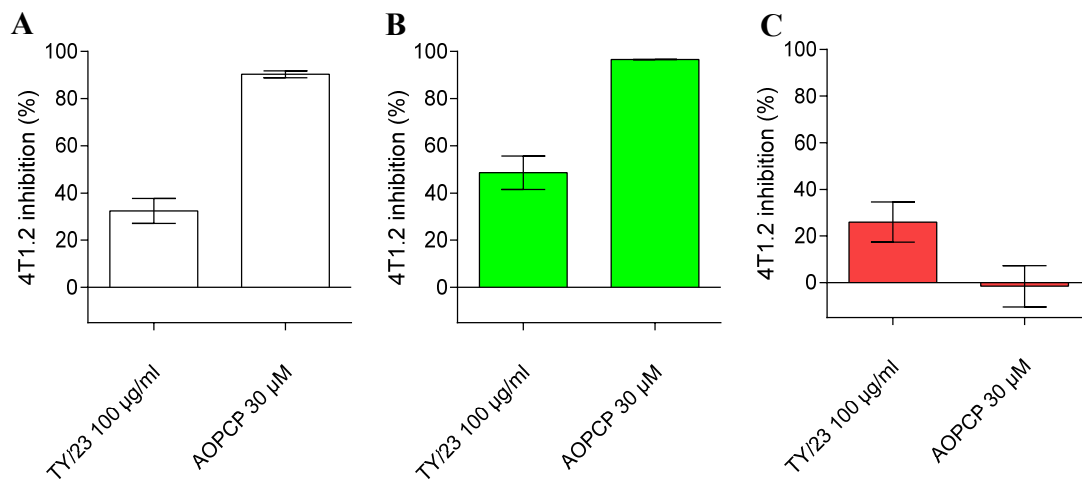
Figure 72. Analysis of mouse CD73-targeting antibody with cell line 4T1.2 under different conditions. **(A)** Preincubation of the antibody in reaction buffer for 30 min, **(B)** for 5 h before initiating the reaction and **(C)** preincubation of the antibody in cell culture media for 5 h with subsequent washing and change to reaction buffer (results of A: n=3, B: n=2 and C: n=1 independent experiments performed in duplicates, error bars represent SEM).

The mouse CD73-targeting antibody **TY/23** inhibited the hydrolysis of AMP at 100 µg/ml by 32% (Figure 72A). This value deviates from the value published by Mark Smith and coworkers (inhibition of around 80%, Figure 73). A preincubation time of 30 min was used, which was also used in our previous experiments. Mark Smith and coworkers treated the cells for 5 h with the antibody. Therefore, the preincubation time was increased to 5 h before starting the reaction. The inhibition increased to 48% (Figure 72B). In a third setup, it was analyzed if the assay reaction buffer might prevent a proper binding of the antibody. Thus, the preincubation was performed for 5 h in cell media instead of reaction buffer. Afterwards, cells were washed with assay reaction buffer and AMP hydrolysis was analyzed resulting in an inhibition of 26% (Figure 72C). The CD73 inhibitor **AOPCP** served as control and showed high inhibition of CD73 in the first two experimental setups. In the third one, it seems that the washing step removed the small molecule from the target and no inhibition of the AMP hydrolysis occurred. Because of the limited amount of the antibody, experimental setup two (Figure 72B) and three (Figure 72C) were performed only twice and once, respectively.
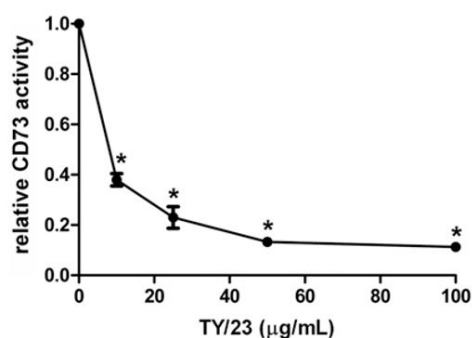
Figure 73. Relative CD73 activity of 4T1.2 cells treated with TY/23 for 5 h (* $P < 0.05$ by Mann–Whitney test; means ± SEs of triplicates are shown).[81]

In conclusion, the bispecific antibody **AD2x1E9** targets CD73 leading to inhibition of enzymatic activity with an IC_{50} of 1.02 µg/ml (6.82 nM) measured on membrane fractions derived from the cell line MDA-MB-231 and with a comparable IC_{50} of 0.648 µg/ml (4.32 nM) on living cells. However, the measured efficacy in the cellular system is lower than in the membrane fractions. To validate the used assay system und to compare the findings with data from an antibody which showed significant effects in *in vivo* studies, the inhibition of AMP hydrolysis by the CD73-targeting antibody **TY/23** was measured in the used radioassay. It showed in our hands a lower inhibition than in the assay system published by Mark Smith. The antibody of this group had shown relevant effects in *in vivo* studies. This suggests that also the bispecific antibody **AD2x1E9** from Denmark, which shows higher inhibition in the radioassay, might show measurable effects in *in vivo* studies. The reason for the incomplete CD73 inhibition by the antibodies is unknown.

Presently, the antibodies are tested *in vivo* in metastasis model as described in the study for the antibody **AD2**.[86] Hereby, CB-17 SCID mice are inoculated with the MDA-MB-231 tumor cells expressing luciferase as reporter. Besides **AD2x1E9**, **b12,** and antibodies with a normal human IgG1 and a mutated (inactive) one are used as controls. The antibodies are injected intraperitoneally 4 d after cancer cell transplantation in an amount of 5 mg/kg. The analysis of tumor growth is monitored by luminescence measurement. This *in vivo* study will demonstrate if the antibody **AD2x1E9** have antitumor efficacy.

Results and Discussion

5   Summary and Outlook

Ecto-5′-nucleotidase (CD73) is an enzyme involved in purinergic signaling. It hydrolyzes extracellular AMP to adenosine and inorganic phosphate. Adenosine activates adenosine receptors that are connected to many physiological and pathophysiological processes, in particular those related to inflammation and immune responses. CD73 has been proposed as a novel drug target for the immunotherapy of cancer, since the enzyme is upregulated under inflammatory and hypoxic conditions, e.g. on cancer cells.

5.1   Expression of CD73 and assay development

For the identification, optimization and characterization of CD73 inhibitors, different sources of CD73 were produced, and assays were developed, established and optimized:

- Human soluble CD73 was successfully expressed in (Sf9) insect cells and purified by affinity chromatography using a C-terminal 6x His-tag.
- Membrane preparations of the triple-negative breast cancer (TNBC) cell line MDA-MB-231 were successfully produced showing high enzymatic activity of CD73.
- A radioassay was optimized for rat and human soluble as well as membrane-bound human CD73; K_M values were determined to be 53.0, 17.0, 14.8 µM and the K_i value of the reference inhibitor **AOPCP** was found to be 167, 49.9 and 39.0 nM, respectively, on these enzyme preparations.

For high-throughput-screening, a malachite green assay was developed leading to the following results:

- The assay was 4-times more sensitive than the procedure described in the literature.
- The enzymatic activity could be stabilized over several hours by the addition of BSA.
- Z′-factors of well above 0.5 were determined for manual and automated pipetting indication the assay's suitability for high-throughput screening (HTS).
- About 5500 compounds were screened at a concentration of 10 µM, in addition to 140 fragments tested at 500 µM concentration. The hit rate was 0.36%, and 20% of the hits could be validated using the sensitive radioassay.

5.2 Nucleotides as CD73 inhibitors

AOPCP was used as a lead structure, and derivatives with substitutions or exchanges of the base adenine, the ribose and the diphosphonate group were investigated with the following results using soluble rat CD73 and the radioassay for testing (Figure 74).

- Modifications of adenine as well as the exchange to substituted pyrimidines were favorable, while modifications of the ribose or bioisosteric replacement of the diphosphonate group were less well tolerated.

- **7-Deaza-AOPCP** was twice as potent as **AOPCP** confirming results from molecular modeling which suggested that the N7 is not interacting with amino acids in the binding site of CD73.

- The exchange of adenine for unsubstituted uracil or cytosine reduced the potency but substituents of both pyrimidine moieties led to potent inhibitors.

- For **COPCP** derivatives it was found that larger lipophilic substituents in the N^4-position like **(N^4-benzoyl)-COPCP (7f)** or substituted alkoxyimino groups like **(3-Me-N^4-benzyloxyimino)-COPCP (9h**, Figure 75A) addressed a large pocket of CD73 which led to an increase in potencies of these inhibitors to low nM K_i values.

- Halogenation of **UOPCP** in the 5-position increased the potency, **5-fluoro-UOPCP (4l**, Figure 75B) being the most potent one.

- Selected inhibitors were analyzed at human soluble and human membrane-bound CD73 showing comparable or slightly higher potency as compared to the rat enzyme.
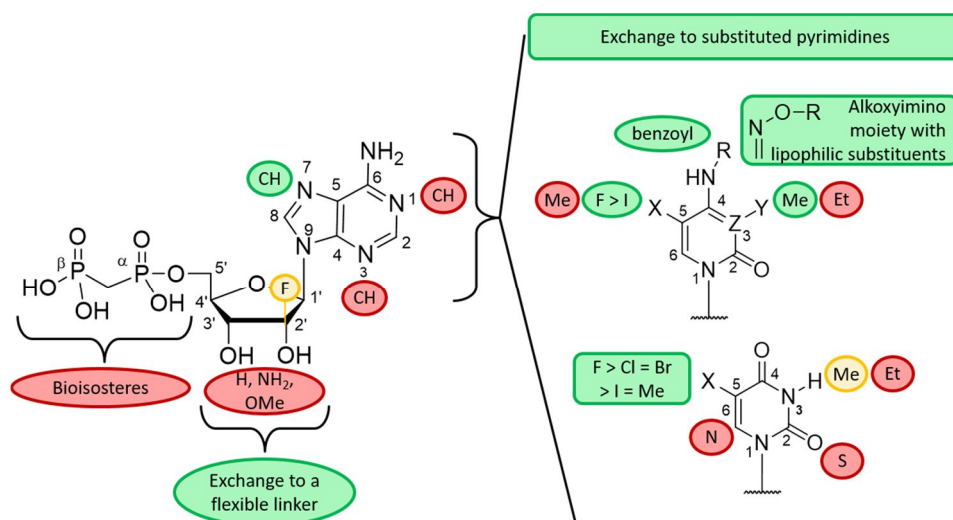
Figure 74. Structure-activity relationships of AOPCP derivatives. Not beneficial (red), accepted (yellow) and beneficial (green) substitutions of the lead compound AOPCP.

The exchange of the ribose by an alkyl linker which connects the 2-chloro- and the N^6-benzyl-N^6-methyl substituted adenine with the diphosphonate moiety led to potent acyclic AOPCP analogs:

- A C5-alkyl linker (**SF-54**) was found to be most potent on rat CD73 resulting in a K_i value in the low μM range, and the C6-alkyl linker (**SF-57,** Figure 75C) was beneficial for human CD73 with a K_i value in the medium nM range and led to the most potent acyclic competitive CD73 inhibitor reported to date.

- Bioisosteres mimicking the diphosphonate group of **AOPCP** were obtained with the aim to avoid negative charges. However, it was not possible to find a sufficiently potent compound, which illustrates that it is difficult to mimic the negative charges and that the negative charges are necessary for obtaining high potencies of AOPCP derivatives.

Summary and Outlook
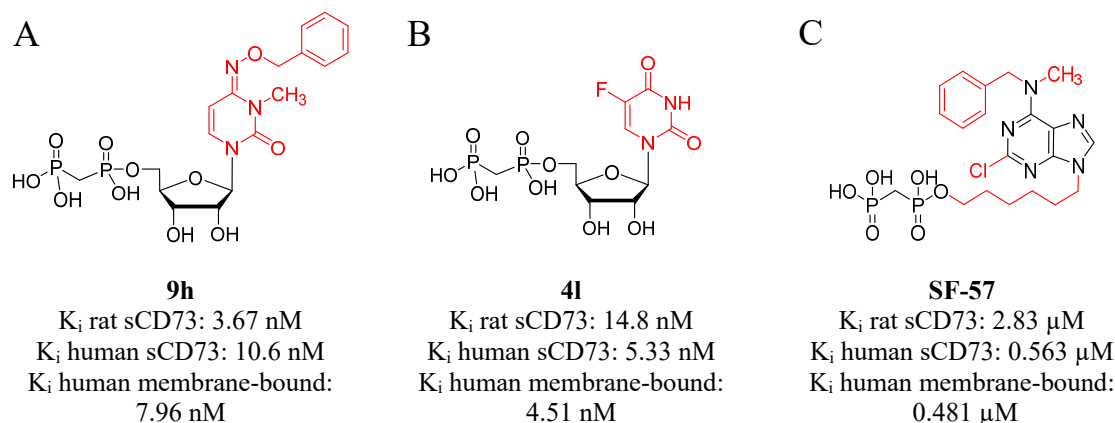
Figure 75. Nucleotide inhibitors of ecto-5′-nucleotidase. (A) Exchange of adenine by cytosine which was substituted with a 3-Me-N^4-benzyloxyimino moiety led to the most potent COPCP derivative. **(B)** In the UOPCP series **5-fluoro-UOPCP** was the most potent inhibitor. **(C)** The most potent acyclic AOPCP analog at human CD73 was the derivative with a C6-alkyl linker (**SF-57**).

Based on these results we suggest further optimization of this class of CD73 inhibitors including:

- methylation of potent COPCP derivatives at the N3-position.
- synthesis of 7-deazaadenine derivatives of potent AOPCP derivatives.
- fluorination of the 8-position of adenine.
- fine-tuning of the linker length of acyclic AOPCP derivatives by introducing heteroatoms or double bonds.

Moreover, co-crystallization of the most potent nucleotidic inhibitors with CD73 for X-ray structure analysis has been performed by a cooperation partner, and ADME properties were analyzed.

5.3   Sulfonamides as CD73 inhibitors

Two different benzenesulfonamide structures, one linked via a hydrazone moiety with a naphthalene group and one linked via an amide with a coumarin moiety originally identified by virtual screening were used as lead structures. The structure-activity relationships of the more potent coumarin series were determined:

- Substitution of the benzenesulfonamide moiety in the 3-position was beneficial, especially with halogen atoms (Br > I > F > Cl, Figure 76A).
- An electron-withdrawing substituent in the 6-position of the coumarin moiety was found to be essential for high potency with 6-chloro substitution being most active.
- In combination with a 3-bromo substitution of the benzenesulfonamide compound **Yazh-937** was 9-fold more potent than the lead structure.
- Interestingly, the compound was found to be similarly potent at soluble human and rat CD73, but appeared to be not active at the human membrane-bound CD73. The reason for this is as yet unclear.
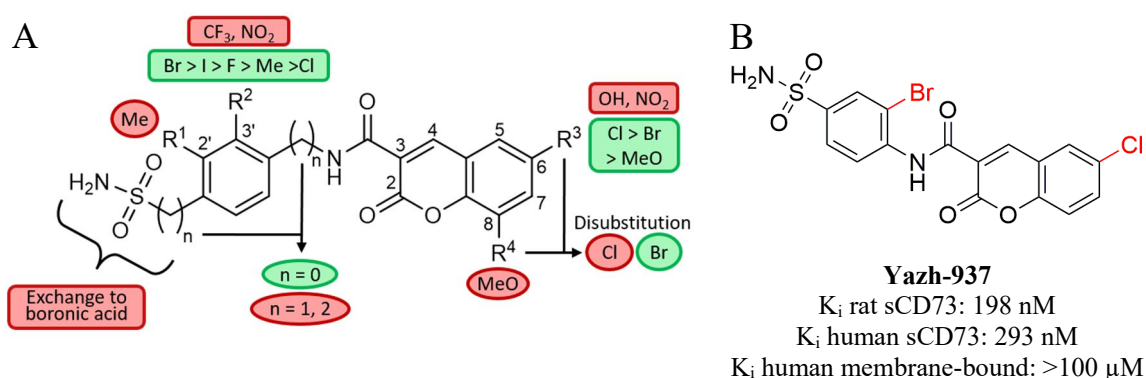
Figure 76. Sulfonamide as CD73 inhibitors. (A) Structure-activity relationships of sulfonamide derivatives with a coumarin moiety analyzed with rat CD73 (not beneficial (red) and beneficial (green) substitutions). **(B)** The most potent sulfonamide derivative with selectivity for soluble human CD73.

**Yazh-937** is currently investigated for co-crystallization with human CD73 for X-ray structure analysis.

5.4 Xanthine derivative as CD73 inhibitors

Most hits identified by high-throughput-screening were tricyclic xanthine derivatives with a mixed inhibition mode and the following structural characteristics (Figure 77A):

- Methylation in the N1- and N3-position.
- Six- or seven-membered heterocycles.
- A *para*-substituted phenyl substituent at the N^8-atom.
- The most potent inhibitor of rat CD73 had a methoxy residue in the *para*-position of a xanthine derivative with a seven-membered heterocycle (**PZB01808057**, IC$_{50}$ rat sCD73: 3.30 μM).

Most derivatives in this series were not active at human soluble CD73. The exception was a six-membered heterocycle with a hydroxy substitution in the *para*-position (**PZB01808014**, Figure 77B), which showed selectivity for the soluble form of CD73, but was inactive at the membrane-bound human CD73.
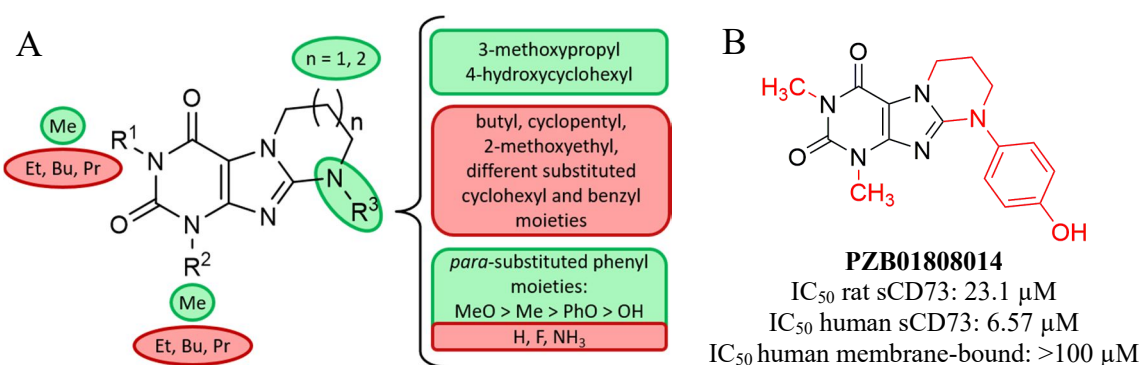
Figure 77. Xanthine derivatives identified by HTS. (A) Structure-activity relationships of xanthine derivatives analyzed with rat CD73 (not beneficial (red) and beneficial (green) substitutions). **(B)** The most potent xanthine derivatives at human CD73 with selectivity for soluble form of CD73.

These results show that species differences as well as differences between human soluble and human membrane-bound CD73 can be observed. Therefore, the malachite green assay should be optimized for cell membrane preparations as a source of CD73 and should be validated for screening campaigns. CMP was suitable as a substrate, as shown by the company Pharmaceutical Vitae Inc. (see introduction, page 30). Thus, high substrate concentrations can be used to maintain good sensitivity and robustness due to the high K$_M$ value of CMP as compared to AMP.

5.5 Development of a radioligand for CD73

To study the direct interaction of compounds with the substrate binding site, we aimed at developing a radioligand using potent AOPCP derivatives as lead structures.

- Propyl-substitution of the N^6-position led to **CS-230**, the most potent compound that could be easily obtained in tritiated form (Figure 78). It was potent on rat and human CD73 in the picomolar range. The radiolabeled version was prepared by the unsaturated precursor by catalytic hydrogenation with tritium gas.

Currently, this radioligand is used for the development of a binding assay.
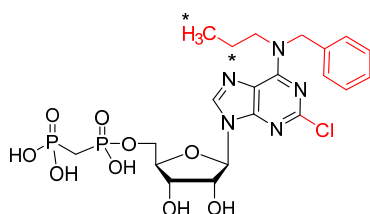
CS-230 (PSB-17230)
K_i rat sCD73: 0.567 nM
K_i human sCD73: 0.0732 nM
K_i human membrane-bound: 0.0891 nM

Figure 78. Radioligand with picomolar potency. CS-230 inhibited CD73 in the picomolar rage and is the template for the later produced radioligand [³H]PSB-17230 (asterisk: tritium atoms).

5.6 CD73-inhibitory potency of bispecific antibodies

A bispecific antibody for CD73 (**AD2x1E9**), different control antibodies as well as **MEDI9447**, a therapeutic antibody which is presently in phase II clinical trials were investigated at membrane fractions and on living TNBC cells with an optimized radioassay. **AD2x1E9** inhibited CD73 in the low nM range on membrane fractions and on living cells. **MEDI9447** was determined to be more potent, but showed lower efficacy than the newly developed bispecific antibody. **AD2x1E9** is currently investigated *in vivo*.

Altogether, we developed and optimized CD73 assays for different applications, and expanded the structure-activity relationships of a variety of scaffolds, including nucleotides, sulfonamides and xanthine derivatives, resulting in potent CD73 inhibitors. These compounds are likely to become useful pharmacological tools to further elucidate the enzyme's (patho)-physiological role and its potential as a drug target in cancer immunotherapy.

Summary and Outlook

6 Appendix

6.1 Methods

6.1.1 Protein sequences of expressed soluble human CD73

pAcG2T-sCD73

<u>MLLVNQSHQGFNKEHTSKMVSAIVLYVLLAAAAHSAFA</u>*DLMSPILGYWKIKGLVQ*
PTRLLLEYLEEKYEEHLYERDEGDKWRNKKFELGLEFPNLPYYIDGDVKLTQSMAIIRYI
ADKHNMLGGCPKERAEISMLEGAVLDIRYGVSRIAYSKDFETLKVDFLSKLPEMLKMFE
DRLCHKTYLNGDHVTHPDFMLYDALDVVLYMDPMCLDAFPKLVCFKKRIEAIPQIDKY
*LKSSKYIAWPLQGWQATFGGGDHPPKSD***LVPRGS**WELTILHTNDVHSRLEQTSEDS
SKCVNASRCMGGVARLFTKVQQIRRAEPNVLLLDAGDQYQGTIWFTVYKGAEVA
HFMNALRYDAMALGNHEFDNGVEGLIEPLLKEAKFPILSANIKAKGPLASQISGLY
LPYKVLPVGDEVVGIVGYTSKETPFLSNPGTNLVFEDEITALQPEVDKLKTLNVNKI
IALGHSGFEMDKLIAQKVRGVDVVVGGHSNTFLYTGNPPSKEVPAGKYPFIVTSD
DGRKVPVVQAYAFGKYLGYLKIEFDERGNVISSHGNPILLNSSIPEDPSIKADINKW
RIKLDNYSTQELGKTIVYLDGSSQSCRFRECNMGNLICDAMINNNLRHADEMFWN
HVSMCILNGGGIRSPIDERNNGTITWENLAAVLPFGGTFDLVQLKGSTLKKAFEHS
VHRYGQSTGEFLQVGGIHVVYDLSRKPGDRVVKLDVLCTKCRVPSYDPLKMDEV
YKVILPNFLANGGDGFQMIKDELLRHDSGDQDINVVSTYISKMKVIYPAVEGRIKF

GGS*HHHHHH*

Theoretical molecular weight: 89.523 kDa with and 85.443 kDa without secretion signal.

Legend: underline: secretion signal (cleaved after bolt A); italic: GST or His-Tag; bolt: Connecting amino acids/thrombin cleavage site (LVPRGS); gray background: CD73

pAcGP67B-sCD73

<u>MLLVNQSHQGFNKEHTSKMVSAIVLYVLLAAAAHSAFA</u>**AADLGS**WELTILHTNDV
HSRLEQTSEDSSKCVNASRCMGGVARLFTKVQQIRRAEPNVLLLDAGDQYQGTIW
FTVYKGAEVAHFMNALRYDAMALGNHEFDNGVEGLIEPLLKEAKFPILSANIKAK
GPLASQISGLYLPYKVLPVGDEVVGIVGYTSKETPFLSNPGTNLVFEDEITALQPEV
DKLKTLNVNKIIALGHSGFEMDKLIAQKVRGVDVVVGGHSNTFLYTGNPPSKEVP
AGKYPFIVTSDDGRKVPVVQAYAFGKYLGYLKIEFDERGNVISSHGNPILLNSSIPE
DPSIKADINKWRIKLDNYSTQELGKTIVYLDGSSQSCRFRECNMGNLICDAMINNN

Appendix

LRHADEMFWNHVSMCILNGGGIRSPIDERNNGTITWENLAAVLPFGGTFDLVQLK GSTLKKAFEHSVHRYGQSTGEFLQVGGIHVVYDLSRKPGDRVVKLDVLCTKCRVP SYDPLKMDEVYKVILPNFLANGGDGFQMIKDELLRHDSGDQDINVVSTYISKMKV IYPAVEGRIKF**GGS***HHHHHH*
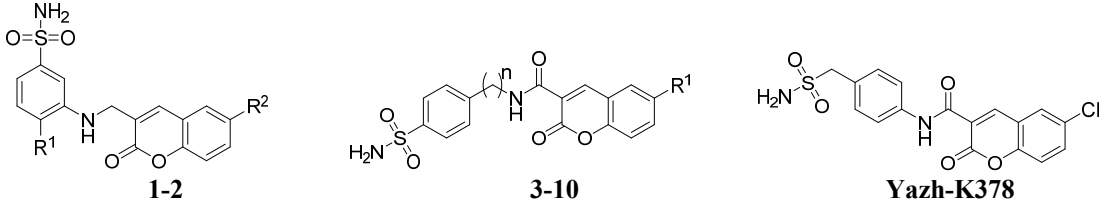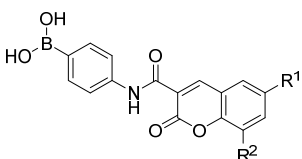
theoretical molecular weight: 63.446 kDa with and 59.366 kDa without secretion signal.

Legend: underline: secretion signal (cleaved after bolt A); italic: His-Tag; bolt: Connecting amino acids/thrombin cleavage site (LVPRGS); gray background: CD73

6.2 Results and Discussion

6.2.1 Structure-activity relationships of sulfonamides as CD73 inhibitors

Table 32. Potencies of coumarin derivatives with a different position of sulfonamide at rat CD73 (means ± SEM from at least three separate experiments performed in duplicates).

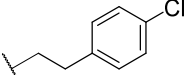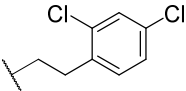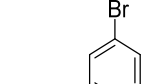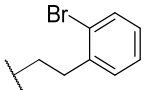|	Compound	n	R^1	R^2	Rat CD73 $K_i \pm$ SEM (nM)*
1	Yazh-K340		H	Br	> 1000 (14%)
2	Yazh-K356		Cl	Cl	> 1000 (7%)
3	Yazh-K327	1	H		> 1000 (-7%)
4	Yazh-K326	2	H		> 1000 (4%)
5	Yazh-K302	1	MeO		> 1000 (2%)
6	Yazh-K315	2	MeO		> 1000 (17%)
7	Yazh-K307	1	Cl		> 1000 (7%)
8	Yazh-K341	2	Cl		> 1000 (13%)
9	Yazh-K309	1	Br		> 1000 (13%)
10	Yazh-K308	2	Br		> 1000 (7%)
11	Yazh-K378				> 1000 (7%)

* or % inhibition at indicated concentration
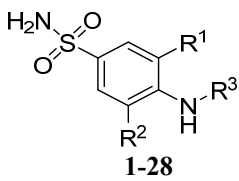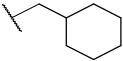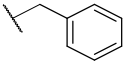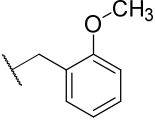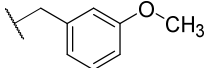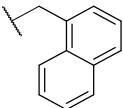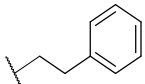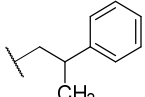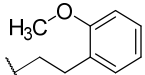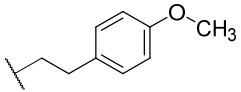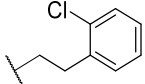
Table 33. Potencies of boronic acid derivatives at rat CD73 (means ± SEM from at least three separate experiments performed in duplicates).

	Compound	R^1	R^2	Rat CD73 $K_i \pm$ SEM (nM)*
1	Yazh-K362	Cl	H	> 1000 (15%)
2	Yazh-K368	Cl	Cl	> 1000 (14%)
3	Yazh-K363	Br	H	> 1000 (18%)
4	Yazh-K365	Br	Br	> 1000 (26%)

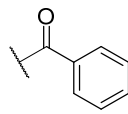* or % inhibition at indicated concentration

Appendix
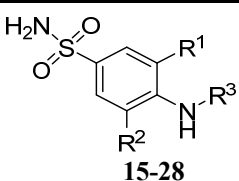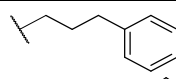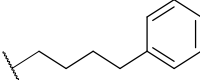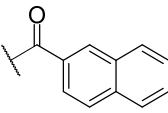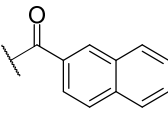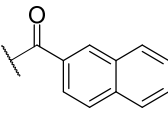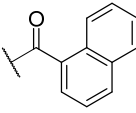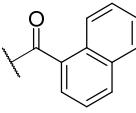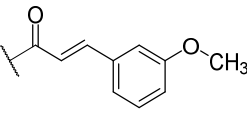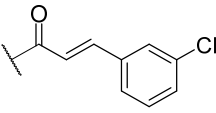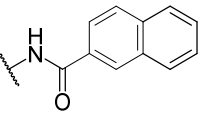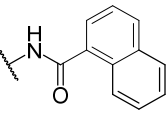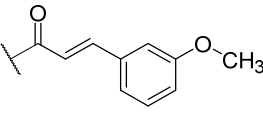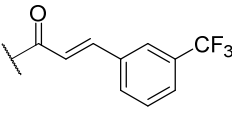
Table 34. Potencies of sulfonamide derivatives at rat CD73 (means ± SEM from at least three separate experiments performed in duplicates).

1-28

	Compound	R^1	R^2	R^3	Rat CD73 K_i ± SEM (nM)*
1	**Yazh-838**	NO_2	H		> 1000 (19%)
2	**Yazh-810**	NO_2	H		> 1000 (22%)
3	**Yazh-835**	NO_2	H		> 1000 (7%)
4	**Yazh-836**	NO_2	H		> 1000 (22%)
5	**Yazh-824**	NO_2	H		> 1000 (22%)
6	**Yazh-826**	NO_2	H		> 1000 (24%)
7	**Yazh-827**	NO_2	H		> 1000 (21%)
8	**Yazh-829**	NO_2	H		> 1000 (21%)
9	**Yazh-834**	NO_2	H		> 1000 (31%)
10	**Yazh-830**	NO_2	H		> 1000 (18%)
11	**Yazh-831**	NO_2	H		> 1000 (17%)
12	**Yazh-832**	NO_2	H		> 1000 (17%)
13	**Yazh-828**	NO_2	H		> 1000 (13%)
14	**Yazh-833**	NO_2	H		> 1000 (20%)

* or % inhibition at indicated concentration
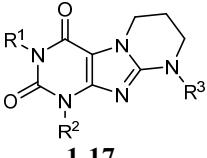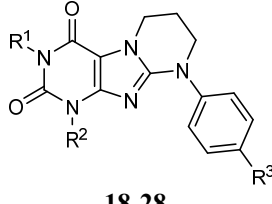
Table 34 (continued). Potencies of sulfonamide derivatives at rat CD73.

15-28

	Compound	R^1	R^2	R^3	Rat CD73 K$_i$ ± SEM (nM)*
15	Yazh-K11	NO$_2$	H		> 1000 (8%)
16	Yazh-K12	NO$_2$	H		> 1000 (2%)
17	Yazh-939	H	Br		> 1000 (1%)
18	Yazh-918	H	CH$_3$		> 1000 (9%)
19	Yazh-943	H	Br		> 1000 (11%)
20	Yazh-892	Br	Br		> 1000 (1%)
21	Yazh-917	H	CH$_3$		> 1000 (1%)
22	Yazh-942	H	Br		> 1000 (7%)
13	Yazh-K347	Br	H		> 1000 (9%)
24	Yazh-K348	Br	H		> 1000 (8%)
25	Yazh-819	NO$_2$	H		> 1000 (21%)
26	Yazh-858	NO$_2$	H		> 1000 (22%)
27	Yazh-K347	Br	H		> 1000 (9%)
28	Yazh-K332	Br	H		> 1000 (1%)

6.2.2 Structure-activity relationships of xanthine derivatives

Table 35. Xanthine derivatives with six-membered heterocycles (error bar: means ± SEM from at least three separate experiments performed in duplicates, ND: not determined).

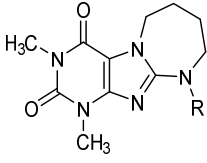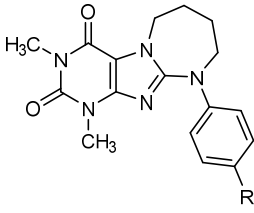|				Rat CD73 Inhibition ± SEM*			
	Compound	**$R^{1,2}$**	**R^3**	**Malachite gr. Assay**	**Radioassay**		
				10 µM	**10 µM**	**1 µM**	**IC_{50} ± SEM**
1	PZB01808308	methyl	hydroxyethyl	-7	ND	ND	ND
2	PZB01808305	methyl	2-hydroxypropyl	5	ND	ND	ND
3	PZB01808172	methyl	isopropyl	ND	13 ± 3	ND	ND
4	PZB01808304	methyl	2-hydroxybutyl	ND	11 ± 7	ND	ND
5	PZB01808232	methyl	2-ethoxyethyl	17	ND	ND	ND
6	PZB01808173	methyl	3-methoxypropyl	40	51 ± 2	23 ± 2	10.0 ± 1.14
7	PZB01808104	propyl	2-methoxyethyl	67	72 ± 0	39 ± 2	5.74 ± 4.05
8	PZB01808231	methyl	2-propoxyethyl	15	ND	ND	ND
9	PZB01808237	methyl	3-ethoxypropyl	13	3 ± 6	3 ± 7	ND
10	PZB01808233	methyl	2-butoxyethyl	ND	8 ± 10	ND	ND
11	PZB01808086	methyl	2-methoxyethyl	24	ND	ND	ND
12	PZB01808204	methyl	4-hydroxycyclohexyl	-14	ND	ND	ND
13	PZB01815044	methyl	2-(piperidin-1-yl)ethyl	ND	14 ± 2	ND	ND
14	PZB01808296	ethyl	4-hydroxyphenethyl	-7	ND	ND	ND
15	PZB01808310	propyl	4-hydroxyphenethyl	-10	ND	ND	ND
16	PZB01808170	ethyl	3-hydroxybenzyl	7	ND	ND	ND
17	PZB01813064	methyl	4-hydroxybenzyl	ND	18 ± 3	ND	ND
18	PZB01808010	methyl	H	-22	ND	ND	ND
19	PZB01808012	methyl	methyl	-10	ND	ND	ND
20	PZB01812013	methyl	amino		16 ± 8	ND	ND
21	PZB01808014	methyl	hydroxy	22	48 ± 9	14 ± 4	23.1 ± 8.3
22	PZB01812022	ethyl	hydroxy	1	ND	ND	ND
23	PZB01812009	propyl	hydroxy	ND	6 ± 5	ND	ND
24	PZB01812008	butyl	hydroxy	1	6 ± 5	ND	ND
25	PZB01808046	methyl	fluoro	ND	15 ± 4	ND	ND
26	PZB01808047	methyl	methoxy	ND	38 ± 5	ND	25.1 ± 7.3
27	PZB01808078	methyl	ethyl	ND	39 ± 3	ND	> 100
28	PZB01808049	methyl	acetoxy	ND	38 ± 2	ND	53.2 ± 34.4

* or % inhibition at indicated concentration

Table 36. Xanthine derivatives with seven-membered heterocycles (error bar: means ± SEM from at least three separate experiments performed in duplicates, ND: not determined).

			Rat CD73 Inhibition ± SEM*			
					Radioassay	
Compound		R	Malachite gr. Assay			
			10 µM	10 µM	1 µM	IC$_{50}$ ± SEM
1	PZB01808208		-5	ND	ND	ND
2	PZB01808238	pemtan-2-yl	-22	ND	ND	ND
3	PZB01808103	butyl	15	ND	ND	ND
4	PZB01808111	*sec*-butyl	10	ND	ND	ND
5	PZB01808116	4-methylpentan-2-yl	ND	6 ± 12	ND	ND
6	PZB01808114	allyl	27	ND	ND	ND
7	PZB01808244	cyclopentyl	6	ND	ND	ND
8	PZB01808113	cyclohexyl	ND	10 ± 7	ND	ND
9	PZB01808243	4-methylcyclohexyl	-5	ND	ND	ND
10	PZB01808117	2-methoxyethyl	31	7 ± 3	ND	ND
11	PZB01808059	4-acetoxycyclohexyl	9	ND	ND	ND
12	PZB01808141	cyclohexylmethyl	2	ND	ND	ND
13	PZB01816039	2-methoxybenzyl	ND	15 ± 5	ND	ND
14	PZB01816041	4-chlorobenzyl	ND	17 ± 1	ND	ND
15	PZB01816033	2-fluorobenzyl	ND	14 ± 8	ND	ND
16	PZB01813008	3,4-dihydroxyphenethyl	9	ND	ND	ND
17	PZB01808055	4-hydroxycyclohexyl	43	43 ± 2	20 ± 8	13.9 ± 1.6
18	PZB01808051	methyl	26	52 ± 5	23 ± 6	8.47 ± 1.32
19	PZB01808054	hydroxy	27	25 ± 4	7 ± 2	106 ± 6
20	PZB01808057	methoxy	49	65 ± 1	31 ± 1	3.30 ± 0.34
21	PZB01808053	ethoxy	ND	33 ±1	ND	ND
22	PZB01808056	acetoxy	23	27 ± 5	ND	ND
23	PZB01808058	fluoro	16	ND	ND	ND
24	PZB01808052	phenoxy	ND	49 ± 3	ND	~ 10**

* or % inhibition at indicated concentration, **problematic to measure, due to solubility issues

Appendix

Table 37. Further explored xanthine derivatives (I) (error bar: means ± SEM from at least three separate experiments performed in duplicates, ND: not determined).

	Compound	n	R	Malachite gr. Assay 10 µM	Rat CD73 Inhibition ± SEM* Radioassay 10 µM	1 µM	IC$_{50}$ ± SEM
1	PZB01808125	1	propyl	-7	ND	ND	ND
2	PZB00908015	1	2,3-dihydro-1H-inden-2-yl	-3	ND	ND	ND
3	PZB00908013	1	naphthalen-1-yl	-2	ND	ND	ND
4	PZB00908009	1	H	-2	ND	ND	ND
5	PZB00908016	1	3-methoxy	-6	ND	ND	ND
6	PZB00908006	1	4-fluoro	-1	ND	ND	ND
7	PZB00908012	1	H	-10	ND	ND	ND
8	PZB00908022	1	4-hydroxy	-10	ND	ND	ND
9	PZB00908080	1	3-methoxy	-4	ND	ND	ND
10	PZB00908081	1	4-methoxy	-3	ND	ND	ND
11	PZB00410060	2	2-chloro	3	ND	ND	ND
12	PZB00908023	1	3-chloro	-7	ND	ND	ND
13	PZB00410060	2	3-chloro	3	ND	ND	ND
14	PZB00908068	1	4-sulfamoyl	-6	ND	ND	ND
15	PZB00908082	1	2,4,6-trimethoxy	-4	ND	ND	ND
16	PZB00908083	1	3,4,5-trimethoxy	-4	ND	ND	ND

* or % inhibition at indicated concentration

Table 38. Further explored xanthine derivatives (II) (error bar: means ± SEM from at least three separate experiments performed in duplicates, ND: not determined).

	Compound	n	Malachite gr. Assay 10 µM	Rat CD73 Inhibition ± SEM* Radioassay 10 µM	1 µM	IC$_{50}$ ± SEM
1	PZB00909048	1	1	ND	ND	ND
2	PZB01808048	1	-6	ND	ND	ND
3	PZB01808050	2	-4	ND	ND	ND

* or % inhibition at indicated concentration

Table 39. Xanthine derivatives with five-membered heterocycles (error bar: means ± SEM from at least three separate experiments performed in duplicates, ND: not determined).
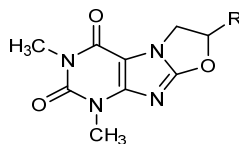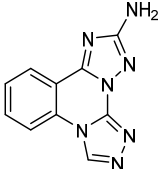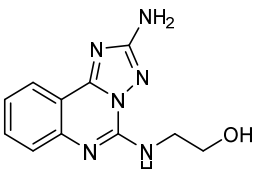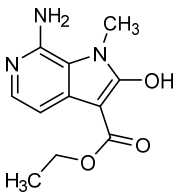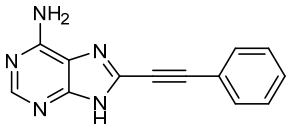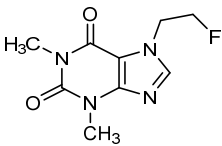
Compound	R	Rat CD73 Inhibition ± SEM*			
		Malachite gr. Assay	Radioassay		
		10 µM	10 µM	1 µM	IC$_{50}$ ± SEM
1 PZB01808001	methyl	2	ND	ND	ND
2 PZB01808003	ethyl	14	ND	ND	ND
3 PZB01808076	hydroxymethyl	1	ND	ND	ND
4 PZB01808002	cloromethyl	47	57 ± 2	37 ± 9	**10.4** ± 1.55
5 PZB01808092	propyl	13	ND	ND	ND
6 PZB01808101	isopropoxymethyl	47	11 ± 4	0 ± 0	ND

* or % inhibition at indicated concentration
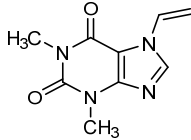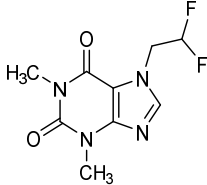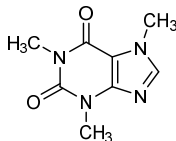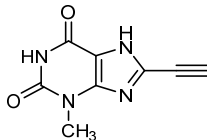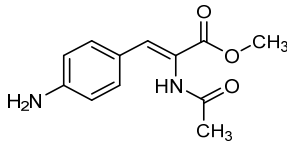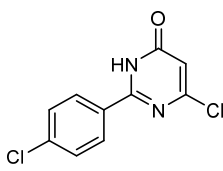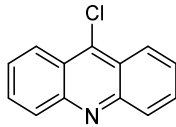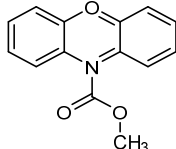
6.2.3 Identified fragments

Table 40. Screening results and potencies of compounds from the fragment library at rat CD73 (error bar: means ± SEM from at least three separate experiments performed in duplicates, ND: not determined).

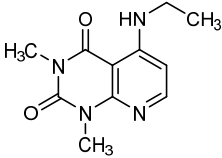| Structure/ Name	Rat CD73 Inhibition ± SEM (%)				Pseudo IC$_{50}$ (µM)	IC$_{50}$ ± SEM (µM)
	Malachite green assay	Radio assay				
	500 µM	500 µM	100 µM	10 µM		
PZB00410018	45	26 ± 15	7 ± 5	1 ± 3	1585	ND
PZB00609010	44	61 ± 5	28 ± 15	19 ± 12	403	ND
PZB00609012	77	76 ± 5	64 ± 3	23 ± 3	43.9	32.6 ± 2.6
PZB00609136	43	86 ± 4	22 ± 3	-5 ± 3	179	ND
PZB00709002	78	89 ± 4	57 ± 1	28 ± 2	63.4	37.4 ± 7.4
PZB01009015	26	83 ± 4	24 ± 9	1 ± 3	197	ND
PZB02109029	34	65 ± 7	14 ± 3	1 ± 2	333	ND

Table 40 (continued). Screening results and potencies of compound from the fragment library at rat CD73 (means ± SEM from at least three separate experiments performed in duplicates, ND: not determined).

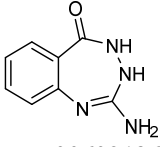| Structure/ Name	RatCD73 Inhibition ± SEM (%)				Pseudo IC$_{50}$ (μM)	IC$_{50}$ ± SEM (μM)
	Malachite green assay	Radio assay				
	500 μM	500 μM	100 μM	10 μM		
PZB02109039A	34	84 ± 6	30 ± 8	5 ± 1	183	ND
PZB02109030	26	58 ± 5	15 ± 8	5 ± 3	417	ND
PZB02109041A	32	42 ± 7	15 ± 3	1 ± 4	694	ND
PZB06114025A	28	26 ± 7	7 ± 8	2 ± 5	1361	ND
PZB09414102A	55	70 ± 5	46 ± 4	28 ± 6	113	96.0 ± 8.0
PZB02909096A	42	48 ± 3	18 ± 12	6 ± 5	598	ND
PZB05311010A	28	42 ± 11	27 ± 7	6 ± 3	760	ND
PZB05311022A	90	42 ± 7	9 ± 9	4 ± 4	651	ND

6.2.4 Binding mode of compound PZB00709002
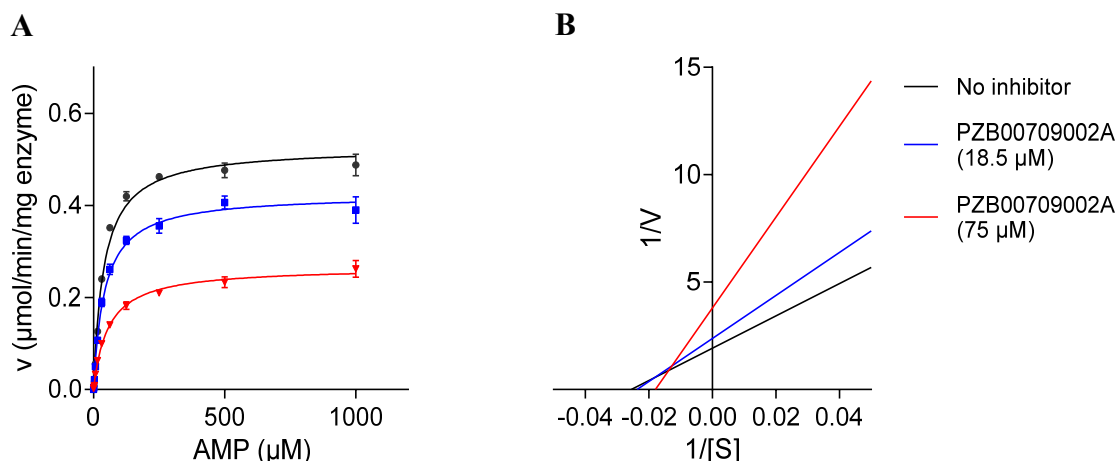
Figure 79. Mixed inhibition mode of PZB00709002. (A) Michaelis-Menten kinetics: V_{max} is decreased at higher inhibitor concentration. The K_M value is increased for higher inhibitor concentrations. **(B)** Lineweaver-Burk plot shows intercept of the lines in quadrant II with $\alpha > 1$ that is typical for a mixed inhibition with a more competitive than uncompetitive character of the inhibition. (Mean of three independent experiments, error bars represent SEM).

6.2.5 Analysis of CD73-targeting antibodies
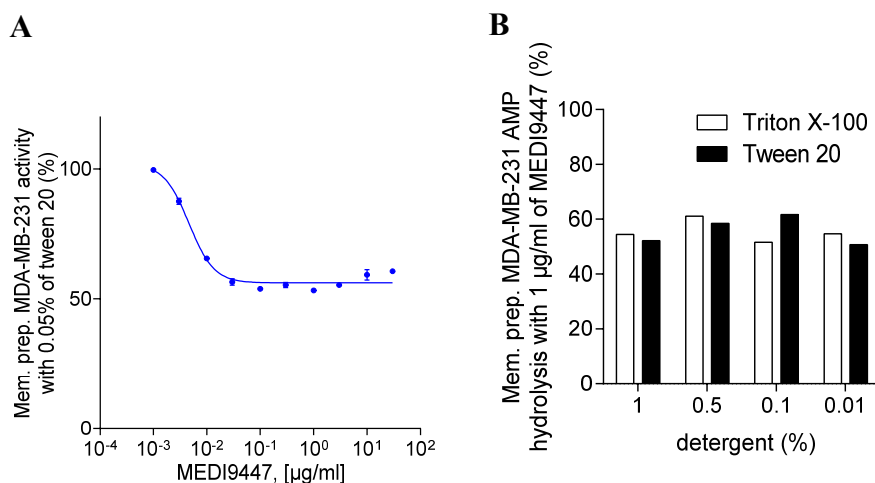
Figure 80. Analysis of MEDI9447 antibody in the presence of detergents. (A) The addition of 0.05% Tween 20 was tried to prevent aggregation of MEDI9447 at higher concentrations. **(B)** Investigation of Tween 20 and Triton X-100 at different concentrations did not increase maximal inhibition.
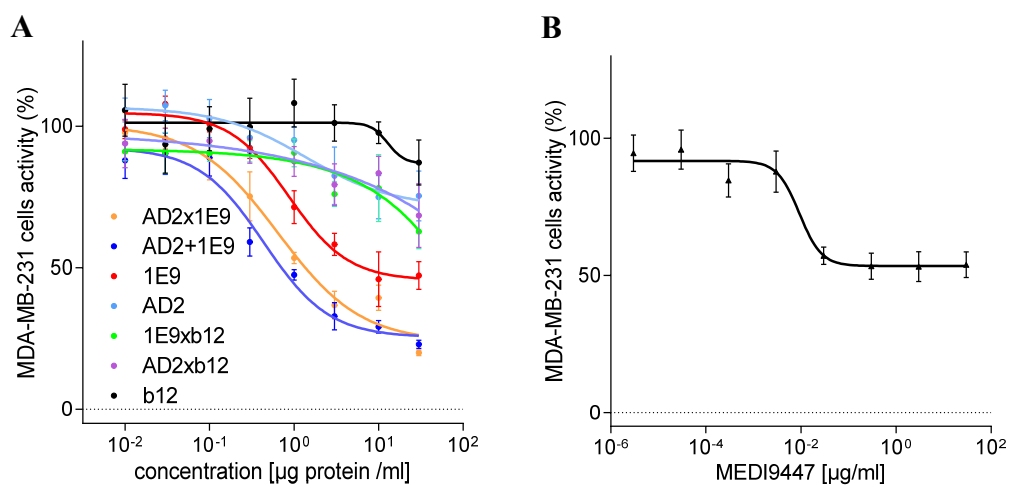
Figure 81. Analysis of CD73-targeting antibodies with cells. **(A)** Bispecific antibodies and **(B)** MEDI9447 (results of at least three independent experiments, error bars represent SEM).
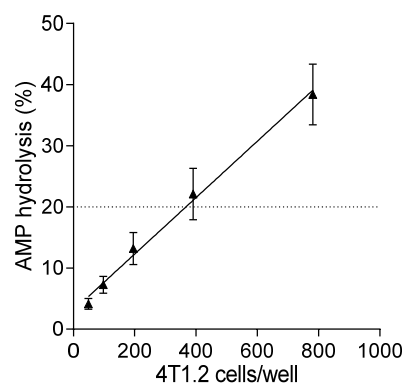
Figure 82. Cell titration with 4T1.2 cells (mean results of three independent experiments, error bars represent SEM).

Appendix

7 Bibliography

(1) Definition of a drug. *Collins English Dictionary - Complete & Unabridged 2012 Digital Edition* [Online]; William Collins Sons & Co. Ltd. 1979, 1986, Harper Collins Publishers 1998, 2000, 2003, 2005, 2006, 2007, 2009, 2012 https://www.dictionary.com/browse/drug (accessed March 13, 2019).

(2) Rang, H. P.; Dale, M. M. *Rang and Dale's pharmacology*; Elsevier Churchill Livingstone: Edinburgh, 2012; 7. ed, p 1.

(3) Vohora, D.; Singh, G. *Pharmaceutical medicine and translational clinical research*; Academic Press an imprint of Elsevier: London, 2018, pp 19-30.

(4) Amoxicillin. *The Drugs.com Database* [Online]; Posted on September 03, 2018. http://www.drugs.com/monograph/amoxicillin.html (accessed March 15, 2019).

(5) Hochhaus, A.; Larson, R. A.; Guilhot, F.; Radich, J. P.; Branford, S.; Hughes, T. P.; Baccarani, M.; Deininger, M. W.; Cervantes, F.; Fujihara, S.; Ortmann, C.-E.; Menssen, H. D.; Kantarjian, H.; O'Brien, S. G.; Druker, B. J. Long-term outcomes of imatinib treatment for chronic myeloid leukemia. *N. Engl. J. Med.* **2017**, *376*, 917–927.

(6) Sebaugh, J. L. Guidelines for accurate EC50/IC50 estimation. *Pharm. Stat.* **2011**, *10*, 128–134.

(7) Rester, U. From virtuality to reality - Virtual screening in lead discovery and lead optimization: a medicinal chemistry perspective. *Curr. Opin. Drug Discov. Devel.* **2008**, *11*, 559–568.

(8) Leeson, P. Drug discovery: chemical beauty contest. *Nature* **2012**, *481*, 455–456.

(9) van Breemen, R. B.; Li, Y. Caco-2 cell permeability assays to measure drug absorption. *Expert Opin. Drug Metab. Toxicol.* **2005**, *1*, 175–185.

(10) Baranczewski, P.; Stańczak, A.; Sundberg, K.; Svensson, R.; Wallin, A.; Jansson, J.; Garberg, P.; Postlind, H. Introduction to in vitro estimation of metabolic stability and drug interactions of new chemical entities in drug discovery and development. *Pharmacol. Rep.* **2006**, *58*, 453–472.

(11) Yan, Z.; Caldwell, G. W. Metabolism profiling, and cytochrome P450 inhibition & induction in drug discovery. *Curr. Top. Med. Chem.* **2001**, *1*, 403–425.

Bibliography

(12) Lambrinidis, G.; Vallianatou, T.; Tsantili-Kakoulidou, A. In vitro, in silico and integrated strategies for the estimation of plasma protein binding. A review. *Adv. Drug Deliv. Rev.* **2015**, *86*, 27–45.

(13) U.S. Food and Drug Administration Homepage. The drug development process https://www.fda.gov/forpatients/approvals/drugs/ (accessed March 11, 2019).

(14) Ciani, O.; Jommi, C. The role of health technology assessment bodies in shaping drug development. *Drug Des. Devel. Ther.* **2014**, *8*, 2273–2281.

(15) van Nooten, F.; Holmstrom, S.; Green, J.; Wiklund, I.; Odeyemi, I. A. O.; Wilcox, T. K. Health economics and outcomes research within drug development: challenges and opportunities for reimbursement and market access within biopharma research. *Drug Discov. Today* **2012**, *17*, 615–622.

(16) Drury, A. N.; Szent-Györgyi, A. The physiological activity of adenine compounds with especial reference to their action upon the mammalian heart. *J. Physiol.* **1929**, *68*, 213–237.

(17) Burnstock, G.; Fredholm, B. B.; North, R. A.; Verkhratsky, A. The birth and postnatal development of purinergic signalling. *Acta Physiol.* **2010**, *199*, 93–147.

(18) Burnstock, G.; Campbell, G.; Satchell, D.; Smythe, A. Evidence that adenosine triphosphate or a related nucleotide is the transmitter substance released by non-adrenergic inhibitory nerves in the gut. *Br. J. Pharmacol.* **1970**, *40*, 668–688.

(19) Burnstock, G. Purinergic nerves. *Pharmacol. Rev.* **1972**, *24*, 509–581.

(20) Abbracchio, M. P.; Burnstock, G. Purinergic signalling: pathophysiological roles. *Jpn. J. Pharmacol.* **1998**, *78*, 113–145.

(21) Fredholm, B. B.; Abbracchio, M. P.; Burnstock, G.; Dubyak, G. R.; Harden, T. K.; Jacobson, K. A.; Schwabe, U.; Williams, M. Towards a revised nomenclature for P1 and P2 receptors. *Trends Pharmacol. Sci.* **1997**, *18*, 79–82.

(22) Gever, J. R.; Cockayne, D. A.; Dillon, M. P.; Burnstock, G.; Ford, A. P. D. W. Pharmacology of P2X channels. *Pflugers Arch.* **2006**, *452*, 513–537.

(23) Rafehi, M.; Müller, C. E. Tools and drugs for uracil nucleotide-activated P2Y receptors. *Pharmacol. Ther.* **2018**, *190*, 24–80.

(24) Freundlieb, M. Entwicklung und Charakterisierung von neuen und selektiven Inhibitoren für die Ecto-5'-Nucleotidase. Dissertation, University of Bonn, 2016.

(25) Müller, C. E. University of Bonn, Bonn, Germany, unpublished work, 2015.

(26) Nehlig, A.; Daval, J.-L.; Debry, G. Caffeine and the central nervous system: mechanisms of action, biochemical, metabolic and psychostimulant effects. *Brain Res. Rev.* **1992**, *17*, 139–170.

(27) Sheth, S.; Brito, R.; Mukherjea, D.; Rybak, L. P.; Ramkumar, V. Adenosine receptors: expression, function and regulation. *Int. J. Mol. Sci.* **2014**, *15*, 2024–2052.

(28) Blackburn, M. R.; Vance, C. O.; Morschl, E.; Wilson, C. N. Adenosine receptors and inflammation. *Handb. Exp. Pharmacol.* **2009**, 215–269.

(29) Takahashi, M.; Fujita, M.; Asai, N.; Saki, M.; Mori, A. Safety and effectiveness of istradefylline in patients with Parkinson's disease: interim analysis of a post-marketing surveillance study in Japan. *Expert Opin. Pharmacother.* **2018**, *19*, 1635–1642.

(30) Townsend, R.; Desai, A.; Rammelsberg, D.; Kowalski, D.; Simmons, N.; Kitt, T. M. Safety and tolerability of intravenous regadenoson in healthy subjects: A randomized, repeat-dose, placebo-controlled study. *J. Nucl. Cardiol.* **2017**, *24*, 57–65.

(31) Lieu, H. D.; Shryock, J. C.; Mering, G. O. von; Gordi, T.; Blackburn, B.; Olmsted, A. W.; Belardinelli, L.; Kerensky, R. A. Regadenoson, a selective A2A adenosine receptor agonist, causes dose-dependent increases in coronary blood flow velocity in humans. *J. Nucl. Cardiol.* **2007**, *14*, 514–520.

(32) U.S. National Institutes of Health Homepage. A phase 2 study of NIR178 in combination with PDR001 in patients with solid tumors and non-hodgkin lymphoma https://clinicaltrials.gov/ct2/show/NCT03207867 (accessed May, 3, 2019).

(33) Corvus Pharmaceuticals Homepage. Our Pipeline; Posted on April 30, 2018 https://www.corvuspharma.com/our-science/our-pipeline/ (accessed May 2, 2019).

(34) Willingham, S. B.; Ho, P. Y.; Hotson, A.; Hill, C.; Piccione, E. C.; Hsieh, J.; Liu, L.; Buggy, J. J.; McCaffery, I.; Miller, R. A. A2AR antagonism with CPI-444 induces antitumor responses and augments efficacy to anti-PD-(L)1 and anti-CTLA-4 in preclinical models. *Cancer Immunol. Res.* **2018**, *6*, 1136–1149.

(35) Ghalamfarsa, G.; Kazemi, M. H.; Raoofi Mohseni, S.; Masjedi, A.; Hojjat-Farsangi, M.; Azizi, G.; Yousefi, M.; Jadidi-Niaragh, F. CD73 as a potential opportunity for cancer immunotherapy. *Expert Opin. Ther. Targets* **2019**, *23*, 127–142.

(36) Kügelgen, I. von. Pharmacological profiles of cloned mammalian P2Y-receptor subtypes. *Pharmacol. Ther.* **2006**, *110*, 415–432.

Bibliography

(37) Patel, A.; Vidula, M.; Kishore, S. P.; Vedanthan, R.; Huffman, M. D. Building the case for clopidogrel as a world health organization essential medicine. *Circ. Cardiovasc. Qual. Outcomes* **2015**, *8*, 447–451.

(38) Plosker, G. L.; Lyseng-Williamson, K. A. Clopidogrel: a review of its use in the prevention of thrombosis. *Drugs* **2007**, *67*, 613–646.

(39) Kaczmarek-Hájek, K.; Lörinczi, E.; Hausmann, R.; Nicke, A. Molecular and functional properties of P2X receptors-recent progress and persisting challenges. *Purinergic Signal.* **2012**, *8*, 375–417.

(40) Surprenant, A.; North, R. A. Signaling at purinergic P2X receptors. *Annu. Rev. Physiol.* **2009**, *71*, 333–359.

(41) North, R. A.; Jarvis, M. F. P2X receptors as drug targets. *Mol. Pharmacol.* **2013**, *83*, 759–769.

(42) Wang, J.; Wang, Y.; Cui, W.-W.; Huang, Y.; Yang, Y.; Liu, Y.; Zhao, W.-S.; Cheng, X.-Y.; Sun, W.-S.; Cao, P.; Zhu, M. X.; Wang, R.; Hattori, M.; Yu, Y. Druggable negative allosteric site of P2X3 receptors. *PNAS* **2018**, *115*, 4939–4944.

(43) Zimmermann, H.; Zebisch, M.; Sträter, N. Cellular function and molecular structure of ecto-nucleotidases. *Purinergic Signal.* **2012**, *8*, 437–502.

(44) Sträter, N. Prof. Dr. Norbert Sträter Homepage; Posted on January 03, 2014 http://research.uni-leipzig.de/straeter/research/purinergicsignaling.html (accessed March 24, 2019).

(45) Sek, K.; Mølck, C.; Stewart, G. d.; Kats, L.; Darcy, P. K.; Beavis, P. A. Targeting adenosine receptor signaling in cancer immunotherapy. *Int. J. Mol. Sci.* **2018**, *19*.

(46) Leone, R. D.; Emens, L. A. Targeting adenosine for cancer immunotherapy. *J. Immunother. Cancer* **2018**, *6*, 57.

(47) Zalatan, J. G.; Fenn, T. D.; Brunger, A. T.; Herschlag, D. Structural and functional comparisons of nucleotide pyrophosphatase/phosphodiesterase and alkaline phosphatase: implications for mechanism and evolution. *Biochemistry* **2006**, *45*, 9788–9803.

(48) Lee, S.-Y.; Müller, C. E. Nucleotide pyrophosphatase/phosphodiesterase 1 (NPP1) and its inhibitors. *Medchemcomm* **2017**, *8*, 823–840.

(49) Gorelik, A.; Randriamihaja, A.; Illes, K.; Nagar, B. A key tyrosine substitution restricts nucleotide hydrolysis by the ectoenzyme NPP5. *FEBS J.* **2017**, *284*, 3718–3726.

(50) Sakagami, H.; Aoki, J.; Natori, Y.; Nishikawa, K.; Kakehi, Y.; Natori, Y.; Arai, H. Biochemical and molecular characterization of a novel choline-specific glycerophosphodiester phosphodiesterase belonging to the nucleotide pyrophosphatase/phosphodiesterase family. *J. Biol. Chem.* **2005**, *280*, 23084–23093.

(51) Aerts, I.; Martin, J.-J.; Deyn, P. P. de; van Ginniken, C.; van Ostade, X.; Kockx, M.; Dua, G.; Slegers, H. The expression of ecto-nucleotide pyrophosphatase/phosphodiesterase 1 (E-NPP1) is correlated with astrocytic tumor grade. *Clin. Neurol. Neurosurg.* **2011**, *113*, 224–229.

(52) Albright, R. A.; Chang, W. C.; Robert, D.; Ornstein, D. L.; Cao, W.; Liu, L.; Redick, M. E.; Young, J. I.; La Cruz, E. M. de; Braddock, D. T. NPP4 is a procoagulant enzyme on the surface of vascular endothelium. *Blood* **2012**, *120*, 4432–4440.

(53) Goding, J. W.; Grobben, B.; Slegers, H. Physiological and pathophysiological functions of the ecto-nucleotide pyrophosphatase/phosphodiesterase family. *Biochim. Biophys. Acta* **2003**, *1638*, 1–19.

(54) Doñate, F.; Raitano, A.; Morrison, K.; An, Z.; Capo, L.; Aviña, H.; Karki, S.; Morrison, K.; Yang, P.; Ou, J.; Moriya, R.; Shostak, Y.; Malik, F.; Nadell, R.; Liu, W.; Satpayev, D.; Atkinson, J.; Joseph, I. B. J.; Pereira, D. S.; Challita-Eid, P. M.; Stover, D. R. AGS16F is a novel antibody drug conjugate directed against ENPP3 for the treatment of renal cell carcinoma. *Clin. Cancer Res.* **2016**, *22*, 1989–1999.

(55) U.S. National Institutes of Health Homepage. A study of AGS-16C3F vs. Axitinib in metastatic renal cell carcinoma https://clinicaltrials.gov/ct2/show/NCT02639182 (accessed .June 28, 2019).

(56) Garavaglia, S.; Bruzzone, S.; Cassani, C.; Canella, L.; Allegrone, G.; Sturla, L.; Mannino, E.; Millo, E.; Flora, A. de; Rizzi, M. The high-resolution crystal structure of periplasmic Haemophilus influenzae NAD nucleotidase reveals a novel enzymatic function of human CD73 related to NAD metabolism. *Biochem. J.* **2012**, *441*, 131–141.

(57) Ogata, S.; Hayashi, Y.; Misumi, Y.; Ikehara, Y. Membrane-anchoring domain of rat liver 5'-nucleotidase: identification of the carboxy-terminal serine-523 covalently attached with a glycolipid. *Biochemistry* **1990**, *29*, 7923–7927.

(58) Sträter, N. Ecto-5'-nucleotidase: structure function relationships. *Purinergic Signal.* **2006**, *2*, 343–350.

Bibliography

(59) Knapp, K.; Zebisch, M.; Pippel, J.; El-Tayeb, A.; Müller, C. E.; Sträter, N. Crystal structure of the human ecto-5'-nucleotidase (CD73). Insights into the regulation of purinergic signaling. *Structure* **2012**, *20*, 2161–2173.

(60) Misumi, Y.; Ogata, S.; Ohkubo, K.; Hirose, S.; Ikehara, Y. Primary structure of human placental 5'-nucleotidase and identification of the glycolipid anchor in the mature form. *Eur. J. Biochem.* **1990**, *191*, 563–569.

(61) Walldén, K.; Stenmark, P.; Nyman, T.; Flodin, S.; Gräslund, S.; Loppnau, P.; Bianchi, V.; Nordlund, P. Crystal structure of human cytosolic 5'-nucleotidase II: insights into allosteric regulation and substrate recognition. *J. Biol. Chem.* **2007**, *282*, 17828–17836.

(62) Sunderman, F. W. The clinical biochemistry of 5'-nucleotidase. *Ann. Clin. Lab. Sci.* **1990**, *20*, 123–139.

(63) Johnson, S. M.; Patel, S.; Bruckner, F. E.; Collins, D. A. 5'-Nucleotidase as a marker of both general and local inflammation in rheumatoid arthritis patients. *Rheumatology (Oxford)* **1999**, *38*, 391–396.

(64) Clayton, A.; Al-Taei, S.; Webber, J.; Mason, M. D.; Tabi, Z. Cancer exosomes express CD39 and CD73, which suppress T cells through adenosine production. *J. Immunol.* **2011**, *187*, 676–683.

(65) Trams, E. G.; Lauter, C. J.; Salem, N.; Heine, U. Exfoliation of membrane ecto-enzymes in the form of micro-vesicles. *Biochim. Biophys. Acta* **1981**, *645*, 63–70.

(66) Fini, C.; Talamo, F.; Cherri, S.; Coli, M.; Floridi, A.; Ferrara, L.; Scaloni, A. Biochemical and mass spectrometric characterization of soluble ecto-5'-nucleotidase from bull seminal plasma. *Biochem. J.* **2003**, *372*, 443–451.

(67) Vogel, M.; Kowalewski, H.; Zimmermann, H.; Hooper, N. M.; Turner, A. J. Soluble low-Km 5'-nucleotidase from electric-ray (Torpedo marmorata) electric organ and bovine cerebral cortex is derived from the glycosyl-phosphatidylinositol-anchored ectoenzyme by phospholipase C cleavage. *Biochem. J.* **1992**, *284*, 621–624.

(68) Reinhardt, J.; Landsberg, J.; Schmid-Burgk, J. L.; Ramis, B. B.; Bald, T.; Glodde, N.; Lopez-Ramos, D.; Young, A.; Ngiow, S. F.; Nettersheim, D.; Schorle, H.; Quast, T.; Kolanus, W.; Schadendorf, D.; Long, G. V.; Madore, J.; Scolyer, R. A.; Ribas, A.; Smyth, M. J.; Tumeh, P. C.; Tüting, T.; Hölzel, M. MAPK signaling and inflammation link melanoma phenotype switching to induction of CD73 during immunotherapy. *Cancer Res.* **2017**, *77*, 4697–4709.

(69) Su, A. I.; Wiltshire, T.; Batalov, S.; Lapp, H.; Ching, K. A.; Block, D.; Zhang, J.; Soden, R.; Hayakawa, M.; Kreiman, G.; Cooke, M. P.; Walker, J. R.; Hogenesch, J. B. A gene atlas of the mouse and human protein-encoding transcriptomes. *PNAS* **2004**, *101*, 6062–6067.

(70) Yang, J.; Jian, R.; Yu, J.; Zhi, X.; Liao, X.; Yu, J.; Zhou, P. CD73 regulates vascular smooth muscle cell functions and facilitates atherosclerotic plaque formation. *IUBMB Life* **2015**, *67*, 853–860.

(71) Jian, R.; Sun, Y.; Wang, Y.; Yu, J.; Zhong, L.; Zhou, P. CD73 protects kidney from ischemia-reperfusion injury through reduction of free radicals. *APMIS* **2012**, *120*, 130–138.

(72) Yang, J.; Liao, X.; Yu, J.; Zhou, P. Role of CD73 in disease: promising prognostic indicator and therapeutic target. *Curr. Med. Chem.* **2018**, *25*, 2260–2271.

(73) Stagg, J.; Smyth, M. J. Extracellular adenosine triphosphate and adenosine in cancer. *Oncogene* **2010**, *29*, 5346–5358.

(74) Synnestvedt, K.; Furuta, G. T.; Comerford, K. M.; Louis, N.; Karhausen, J.; Eltzschig, H. K.; Hansen, K. R.; Thompson, L. F.; Colgan, S. P. Ecto-5'-nucleotidase (CD73) regulation by hypoxia-inducible factor-1 mediates permeability changes in intestinal epithelia. *J. Clin. Invest.* **2002**, *110*, 993–1002.

(75) Zhang, B. CD73 promotes tumor growth and metastasis. *Oncoimmunology* **2012**, *1*, 67–70.

(76) Gao, Z.-w.; Wang, H.-p.; Lin, F.; Wang, X.; Long, M.; Zhang, H.-z.; Dong, K. CD73 promotes proliferation and migration of human cervical cancer cells independent of its enzyme activity. *BMC Cancer* [Online] **2017**, *17*. https://www.ncbi.nlm.nih.gov/pmc/articles/PMC5311855/pdf/12885_2017_Article_3128.pdf (accessed June 25, 2019).

(77) Leth-Larsen, R.; Lund, R.; Hansen, H. V.; Laenkholm, A.-V.; Tarin, D.; Jensen, O. N.; Ditzel, H. J. Metastasis-related plasma membrane proteins of human breast cancer cells identified by comparative quantitative mass spectrometry. *Mol. Cell. Proteomics* **2009**, *8*, 1436–1449.

(78) Foulkes, W. D.; Smith, I. E.; Reis-Filho, J. S. Triple-negative breast cancer. *N. Engl. J. Med.* **2010**, *363*, 1938–1948.

(79) Buisseret, L.; Pommey, S.; Allard, B.; Garaud, S.; Bergeron, M.; Cousineau, I.; Ameye, L.; Bareche, Y.; Paesmans, M.; Crown, J. P. A.; Di Leo, A.; Loi, S.; Piccart-Gebhart, M.; Willard-Gallo, K.; Sotiriou, C.; Stagg, J. Clinical significance of CD73 in triple-negative

breast cancer: multiplex analysis of a phase III clinical trial. *Ann. Oncol.* **2018**, *29*, 1056–1062.

(80) Stagg, J.; Divisekera, U.; Duret, H.; Sparwasser, T.; Teng, M. W. L.; Darcy, P. K.; Smyth, M. J. CD73-deficient mice have increased antitumor immunity and are resistant to experimental metastasis. *Cancer Res.* **2011**, *71*, 2892–2900.

(81) Stagg, J.; Divisekera, U.; McLaughlin, N.; Sharkey, J.; Pommey, S.; Denoyer, D.; Dwyer, K. M.; Smyth, M. J. Anti-CD73 antibody therapy inhibits breast tumor growth and metastasis. *PNAS* **2010**, *107*, 1547–1552.

(82) Airas, L.; Niemelä, J.; Jalkanen, S. CD73 engagement promotes lymphocyte binding to endothelial cells via a lymphocyte function-associated antigen-1-dependent mechanism. *J. Immunol.* **2000**, *165*, 5411–5417.

(83) Jin, D.; Fan, J.; Wang, L.; Thompson, L. F.; Liu, A.; Daniel, B. J.; Shin, T.; Curiel, T. J.; Zhang, B. CD73 on tumor cells impairs antitumor T-cell responses: a novel mechanism of tumor-induced immune suppression. *Cancer Res.* **2010**, *70*, 2245–2255.

(84) Häusler, S. F. M.; Montalbán del Barrio, I.; Strohschein, J.; Chandran, P. A.; Engel, J. B.; Hönig, A.; Ossadnik, M.; Horn, E.; Fischer, B.; Krockenberger, M.; Heuer, S.; Seida, A. A.; Junker, M.; Kneitz, H.; Kloor, D.; Klotz, K.-N.; Dietl, J.; Wischhusen, J. Ectonucleotidases CD39 and CD73 on OvCA cells are potent adenosine-generating enzymes responsible for adenosine receptor 2A-dependent suppression of T cell function and NK cell cytotoxicity. *Cancer Immunol. Immunother.* **2011**, *60*, 1405–1418.

(85) U.S. National Institutes of Health Homepage. A study to investigate the safety of AB680 in healthy volunteers https://clinicaltrials.gov/ct2/show/NCT03677973?term=NCT03677973&rank=1 (accessed May 3, 2019).

(86) Terp, M. G.; Olesen, K. A.; Arnspang, E. C.; Lund, R. R.; Lagerholm, B. C.; Ditzel, H. J.; Leth-Larsen, R. Anti-human CD73 monoclonal antibody inhibits metastasis formation in human breast cancer by inducing clustering and internalization of CD73 expressed on the surface of cancer cells. *J. Immunol.* **2013**, *191*, 4165–4173.

(87) Hay, C. M.; Sult, E.; Huang, Q.; Mulgrew, K.; Fuhrmann, S. R.; McGlinchey, K. A.; Hammond, S. A.; Rothstein, R.; Rios-Doria, J.; Poon, E.; Holoweckyj, N.; Durham, N. M.; Leow, C. C.; Diedrich, G.; Damschroder, M.; Herbst, R.; Hollingsworth, R. E.;

Sachsenmeier, K. F. Targeting CD73 in the tumor microenvironment with MEDI9447. *Oncoimmunology* **2016**, *5*, e1208875.

(88) U.S. National Institutes of Health. MEDI9447 alone and in combination with MEDI4736 in adult subjects with select advanced solid tumors https://clinicaltrials.gov/ct2/show/NCT02503774 (accessed January 28, 2017).

(89) Voet, D.; Voet, J. G.; Pratt, C. W.; Beck-Sickinger, A.; Hahn, U.; Häcker, B. *Lehrbuch der Biochemie*; Wiley-VCH-Verl.: Weinheim, 2010; 2. ed, pp 400-418.

(90) Voet, D.; Voet, J. G. *Biochemistry*; Wiley: New York, 2011; 4. ed., pp 488-496.

(91) GraphPad Prism Homepage. GraphPad Curve Fitting Guide (Equation: Michaelis-Menten model); Posted on April 09, 2018 https://www.graphpad.com/guides/prism/7/curve-fitting/index.htm?reg_michaelis_menten_enzyme.htm (accessed February 11, 2019).

(92) Cheng, Y.; Prusoff, W. H. Relationship between the inhibition constant (K_I) and the concentration of inhibitor which causes 50 per cent inhibition (I_{50}) of an enzymatic reaction. *Biochem. Pharmacol.* **1973**, *22*, 3099–3108.

(93) Iqbal, J.; Jirovsky, D.; Lee, S.-Y.; Zimmermann, H.; Müller, C. E. Capillary electrophoresis-based nanoscale assays for monitoring ecto-5'-nucleotidase activity and inhibition in preparations of recombinant enzyme and melanoma cell membranes. *Anal. Biochem.* **2008**, *373*, 129–140.

(94) Bhattarai, S.; Freundlieb, M.; Pippel, J.; Meyer, A.; Abdelrahman, A.; Fiene, A.; Lee, S.-Y.; Zimmermann, H.; Yegutkin, G. G.; Sträter, N.; El-Tayeb, A.; Müller, C. E. α,β-Methylene-ADP (AOPCP) derivatives and analogues: development of potent and selective ecto-5′-Nucleotidase (CD73) inhibitors. *J. Med. Chem.* **2015**, *58*, 6248–6263.

(95) Myers, T. C.; Nakamura, K.; Danielzadeh, A. B. Phosphonic acid analogs of nucleoside phosphates. III. The synthesis of adenosine-5'-methylenediphosphonate, a phosphonic acid analog of adenosine-5'-diphosphate. *J. Org. Chem.* **1965**, *30*, 1517–1520.

(96) Burger, R. M.; Lowenstein, J. M. Preparation and properties of 5'-nucleotidase from smooth muscle of small intestine. *J. Biol. Chem.* **1970**, *245*, 6274–6280.

(97) Tomczyk, M.; Mierzejewska, P.; Slominska, E. M.; Smolenski, R. T. The metabolism of ecto-5'-nucleotidase (CD73) inhibitor-α,β-methylene adenosine diphosphate in BALB/c mice. *Nucleosides Nucleotides Nucleic Acids* **2018**, *37*, 709–716.

(98) Lawson KV, Jin L, Jeffrey J, Kalisiak J, Yin F, Zhang K, Chen A, Swinarski D, Walters MJ, Young S, Schindler U, Powers JP. Discovery and characterization of AB680, a potent

Bibliography

and selective small-molecule CD73 inhibitor for cancer immunotherapy [Online] https://www.arcusbio.com/wp-content/uploads/2018/04/AACR_AB680_1756_final_ 90x42-abstract-4886.pdf (accessed May 23, 2019).

(99) Tiley, S.; Claxton, D. Clofarabine in the treatment of acute myeloid leukemia in older adults. *Ther. Adv. Hematol.* **2013**, *4*, 5–13.

(100) Dumontet, C.; Peyrottes, S.; Rabeson, C.; Cros-Perrial, E.; Géant, P. Y.; Chaloin, L.; Jordheim, L. P. CD73 inhibition by purine cytotoxic nucleoside analogue-based diphosphonates. *Eur. J. Med. Chem.* **2018**, *157*, 1051–1055.

(101) Li, W. Therapeutically important enzymes with polar substrates or products: characterization by capillary electrophoresis and identification of inhibitors. Dissertation, University of Bonn, 2014.

(102) Brunschweiger, A. Darstellung und Charakterisierung von Uracil- und Adeninnucleotid-Mimetika als selektive Ectonucleotidase-Inhibitoren. Dissertation, University of Bonn, 2007.

(103) Cacatian, S.; Claremon, D. A.; Jia, L.; Morales-Ramos, A.; Singh, S. B.; Venkat-Raman, S.; Xu, Z.; Zheng, Y. Purine derivatives as CD73 inhibitors for the treatment of cancer. International patent application WO2015164573, applicant: Vitae Pharmaceuticals Inc., October 29, 2015.

(104) Heuts, D. P. H. M.; Weissenborn, M. J.; Olkhov, R. V.; Shaw, A. M.; Gummadova, J.; Levy, C.; Scrutton, N. S. Crystal structure of a soluble form of human CD73 with ecto-5'-nucleotidase activity. *Chembiochem* **2012**, *13*, 2384–2391.

(105) Billedeau, R. J.; Li, J.; Chen, L. Ectonucleotidase inhibitors and methods the use there of. U.S. Patent application publication US 2018/0186827 A1, applicant: Calithera Biosciences Inc., July 5, 2018.

(106) Giordani, R. B.; Weizenmann, M.; Rosemberg, D. B.; Carli, G. A. de; Bogo, M. R.; Zuanazzi, J. A. S.; Tasca, T. Trichomonas vaginalis nucleoside triphosphate diphosphohydrolase and ecto-5'-nucleotidase activities are inhibited by lycorine and candimine. *Parasitol. Int.* **2010**, *59*, 226–231.

(107) Kao, D. J.; Saeedi, B. J.; Kitzenberg, D.; Burney, K. M.; Dobrinskikh, E.; Battista, K. D.; Vázquez-Torres, A.; Colgan, S. P.; Kominsky, D. J. Intestinal epithelial ecto-5'-nucleotidase (CD73) regulates intestinal colonization and infection by nontyphoidal *Salmonella*. *Infect. Immun.* **2017**, *85*.

(108) Alam, M. S.; Kuo, J. L.; Ernst, P. B.; Derr-Castillo, V.; Pereira, M.; Gaines, D.; Costales, M.; Bigley, E.; Williams, K. Ecto-5′-nucleotidase (CD73) regulates host inflammatory responses and exacerbates murine salmonellosis. *Sci. Rep.* **2014**, *4*.

(109) Kavutcu, M.; Melzig, M. F. In vitro effects of selected flavonoids on the 5'-nucleotidase activity. *Pharmazie* **1999**, *54*, 457–459.

(110) Braganhol, E.; Tamajusuku, A. S. K.; Bernardi, A.; Wink, M. R.; Battastini, A. M. O. Ecto-5'-nucleotidase/CD73 inhibition by quercetin in the human U138MG glioma cell line. *Biochim. Biophys. Acta* **2007**, *1770*, 1352–1359.

(111) Baqi, Y. Ecto-nucleotidase inhibitors: recent developments in drug discovery. *Mini Rev. Med. Chem.* **2015**, *15*, 21–33.

(112) Fredholm, B. B.; Hedqvist, P.; Vernet, L. Effect of theophylline and other drugs on rabbit renal cyclic nucleotide phosphodiesterase, 5′-nucleotidase and adenosine deaminase. *Biochem. Pharmacol.* **1978**, *27*, 2845–2850.

(113) Heyliger, C. E.; Panagia, V.; Dhalla, N. S. Effect of cyclic AMP phosphodiesterase inhibitors on cardiac sarcolemmal 5'-nucleotidase. *J. Pharmacol. Exp. Ther.* **1981**, *217*, 489–493.

(114) Baqi, Y.; Lee, S.-Y.; Iqbal, J.; Ripphausen, P.; Lehr, A.; Scheiff, A. B.; Zimmermann, H.; Bajorath, J.; Müller, C. E. Development of potent and selective inhibitors of ecto-5'-nucleotidase based on an anthraquinone scaffold. *J. Med. Chem.* **2010**, *53*, 2076–2086.

(115) Raza, R.; Saeed, A.; Lecka, J.; Sévigny, J.; Iqbal, J. Identification of small molecule sulfonic acids as ecto-5'-Nucleotidase inhibitors. *Med. Chem.* **2012**, *8*, 1133–1139.

(116) Iqbal, J.; Saeed, A.; Raza, R.; Matin, A.; Hameed, A.; Furtmann, N.; Lecka, J.; Sévigny, J.; Bajorath, J. Identification of sulfonic acids as efficient ecto-5'-nucleotidase inhibitors. *Eur. J. Med. Chem.* **2013**, *70*, 685–691.

(117) Olender, D.; Żwawiak, J.; Zaprutko, L. Multidirectional efficacy of biologically active nitro compounds included in medicines. *Pharmaceuticals* **2018**, *11*.

(118) Nepali, K.; Lee, H.-Y.; Liou, J.-P. Nitro-group-containing drugs. *J. Med. Chem.* **2018**.

(119) Channar, P. A.; Shah, S. J. A.; Hassan, S.; Nisa, Z. U.; Lecka, J.; Sévigny, J.; Bajorath, J.; Saeed, A.; Iqbal, J. Isonicotinohydrazones as inhibitors of alkaline phosphatase and ecto-5'-nucleotidase. *Chem. Biol. Drug Des.* **2017**, *89*, 365–370.

(120) Kalia, J.; Raines, R. T. Hydrolytic stability of hydrazones and oximes. *Angew. Chem.* **2008**, *47*, 7523–7526.

Bibliography

(121) Hassan, S.; Channar, P. A.; Larik, F. A.; Saeed, A.; Shah, H. S.; Lecka, J.; Sévigny, J.; Iqbal, J. Synthesis of novel (E)-1-(2-(2-(4(dimethylamino) benzylidene) hydrazinyl)-4-methylthiazol-5-yl)ethanone derivatives as ecto-5'-nucleotidase inhibitors. *R. Soc. Open Sci.* **2018**, *5*, 180837.

(122) Maliga, Z.; Kapoor, T. M.; Mitchison, T. J. Evidence that monastrol is an allosteric inhibitor of the mitotic kinesin Eg5. *Chem. Biol.* **2002**, *9*, 989–996.

(123) Mayer, T. U.; Kapoor, T. M.; Haggarty, S. J.; King, R. W.; Schreiber, S. L.; Mitchison, T. J. Small molecule inhibitor of mitotic spindle bipolarity identified in a phenotype-based screen. *Science* **1999**, *286*, 971–974.

(124) Figueiró, F.; Mendes, F. B.; Corbelini, P. F.; Janarelli, F.; Jandrey, E. H. F.; Russowsky, D.; Eifler-Lima, V. L.; Battastini, A. M. O. A monastrol-derived compound, LaSOM 63, inhibits ecto-5'nucleotidase/CD73 activity and induces apoptotic cell death of glioma cell lines. *Anticancer Res.* **2014**, *34*, 1837–1842.

(125) Gong, Y.-P.; Wan, R.-Z.; Liu, Z.-P. Evaluation of WO2017098421: GSK's benzothiazine compounds as CD73 inhibitor filings. *Expert Opin. Ther. Pat.* **2018**, *28*, 167–171.

(126) Rahimova, R.; Fontanel, S.; Lionne, C.; Jordheim, L. P.; Peyrottes, S.; Chaloin, L. Identification of allosteric inhibitors of the ecto-5'-nucleotidase (CD73) targeting the dimer interface. *PLoS Comput. Biol.* [Online] **2018**, *14.* https://www.ncbi.nlm.nih.gov/pmc/articles/PMC5805337/pdf/pcbi.1005943.pdf (accessed June 25, 2019).

(127) Ripphausen, P.; Freundlieb, M.; Brunschweiger, A.; Zimmermann, H.; Müller, C. E.; Bajorath, J. Virtual screening identifies novel sulfonamide inhibitors of ecto-5′-nucleotidase. *J. Med. Chem.* **2012**, *55*, 6576–6581.

(128) McManus, J.; He, T.; Gavigan, J.-A.; Marchand, G.; Vougier, S.; Bedel, O.; Ferrari, P.; Arrebola, R.; Gillespy, T.; Gregory, R. C.; Licht, S.; Cheng, H.; Zhang, B.; Deng, G. A robust multiplex mass spectrometric assay for screening small-molecule inhibitors of CD73 with diverse inhibition modalities. *SLAS Discov.* **2018**, *23*, 264–273.

(129) Hasenknopf, B. Polyoxometalates: introduction to a class of inorganic compounds and their biomedical applications. *Front. Biosci.* **2005**, *10*, 275–287.

(130) Lee, S.-Y.; Fiene, A.; Li, W.; Hanck, T.; Brylev, K. A.; Fedorov, V. E.; Lecka, J.; Haider, A.; Pietzsch, H.-J.; Zimmermann, H.; Sévigny, J.; Kortz, U.; Stephan, H.; Müller,

C. E. Polyoxometalates-potent and selective ecto-nucleotidase inhibitors. *Biochem. Pharmacol.* **2015**, *93*, 171–181.

(131) Broadway, N. How to develop assays: 5 considerations and 8 fundamentals. *Mater. Methods* **2012**, *2*.

(132) Iternational Conference on Harmonization of Technical Requirements for Registration of Pharmaceuticals for Human Use. Validation of analytical procedures: text and methodology, Q2 (R1) **2005**.

(133) Zhang; Chung; Oldenburg. A Simple Statistical Parameter for Use in Evaluation and Validation of High Throughput Screening Assays. *J. Biomol. Screen.* **1999**, *4*, 67–73.

(134) Baykov, A. A.; Evtushenko, O. A.; Avaeva, S. M. A malachite green procedure for orthophosphate determination and its use in alkaline phosphatase-based enzyme immunoassay. *Anal. Biochem.* **1988**, *171*, 266–270.

(135) Amici, A.; Emanuelli, M.; Raffaelli, N.; Ruggieri, S.; Magni, G. One-minute high-performance liquid chromatography assay for 5'-nucleotidase using a 20-mm reverse-phase column. *Anal. Biochem.* **1994**, *216*, 171–175.

(136) Chatterjee, S. K.; Bhattacharya, M.; Barlow, J. J. A simple, specific radiometric assay for 5′-nucleotidase. *Anal. Biochem.* **1979**, *95*, 497–506.

(137) Ellims, P. H.; Bailey, L.; van der Weyden, M. B. An improved method for the determination of human erythrocyte pyrimidine 5'-nucleotidase activity. *Clin. Chim. Acta* **1978**, *88*, 99–103.

(138) Dooley, J. F.; Racich, L. A new kinetic determination of serum 5'-nucleotidase activity, with modifications for a centrifugal analyzer. *Clin. Chem.* **1980**, *26*, 1291–1297.

(139) Garvey, E. P.; Lowen, G. T.; Almond, M. R. Nucleotide and nucleoside analogues as inhibitors of cytosolic 5'-nucleotidase I from heart. *Biochemistry* **1998**, *37*, 9043–9051.

(140) Gentry, M. K.; Olsson, R. A. A simple, specific, radioisotopic assay for 5′-nucleotidase. *Anal. Biochem.* **1975**, *64*, 624–627.

(141) Janero, D. R.; Yarwood, C.; Thakkar, J. K. Application of solid-phase extraction on anion-exchange cartridges to quantify 5'-nucleotidase activity. *J. Chromatogr. B Biomed. Sci. Appl.* **1992**, *573*, 207–218.

(142) Lanzetta, P. A.; Alvarez, L. J.; Reinach, P. S.; Candia, O. A. An improved assay for nanomole amounts of inorganic phosphate. *Anal. Biochem.* **1979**, *100*, 95–97.

(143) Perez, S.; Courtis, N.; Kokkinopoulos, D.; Papamichail, M.; Tsiapalis, C. M.; Trangas, T. A colorimetric assay for the determination of 5′-nucleotidase activity. *J. Immunol. Methods* **1987**, *101*, 73–78.

(144) Plagemann, P. G.; Wohlhueter, R. M.; Kraupp, M. Adenine nucleotide metabolism and nucleoside transport in human erythrocytes under ATP depletion conditions. *Biochim. Biophys. Acta* **1985**, *817*, 51–60.

(145) Price, C. P.; Hill, P. G.; Sammons, H. G. A comparison of two colorimetric procedures for the assay of 5'-nucleotidase. *Clin. Chim. Acta* **1971**, *33*, 260–263.

(146) Sachsenmeier, K. F.; Hay, C.; Brand, E.; Clarke, L.; Rosenthal, K.; Guillard, S.; Rust, S.; Minter, R.; Hollingsworth, R. Development of a novel ectonucleotidase assay suitable for high-throughput screening. *J. Biomol. Screen.* **2012**, *17*, 993–998.

(147) Suran, A. A. A simple microradioisotopic assay for 5′-nucleotidase activity. *Anal. Biochem.* **1973**, *55*, 593–600.

(148) Tucker-Pian, C.; Bakay, B.; Nyhan, W. L. 5'-Nucleotidase: solubilization, radiochemical analysis, and electrophoresis. *Biochem. Genet.* **1979**, *17*, 995–1005.

(149) Yegutkin, G. G.; Henttinen, T.; Jalkanen, S. Extracellular ATP formation on vascular endothelial cells is mediated by ecto-nucleotide kinase activities via phosphotransfer reactions. *FASEB J.* **2001**, *15*, 251–260.

(150) Chalmers, A. H.; Hare, C. A semi-automated method for 5'-ectonucleotidase measurement in lymphocytes. *Immunol. Cell Biol.* **1990**, *68 (Pt 2)*, 75–79.

(151) Freundlieb, M.; Zimmermann, H.; Müller, C. E. A new, sensitive ecto-5′-nucleotidase assay for compound screening. *Anal. Biochem.* **2014**, *446*, 53–58.

(152) Cogan, E. B.; Birrell, G. B.; Griffith, O. H. A robotics-based automated assay for inorganic and organic phosphates. *Anal. Biochem.* **1999**, *271*, 29–35.

(153) Heinz, F.; Pilz, R.; Reckel, S.; Kalden, J. R.; Haeckel, R. A new spectrophotometric method for the determination of 5′-nucleotidase. *Clin. Chem. Lab. Med.* **1980**, *18*, 2034.

(154) Bethune, V. G.; Fleisher, M.; Schwartz, M. K. Automated method for determination of serum 5'-nucleotidase activity. *Clin. Chem.* **1972**, *18*, 1524–1528.

(155) Zimmermann, H. 5'-Nucleotidase: molecular structure and functional aspects. *Biochem. J.* **1992**, *285*, 345–365.

(156) Hunsucker, S. A.; Mitchell, B. S.; Spychala, J. The 5'-nucleotidases as regulators of nucleotide and drug metabolism. *Pharmacol. Ther.* **2005**, *107*, 1–30.

(157) Marin, R. M.; Franchini, K. G.; Rocco, S. A. Analysis of adenosine by RP-HPLC method and its application to the study of adenosine kinase kinetics. *J. Sep. Sci.* **2007**, *30*, 2473–2479.

(158) Servos, J.; Reilnder, H.; Zimmermann, H. Catalytically active soluble ecto-5'-nucleotidase purified after heterologous expression as a tool for drug screening. *Drug Dev. Res.* **1998**, *45*, 269–276.

(159) BD Biosciences. BD BaculoGold™ Baculovirus Expression System Innovative Solutions for Proteomic; Posted on March 22, 2007 https://www.bdj.co.jp/pdf/55-02_03-7900030-23-A1.pdf (accessed July 3, 2019).

(160) Lowry, O. H.; Rosenbrough, N. J.; Farr, A. L.; Randall, R. J. Protein measurement with the Folin phenol reagent. *J. Biol. Chem.* **1951**, *193*, 265–275.

(161) Laemmli, U. K. Cleavage of structural proteins during the assembly of the head of bacteriophage T4. *Nature* **1970**, *227*, 680–685.

(162) Bio-Rad Laboratories Homepage. Mini-trans-blot electrophoretic transfer cell, instruction manual www.bio-rad.com/webroot/web/pdf/lsr/literature/M1703930.pdf (accessed June 28, 2019).

(163) Malo, N.; Hanley, J. A.; Cerquozzi, S.; Pelletier, J.; Nadon, R. Statistical practice in high-throughput screening data analysis. *Nat. Biotechnol.* **2006**, *24*, 167–175.

(164) Pharma-Zentrums-Bonn Homepage. Substanzbibliothek — Fachgruppe Pharmazie https://www.pharmchem1.uni-bonn.de/ak-mueller/bibliothek (accessed March 1, 2019).

(165) Tocris Homepage. Tocriscreen Kinase Inhibitor Toolbox https://www.tocris.com/products/tocriscreen-kinase-inhibitor-toolbox_3514 (accessed March 3, 2019).

(166) Tocris Homepage. Tocriscreen Mini https://www.tocris.com/products/tocriscreen-mini_2890 (accessed March 8, 2019).

(167) Bhattarai, S. Synthesis and structure-activity relationships of α,β-methylene-ADP derivatives: potent and selective ecto-5′-nucleotidase inhibitors. Dissertation, University of Bonn, 2015.

Bibliography

(168) Altschul, S. F.; Madden, T. L.; Schäffer, A. A.; Zhang, J.; Zhang, Z.; Miller, W.; Lipman, D. J. Gapped BLAST and PSI-BLAST: a new generation of protein database search programs. *Nucleic Acids Res.* **1997**, *25*, 3389–3402.

(169) Altschul, S. F.; Wootton, J. C.; Gertz, E. M.; Agarwala, R.; Morgulis, A.; Schäffer, A. A.; Yu, Y.-K. Protein database searches using compositionally adjusted substitution matrices. *FEBS J.* **2005**, *272*, 5101–5109.

(170) Furtmann, N.; Bajorath, J. Evaluation of molecular model-based discovery of ecto-5'-nucleotidase inhibitors on the basis of X-ray structures. *Bioorg. Med. Chem.* **2013**, *21*, 6616–6622.

(171) Radner, S.; Celie, P. H. N.; Fuchs, K.; Sieghart, W.; Sixma, T. K.; Stornaiuolo, M. Transient transfection coupled to baculovirus infection for rapid protein expression screening in insect cells. *J. Struct. Biol.* **2012**, *179*, 46–55.

(172) Ustün-Aytekin, O.; Gürhan, I. D.; Ohura, K.; Imai, T.; Ongen, G. Monitoring of the effects of transfection with baculovirus on Sf9 cell line and expression of human dipeptidyl peptidase IV. *Cytotechnology* **2014**, *66*, 159–168.

(173) Tamiya, T.; Okahashi, N.; Sakuma, R.; Aoyama, T.; Akahane, T.; Matsumoto, J. J. Freeze denaturation of enzymes and its prevention with additives. *Cryobiology* **1985**, *22*, 446–456.

(174) Millipore Corporation Homepage. Amicon® Ultra-15 Centrifugal Filter Devices, User Guide http://www.emdmillipore.com/Web-PR-Site/en_CA/-/USD/ShowDocument-File?ProductSKU=MM_NF-C7715 &DocumentId=201501.108.ProNet& DocumentType =UG&Language=EN&Country=NF&Origin=PDP (accessed June 28, 2019).

(175) Loi, S.; Pommey, S.; Haibe-Kains, B.; Beavis, P. A.; Darcy, P. K.; Smyth, M. J.; Stagg, J. CD73 promotes anthracycline resistance and poor prognosis in triple negative breast cancer. *PNAS* **2013**, *110*, 11091–11096.

(176) Young, A.; Ngiow, S. F.; Barkauskas, D. S.; Sult, E.; Hay, C.; Blake, S. J.; Huang, Q.; Liu, J.; Takeda, K.; Teng, M. W. L.; Sachsenmeier, K.; Smyth, M. J. Co-inhibition of CD73 and A2AR adenosine signaling improves anti-tumor immune responses. *Cancer Cell* **2016**, *30*, 391–403.

(177) Allard, D.; Chrobak, P.; Allard, B.; Messaoudi, N.; Stagg, J. Targeting the CD73-adenosine axis in immuno-oncology. *Immunol. Lett.* **2018**, *205*, 31–39.

(178) Nassir, M.; Arad, U.; Lee, S.-Y.; Journo, S.; Mirza, S.; Renn, C.; Müller, C. E.; Fischer, B. Identification of adenine-N9-(methoxy)ethyl-β-bisphosphonate as NPP1 inhibitor attenuating undesired NPPase activity in human osteoarthritic chondrocytes. *Purinergic Signal.* [Online] **2019.** https://link.springer.com/content/pdf/10.1007%2Fs11302-019-09649-2.pdf (accessed June 25, 2019).

(179) Junker, A.; Renn, C.; Dobelmann, C.; Namasivayam, V.; Jain, S.; Losenkova, K.; Irjala, H.; Duca, S.; Balasubramanian, R.; Chakraborty, S.; Börgel, F.; Zimmermann, H.; Yegutkin, G. G.; Müller, C. E.; Jacobson, K. A. Structure-Activity Relationship of Purine and Pyrimidine Nucleotides as Ecto-5'-Nucleotidase (CD73) Inhibitors. *J. Med. Chem.* **2019**, *62*, 3677–3695.

(180) Grubbs, F. E. Sample criteria for testing outlying observations. *Ann. Math. Statist.* **1950**, *21*, 27–58.

(181) Duan, G.; Walther, D. The roles of post-translational modifications in the context of protein interaction networks. *PLoS Comput. Biol.* [Online] **2015**, *11*. https://www.ncbi.nlm.nih.gov/pmc/articles/PMC4333291/pdf/pcbi.1004049.pdf (accessed June 25, 2019).

(182) Koch, P.; Brunschweiger, A.; Namasivayam, V.; Ullrich, S.; Maruca, A.; Lazzaretto, B.; Küppers, P.; Hinz, S.; Hockemeyer, J.; Wiese, M.; Heer, J.; Alcaro, S.; Kiec-Kononowicz, K.; Müller, C. E. Probing substituents in the 1- and 3-position: tetrahydropyrazino-annelated water-soluble xanthine derivatives as multi-target drugs with potent adenosine receptor antagonistic activity. *Front. Chem.* **2018**, *6*, 206.

(183) Brunschweiger, A.; Koch, P.; Schlenk, M.; Pineda, F.; Küppers, P.; Hinz, S.; Köse, M.; Ullrich, S.; Hockemeyer, J.; Wiese, M.; Heer, J.; Müller, C. E. 8-Benzyltetrahydropyrazino[2,1-f]purinediones: water-soluble tricyclic xanthine derivatives as multitarget drugs for neurodegenerative diseases. *ChemMedChem* **2014**, *9*, 1704–1724.

(184) Brunschweiger, A.; Koch, P.; Schlenk, M.; Rafehi, M.; Radjainia, H.; Küppers, P.; Hinz, S.; Pineda, F.; Wiese, M.; Hockemeyer, J.; Heer, J.; Denonne, F.; Müller, C. E. 8-Substituted 1,3-dimethyltetrahydropyrazino[2,1-f]purinediones: wter-soluble adenosine receptor antagonists and monoamine oxidase B inhibitors. *Bioorg. Med. Chem.* **2016**, *24*, 5462–5480.

(185) Koch, P.; Akkari, R.; Brunschweiger, A.; Borrmann, T.; Schlenk, M.; Küppers, P.; Köse, M.; Radjainia, H.; Hockemeyer, J.; Drabczyńska, A.; Kieć-Kononowicz, K.; Müller, C. E. 1,3-Dialkyl-substituted tetrahydropyrimido[1,2-f]purine-2,4-diones as multiple target

drugs for the potential treatment of neurodegenerative diseases. *Bioorg. Med. Chem.* **2013**, *21*, 7435–7452.

(186) Drabczyńska, A.; Karcz, T.; Szymańska, E.; Köse, M.; Müller, C. E.; Paskaleva, M.; Karolak-Wojciechowska, J.; Handzlik, J.; Yuzlenko, O.; Kieć-Kononowicz, K. Synthesis, biological activity and molecular modelling studies of tricyclic alkylimidazo-, pyrimido- and diazepinopurinediones. *Purinergic Signal.* **2013**, *9*, 395–414.

(187) Drabczyńska, A.; Müller, C. E.; Karolak-Wojciechowska, J.; Schumacher, B.; Schiedel, A.; Yuzlenko, O.; Kieć-Kononowicz, K. N9-Benzyl-substituted 1,3-dimethyl- and 1,3-dipropyl-pyrimido[2,1-f]purinediones: synthesis and structure-activity relationships at adenosine A1 and A2A receptors. *Bioorg. Med. Chem.* **2007**, *15*, 5003–5017.

(188) Drabczyńska, A.; Müller, C. E.; Schiedel, A.; Schumacher, B.; Karolak-Wojciechowska, J.; Fruziński, A.; Zobnina, W.; Yuzlenko, O.; Kieć-Kononowicz, K. Phenylethyl-substituted pyrimido[2,1-f]purinediones and related compounds: structure-activity relationships as adenosine A(1) and A(2A) receptor ligands. *Bioorg. Med. Chem.* **2007**, *15*, 6956–6974.

(189) Drabczyńska, A.; Yuzlenko, O.; Köse, M.; Paskaleva, M.; Schiedel, A. C.; Karolak-Wojciechowska, J.; Handzlik, J.; Karcz, T.; Kuder, K.; Müller, C. E.; Kieć-Kononowicz, K. Synthesis and biological activity of tricyclic cycloalkylimidazo-, pyrimido- and diazepinopurinediones. *Eur. J. Med. Chem.* **2011**, *46*, 3590–3607.

(190) Drabczyńska, A.; Müller, C. E.; Schumacher, B.; Hinz, S.; Karolak-Wojciechowska, J.; Michalak, B.; Pekala, E.; Kieć-Kononowicz, K. Tricyclic oxazolo[2,3-f]purinediones: potency as adenosine receptor ligands and anticonvulsants. *Bioorg. Med. Chem.* **2004**, *12*, 4895–4908.

(191) Drabczyńska, A.; Schumacher, B.; Müller, C. E.; Karolak-Wojciechowska, J.; Michalak, B.; Pekala, E.; Kieć-Kononowicz, K. Impact of the aryl substituent kind and distance from pyrimido[2,1-f]purinediones on the adenosine receptor selectivity and antagonistic properties. *Eur. J. Med. Chem.* **2003**, *38*, 397–402.

(192) Docampo, R.; Moreno, S. N. The metabolism and mode of action of gentian violet. *Drug Metab. Rev.* **1990**, *22*, 161–178.

(193) Maley, A. M.; Arbiser, J. L. Gentian violet: a 19th century drug re-emerges in the 21st century. *Exp. Dermatol.* **2013**, *22*, 775–780.

(194) Gold, L. S.; Ames, B. N.; Bernstein, L.; Blumenthal, M.; Chow, K.; Da Costa, M.; Veciana, M. de; Eisenberg, S.; Garfinkel, G. B.; Haggin, T.; Havender, W. R.; Hooper, K.; Levinson, R.; Lopipero, P.; Magaw, R.; Manley Neela B.; MacLeod, P. M.; Peto, R.; Pike, M. C.; Rohrbach, L.; Sawyer, C. B.; Slone, T. H.; Smith, M.; Stern, B. R.; Wong, M. *The Carcinogenic Potency Database (CPDB)* [Online]; Posted on February 14, 2013 https://toxnet.nlm.nih.gov/cpdb/chempages/GENTIAN%20VIOLET.html (accessed March 5, 2019).

(195) Littlefield, N. A.; Blackwell, B. N.; Hewitt, C. C.; Gaylor, D. W. Chronic toxicity and carcinogenicity studies of gentian violet in mice. *Fundam. Appl. Toxicol.* **1985**, *5*, 902–912.

(196) Bingham, E.; Cohrssen, B.; Patty, F. A. *Patty's toxicology*; John Wiley & Sons: New York, 2012; 6. ed, p 585.

(197) Mani, S.; Bharagava, R. N. Exposure to Crystal Violet, Its Toxic, Genotoxic and Carcinogenic Effects on Environment and Its Degradation and Detoxification for Environmental Safety. *Rev. Environ. Contam. Toxicol.* **2016**, *237*, 71–104.

(198) Mullur, R.; Liu, Y.-Y.; Brent, G. A. Thyroid hormone regulation of metabolism. *Physiol. Rev.* **2014**, *94*, 355–382.

(199) Salvatore, D.; Simonides, W. S.; Dentice, M.; Zavacki, A. M.; Larsen, P. R. Thyroid hormones and skeletal muscle — new insights and potential implications. *Nat. Rev. Endocrinol.* **2013**, *10*, 206–214.

(200) Meyer, A. Chromen-4-ones as novel potent and selective ligands for purinoceptor-related class A δ-branch orphan G protein-coupled receptors. Dissertation, University of Bonn, 2017.

(201) Ghose, A. K.; Crippen, G. M. Atomic physicochemical parameters for three-dimensional-structure-directed quantitative structure-activity relationships. 2. Modeling dispersive and hydrophobic interactions. *J. Chem. Inf. Model.* **1987**, *27*, 21–35.

(202) Bylund, D. B.; Toews, M. L. Radioligand binding methods: practical guide and tips. *Am. J. Physiol.* **1993**, *265*, L421-L429.

(203) Thomson, L. F.; Ruedi, J. M.; Glass, A.; Moldenhauer, G.; Moller, P.; Low, M. G.; Klemens, M. R.; Massaia, M.; Lucas, A. H. Production and characterization of monoclonal antibodies to the glycosyl phosphatidylinositol-anchored lymphocyte differentiation antigen ecto-5′-nucleotidase (CD73). *Tissue Antigens* **1990**, *35*, 9–19.

(204) Ashish; Solanki, A. K.; Boone, C. D.; Krueger, J. K. Global structure of HIV-1 neutralizing antibody IgG1 b12 is asymmetric. *Biochem. Biophys. Res. Commun.* **2010**, *391*, 947–951.

(205) Ditzel, H. University of Southern Denmark, Odense, Denmark, unpublished work, 2016.

(206) Ryan, A. J.; Gray, N. M.; Lowe, P. N.; Chung, C.-w. Effect of detergent on "promiscuous" inhibitors. *J. Med. Chem.* **2003**, *46*, 3448–3451.

(207) Acker, M. G.; Auld, D. S. Considerations for the design and reporting of enzyme assays in high-throughput screening applications. *Perspect. Sci.* **2014**, *1*, 56–73.

(208) Eckhardt, B. L.; Parker, B. S.; van Laar, R. K.; Restall, C. M.; Natoli, A. L.; Tavaria, M. D.; Stanley, K. L.; Sloan, E. K.; Moseley, J. M.; Anderson, R. L. Genomic analysis of a spontaneous model of breast cancer metastasis to bone reveals a role for the extracellular matrix. *Mol. Cancer Res.* **2005**, *3*, 1–13.

8   Publications

Based on this thesis:

Junker, A.; **Renn, C.**; Dobelmann, C.; Namasivayam V.; Jain, S.; Duca, S.; Balasubramanian, R,; Chakraborty S.; Börgel, F.; Losenkova K.; Irjalab H.; Yegutkin, G. G.; Zimmermann H.; Müller, C. E.; Jacobson, K. A. Structure-activity relationship of purine and pyrimidine nucleotides as ecto-5′-nucleotidase (CD73) inhibitors. *J. Med. Chem.* **2019**, *62*, 3677–3695.

U.S. Patent Application No. 62/719,492 filed August 17, **2018** 'Purine and Pyrimidine Nucleotides as Ecto-5′-Nucleotidase Inhibitors'. HHS, E-132-2018-0-US-01

Nassir, M.; Arad, U.; Lee, S.; Journo, S.; Mirza S.; **Renn, C.**; Müller, C. E.; Fischer, B. Synthesis and evaluation of AMP and ADP mimics identifies adenine-N9-(methoxy)ethyl-β-bisphosphonate as NPP1 inhibitor attenuating undesired NPPase activity in human osteoarthritic chondrocytes. *Purinergic Signal.* **2019**

Previous publications:

Bethke, E.; Pinchuk, B.; **Renn, C.**; Witt, L.; Schlosser, J.; Peifer, C. From Type I to Type II: Design, synthesis, and characterization of potent pyrazin-2-ones as DFG-Out inhibitors of PDGFRβ. *ChemMedChem*. **2016**, 11, 2664–2674.

Phoa, A.; Browne, S.; Gurgis, F.; Åkerfeldt, M.; Döbber, A.; **Renn, C.**; Peifer, C.; Stringer, B.; Day, B.; Wong, C.; Chircop, M.; Johns, T.; Kassiou, M.; Munoz, L. Pharmacology of novel small-molecule tubulin inhibitors in glioblastoma cells with enhanced EGFR Signalling, *Biochem Pharmacol*. **2015**, *98,* 587–601.

Zindler, M.; Pinchuk, B.; **Renn, C.**; Horbert, R.; Döbber, A.; Peifer, C. Design, synthesis, and characterization of a photoactivatable caged prodrug of imatinib. *ChemMedChem*. **2015**, *10*, 1335-1338.

9   Danksagung

<div align="center">

Danke

</div>

an alle, die mich darin unterstützt haben, diese Arbeit zu verfassen!